Quantifying carbon fixation in microbial dark matter from low-temperature hydrothermal settings: experimental validation using quantitative stable isotope probing

Ömer Kürşat Coşkun

München 2022

Quantifying carbon fixation in microbial dark matter from low-temperature hydrothermal settings: experimental validation using quantitative stable isotope probing

Ömer Kürşat Coşkun

Dissertation zur Erlangung des Doktorgrades
an der Fakultät für Geowissenschaften
der Ludwig-Maximilians-Universität
München

vorgelegt von

Ömer Kürşat Coşkun

München, den 02. März 2022

Erstgutachter/in: **Prof. Dr. William D. Orsi**
Zweitgutachter/in: **Dr. Stefan M. Sievert**

Tag der mündlichen Prüfung: 21.07.2022

Table of Contents

List of published articles and papers in preparation.

Ömer K Coskun, Aurèle Vuillemin, Florence Schubotz, Frieder Klein, Susanna E Sichel, Wolfgang Eisenreich, William D Orsi (2021). Quantifying the effects of hydrogen on carbon assimilation in a seafloor microbial community associated with ultramafic rocks.
Published in: *The ISME journal*, Volume 16, Issue 1, January 2022, Pages 257-271, https://doi.org/10.1038/s41396-021-01066-x **(Chapter 2)**

Ömer K Coskun, Volkan Özen, Scott D Wankel, William D Orsi (2019). Quantifying population-specific growth in benthic bacterial communities under low oxygen using $H_2{}^{18}O$.
Published in: *The ISME journal*, Volume 13, Issue 6, June 2019, Pages 1546-1559, https://doi.org/10.1038/s41396-019-0373-4 **(Chapter 3)**

Ömer K Coskun, Murat Beren, Doğacan Özcan, Suna D. Günay, Viktor Elkin, Hakan Hoşgörmez, Florian Einsiedl and William D Orsi. Bicarbonate concentrations drive primary production by microbial dark matter in a subsurface hydrothermal aquifer.
This manuscript is in preparation for standalone publication **(Chapter 4)**

Ömer K Coskun, Murat Beren, Doğacan Özcan,Hakan Hoşgörmez, Florian Einsiedl and William D. Orsi. Wood-Ljungdahl pathway in *Candidatus* Bipolaricaulota thriving in thermal waters in Biga Peninsula.
This manuscript is in preparation for standalone publication **(Chapter 5)**

APPENDIX

Valentine Puzenat, Javier Escartin, Jean-Emmanuel Martelat, Thibaut Barreyre, Sven Le Moine Bauer, Paraskevi Nomikou, Nuno Gracias, Pascal Allemand, Varvara Antoniou, **Ömer Coskun**, Rafael Garcia, Philippe Grandjean, Steffen Leth Jørgensen, Lluís Magí, Manolis Mandalakis, William Orsi, Paraskevi Polymenakou, Anders Schouw, Guillem Vallicrosa, Othonas Vlasopoulos (2021). Shallow-water hydrothermalism at Milos (Greece): Nature, distribution, heat fluxes and impact on ecosystems.
Published in: *Marine Geology*, Volume 438, August 2021, Pages 106521, https://doi.org/10.1016/j.margeo.2021.106521 **(Paper 1)**

William D Orsi, Aurèle Vuillemin, Paula Rodriguez, **Ömer K Coskun**, Gonzalo V Gomez-Saez, Gaute Lavik, Volker Mohrholz, Timothy G Ferdelman (2020). Metabolic activity analyses demonstrate that Lokiarchaeon exhibits homoacetogenesis in sulfidic marine sediments.
Published in: *Nature Microbiology*, Volume 5, Issue 2, February 2020, Pages 248-255, https://doi.org/10.1038/s41564-019-0630-3 **(Paper 2)**

Florian Einsiedl, Anja Wunderlich, Mathieu Sebilo, **Ömer K Coskun**, William D Orsi, Bernhard Mayer (2020). Biogeochemical evidence of anaerobic methane oxidation and anaerobic ammonium oxidation in a stratified lake using stable isotopes.
Published in: Biogeosciences, Volume 17, Issue 20, October 2020, Pages 5149-5161 https://bg.copernicus.org/articles/17/5149/2020/ **(Paper 3)**

Aurèle Vuillemin, Sergio Vargas, **Ömer K Coskun**, Robert Pockalny, Richard W Murray, David C Smith, Steven D'Hondt, William D Orsi (2020). Atribacteria Reproducing over Millions of Years in the Atlantic Abyssal Subseafloor.
Published in: mBio, Volume 11, Issue 5, October 2020, Pages e01927-20, https://doi.org/10.1128/mBio.01937-20 **(Paper 4)**

Aurèle Vuillemin, Scott D Wankel, **Ömer K Coskun**, Tobias Magritsch, Sergio Vargas, Emily R Estes, Arthur J Spivack, David C Smith, Robert Pockalny, Richard W Murray, Steven D'Hondt, William D Orsi (2019). Archaea dominate oxic subseafloor communities over multi million-year time scales.
Published in: Science Advances, Volume 5, Issue 6, June 2019, Pages eaaw4108, doi:10.1126/sciadv.aaw4108 **(Paper 5)**

William D Orsi, Aurèle Vuillemin, **Ömer K Coskun**, Paula Rodriguez, Yanik Oertel, Jutta Niggemann, Volker Mohrholz, Gonzalo V Gomez-Saez (2021). Carbon assimilating fungi from surface ocean to subseafloor revealed by coupled phylogenetic and stable isotope analysis.
Published in: The ISME Journal, December 2021, Pages 1751-7370, https://doi.org/10.1038/s41396-021-01169-5 **(Paper 6)**

Authors Contributions

Chapter 2: WDO, WE, FK, and FS conceived the idea for the study. FS, WDO and OKC designed the experiments. FS conducted the experiments. OKC performed DNA extraction, DNA-SIP analysis. AV and OKC prepared metagenomic analysis. OKC performed quantitative stable isotope probing analysis and phylogenetic analyses. OKC and WDO, FK, and FS prepared the figures. OKC, WDO, FK, and FS wrote the paper. OKC, AV, FS, FK, SES, WE, and WDO revised the manuscript. WDO, FS, and FK secured the funding.

Chapter 3: SDW and WDO designed the study. SDW, WDO, and OKC conducted the experiments. OKC and VO worked on the statistical calculations and generated the first figures. OKC, VO, SDW, and WDO drafted the manuscript and figures. All authors revised the manuscript. SDW and WDO secured the funding.

Chapter 4: OKC and WDO designed the study. OKC, MB, DÖ conducted the field trip and the experiments. OKC performed DNA extraction, DNA-SIP analysis and metagenomic analysis. OKC performed quantitative stable isotope probing and the metagenomic workflow. OKC performed the bioinformatic analyses. SDG and VE partially helped with the laboratory work to generate the data. FE performed water chemistry analyses and isotope measurements. OKC, WDO drafted the manuscript and figures. OKC, MB, DÖ, SDG, VE, FE, and WDO revised the manuscript. WDO secured the funding.

Chapter 5: OKC and WDO designed the study. OKC, MB, DÖ conducted the field trip and the experiments. OKC performed DNA extraction, DNA-SIP analysis and metagenomic analysis. OKC performed quantitative stable isotope probing, metagenomic workflow and pangenome analysis. OKC performed the bioinformatic analyses. FE performed water chemistry analyses and isotope measurements. OKC, WDO drafted the manuscript and figures. OKC, MB, DÖ, FE, and WDO revised the manuscript. WDO secured the funding.

SUMMARY

Last common universal ancestor of all cells (LUCA or progenote) is in the center of Origin-of-life related studies. Phylogenetic and genetic analysis indicate that LUCA was an anaerobic single celled thermophile which was able to fix carbon-dioxide using hydrogen-dependent reductive acetyl-CoA (Wood-Ljungdahl pathway; abbreviated as WL pathway hereon). Besides WL pathway, reductive tricarboxylic acid pathway (rTCA) was also proposed as a candidate primordial carbon fixation mechanism at the dawn of the origin of life. Apart from proposed metabolisms, it has been hypothesized that serpentinization-driven hydrothermal vents and hot springs could be the possible birthplace where life could have originated and evolved. The data also supports this idea that LUCA might have existed in a hydrothermal setting. However, quantitative experimental data to better understand the ecology of the modern-day microbes utilizing rTCA and WLP in hydrothermal vents, deep-subsurface and hot springs is lacking.

In this project we sampled the environments where the first functional cellular life could have proliferated. We conducted for the first time quantitative stable isotope probing experiments (qSIP) on the samples taken from a possible serpentinization-driven setting, hot springs and shallow water hydrothermal systems using ^{13}C-labeled carbon sources. Main objectives of this study were [1] to better understand the controlling parameters underlying the function of proposed ancestral pathways and [2] potentially other mechanisms hypothesized to be rooted from prebiotic mechanisms, [3] to gain understanding of carbon cycling performed by indigenous microbes dwelling in hydrothermal systems, [4] to elucidate the microbial interactions under different conditions by changing the substrate additions and concentrations, and [5] to find out novel microbes which are relevant to origin-of-life studies. In the introduction section (**Chapter 1**) the background information, terminology, and the relevant concepts for the origin of life are provided.

In **Chapter 2**, the effect of hydrogen on microbial carbon assimilation dynamics in a partially serpentinized peridotite-associated environment is described. Serpentinization is a natural process that results in production of hydrogen and methane as the main products and hypothesized to be modern analogue for origin-of-life related studies. H_2 utilization is a favorable energy source for microbial life and this chapter addresses how the hydrogen affects the anabolic processes in seafloor associated communities. By applying quantitative stable isotope probing experiments using ^{13}C-bicarbonate -acetate and -formate in the presence/absence of molecular hydrogen, increase in bicarbonate and acetate assimilation was observed with the addition hydrogen and correlated with increase in NiFe-hydrogenases. Hydrogen decreased the assimilation of formate by rock-associated microbes. Because ultramafic rocks are widespread in oceanic lithosphere, continental margins, and subduction zones where H_2 is formed in copious amounts, the link between H_2 and carbon assimilation demonstrated here may be widespread in geological settings around the globe and may shed light on earliest biochemical pathways driven by H_2 in serpentinization-driven ecosystems.

Chapter 3 aimed to comprehend the growth dynamics of microbes in marine sediments using qSIP with $H_2{}^{18}O$. It closely focuses on how the oxygen depletion in benthos shapes growth, mortality, and

reproduction rates of uncultivated microbial populations, which a huge gap is present in our current understanding. The oxygen-labeling helped us categorize the microbial population based on their growth characteristics, i.e., spanning from aerobic to anaerobic lifestyle. Further investigation on the genes encoding dissimilatory sulfite reductase β-subunit (*dsrB*) revealed novel Acidobacteria, highlighting their importance for sulfur cycling in estuarine sediments. This chapter helped me improve my skills on qSIP and understand the importance of the effect of oxygen on microbial communities, which is mostly overlooked in closed incubational setups.

Chapter 4 aimed to better understand how different bicarbonate concentrations affect the microbial carbon fixation in deep subsurface geothermal aquifer systems. Continental deep subsurface environments provide an analogous environment for any crustal subsurface in rocky or icy planetary bodies as lithogenic substrates produced through the water-rock interactions may provide an energy source for first microbial life away from the pre-ozone early Earth. The ^{13}C-bicarbonate qSIP incubations using 750-meter-deep thermal water pumped to a private hotel showed novel bicarbonate-utilizing bacteria and archaea. Interestingly, the incubations receiving low bicarbonate addition revealed higher utilization rate of bicarbonate performed by higher biodiversity compared to the incubations amended with those of higher concentrations. Metagenomic data uncovered taxonomically unassigned taxa, reflecting the uniqueness of the studied area with metabolic capacity to fix carbon through WL pathway, rTCA and CBB cycles. Our data may shed light onto how life may emerge and evolve in geothermal systems by underlying the diverse microbial metabolic capacities in modern, deep, and hot subsurface environments.

Chapter 5 targets to reveal metabolic potentials of reconstructed metagenome-assembled-genomes (MAGs) affiliated to *Canditatus* Bipolaricaulota (Formerly, *Candidatus* OP1, Acetothermia) by applying a pangenome approach. We reconstructed 5 high to medium quality MAGs and compared them to 19 publicly available (complete to incomplete) MAGs. The pangenomic approach has uncovered complete – nearly complete WL pathway in more than half of the MAGs of *Ca.* Bipolaricaulota studied here, which was in line with the literature. It has been shown and predicted that WL pathway in this deeply branching phylum is versatile and mainly used in homoacetogenic fermentation and syntrophic acetate oxidation. The lack of representative cultures and isolates makes it difficult to assess which way WL pathway is working; however, the results from quantitative stable isotope probing (qSIP) experiment in **Chapter 4** helped us to unearth carbon fixing OTUs affiliated with *Ca.* Bipolaricaulota. Furthermore, 3 actively carbon fixing OTUs associated with *Ca.* Bipolaricaulota, found in all the sampled hydrothermal spots except Entur, were the major taxa in Tuzla sample, which is a hypersaline geothermal brine, suggesting halotolerant ecophysiology of this phylum.

Summary of the papers published during my Ph.D.

This study **(Paper 1)** aimed to comprehend the hydrothermal outflow at shallow-water hydrothermal system of Milos, Greece where an underwater survey coupled with drone imagery was conducted. Shallow-water hydrothermal systems may provide the necessary ingredients for life- carbon sources, chemical energy from thermodynamic disequilibrium, mineral surfaces, and compositional gradients. Although U-V light might be a problem for life to exist in the emergence of life, seabed may be a protecting area for life to thrive. Therefore, a field work was conducted in Paleochori Bay in Milos to investigate the microbial carbon cycling. Aside from the published paper, DNA-SIP experiments were conducted in the field using sediment samples exhibiting >60 ^{o}C, but none of them showed a clear shift due to low amount of biomass and experimental setup. However, this helped us change our experimental setup for the future experiments.

This study **(Paper 2)** focuses on metabolic capability of representatives of Lokiarchaeon using metatranscriptomics coupled with quantitative stable isotope probing technique. *Candidatus* Lokiarchaeota is at the heart of studies investigating the eukaryotic evolution as it has been hypothesized that a Lokiarcheon was the host cell acquiring the mitochondrion which led to eukaryotic dispersion around the globe. Our data has expanded our knowledge on the metabolic capacity of *Candidatus* Lokiarchaeota. It has been revealed that homoacetogenesis was performed by representatives of *Candidatus* Lokiarchaeota.

Papers 3-6 consist of the publications that I have contributed on but are also irrespective of origin of life-related studies. **Paper 3** presents vertical concentration and stable isotope profiles of CH_4, NO_3^-, NO_2^-, and NH_4^+ in the water column of Fohnsee (Bavaria, Germany) using geochemical data coupled with 16S rRNA gene sequencing. Nitrate pollution of freshwater systems and methane emissions to the atmosphere are two important factors in lowering the quality of drinking water and in increasing global warming. This chapter linked geochemical data to microbial populations driving nitrite-dependent anaerobic methane oxidation (n-damo), nitrate-dependent anaerobic methane oxidation and the anaerobic oxidation of ammonium (anammox). **In Paper 4,** the metabolism of *Candidatus* Atribacteria was discussed. The members of this phylum were found to be dominant microorganism in an anoxic energy-limited abyssal clay in North Atlantic Ocean that are million years old. These microbes exhibited increased transcription of genes associated with acetogenic fermentation and reproduction. **Paper 5** was a complementary study of **Paper 4** and provided a better understanding of how microbial communities thrived in the oxic, but energy-starved abyssal clay of North Atlantic Ocean. Ammonia-oxidizing archaea (AOA) dominated the microbial community in which their abundance showed a positive correlation with the rates of nitrification. This chapter shed light on how AOA could subsist in larger abundance under constant energetic stress in oxic subseafloor sediment. Lastly, in **Paper 6**, qSIP, metagenomic and metatranscriptomic approaches were coupled to unravel carbon cycling mediated by Fungi in marine ecosystems. ^{13}C-labeling of Fungi utilizing diatom extracellular polymeric substances correlated with the expression of fungal genes encoding carbohydrate-active enzymes. This paper

showed how marine fungi play an important role in the cycling of marine organic matter in the water column and sediment.

This dissertation contributes to our understanding of microbial carbon cycling in environmental setting associated with origin of life by specifically focusing on the proposed primordial carbon fixation mechanisms, namely rTCA and WL pathways. This thesis has three main objectives. First objective is to investigate microbial carbon assimilation dynamics under varying conditions such as addition of H_2 (**Chapter 2**), or differential bicarbonate concentrations (**Chapter 4**). Secondly, it targets to find novel microbes mediating carbon fixation in hydrothermal environments which exhibits variable geochemical characteristics (**Chapter 5**). Finally, it aims to better understand the microbial growth dynamic in an environment which is subjected to perturbations in chemical gradients (**Chapter 3**). The latter objective was not directly related to origin-of-life studies, but the early environments where life has emerged was not different than today's environments (except especially O_2 and CO_2 levels) where chemical gradients are disturbed regularly. Therefore, organisms should adapt to these conditions by employing genetic capability to withstand. These perturbations likely played an important role in microbial diversification in the Early Earth, and I have shown that some microbial populations in Estuarine sediments can grow in both anoxic and oxic conditions which bolsters survivability in the nature (**Chapter 3**). In conclusion, at least 4 billion years of evolution in microbes has tremendously shaped microbial metabolism, leading to a huge diversification in the microbial world. However, ancient imprints may still be present in the modern microbial world and this dissertation seeks microbes carrying ancient genes that have survived since the origin of life in the environmental ecosystems where life could have emerged and evolved.

Chapter 1

Introduction

Chapter 1
Introduction

In 1929, John Burdon Sanderson Haldane published an article titled “The Origin of Life”, explaining the concept of “prebiotic soup” in the Early Earth conditions (Haldane 1929). According to this scenario, first organic molecules were assembled from methane, ammonia and water by UV radiation and these molecules started to accumulate to produce even larger molecules. Without an existing life consuming these organics, first anaerobic fermenters emerged and started utilizing the rest of the concentrated prebiotic soup as an energy source. This led to the diversification of the first organism until the prebiotic soup had been used up. Prebiotic soup theory received support from a well-known experiment, Miller’s experiment, which showed that organic molecules could be synthesized with a simulated lightning from CH_4, H_2 and NH_3 which was thought to be Early Earth’s atmospheric composition (Miller 1953). This hypothesis was assuming life’s creation out of an homologous soup which had already reached a thermodynamic equilibrium; therefore, no further reactions could have taken place (Lane et al. 2010). His theory was missing an energy flux which life requires.

In the late 1970s, submarine hydrothermal vents, known as black smokers, were discovered in the deep ocean waters near Galapagos Island (Corliss et al. 1979; Baross and Hoffman 1985). Although the thermodynamic non-equilibrium conditions were governing in the vents where emanating mineral-rich fluid meets with oceanic cold water, the environment itself was too hot for life’s emergence. However, this discovery led to an origin of life hypotheses since the vent system was chemically reactive environments that would have created suitable conditions for prebiotic synthesis (Baross and Hoffman 1985; Martin et al. 2008).

In the late 1980’s novel geochemical evidence from deep-sea hydrothermal vents led to the hypothesis that warm, alkaline (basic) springs at the bottom of the acidic Hadean Ocean could have provided the conditions that were suitable for the emergence of the life (Russell et al. 1989; Martin et al. 2008; Russell et al. 2010).

1.1 The Alkaline hydrothermal vents (AHVs) theory

The gradients of temperature and pH around alkaline hydrothermal vents (AHVs) would have provided potential energy for proto-life and dissolved compounds are proposed to have fallen out of solution and formed insoluble solids when mixed with the chemicals in the cooler Hadean seawater, thereby generating towering mounds of precipitated carbonate, silica, clays, and iron-

nickel sulfides that surrounded such springs. Particularly, continuous supply of hydrogen, methane, formate and acetate through serpentinization to carbonic Hadean ocean are speculated to have fueled anaerobic ecosystems in the Early Earth (Russell et al. 2010). This submarine AHV theory for the emergence of life postulates that reactive Ni-Fe-S mineral surfaces formed across eH-pH gradients and served as catalytic sites for abiotic organic synthesis reactions (Martin et al. 2008; Sojo et al. 2016). New laboratory experiments are able to simulate AHV models under simulated Hadean Ocean conditions identified the growth of catalytic mineral membranes and chambers inside of the chimneys that catalyze CO_2 reduction and thus provide a constant source of energy for proto-cells and reduced carbon to sustain early life in submarine AHVs (Herschy et al. 2014; Barge et al. 2019; Barge et al. 2020). Furthermore, the serpentinization has potentially significant implications for the other planets as it may be presently going on in "ocean worlds" such as Europa and Enceladus (Glein et al. 2015; Waite et al. 2017).

1.1.1 Low-temperature serpentinization

In 2000, The Lost City hydrothermal vent field (LCHF) was discovered 15 km away from Mid Atlantic Ocean ridge (MAR) at a water depth of 750-900 meters which was away from the maximum depth the sunlight could penetrate (Kelley et al. 2001). It became one of the most extensively studied sites for active serpentinization since its discovery. The temperature of emanating fluids from hydrothermal vents at LCHF ranged from 41 - 91 ^{o}C and was rich in hydrogen and methane (Kelley et al. 2005). It has been estimated that hydrothermal activity has been active for at least >30,000 years as shown by ^{14}C and U/Th dating of calcium carbonate chimney deposits (Früh-Green et al. 2003). The hydrothermal fluid had pH from 9 to 11, providing a highly reduced alkaline condition driven by active serpentinization.

Serpentinization is the aqueous alteration of ultramafic rocks (high Fe^{+2}, Mg^{+2} and low silica) which generates H_2, methane (CH_4), alkaline fluids (only at low temperature serpentinization) and low-molecular-weight organic compounds (Bach et al. 2006) (reaction 1). The interaction of produced H_2 with carbon produces the methane via Fischer-Tropsch Type reaction and other carbons such as formate and released to the environment through fractures (McCollom and Seewald 2007; Etiope 2017). The source of carbon dioxide may be ocean water infiltrating through the cracks, or the mantle beneath (Russell et al. 2010). Recently, it has been also shown that serpentinization occurs in fluid inclusions trapped in olivine systems when the temperatures are lower than 340 ^{o}C and a significant amount H_2 and CH_4 can be stored until extracted by dissolution and fracturing (Klein et al. 2019). It has been estimated that the rate of H_2 production through serpentinization within the oceanic lithosphere is ~10^{12} mol H_2/yr (2 Tg/yr), which exceeds continental production by an order of magnitude (Worman et al. 2016).

Reaction 1: The overall process of serpentinization taken from (McCollom and Seewald 2013)

Olivine + pyroxene + H_2O ---> serpentinite ± brucite ± magnetite ± H_2

1.1.2 Microbial communities in serpentinization-driven ecosystems

Alkaline fluids emanating from serpentinization process are rich in electron donors H_2, CH_4, short-chain hydrocarbons and in some cases formate that can fuel the microbial communities, although the electron acceptors and dissolved carbon are often limited (Schrenk et al. 2013). It is usually observed that alkaline fluids at many sites demonstrates low cell abundances and low taxonomic diversity; however, surface-attached habitats where the ambient water mixes with those fluids may exhibit greater biomass such as the biofilms on carbonate chimneys of Lost-City low-temperature hydrothermal vent field (Kelley et al. 2005; Schrenk et al. 2013). Diverse metabolic strategies possessed by microorganisms could be found in the extremely basic serpentinite systems due to the high concentrations of electron donors but coping with the electron acceptors seems to be the reason which keeps the biodiversity at low levels. In those systems, methane, hydrogen, sulfur and fermentative processes (see table 1) are the main metabolic capabilities activities that shape the biological cycling of important elements such as hydrogen, carbon and sulfur (Schrenk et al. 2013). One of the features of serpentinization-fueled chimneys is that the transition of microbial communities from hot chimney interior where anoxic conditions prevail to cold oxic conditions where the diffusing water is mixed with the ambient water. The chimney interior is mainly dominated by thermophilic anaerobes such as methanogens and sulfate-reducers while the exterior favors for meso- and physophillic aerobes such as methanotrophs and H_2-oxidizing microorganisms (McCollom and Seewald 2013).

TABLE 1: Main metabolic energy sources for chemosynthetic microorganisms in serpentinite-fueled environments (taken and modified from (McCollom and Seewald 2013).

Metabolic energy source	Overall chemical reaction
Hydrogen oxidation	$H_2 + {}^1/_2\, O_2 \rightarrow H_2O$
Methanotrophy	$CH_4 + 2\, O_2 \rightarrow HCO_3^- + H^+ + H_2O$
Methanogenesis	$CO_2 + 4\, H_2 \rightarrow CH_4 + 2H_2O$
Sulfate reduction	$SO_4^{2-} + 2\, H^+ + 4\, H_2 \rightarrow H_2S + 4H_2O$
Anaerobic methane oxidation (AMO)	$SO_4^{2-} + 2\, H^+ + CH_4 \rightarrow CO_2 + H_2S + 4H_2O$

1.2 The hot, deep biosphere and hot spring theory of origin of life

The deep biosphere is defined as the permanently dark environments that organisms can sustain themselves using geochemical sources (Gold 1992). Thomas Gold in his famous paper argued that life might have emerged and evolved at the deep depth in the pores spaces between rock grains and in the cracks, where Earth's dynamic interior and host rock supplied sources needed for life at temperatures exceeding known limits of life (Gold 1992; Colman et al. 2017). It was also hypothesized that deep rock bodies containing H_2, CH_4 and other chemicals important to life can be

the most plausible starting point for the emergence of life. Life's evolution later on must have been followed by lateral expansion in the deep and eventually upward progression where it met with lower temperatures. Besides, it has been suggested that subsurfaces must play an important role in the origin of life by preventing devastating effects of meteorites and high radiation of the early solar system (Edwards et al. 2012; Stevens 2018).

Hot spring hypothesis of the origin of life is one of the famous concepts put forth by Darwin in a letter which he wrote to his friend J.D.Hooker in 1871 (Darwin 1871; Damer and Deamer 2019). He described that a "warm little pond" could provide conditions that facilitated the life's emergence The modern hot spring theories is built upon this first idea and states the hydrothermal fields with multiple hot spring spots on volcanic islands above the sea level (Van Kranendonk 2010; Bada and Korenaga 2018) would provide sources of heat and geochemical energy to stimulate the accumulation, concentration and synthesis of organic polymers on the mineral surfaces driven by intense and fast wet-dry cycles (Damer and Deamer 2019).

1.3 Relevance of carbon fixation in origin of life: Implications for metabolism of Last Universal Common Ancestor (LUCA)

All life on Earth builds itself from CO_2 (Fuchs 2011), and we agree with the argument that this was no different at the emergence of life (Martin et al. 2008; Russell et al. 2014). The evolutionary metabolic analysis of all available genomic data indicates the last universal common ancestor (LUCA) was likely an H_2-utilizing autotroph (Wimmer et al. 2021). Related to this important point, it was recently shown that the iron-sulfur mineral greigite (Fe_3S_4) can catalyze abiotic reduction of CO_2 from H_2, forming pyruvate and a series of other reduced carbon compounds (Preiner et al. 2020). Moreover, it was shown that native transition metals (Fe^0, Ni^0, Co^0) can reduce CO_2 into intermediates and end products of the acetyl-CoA fixation pathway (Varma et al. 2018; Muchowska et al. 2019b). High CO_2 partial pressures, which were present during Hadean, were also shown to stimulate carbon fixation in an otherwise heterotrophic organism thus driving the TCA cycle backwards towards autotrophy (Steffens et al. 2021). These recent results provide strong support for the hypothesis that emergence of life occurred in a CO_2 environment enriched with metals and iron sulfide minerals and was characterized by H_2 dependent CO_2 reduction (Martin et al. 2008). Two of carbon fixation pathways, the reductive tricarboxylic acid (rTCA) and reductive acetyl-CoA pathways, are present in modern hydrothermal microbes and thought to be the most ancient primordial metabolism (Wächtershäuser 1990; Smith and Morowitz 2004; Braakman and Smith 2012, 2013).

1.3.1 Wood-Ljungdahl pathway

Among the seven known pathways (Fuchs 2011; Sánchez-Andrea et al. 2020), the only carbon fixation pathway found in both archaea and bacteria is reductive acetyl-CoA pathway, known as Wood-Ljungdahl pathway. In this pathway, ATP is generated simultaneously by converting acetyl-

CoA to acetate while fixing CO_2, making the WL pathway unique among the others (Fuchs 2011) (Figure 1b-c). It is also surprising finding that the chemistry facilitated by WL pathway, i.e., the reduction in CO_2 to organic one-carbon moieties, is similar to spontaneous geochemical reactions occurring in hydrothermal systems (Seewald et al. 2006; Schrenk et al. 2013; McCollom 2016) (Figure 1a). The WL pathway consists of O_2 sensitive catalysts, as its enzymes containing iron, nickel and sulfur in their center performs electron transfer and catalysis (Russell and Martin 2004; Ragsdale and Pierce 2008). Interestingly, the atomic structure of these enzymes are very similar to minerals found in hydrothermal vents such as greigite (Fe_3S_4), highlighting the importance of the catalytic activity of naturally occurring minerals in the presence of proteins (Russell and Martin 2004). Phylogenetic reconstruction of LUCA has shown that it might have deployed this pathway to fix inorganic carbon into biomass (Weiss et al. 2016). Thus, these findings strongly present a plausible starting point for metabolic evolution.

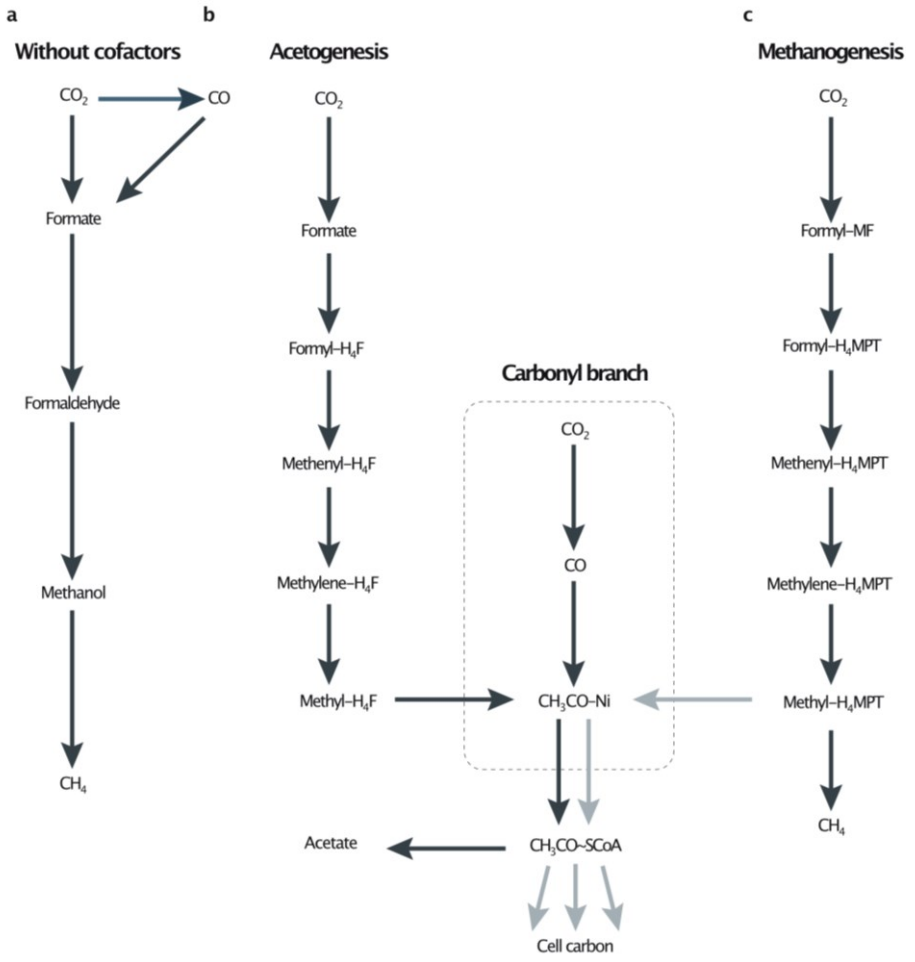

Figure 1. Figure is deciphering the CO_2 reduction to methane without cofactors (a) and with enzymes in acetogens (b and c). Figure is taken from (Martin et al. 2008).

1.3.2 Reductive tricarboxylic acid cycle (rTCA)

The other carbon fixation pathway associated with the origin of life is the rTCA cycle, known also as reverse Krebs cycle or Arnon-Buchanan cycle (Mall et al. 2018; Kitadai et al. 2017; Wächtershäuser 1990). It has been shown that 6 reactions in the rTCA cycle (out of 11) can be promoted by metals in acidic aqueous solutions (Muchowska et al. 2017). The incomplete version of rTCA, known as horseshoe rTCA, exists in bacteria and archaea, which is performed to build up C4 and C5 intermediates for amino acid and other metabolic products (Martin and Russell 2007; Fuchs 2011; Martin 2020; Wimmer et al. 2021). Nevertheless, this work together with acetyl-CoA pathway and is non-autocatalytic although it contains all five universal metabolic precursors related to origin of life (Muchowska et al. 2019a)

1.4 Nature of dark microbial matter: requirement of quantitative stable isotope probing (qSIP) to quantify carbon fixation in these complex communities

Microbes are the most abundant living organisms on Earth. Microbes can be found in any habitable environment on Earth because they had an immense amount of time to diversify on Earth without having the third domain of life, eukaryotes. It is also the fact that eukaryotes emerged on Earth which is explained by endosymbiotic theory (please visit the paper explained in Paper 2 (Orsi et al. 2020b)) . However, it is estimated that more than 99% of microbes have not been brought to the laboratory environment in pure cultures (Rappé and Giovannoni 2003; Yarza et al. 2014; Jiao et al. 2021). Thanks to the cultivation-independent technologies such shotgun metagenomics (Quince et al. 2017), we are able to target whole microbial genomes present in a sample, including the major unexplored portion of microbial diversity, called as Microbial Dark Matter (MDM) (Marcy et al. 2007; Rinke et al. 2013). The microbes that fit into MDM classification, for example in hydrothermal settings, are phyla Thermoprotei, Thaumarchaeota, Aigarchaeota, Aenigmarchaea, Thermotogae, Fervidibacteria and many others without any cultivated representatives (Rinke et al. 2013). It should be kept in mind that MDM may indicate any understudied or uncultured or underexplored lineages which do not possess a cultivated strain in laboratory conditions.

One of the major challenges in microbial ecology is to link the identities of microorganisms to the roles they play in natural environment systems. The study of microorganisms in pure culture reveals their genomic content and potential functions but may not reflect the activities of organisms in their natural communities. Cultivation-independent studies provide community structure (such as 16S rRNA gene-targeted researchs) and genomic capability of the microbes living in a particular environment (shotgun metagenomics). Metatranscriptomic and metaproteomic studies give a better understanding of microbial metabolic activity. However, linkage between community members to functional activity in natural environment is often challenging. DNA-SIP is a powerful technique which uses the labeled carbon (^{13}C), nitrogen (^{15}N) or oxygen (^{18}O) substrates to identify the organisms assimilating the provided sources (Neufeld et al. 2007a) and can link the identity and functional activity of specific organisms in natural community.

The labeled substrates incorporate with DNA when cellular growth or nucleotide repair is taking

place. As a result, DNA of an incorporator gets heavier with labeled substrates and can be tracked using density-gradient ultracentrifugation coupled with sequencing of DNA (Neufeld et al. 2007b). Conventional DNA-SIP application (referred as Heavy-SIP in (Youngblut et al. 2018b)) tries to identify the "heavy" and "light" regions after an incubation period. An incorporator is determined if its SSU rRNA exists in the 'heavy' fractions but not in the 'light' fractions (Radajewski et al. 2003; Lueders et al. 2004). The position of DNA in CsCl density gradient is dependent on one main factor: its buoyant density (BD). BD of a DNA fragment is influenced by G + C content and isotopic composition of its atoms (Youngblut and Buckley 2014). Therefore, selecting 'heavy' and 'light' regions may create a G + C bias, i.e., high G + C content DNA fragment might be in the heaviest DNA fractions which might be taken into consideration for downstream analysis. Usually, when peaks are determined using DNA quantification of the fractions, the lightest and the heaviest fractions contain minimal DNA concentration; therefore, left out of the analysis. For example, unlabeled DNA with high G+C content tends to shift towards the heavier regions of DNA-SIP experiment and may cause a false positive signal (Chen and Murrell 2010). Therefore, a modification in conventional-SIP method, known as quantitative stable isotope probing (qSIP), was proposed as a robust method (Hungate et al. 2015) which calculates each microbial taxon's density shift using labeled and unlabeled density fractions. qSIP is a method that can link the identity and functional activity of specific microorganisms in natural communities (Hungate et al. 2015) while providing how much of labeled substrate gets incorporated into a specific taxon's DNA in terms of atom excess fraction (EAF) which ranges between 0 (no assimilation of the labeled substrate) – 1 (Fully-labeled DNA). In brief, 16S rRNA relative abundances of each taxon are transformed into gene copy number of that taxon using total bacterial 16S rRNA present in each fraction. These normalized 16S rRNA gene copies of each taxon are used to obtain weighted average buoyant densities (WAD) for each taxon in both unlabeled and labeled replicate sets. Triplicates of same experiment (biological replicates) or triplicates of DNA extraction (technical replicates) are required to apply qSIP methodology. Afterwards, the shifts in density caused by labeling incorporation are converted to isotopic enrichment. Assimilators are then determined using the WAD values of each taxon in each unlabeled and labeled dataset using the following formula:

$$A_{CARBONi} = \frac{M_{LABi} - M_{LIGHTi}}{M_{HEAVYMAXi} - M_{LIGHTi}} . (1 - 0.01111233)$$

where M_{LABi} is the molecular weight of the 16S gene for taxon i in the labeled treatment, M_{LIGHTi} is the molecular weight of the 16S gene for taxon i in the unlabeled treatment, and $M_{HEAVYMAXi}$ is the theoretical maximum molecular weight of a fully labeled 16S gene with ^{13}C. If the labeled substrate is ^{18}O such as in Chapter 2 of this thesis (Coskun et al. 2019), the multiplier changes to (1-0.002000429). The lowest detection limit in the density shifts were proposed as 0.0034 to 0.0042 g/ml^{-1} (Hungate et al. 2015). Using the triplicates of calculated excess atom fraction (EAF, A value) from labeled and unlabeled datasets, mean differences in EAFs are resampled with replacement (bootstrapping) to determine 90% confidence intervals (CI). If the lower confidence boundary of a taxon is higher than 0, then that taxon is considered as an assimilator in qSIP. This methodology ensures that density shift of each taxon due to isotopic enrichment is not occurring by chance.

qSIP is not the only methodology that combines high throughput sequencing with SIP. High resolution stable isotope probing (HR-SIP) (Pepe-Ranney et al. 2016a; Pepe-Ranney et al. 2016b) and multi window high resolution stable isotope probing (MW-HR-SIP) (Youngblut et al. 2018b; Barnett et al. 2019) have been also proposed. HR-SIP uses differential abundances between "heavy" fractions of labeled and unlabeled SIP-incubations and MW-HR-SIP considers "heavy" fractions within multiple windows such as 1.70–1.73, 1.72–1.75, 1.74–1.77 g ml^{-1} (Youngblut et al. 2018b; Barnett et al. 2019). A simulation study has concluded that qSIP and MW-HR-SIP are more robust and accurate than conventional DNA-SIP techniques (Heavy-SIP) (Youngblut et al. 2018b). qSIP has been shown to have high sensitivity, but creating more false positives than MW-HR-SIP methodology (Youngblut et al. 2018b).

SIP studies can be expensive to apply depending on the experimental design (Angel 2019). There are multiple factors that directly affect the cost of the SIP such as number of replicates, number of fractions, molarity of isotopes used, labor and sequencing (Sieradzki et al. 2020). Number of collected fractions increase the cost, but it is an important factor on DNA-SIP accuracy. It has been also shown that increase in fraction numbers tends to improve the sensitivity in MW-HR-SIP, HR-SIP and qSIP (Youngblut et al. 2018b). In qSIP, number of fractions have been shown to reduce the variance; however, nine density fractions seem to be an optimal trade-off between cost and precision for most of the qSIP applications (Sieradzki et al. 2020). On the other hand, low-biomass samples should be treated more carefully, and 20 fractions are found to provide improved resolution detecting a clear shift in DNA buoyant density between unlabeled and labeled treatments (Unpublished Chapter 4 and 5).

To better understand the microbial ecology of a vast number of uncultured microorganisms in their natural environment, qSIP (Hungate et al. 2015)was used in this dissertation. All in all, qSIP method was selected to elucidate taxon-specific activities driving important cycling of elements in nearly intact communities (Hungate et al. 2015).

1.5 Aims of the study

The main goal of this project was to provide experimental and field constraints on ancestral carbon fixation pathways postulated to be remnants of the "Ur-Metabolism" in hypothesized settings where emergence of life might have taken place. To achieve this goal, this dissertation aimed to answer the following specific research questions using the natural samples taken from a possible serpentinization-driven ecosystem in St. Paul's and St. Peter's Rocks, shallow-water hydrothermal system in Milos, Greece and tectonically driven thermal waters in Biga peninsula, Turkey:

1. Which organisms utilize the ancient reductive acetyl-CoA pathway and rTCA *in situ*?
2. Do their genomes exhibit ancestral signatures of the acetyl-CoA and rTCA pathways?
3. How does the diversity of life correlate with the surrounding chemistry of the hydrothermal

systems examined in this study?

Aside from these main questions in search of the primordial carbon metabolism utilized by microbes, we tried to unravel the carbon assimilation dynamics in natural communities:

1. What is the effect of hydrogen on the rate of acetate, formate, and bicarbonate assimilation by the microorganisms in a partially serpentinized, possibly active serpentinization-driven ecosystem?
2. What is the effect of bicarbonate concentration on the carbon cycling mediated by chemolithoautotrophs in a thermal water coming to the surface from 750 meters depth? Does bicarbonate concentration directly affect the carbon dynamics of carbon-fixing microbes and favor specific communities?
3. What are the microbial communities living in the thermal waters of the Biga peninsula, Turkey? Is there any compositional difference between the hot springs and deep subsurface wells and can they be correlated to chemical composition of the fluids?

Quantitative stable isotope was used to gain an understanding of microbial carbon cycling with a focus on the genes and pathways hypothesized to be ancient.

Chapter 2

Quantifying the effects of hydrogen on carbon assimilation in a seafloor microbial community associated with ultramafic rocks

Ömer K. Coskun[1], Aurèle Vuillemin[3], Florence Schubotz[3], Frieder Klein[4], Susanna E. Sichel[5], Wolfgang Eisenreich[6] and William D. Orsi[1,2,§]

[1]Department of Earth and Environmental Sciences, Ludwig-Maximilians-Universität, 80333 Munich, Germany.

[2]GeoBio-Center[LMU], Ludwig-Maximilians-Universität München, 80333 Munich, Germany

[3] MARUM Center for Marine Environmental Sciences, University of Bremen, 28359, Bremen, Germany

[4] Woods Hole Oceanographic Institution, Woods Hole, Massachusetts 02543, USA

[5] Departamento de Geologia e Geofísica/LAGEMAR–Universidade Federal Fluminense-Brazil, Niterói, RJ, Brazil

[6] Lehrstuhl für Biochemie, Department Chemie, Technische Universität München, Lichtenbergstraße 85748 Garching, Germany

[§]Corresponding author: w.orsi@lrz.uni-muenchen.de

Published in: **The ISME Journal, Nature Publishing Group**

Accepted: 09 July 2021

2.1 Abstract

Thermodynamic models predict that H_2 is energetically favorable for seafloor microbial life, but how H_2 affects anabolic processes in seafloor-associated communities is poorly understood. Here, we used quantitative ^{13}C DNA stable isotope probing (qSIP) to quantify the effect of H_2 on carbon assimilation by microbial taxa synthesizing ^{13}C-labeled DNA that are associated with partially serpentinized peridotite rocks from the equatorial Mid-Atlantic Ridge. The rock-hosted seafloor community was an order of magnitude more diverse compared to the seawater community directly above the rocks. With added H_2, peridotite-associated taxa increased assimilation of ^{13}C-bicarbonate and ^{13}C-acetate into 16S rRNA genes of operational taxonomic units by 146% (±29%) and 55% (±34%), respectively, which correlated with enrichment of H_2-oxidizing NiFe-hydrogenases encoded in peridotite-associated metagenomes. The effect of H_2 on anabolism was phylogenetically organized, with taxa affiliated with Atribacteria, *Nitrospira*, and Thaumarchaeota exhibiting the most significant increases in ^{13}C-substrate assimilation in the presence of H_2. In SIP incubations with added H_2, an order of magnitude higher number of peridotite rock-associated taxa assimilated ^{13}C-bicarbonate, ^{13}C-acetate, and ^{13}C-formate compared to taxa that were not associated with peridotites. Collectively, these findings indicate that the unique geochemical nature of the peridotite-hosted ecosystem has selected for H_2-metabolizing, rock-associated taxa that can increase anabolism under high H_2 concentrations. Because ultramafic rocks are widespread in slow-, and ultraslow-spreading oceanic lithosphere, continental margins, and subduction zones where H_2 is formed in copious amounts, the link between H_2 and carbon assimilation demonstrated here may be widespread within these geological settings.

2.2 Introduction

The oxidation of molecular hydrogen (H_2) is an important source of bioavailable energy in anoxic environments, and H_2 represents a key metabolic intermediate in anaerobic syntrophy (Schink 1997; Vignais and Billoud 2007). Recently, aerobic H_2 oxidation was discovered to be widespread amongst microbial "dark matter" (Wolf et al. 2016; Ji et al. 2017; Islam et al. 2020), with many aerobic microbial groups being capable of scavenging trace concentrations of atmospheric H_2 as an energy source (Greening et al. 2016). However, the effects of H_2 on carbon utilization rate in marine microbial communities under low-oxygen conditions are poorly understood. The oxidation of H_2 with O_2 is predicted to be a thermodynamically favorable energy source for peridotite-associated microbial communities over a wide range of temperatures in ultramafic-hosted systems (Amend et al. 2011) and thus has the potential to provide important catabolic energy for seafloor-associated communities that live in the vicinity of a geological H_2 source (Amend et al. 2011; Reveillaud et al. 2016). Indeed, a linkage between H_2 and microbial activity has been demonstrated in several high-temperature hydrothermal settings (Reveillaud et al. 2016; Perner et al. 2013; Schubotz et al. 2015; Fortunato and Huber 2016; McNichol et al. 2018).

To better understand the effects of H_2 on carbon anabolism in seafloor microbial communities associated with ultramafic rocks, we used ^{13}C quantitative DNA stable isotope probing (qSIP)

(Hungate et al. 2015; Coskun et al. 2018) with ^{13}C-labeled bicarbonate, acetate, and formate in H_2 incubation experiments. The ^{13}C DNA-qSIP approach identifies microbial taxa that are synthesizing new ^{13}C-labeled DNA from the added ^{13}C substrates, which occurs during genome replication (Tuorto et al. 2014). We applied this method to microbial communities associated with partially serpentinized peridotite mylonite from Saint Peter and Saint Paul Archipelago (Arquipélago de São Pedro e São Paulo, Brazil 'SPSPA') at the equatorial Mid-Atlantic Ridge.

The SPSPA is mainly composed of strongly deformed, partially serpentinized Mg- and Fe-rich (i.e. ultramafic) rocks (Maia et al. 2016). Serpentinization of ultramafic rocks involves the oxidation of ferrous iron in primary minerals to ferric iron in secondary minerals by water which generates abundant H_2 that can be used to conserve energy by H_2-oxidizing microbes (Klein et al. 2020). During a recent expedition to SPSPA (AL170602) onboard the MV ALUCIA in 2017, geochemical evidence for H_2 formation was found to be recorded in serpentinized rocks and H_2 is likely generated today at SPSPA through low-temperature aqueous alteration of peridotite, mechanoradical H_2 formation, or radiolysis (Klein et al. 2020), albeit at slow rates. Thus, we incubated partially serpentinized peridotite from SPSPA with ^{13}C-bicarbonate, ^{13}C-acetate, and ^{13}C-formate in incubations with and without H_2, and then applied qSIP (Coskun et al. 2018; Hungate et al. 2015) to quantify the effects of H_2 on ^{13}C-substrate assimilation by specific operational taxonomic units (OTUs) that were associated with the ultramafic rocks.

2.3 Material and methods

2.3.1 Sampling

Partially serpentinized peridotite (DR541-R3; 00°55.56'N; 29°19.70'W) and bottom seawater samples were collected from a yellowish-brown outcrop using the Deep Rover submersible in July 2017 at 327 m water depth from the northern slope east of the SPSPA, Brazil (M/V Alucia Expedition AL170602, 00°55'N; 29°21'W), a remote group of islets in the equatorial Atlantic Ocean, on the Mid-Atlantic ridge (Fig. 1A). The SPSPA belongs to the Brazilian Exclusive Economic Zone and is located within the Fernando de Noronha Environmental Protection Area. Conductivity, temperature, and density profiles were taken from several stations around the SPSPA to explore ongoing hydrothermal activity which could not be detected. The alteration mineralogy of serpentinized peridotite mylonite and fluid inclusion contents in primary minerals were determined in thin sections using a petrographic microscope and a confocal Raman spectrometer (Horiba LabRAM HR) equipped with a 20 mW 473 nm laser, astigmatic flat field spectrograph with a focal length of 800 mm, and a multichannel air-cooled (−70 °C) CCD detector.

Seawater was collected from directly above the peridotite rocks using an isobaric gas-tight (IGT) fluid sampler (Seewald et al. 2002). In addition, seawater was collected with a Niskin rosette from three nearby sites (Fig. 1A), two from 300 to 330 m water depth to serve as a background seawater microbial community comparison to the IGT fluids and peridotite rocks collected from dive DR541. Niskin (4–8 L) and IGT (18–75 mL) seawater for the t0 comparisons were filtered onto 0.2 µm

polycarbonate filters using a peristaltic pump and frozen immediately at −20 °C.

Sediments were collected from two nearby sites (Fig. 1A) using the slurp suction sampler onboard the Deep Rover submersible. Sediments were stored in 50 mL falcon tubes at −20 °C until DNA extraction.

2.3.2 DNA extraction

DNA was extracted from the seawater samples (frozen filters) using a protocol described previously (Orsi et al. 2016). In order to avoid cross-sample contamination with the rock samples, DNA was extracted from 10 to 12 g of rock samples on a separate day (Fig. 2A), in a laminar flow clean bench with pipettors that were autoclaved immediately before use (to remove contaminating DNA on the pipettors). DNA was extracted from three separate peridotite rock samples (subsamples of the same rock). These t0 rock samples were collected from the same dive (DR541-R3; Fig. 1B) where peridotite rocks were sampled for the qSIP incubations (Fig. 1A). In addition, two separate carbonate rock replicates (subsamples of the same rock) were collected from dive DR540 (DR540-R3 and R4) (Fig. 1A). All t0 rock samples were stored in 50 mL RNA/DNA clean falcon tubes (Fig. 2A), and DNA was extracted according to a previously published protocol (Vuillemin et al. 2019). The only deviation from the previous protocol was that silica glass beads from three Lysing Matrix E tubes (MP Biomedicals) were directly added to the 50 mL falcon tubes containing the rocks (Fig. 2A), which were homogenized with 10 mL C1 extraction buffer (Vuillemin et al. 2019).

The t0 peridotite rocks (DR541-R3) serve as a reference for the in situ peridotite-associated microbial community and allow comparison against the “rock-free” community from the seawater samples. Moreover, because the t0 peridotite rocks (DR541-R3) were collected from the same location as the peridotites that were used for setting up the ^{13}C-SIP incubations, we could identify “rock-associated” OTUs (detected in the peridotite t0 samples) that became labeled in the qSIP incubations that were, or were not, detected in seawater. For DNA extraction from sediments, we used the same protocol that we applied for the carbonate and peridotite rock samples, with the main difference that only 0.5 g of sediment was extracted in 2 mL lysing matrix E tubes with 1 mL of C1 extraction buffer (Vuillemin et al. 2019). Such a relatively small volume was required given the orders of magnitude higher microbial abundance in the sediment samples compared to the rocks (Fig. 2B).

2.3.3 Experimental setup for SIP incubations

For incubation experiments, the outermost ~3 cm of rock sample DR541-R3 was carefully removed with a sterile hammer to retrieve the rock interior. The rock interior was subsequently crushed into mm-sized fragments on a sterile surface (ethanol washed) in a fume hood for incubations. For the inocula in the SIP incubations, 2 g of crushed rock fragments from the interior of the peridotites were placed into 20 mL gas-tight glass vials which had been heated to 450 °C for 10 h prior to use. In addition, 10 mL sterile-filtered seawater (using 0.2 µm polycarbonate filters) was added to each vial containing the crushed peridotite rocks. Therefore, the living cells in the SIP incubations should

be primarily rock-associated and derived from the interior of the peridotites, as sterile filtration should have removed cells >0.2 µm in size from the added seawater. However, it is possible that some ultra-small seawater cells <0.2 µm could have passed through and made it into the SIP incubations.

Each vial was amended with either 10 mM sodium-[^{13}C]bicarbonate (99% ^{13}C-content, Sigma-Aldrich, Darmstadt, Germany), 2 mM sodium-[^{13}C1]acetate or 10 mM sodium-[^{13}C]formate (99% ^{13}C-content, Cambridge Isotope Laboratories, Andover, MA, USA) and crimp-sealed using KOH-washed butyl stoppers (Oremland et al. 1987). We acknowledge that the high concentrations of ^{13}C-acetate and ^{13}C-formate that were added are orders of magnitude higher compared with the measured concentrations of acetate and formate in fluids venting from the Lost City Hydrothermal field (Lang et al. 2010). All glass vials were crimp-sealed with a butyl rubber stopper creating gas-tight conditions and the atmosphere was replaced with nitrogen gas (N_2) for 10 min to create low oxygen conditions. Afterward, one set of flasks was amended with H_2 added to the headspace (1.5 bar), with a second set as a control that did not receive H_2. We acknowledge that these concentrations are higher than those at most hydrothermal systems (Amend et al. 2011).

Although the O_2 was not measured in the incubations, we assume dissolved oxygen concentration was reduced down ca. 10-fold compared to the ambient concentration of ca. 120 µM by purging the incubation medium for a minimum of 10 min with N_2 (Butler et al. 1994). The resulting low O_2 conditions of assumed 10–15 µM were likely further drawn down by aerobic respiration during the course of the experiment (Ortega-Arbulú et al. 2019).

As is common practice for all DNA-SIP studies, control vials were also prepared with the same unlabeled carbon sources (referred to as “unlabeled control”) to compare the extent of ^{13}C-labeling from the labeled incubations. The glass vials containing unlabeled control and ^{13}C-substrates were incubated at room temperature (ca. 25 °C) terminated after 35 h and stored at −60 °C for onshore analysis. DNA was extracted from 1 g of slurry in triplicate using the same method as described above (Vuillemin et al. 2019) and quantified fluorometrically using Qubit 3.0 fluorometer (Invitrogen, Eugene, OR, USA).

2.3.4 Density gradient centrifugation and gradient fraction

DNA samples were prepared for density gradient centrifugation according to previously defined protocols for qSIP (Hungate et al. 2015; Coskun et al. 2018). DNA of density fractions was resuspended with 30 µl molecular-grade (DEPC-treated) water and quantified fluorometrically using a Qubit fluorometer.

2.3.5 Quantitative PCR (qPCR)

Universal primers targeting the V4 hypervariable region of 16S ribosomal RNA (rRNA) genes were used in qPCR to determine density shifts in the peak DNA of buoyant density (BD) for each incubation. We used a version of the 515F primer with a single-base change (in bold) to increase the

coverage of archaeal groups (515F-Y, 5'-GTGYCAGCMGCCGCGGTAA (Parada et al. 2016)). qPCR was carried out as described previously (Coskun et al. 2019). 16S rRNA gene quantities of the density fractions were plotted against their corresponding densities and 10 fractions (on average) from each replicate set were selected for sequencing (Fig. S1; gray shaded area). Two 16S rRNA gene PCR amplicons from each density fraction (technical replicates to reduce PCR bias) were pooled and subjected to dual-indexed barcoded sequencing of 16S rRNA gene amplicons on the MiniSeq (Illumina) as described previously (Pichler et al. 2018).

2.3.6 Bioinformatic and qSIP analysis

The MiniSeq reads were quality trimmed and assembled using USEARCH version 11.0.667 with the default parameters (Edgar 2010) resulting in 6.8 million quality checked V4 reads. Reads were then de novo clustered at 97% identity using UPARSE; OTUs represented by a single sequence were discarded (Edgar 2013). Taxonomic assignments were generated by QIIME 1.9.1 (Caporaso et al. 2010) using the implemented BLAST method against the SILVA rRNA gene database release 132 (Quast et al. 2013). The raw OTU table consisted of 10,654 OTUs which were further quality-filtered. The level of contamination in each density fraction for qSIP analysis was determined using previously sequenced DNA sequences from dust samples collected from three different laboratories in our building where the samples are processed (Pichler et al. 2018). If the total number reads per OTU in the samples was 10 times greater compared to that of contaminant sequence reads, the OTU was considered to be endemic to the sample. 1662 contaminant-related OTUs such as Pseudomonas, Ralstonia, Variovorax, or Streptococcus (Salter et al. 2014) were deleted based on comparing contaminant sample sequence reads to the samples, comprising 2.34% of the whole 16S rRNA gene dataset (188,273 sequence reads out of 8,046,165). Only OTUs having >12 sequences in total in each replicate (summed across all density fractions) were selected for further study since low abundance taxa cause artificial variations in qSIP calculations (Morrissey et al. 2016). Intermediate files in data removal of contaminants, quality filtering, and detailed explanations of the intermediate files can be found in the following data repository: https://doi.org/10.6084/m9.figshare.13341443.v1.

Excess atomic fraction ^{13}C (EAF) values were calculated for the 16S rRNA genes corresponding to OTUs according to a previously described study (Hungate et al. 2015) using a qSIP workflow embedded in the HTS-SIP R package (Youngblut et al. 2018a). To calculate the bootstrap confidence intervals (CI) for significant isotope incorporation, bootstrap replicates (n = 1000) were run with the HTS-SIP R package; an OTU was considered as a ^{13}C-assimilator if the lower boundary of CI was above the 0% EAF cutoff (Hungate et al. 2015). Statistical analyses and plots were performed using R.Studio Version 3.3.0 (Team and Others 2015).

qSIP measurements of OTU-specific ^{13}C-substrate assimilation with and without H_2 allowed us to test whether the activity of microbial communities in the presence of H_2 was significantly restricted to specific phylogenetic clades (e.g., "phylogenetic signal" (Morrissey et al. 2016)). Pagel's λ and Blomberg's K were calculated as two independent indices of the phylogenetic signal (Blomberg et al. 2003; Pagel 1999): shared traits (e.g., ^{13}C-assimilation patterns) in the context of evolutionary

history (e.g., 16S rRNA gene phylogenetic relation).

2.3.7 Metagenomic analysis of rock, seawater, and SIP samples

Given the shifts in buoyant density of 16S rRNA genes in the ^{13}C-SIP incubations (Fig. S1), we produced metagenomes from "heavy" fractions of the density gradients that indicated ^{13}C labeling (Fig. S1). The DNA contained within the density fraction for each of these "heavy" metagenomes was chosen for metagenomic shotgun sequencing based on the region of the CsCl gradient that exhibited a peak in the ^{13}C-substrate incubation that had a higher CsCl density compared to the unlabeled control experiment (Fig. S1). Metagenomic libraries were prepared using Nextera XT DNA Library Prep Kit (Illumina) and following the manual provided by the manufacturer with minor modifications. The starting concentration of genomic DNA could not be set to 0.2 ng as suggested by the manufacturer's manual due to low DNA content in the labeled SIP fractions. Instead, the PCR program in the amplification step of the fragmented DNA was increased from 12 to 15 cycles. Metagenomic libraries from the rock and seawater t0 samples were prepared from the extracted DNA (see above) with unique barcodes using the same Nextera XT kit, were diluted to 1 nM, and pooled together for sequencing on the MiniSeq (Illumina) platform.

Paired-end reads were trimmed and assembled into contigs using CLC Genomics Workbench 9.5.4 (Qiagen, Hilden, Germany), using a word size of 20, bubble size of 50, and a minimum contig length of 300 nucleotides. Reads were then mapped to the contigs using the following parameters (mismatch penalty, 3; insertion penalty, 3; deletion penalty, 3; minimum alignment length, 50% of reading length; minimum percent identity, 95%). Coverage values were obtained from the number of reads mapped to a contig divided by its length (i.e., average coverage). This protocol does not assemble rRNA genes (Orsi et al. 2020a); thus, results are only discussed in terms of protein-encoding genes.

For annotating putative functions of ORFs in metagenomes from particular "higher-level" taxonomic groups of microorganisms, we applied a previously published bioinformatics pipeline (Orsi et al. 2020a). This pipeline extracts protein-encoding ORFs from de novo-assembled contigs using FragGeneScan v. 1.30 (Rho et al. 2010), and functionally annotates ORFs against a large aggregated database ("MetaProt") (Orsi et al. 2020a) using DIAMOND version 0.9.24 (Buchfink et al. 2015). The MetaProt database contained predicted proteins from all protist, fungal, bacterial, and archaeal genomes (and MAGs) in the JGI and NCBI databases as of January 2021. The MetaProt database (Orsi et al. 2020a) also contains ORFs from all of the transcriptomes of microbial eukaryotes from the MMETS project (Keeling et al. 2014). The MetaProt database is available as a single 32 GB amino acid fasta file on the LMU Open Data website (https://data.ub.uni-muenchen.de/183/). Cutoff values for assigning hits to specific taxa were performed at a minimum bit score of 50, the minimum amino acid similarity of 60, and an alignment length of 50 residues. All scripts and code used to produce the analysis have been posted on GitHub (https://github.com/williamorsi/MetaProt-database). This approach assigns ORFs to higher-level taxonomic groups (Orsi et al. 2020a). As is the case in all metagenomic studies, the incomplete nature of genomes in databases, together with the lower representation of sequenced genomes from candidate clades than from cultured ones, makes

it likely that our pipeline misses annotation of ORFs that are derived from as-yet-unsequenced genomes.

The 16S rRNA gene amplicon sequences and metagenomic sequence data were entered in the NCBI Sequence Read Archive under BioProject ID PRJNA679196. The CTD data, metagenomic dataset, and intermediate files to produce qSIP results were deposited under https://figshare.com/authors/_mer_Coskun/9725927.

2.3.8 Assessing biases in metagenomes from density fractions containing ^{13}C-enriched DNA

Sequencing metagenomic DNA from only a single ^{13}C-enriched fraction (Fig. S1) may be biased due to (Schink 1997) low GC genomes that might not be detected in ^{13}C-enriched fraction even though they highly incorporate the labeled source, and (Vignais and Billoud 2007) abundant organisms can sometimes be found in all fractions irrespectively of labeling (Sieradzki et al. 2020; Youngblut et al. 2018a). However, many abundant ^{13}C-labeled OTUs were determined with statistical significance via qSIP related to Marinobacter, Alteromonas, Thaumarchaeota, 'Ca. Rokubacteria', or Nitrospinae, were represented in the ^{13}C-metagenomes. The overlapping taxa labeled in qSIP and metagenomes from ^{13}C-enriched SIP fractions indicate that the metagenomic sequences obtained from the selected SIP fractions are derived to a large extent from taxa that were ^{13}C-labeled.

2.3.9 Phylogenetic analyses

For phylogenetic analyses of ^{13}C-labeled 16S rRNA genes, OTUs which were at least occurring in one of the experiments were selected for alignment with MUSCLE (Edgar 2004) using SeaView (Gouy et al. 2010). The resulting fasta file was imported into W-IQ-TREE (Trifinopoulos et al. 2016) with an option to select the best phylogenetic model using Bayesian criterion, which resulted in TIM3e + R10 algorithm using ModelFinder (Kalyaanamoorthy et al. 2017). The phylogenetic tree was visualized and edited using iTOL (Letunic and Bork 2016). Statistical analyses and plots were performed using R.Studio Version 3.3.0 (Team and Others 2015). Pagel's λ (Pagel 1999) and Blomberg's K (Blomberg et al. 2003) tests for significantly non-random phylogenetic distributions of ^{13}C-utiliziers from qSIP were calculated using the phylosignal R package (Keck et al. 2016).

For phylogenetic analyses of ORFs from metagenomes with similarity to *HypE*, *nirS*, and *coxL* based on BLASTp searches against the MetaProt database (Orsi et al. 2020a), ORFs were aligned against their top BLASTp hits using MUSCLE (Edgar 2004). Phylogenetic analysis of the resulting amino acid alignments of the predicted proteins was conducted in SeaView using RAxML (Stamatakis 2006) with BLOSUM62 as the evolutionary model and 100 bootstrap replicates. The resulting phylogenetic trees were displayed as unrooted cladograms using FigTree (http://tree.bio.ed.ac.uk/software/figtree/).

2.4 Results

2.4.1 Rock description

Thin section petrography and Raman analysis revealed that rock sample DR541-R3 (used as the inoculum for the qSIP incubations) is a partially serpentinized peridotite mylonite that is chiefly composed of olivine and orthopyroxene, minor amounts of clinopyroxene, and traces of Cr-spinel (Fig. 1D). Primary minerals are partially altered to serpentine, magnetite, tremolite, calcite, and aragonite which chiefly occur in veins cutting across the mylonite matrix. We observed methane-rich fluid inclusions at other locations at SPSPA but not at the sampling location (Fig. 1D). For comparison, we obtained thin sections of two additional samples from the same dive (samples DR541-R1 and DR541-R4) which revealed structural and alteration patterns similar to those of DR541-R3 suggesting all three samples experienced extensive ductile and brittle deformation followed by serpentinization.

Microbial abundance and diversity of the ultramafic-rock associated community
The concentration of 16S rRNA genes from the peridotite rock samples was 2.6 (±2) $\times 10^4$ copies per g of rock, compared to 7 (±1) $\times 10^4$ and 0.5 (±0.06) $\times 10^4$ 16S rRNA gene copies per mL seawater collected with the IGT fluid samplers and Niskin rosette, respectively (Fig. 2B). qPCR quantification of 16S rRNA gene copies from the frozen peridotite rock samples showed cycle threshold (Ct) values ranging between 25 and 30 cycles, which strongly indicates that our amplified 16S rRNA genes are derived from in situ microbes associated with the rocks as opposed to contamination because all contamination controls (extraction blanks and qPCR no template controls) consistently had Ct values >35. The Chao diversity index based on the 16S rRNA gene data shows that the rock-associated community is significantly more diverse (two-sided T-test: $P < 0.0001$) compared to the seawater communities (Fig. 3B). 16S rRNA gene data also shows that the microbial community composition between the peridotite-associated and the seawater communities was significantly different (Analysis of Similarity [ANOSIM] R: 0.87, $P < 0.0001$), with approximately two-thirds of all detected OTUs being found on the peridotite rock samples and not in any seawater samples (Fig. 3C). The peridotite-associated communities included taxa that are common to hydrothermal (Meier et al. 2019) and ultramafic rock habitats (Lecoeuvre et al. 2021; Mason et al. 2009) including Nitrospirae, Rokubacteria, Entotheonellaeota, Gemmatimonadetes, and Alphaproteobacteria (Fig. 3A). These comparisons reveal a unique microbial community inhabiting the peridotite rocks compared to the seawater that was collected directly above these rocks with the IGT fluid samplers.

2.4.2 Identifying ^{13}C-labeling for qSIP

^{13}C-labeling of 16S rRNA genes (defined by a shift in peak DNA buoyant density) was observed in all incubations, with average shifts in the peak ^{13}C-DNA buoyant densities compared to control-incubations between 0.0018 ± 0.0037 and 0.0279 ± 0.0076 g ml−1 (Fig. S1). This highlights biological variability in ^{13}C-assimilation in our replicate treatments, but despite this variability, the average density shift in the replicate treatments shows a clear trend of ^{13}C-enriched DNA from 16S rRNA genes compared to the unlabeled controls (Fig. S1). Therefore, ^{13}C-labeling of microbes synthesizing new DNA occurred in all incubations. The use of replicates in qSIP allows for statistically constrained estimations of ^{13}C-assimilation in all detectable OTUs (Hungate et al. 2015). Namely, ^{13}C-qSIP allows

for the calculation of the ^{13}C-excess atomic fraction (EAF) for all detectable OTUs within a microbial community, together with a confidence interval (CI) that provides to test statistical significance for OTU-specific ^{13}C-assimilation (Hungate et al. 2015). We thus applied the qSIP protocol to estimate the ^{13}C-EAF (with CI) for all detected OTUs within each experimental treatment.

2.4.3 Significance of H_2 on the phylogenetic organization of ^{13}C-utilizing taxa

Phylogenetic signal analyses showed that H_2 had a statistically significant (non-random) effect on the phylogenetic organization of the ^{13}C-assimilating taxa in each of the three substrates tested (Table 1). Thus, the effect of H_2 on increased ^{13}C-labeling of clades with ^{13}C-bicarbonate and ^{13}C-acetate, and to a lesser extent ^{13}C-formate, was statistically significant in terms of the non-random distribution of specific taxa that increased their anabolism with added H_2.

With added H_2, OTUs increased assimilation of ^{13}C-bicarbonate and ^{13}C-acetate on average by 146% (±29%) and 55% (±34%), respectively (Fig. 4). Moreover, within the peridotite rock-associated OTUs, 54 genus-level taxonomic groups were ^{13}C-labeled in qSIP incubations containing added H_2 (Fig. 5). This was more than an order of magnitude higher compared to seawater-specific ^{13}C-labeled taxa, as well as seafloor-associated ^{13}C-labeled taxa not detected on peridotite rocks (only detected on carbonate rocks and sediments) (Fig. 5).

2.4.4 The effects of H_2 on bicarbonate assimilation

Compared to controls (^{13}C-bicarbonate incubations that did not receive H_2) H_2 addition was correlated with an overall increase in ^{13}C-assimilation by OTUs with EAF values increasing on average from 0.13 ± 0.009 to 0.32 ± 0.051 ($146 \pm 29\%$ increase) (Fig. 4). Most of these OTUs were rock-associated (Fig. 5). H_2 addition coincided with a two-fold drop in ^{13}C-labeled Gammaproteobacterial OTUs (Fig. 4). In contrast, the abundance and ^{13}C-bicarbonate assimilation (EAF) of Thaumarchaeal OTUs in the presence of H_2 increased to 7.79% and 0.38 ± 0.34, respectively (Fig. 4), which were associated with the peridotite rocks (Fig. 5). H_2 addition coincided with a ^{13}C-bicarbonate assimilating peridotite-associated OTU affiliated with the Atribacteria (JS1 clade) having the highest EAF of all OTUs in the ^{13}C-bicarbonate incubations amended with H_2 (EAF: 0.87) (Fig. 4). In total, 85% of the ^{13}C-bicarbonate assimilating taxa were associated with the peridotite rocks (Fig. 5).

2.4.5 Effects of H_2 on acetate assimilation

In ^{13}C-acetate incubations with added H_2, the EAF value per OTU increased from 0.27 ± 0.010 to 0.42 ± 0.011 ($55 \pm 34\%$ increase) relative to control incubations that did not receive H_2 (Fig. 4). Gammaproteobacteria and Thaumarchaeota had the highest number of OTUs that increased ^{13}C-acetate assimilation in the presence of H_2 (Fig. 4). The genera showing the highest ^{13}C-acetate assimilation in the presence of H_2 were *Arcobacter* (0.91 EAF), *Marinobacterium* (0.54 EAF), *Nitrosomonas* (0.49 EAF), *Alteromonas* (0.42 EAF), Nitrosopumilaceae (0.4 EAF), and *Nitrospira* (0.14 EAF) (Fig. 4). All of the acetate assimilating Nitrosopumilaceae (Thaumarchea) and Nitrospira taxa were peridotite-associated (Fig. 5).

2.4.6 Effects of H_2 on formate assimilation

In contrast to acetate and bicarbonate incubations, OTUs assimilating ^{13}C-formate in the presence of H_2 had on average lower EAF values compared to the control ^{13}C-formate qSIP incubations that did not receive H_2 (Figs. 4 and 5) (average 0.32 ± 0.01–0.14 ± 0.02 EAF; 139 ± 11% decrease). This shows that the utilization of formate by most microbial groups was reduced in the presence of H_2. The composition of the community in the H_2-supplemented formate incubation changed substantially, with OTUs belonging to the Planctomycetes (Family Pirellulaceae) and Entotheonellaeota exhibiting the highest EAF values from ^{13}C-formate (up to 0.89 EAF) (Figs. 4 and 5). All of the Planctomycetes and Entotheonellaeota formate assimilating taxa were associated with the peridotite rocks (Fig. 5).

2.4.7 Functional gene diversity in peridotite-associated clades assimilating ^{13}C-substrates

In the heavy metagenomes, approximately one-third of ORFs were associated with peridotite rocks and not with seawater (Fig. 6A). This is evidence of a rock-associated community with unique protein-encoding gene content that was assimilating ^{13}C. Within the heavy metagenomes, diversity of carbon monoxide dehydrogenase (*coxL*: Fig. 6B), H_2-oxidizing NiFe-hydrogenase assembly proteins (*HypE*: Fig. 7A), and dissimilatory nitrite reductase (*nirS*: Fig. 7B) all show bootstrap supported clades that contained ORFs from the heavy metagenomes and peridotite metagenomes. The majority (>75%) of these clades did not include any ORFs from seawater metagenomes (Figs. 6 and 7). This indicates that most of the *coxL*, *HypE* and *nirS* encoding organisms that assimilated the ^{13}C-substrates in the SIP incubations were associated primarily with the peridotites.

In the peridotite rock metagenomes, there was an increased relative abundance of ORFs encoding *nirS* and NiFe-hydrogenase assembly proteins involved in H_2 oxidation (*HypABCDEF*) (Koch et al. 2014) compared to Niskins and IGT collected water, which was consistent across biological replicates (Fig. 7C and D). Relative abundance of *HypABCDEF* and *nirS* encoding ORFs in heavy metagenomes from SIP-incubations were also higher compared to seawater metagenomes (Fig. 7C and D).

Phylogenetic analysis of the carbon monoxide dehydrogenase large subunit (*coxL*) encoding ORFs reveals nine major bootstrap-supported *coxL* clades that include ORFs from heavy metagenomes and peridotite rock metagenomes but did not contain any *coxL* ORFs from seawater metagenomes (Fig. 6B). The peridotite-associated *coxL* clades contain a four-fold higher number (6 compared to 25) of heavy ORFs compared to seawater-associated *coxL* clades, and were affiliated with *Labrenzia*, *Pelomicrobium*, *Denitrobaculum*, *Nitrolancetus*, *Litorilnea*, uncultivated Actinobacteria, SAR116 clade, and '*Ca.* Rokubacteria' (Fig. 6B).

2.5 Discussion

The increased diversity of the peridotite-associated community compared to seawater microbial communities (Fig. 3B) is consistent with prior studies of seafloor communities associated with

basaltic rocks (Santelli et al. 2008). The majority of taxa that assimilated ^{13}C in the presence of H_2 were derived from this diverse peridotite-associated community as opposed to being specific to seawater (Fig. 5). Therefore, the peridotite-associated communities are enriched with the capability to utilize H_2 to increase their carbon assimilation from CO_2, acetate, and formate. Since H_2, acetate, and formate are formed during serpentinization (Schrenk et al. 2013), our results highlight the importance of H_2 in influencing carbon cycling in rock-hosted microbial communities.

The presence of magnetite in the serpentinized rock matrix suggests that temperatures exceeded 200 °C when rocks underwent serpentinization (Klein et al. 2014). Because its formation requires the oxidation of ferrous iron originally contained in primary minerals to ferric iron in magnetite with water as the oxidizing agent, H_2 was generated during serpentinization of mylonite at St. Paul's Rocks. Because the mylonite was only partially serpentinized, it is likely that low-temperature aqueous alteration at SPSPA is currently ongoing—albeit at slow rates—which would be a source of H_2 for the peridotite-hosted communities. Unlike peridotite-hosted alkaline hydrothermal vents with a focused flow such as the Atlantis Massif (Kelley et al. 2005), we found no firm evidence of H_2 anomalies in the water column at SPSPA indicating that any H_2 had already been oxidized in the water column that has ca. 100 µM O_2 (Fig. 1C). However, H_2 in diffuse fluids emanating from the subseafloor of SPSPA could be oxidized by the rock-associated seafloor microbes (Figs. 3C, 5) before diffusing into the oxidized water column, as indicated previously by geochemical evidence in diffuse vents from the Juan de Fuca Ridge (Wankel et al. 2011).

2.5.1 Carbon assimilation in an ultramafic rock-associated community

The observation that most ^{13}C-assimilating taxa were peridotite-associated (Fig. 5), indicates that many taxa within this relatively diverse community (Fig. 3B) have a high affinity for the added substrates compared to the seawater microbes living directly above the rocks. Gammaproteobacteria dominate the ^{13}C-labeled taxa that were detected in seawater, but the ^{13}C-assimilating taxa detected only in the seafloor samples were by comparison more diverse and instead consist of Thaumarchaea, Rokubacteria, Planctomycetes, Acidobacteria, Entotheonellaeota, Deltaproteobacteria, and Gemmatimonadaceae (Fig. 5). The qSIP results show that the effect of H_2 on increased carbon assimilation is phylogenetically organized in this unique rock-associated community, with specific peridotite-associated taxa assimilating more carbon in the presence of H_2 compared to seawater-associated taxa (Fig. 5).

The phylogenetic signal analysis based on Blomberg's K (Blomberg et al. 2003) reveals H_2 utilization as a shared trait in ^{13}C-assimilating taxa, compared to the incubations that did not receive H_2 (Table 1, Fig. S2). This significant phylogenetic signal within ^{13}C-assimilating taxa in the presence of added H_2 coincides with an order of magnitude higher number of peridotite rock associated taxa having an increased anabolism in the presence of added H_2, compared to taxa not detected on the ultramafic rocks (Fig. 5). These relations point to ongoing H_2 production via low-temperature aqueous alteration of peridotite (Fig. 1D) which supports a unique peridotite-associated community with higher diversity (Fig. 3B) that is relatively enriched with the ability to metabolize H_2 compared to the overlying seawater communities (Fig. 7C).

2.5.2 Differential effects of H_2 on the assimilation of acetate, bicarbonate, and formate

The increased ^{13}C-assimilation with added H_2 (Figs. 4 and 5) is supported by a higher relative abundance of the *HypABCDEF* [NiFe]-hydrogenase locus in heavy metagenomes from H_2-amended incubations (Fig. 7C). The *HypABCDEF* locus is responsible for the maturation of NiFe-hydrogenase in bacteria and aerobic H_2 oxidation [54]. The *HypE* ORFs within clades exhibiting ^{13}C assimilation were affiliated with uncultured Nitrospinae bacteria, *Nitrosococcus*, '*Ca.* Entotheonella', and *Alteromonas* (Fig. 7A), which were all groups identified in qSIP as being rock-associated with increased carbon assimilation in the presence of H_2 (Fig. 5). The higher carbon assimilation in the presence of added H_2 in several rock-associated groups (Fig. 5) are consistent with H_2 oxidation via *HypABCDEF*, and could be related to higher H_2 concentrations in the peridotite ecosystem.

The correlation of added H_2 with a decreased formate assimilation by most OTUs (Fig. 4) is possibly due to inhibition of the hydrogenase unit of formate hydrogen lyase that is caused by high H_2 concentrations (McDowall et al. 2014). This has been observed in previous SIP studies, where H_2 had an inhibitory effect on formate assimilation in hot springs (Schubotz et al. 2015). However, microcosm experiments with H_2 and formate in terrestrial alkaline fluids in the Samail Ophiolite showed that under high H_2 concentrations (20%, excess atmospheric pressure) certain methanogens increase methane production from formate, presumably via formate dehydrogenase (Fones et al. 2021). Therefore, in serpentinization settings the inhibition or stimulation of formate metabolism by increased H_2 concentrations is likely to be dependent on the redox potential of the environment.

2.5.3 Atribacteria exhibit H_2-dependent carbon fixation

Of the all OTUs that had enhanced carbon assimilation in H_2-amended ^{13}C-bicarbonate incubations, a single rock-associated OTU affiliated with Atribacteria had the highest EAF value (0.87; Fig. 4). This fits with the presence of an H_2-dependent CO_2 fixation pathway (Wood–Ljungdahl pathway) encoded in Atribacteria genomes (Carr et al. 2015; Nobu et al. 2016). The labeling of the Atribacteria OTU with ^{13}C-bicarbonate was not observed in the absence of H_2 (Fig. 4), indicating that H_2 is needed to fix bicarbonate by this taxon.

The same rock-associated Atribacteria OTU also incorporated ^{13}C-acetate, but only in the absence of H_2 (Fig. 4). However, the amount of ^{13}C-acetate assimilated by this OTU was ca. 50% less compared to its assimilation of ^{13}C-bicarbonate in the presence of H_2. These results possibly reflect the reversibility of the Wood–Ljungdahl pathway encoded in the Atribacteria genomes (Carr et al. 2015; Nobu et al. 2016). For example, when H_2 is present Atribacteria use the Wood–Ljungdahl pathway in the forward direction to fix CO_2 and produce either acetyl-CoA or acetate (Schuchmann and Müller 2016). However, when H_2 is not present the activity of acetate kinase may be reversed and acetate is assimilated (Schuchmann and Müller 2016). In line with our finding, it has been recently discussed that Atribacteria could use WLP either in catabolic or anabolic directions in deep subseafloor sediments (Vuillemin et al. 2020).

Atribacteria typically dominates CH_4-rich anoxic environments such as gas hydrate-containing sediments, and methanogenic meromictic lakes (Rinke et al. 2013). Since our sampled environment was oxic at the time of sampling (Fig. 1C), it seems that some Atribacteria is able to persist under these conditions and increase their carbon fixation activity upon the addition of H_2.

2.5.4 Effects of H_2 on carbon assimilation by nitrogen-cycling Bacteria and Archaea

OTUs belonging to the ammonia-oxidizing Thaumarchaeota (Nitrosopumilaceae) had a significant increase in EAF values in the presence of added H_2 in the ^{13}C-bicarbonate and ^{13}C-acetate incubations (Fig. 4). All of these OTUs were peridotite-associated (Fig. 5). To our knowledge, there are no experimental studies with pure cultures demonstrating that Thaumarchaea catabolize H_2. However, the genomes of some ammonia-oxidizing archaea (AOA) encode NiFe hydrogenase genes that may potentially be involved in H_2 oxidation (Bryant and Adams 1989; Berney et al. 2014; Kwan et al. 2015; Daebeler et al. 2018) which might explain the increased ^{13}C-assimilation of Thaumarchaea in the presence of H_2 seen here.

The increased assimilation of ^{13}C-bicarbonate and ^{13}C-acetate by rock-associated Thaumarchaeal OTUs in H_2 amended incubations with (Figs. 4, 5) indicates many of the AOA used H_2 to increase their mixotrophic activity. Mixotrophy by AOA is a well-known feature (Qin et al. 2014; Seyler et al. 2018), and our data indicate it can be increased in the presence of H_2. However, some AOA have higher ammonia oxidation rates at lower oxygen concentrations (Bristow et al. 2016), and the H_2 amended incubations should have promoted lower oxygen conditions. It is thus possible that higher activity in some rock-associated Thaumarchaeota was further stimulated by reduced oxygen concentrations. Additional experiments are required to determine whether the increased ^{13}C assimilation of mixotrophic AOA seen here is due to H_2 oxidation, low oxygen, or a combination of both.

Nitrospirae are nitrite-oxidizing bacteria (NOB) and were found to be enriched in peridotite rock samples (Figs. 3 and 5) and also exhibited a ^{13}C-labeling pattern consistent with a H_2 catabolism. Namely, Nitrospira-affiliated OTUs increased their assimilation of acetate in the H_2-amended incubations by 64.6% (±36%) (Figs. 4 and 5). This is in line with H_2 oxidation demonstrated for NOB in pure culture experiments (Koch et al. 2014).

The higher relative abundance of *nirS* encoding ORFs in peridotite rock and IGT metagenomes compared to the Niskin seawater metagenomes (Fig. 7D) could be explained by low-oxygen levels commonly experienced at the benthic-seawater interface selecting for anaerobic, nitrite respiring bacteria (Díaz and Rosenberg 1995). The relative abundance of heavy *nirS* ORFs was higher in the presence of added H_2 (Fig. 7D), which indicates that the H_2 was selected for nitrite respiring bacteria. Most of the heavy *nirS* ORFs were affiliated with *Marinobacter* and *Amphritea* (Fig. 7B), which rock-associated and exhibited some of the highest levels of ^{13}C-assimilation with added H_2 (Figs. 4 and 5). Taken together, these results indicate that the addition of H_2 promoted increased assimilation of ^{13}C via anaerobic nitrate-reducing bacteria, including peridotite-associated *Marinobacter* and

Amphritea.

The addition of H_2 affected increased carbon assimilation of peridotite-associated ammonia and nitrite-oxidizing consortia (Fig. 5) that are responsible for nitrification. Together with the activity of rock-associated nitrite reducing bacteria (Fig. 7), our results show the potential for H_2 to effect coupled nitrification and denitrification in the rock-associated community. Coupled nitrification and denitrification influence the loss of fixed nitrogen from benthic ecosystems (Jenkins and Kemp 1984). Our findings raise the possibility that serpentinization derived H_2 may influence fixed nitrogen loss (as N2 gas) from the peridotite-rock associated ecosystem, by stimulating the activity of nitrifiers and denitrifiers. Nitrogen cycling consortia have been found in terrestrial serpentinization systems as well, such as the Somali Ophiolite system in Oman (Rempfert et al. 2017). The possibility for abiotically produced H_2 from serpentinization reactions to influence fixed nitrogen loss via coupled nitrification and denitrification in ultramafic rock ecosystems is a topic worthy of future study.

2.5.5 Carbon assimilation by CO oxidizers in the rock-associated community

Carbon monoxide can serve as the sole source of carbon and energy for life in environments that are low in an organic matter (Ragsdale 2004), including terrestrial serpentinization settings (Fones et al. 2021; Morrill et al. 2014). The *coxMSL* enzyme (carbon monoxide dehydrogenase) catalyzes the oxidation of CO (carbon monoxide) to CO_2 in bacteria (Wilcoxen et al. 2011), and is a widespread mechanism supporting microbial survival (Cordero et al. 2019; Seewald et al. 2006), particularly in extreme habitats experiencing low levels of productivity (Ji et al. 2017). The bootstrap-supported separation of seawater and rock-associated *coxL* clades indicate a unique rock-associated community capable of using CO as an energy source. The substrate utilization within these peridotite-rock-associated clades of *coxL* encoding organisms appears to have been affected by H_2 amendments. For example, heavy *coxL* ORFs from SIP incubations amended with H_2 were detected within bootstrap-supported peridotite-associated clades affiliated with the '*Ca.* Rokubacteria', Gemmatimonadales, and SAR202 clade (Fig. 6B). This raises the possibility that CO oxidation might be related to anabolism at relatively high H_2 concentrations by some taxa within these groups.

The carbon assimilation by CO-oxidizing bacteria associated with ultramafic rocks seen here could be explained by the water–gas shift reaction ($CO_2 + H_2 = CO + H_2O$) (Can et al. 2014). Our data shows that in seafloor ultramafic rock settings where O_2 is above detection and H_2 is likely produced via serpentinization or related low-temperature alteration processes, aerobic CO-oxidizing organisms become stimulated by CO that is produced via the abiotic reduction of CO_2 with H_2. All of the CO-dehydrogenases that we detected were the molybdenum–copper-containing form which functions in aerobic CO-oxidation to CO_2, as opposed to the NiFe CO-dehydrogenases that function in anaerobic CO_2 reduction to CO (Can et al. 2014). Our results from peridotite-associated communities at SPSPA are similar to terrestrial serpentinization settings, where aerobic CO oxidation supports life that survives under alkaline conditions (Fones et al. 2021; Morrill et al. 2014).

Taken together, the phylogenetic analysis of *coxL*, *HypE*, and *nirS* show a similar pattern: the

majority of heavy ORFs cluster together in bootstrap supported clades of peridotite rock-associated taxa. This trend suggests that the oxidation of H_2 and carbon monoxide, as well as dissimilatory nitrite reduction, are widespread and important physiological features for taxa that were assimilating ^{13}C within the peridotite-associated microbial community.

2.5.6 Assessing effects of the qSIP incubation conditions

A comparison of effects of the substrates (acetate, formate, bicarbonate) is problematic due to the extraordinarily high concentrations of acetate and formate added relative to the in situ conditions, and potential substrate inhibition, toxicity, and pH alterations. Therefore, we do not compare the effects of the substrates to one another (e.g., we do not claim that bicarbonate is a more important carbon source compared to formate, despite the clear differences in qSIP results) but rather compare assimilation of a particular substrate with, and without, added H_2. While the added concentrations in our incubations are higher than the in situ abundances (no H_2 above background was detected in the water column), our experimental approach provides initial boundary conditions on the stimulation of carbon assimilation by H_2 for specific substrates, by specific peridotite-associated taxa in an ultramafic seafloor setting undergoing low-temperature aqueous alteration.

An increased temperature of the incubations (room temperature) relative to the in situ temperature (10–12 °C), probably led to elevated microbial activity and rates of ^{13}C substrate assimilation as shown previously for benthic microbes (Gudasz et al. 2010). Moreover, purging of the incubation flasks with N2 created dissolved O_2 concentrations at low oxygen levels (see the "Methods" section), and the labeling of known strictly anaerobic taxa indicates that anoxic regions were established during the incubation. Because O_2 was available at low concentrations in the flasks (ca. 10 µM), this explains why many of the most highly ^{13}C-enriched taxa in the qSIP are known aerobic or facultatively anaerobic taxa (Figs. 4 and 5). However, at the flask bottom below the 3 cm column of crushed peridotite rock, anoxic conditions likely established due to a vertical O_2 gradient in the flask that commonly occurs in this experimental setup due to increased rates of aerobic respiration at the benthic–water interface (Ortega-Arbulú et al. 2019). Anoxic conditions in the crushed rocks at the bottom of the flasks likely promoted carbon assimilation by rock-associated strict anaerobes that also were using H_2 to increase their anabolism from the added ^{13}C-labeled substrates. For example, this is seen in the Atribacteria that are strict anaerobes (Katayama et al. 2020) that exhibited the highest ^{13}C-bicarbonate assimilation in the presence of H_2 (Fig. 4). Moreover, the ^{13}C-labeling of a peridotite-associated taxon affiliated with the Firmicute *Paramaledivibacter* (Fig. 5) indicates anoxic conditions, as this is a strictly anaerobic organism originally isolated from a deep-sea hydrothermal vent from the Mid-Atlantic Ridge (Brisbarre et al. 2003).

2.5.7 Assessing cross-feeding of ^{13}C-labeled substrates

Cross feeding is an issue inherent to all SIP studies. It is possible that some of the ^{13}C was fixed from bicarbonate into organic molecules and subsequently assimilated by heterotrophs. The labeling of heterotrophic taxa with ^{13}C-bicarbonate indicates that some of the ^{13}C-bicarbonate was taken up by autotrophs and assimilated by heterotrophs as DOM or POM. Alternatively, heterotrophic carbon fixation occurs through anaplerotic carbon fixation reactions in heterotrophs that can account for

2–8% of cell carbon (Roslev et al. 2004; Spona-Friedl et al. 2020) and could explain a portion of the ^{13}C labeling in heterotrophs seen here. It is not possible that the ^{13}C from the organic substrates would be remineralized and be taken up as bicarbonate because the natural bicarbonate concentration in seawater is ~2.3 mM and will dilute the remineralized ^{13}C label to undetectable levels (Orsi et al. 2016). Therefore, the results in bicarbonate incubations not only show the primary utilizers but underpin complex ecological interactions in the microbial food web. We also note that formate can rapidly interconvert with CO_2 and therefore some of the formate may have been taken up as ^{13}C-bicarbonate (Jansen et al. 1984). These results support the hypothesis that anaplerotic carbon fixation reactions in heterotrophs represent an important, yet underappreciated, component of the global marine carbon cycle (Braun et al. 2021).

2.6 Conclusions

Our findings demonstrate that H_2 has a quantitatively significant impact on microbial carbon assimilation in seafloor ultramafic rock microbial ecosystems (Fig. 8). The qSIP results show that this effect of H_2 on increased carbon assimilation is phylogenetically organized, and the distribution of the carbon assimilating taxa shows a higher diversity of peridotite-associated taxa assimilating carbon in the presence of H_2 compared to taxa that were not detected on the ultramafic rocks. The data support thermodynamic predictions that oxidation of H_2 is energetically favorable for seafloor-associated microbial life in settings where H_2-containing aqueous solutions mix with seawater (Amend et al. 2011), including those where H_2 is formed via high-temperature or low-temperature aqueous alteration (Russell et al. 2010; Martin et al. 2008), rock comminution in fault zones, and radiolysis.

FIGURES AND TABLES

Table 1 The result of phylogenetic signal tests (Blomberg's K and Pagel's λ) analysis on the effect of H_2 on carbon assimilation.

	K	***λ***	**Labeled OTUs**	**Unlabeled OTUs**	**Labeled OTUs (%)**
Bicarbonate	0.13	0	81	58	58.3
Bicarbonate + H_2	0.26*	0.64	26	61	29.9
Acetate	0.11	0	73	79	48
Acetate + H_2	0.25*	0.82	81	17	82.7
Formate	0.16	0	59	6	90.8
Formate + H_2	0.25*	0.64	37	129	22.3
Total number of OTUs	–	–	107	203	34.5

*$p \leq 0.05$.

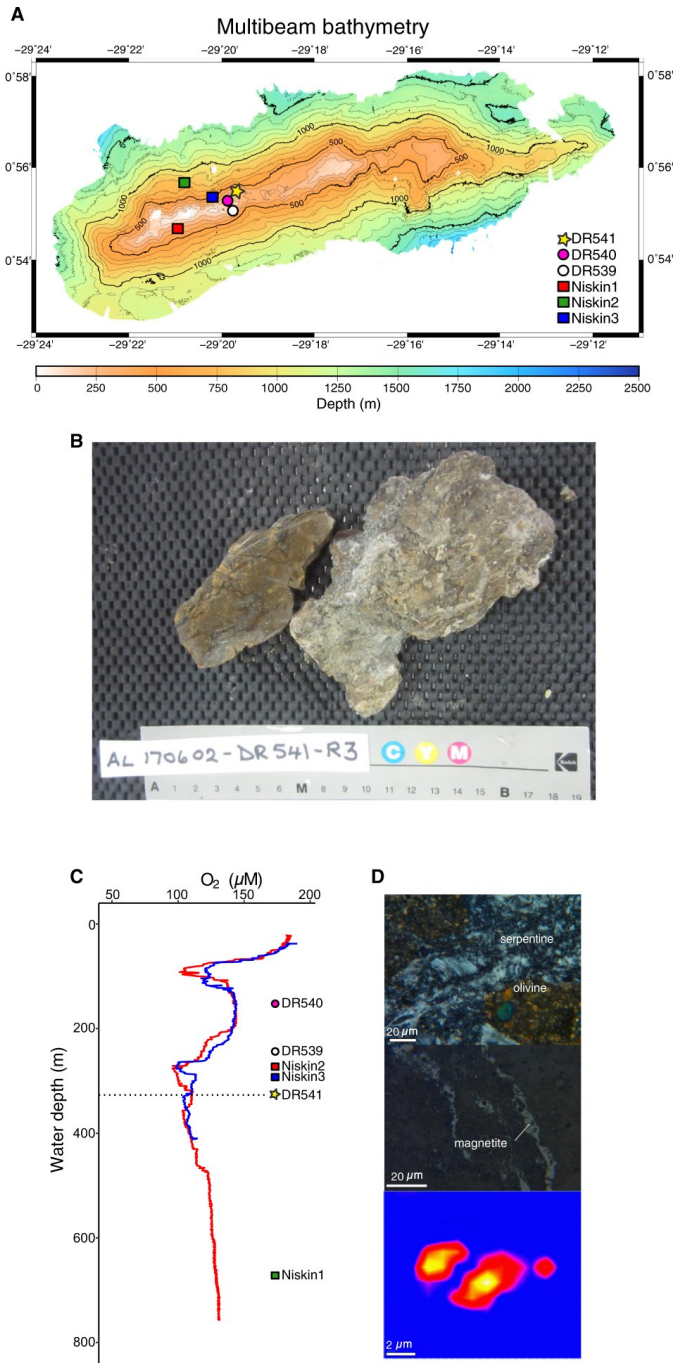

Figure 1: **A** Bathymetry of SPSPA and sampling locations for Niskin, IGT fluids, sediments, and rocks. The location for the qSIP experiment (D541) is shown with a yellow star. **B** Photo of partially serpentinized peridotite collected from St. Pauls Rocks, the interior of the rock was used for the qSIP incubations. **C** Dissolved oxygen vertical profiles from two sites (Niskin2, Niskin3) in close proximity to the location for qSIP (D541). The horizontal dashed line represents the depth where samples were taken for qSIP (327 meters). The other labels indicate the water depths at which those samples were taken (see map in panel A). **D** Thin section photomicrographs of sheared peridotite from SPSPA. The presence of serpentine and magnetite (top two panels) is indicative of H_2 generation. Hyperspectral Raman map (bottom panel) showing a CH_4-rich inclusion in amphibole sampled from the close vicinity of the studied area.

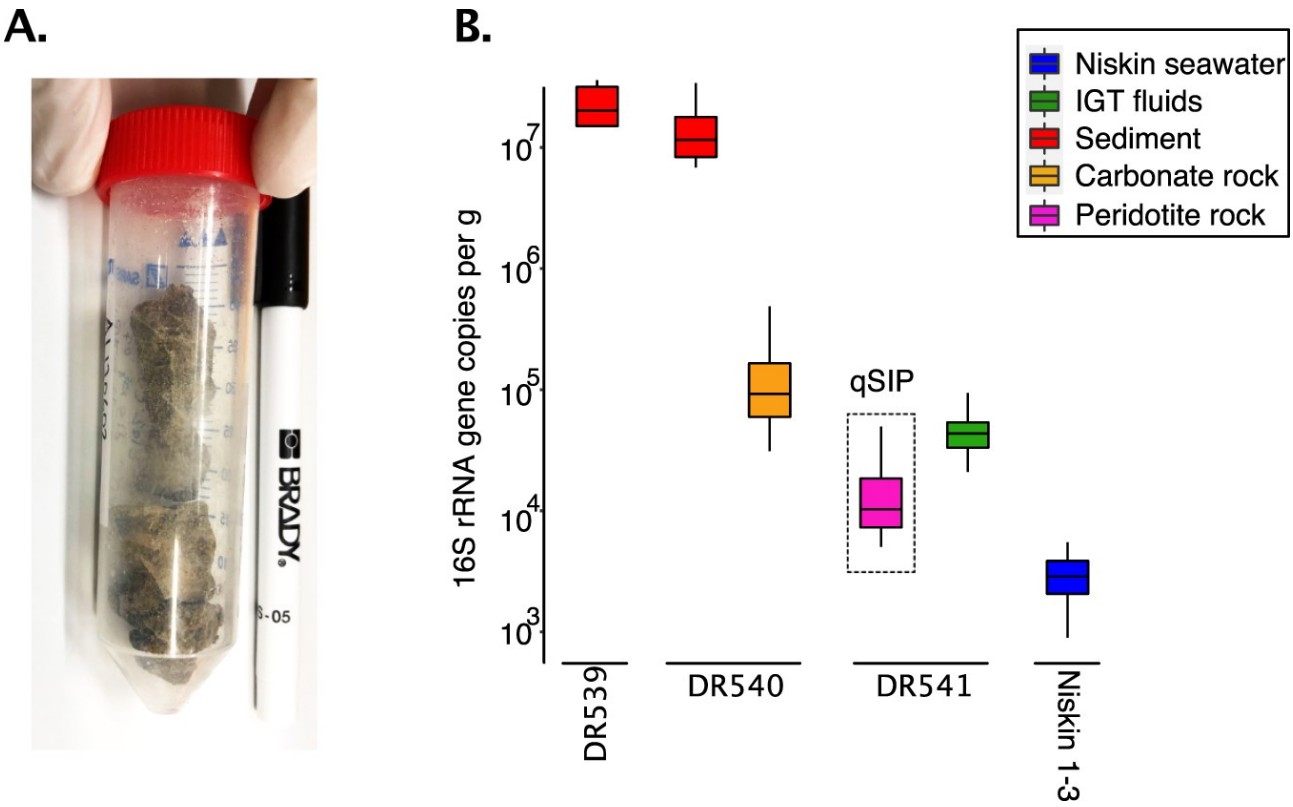

Figure 2: **A** Photograph of peridotite rock samples (dive D541) prior to DNA extraction. **B** Concentration of 16S rRNA genes from sediments, rocks, IGT fluids, and Niskin collected seawater. Concentrations are normalized to per gram for sediment and rock samples, and per mL for seawater samples (IGT fluids and Niskins).

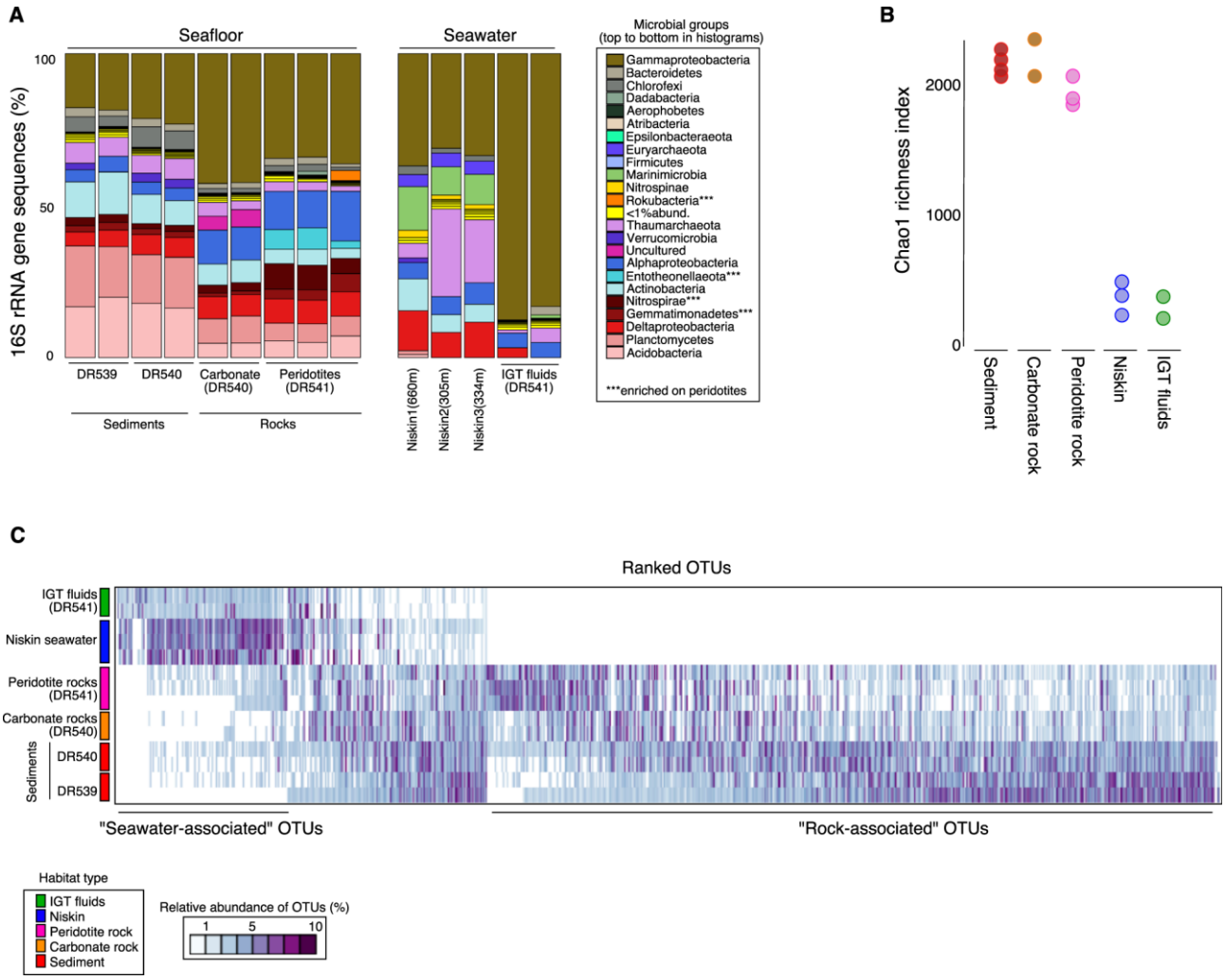

Figure 3: **A** The taxonomic composition of sediment, rock, and seawater communities. **B** Chao1 estimated microbial richness, showing a significantly higher richness in the rock and sediments samples, compared to the seawater communities (two-sided *T*-test: $P = e^{-8}$). **C** Heatmap showing the relative abundance of OTUs (columns) per sample (rows) and their distribution across sample types. The community detected on the ultramafic rocks was significantly different compared to the seawater communities (ANOSIM: P = 0.001). More than half of the total OTUs detected were found only in the seafloor samples (rocks and sediments).

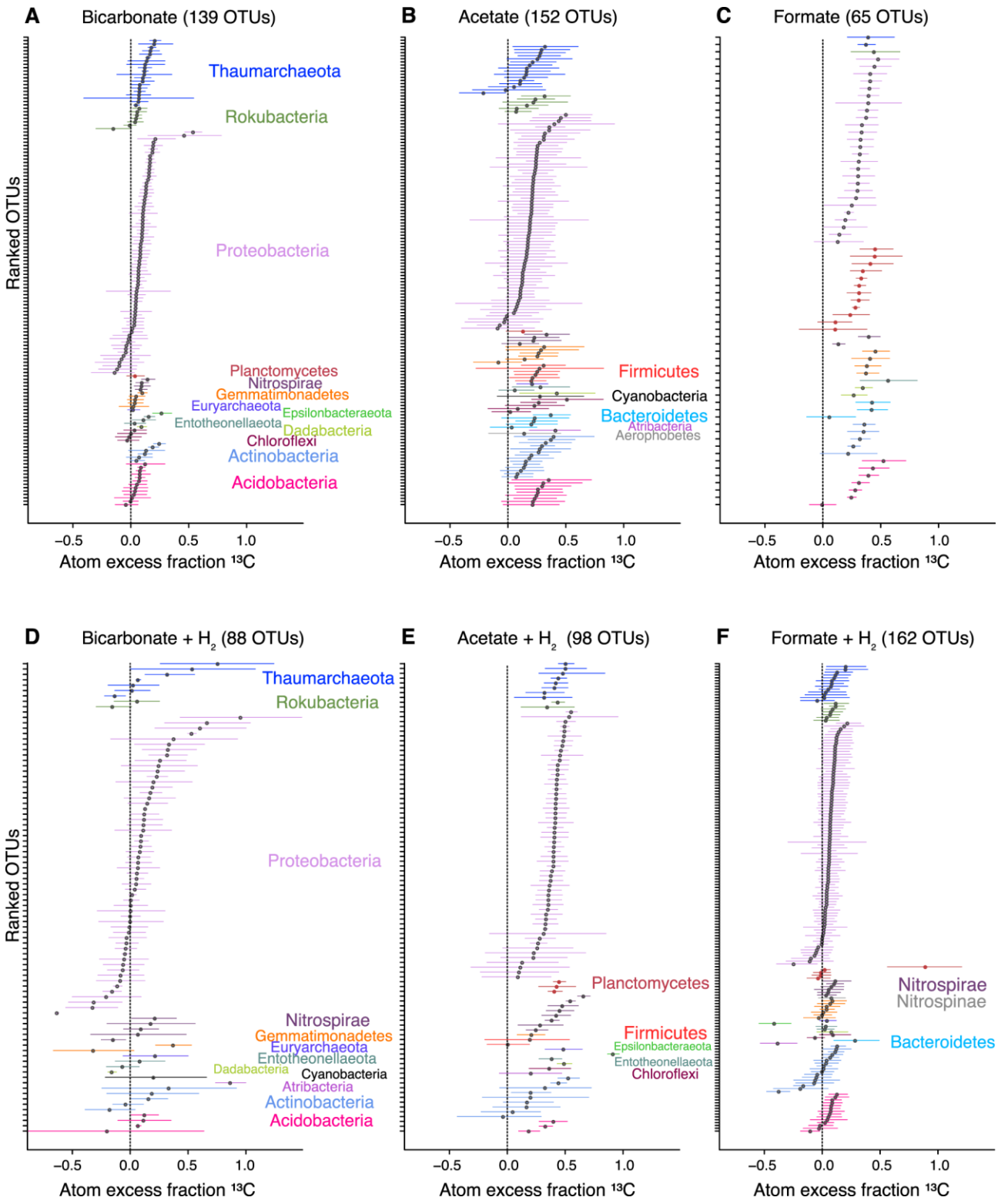

Figure 4: Individual points represent EAF values of specific OTUs, which are colored by Phylum for qSIP incubations that did not (**A–C**), or did (**D–F**), receive H_2. The error bars correspond to 90% CI across three biological replicates. OTUs that do not have a 90% CI overlapping with 0 are considered to be 13C labeled.

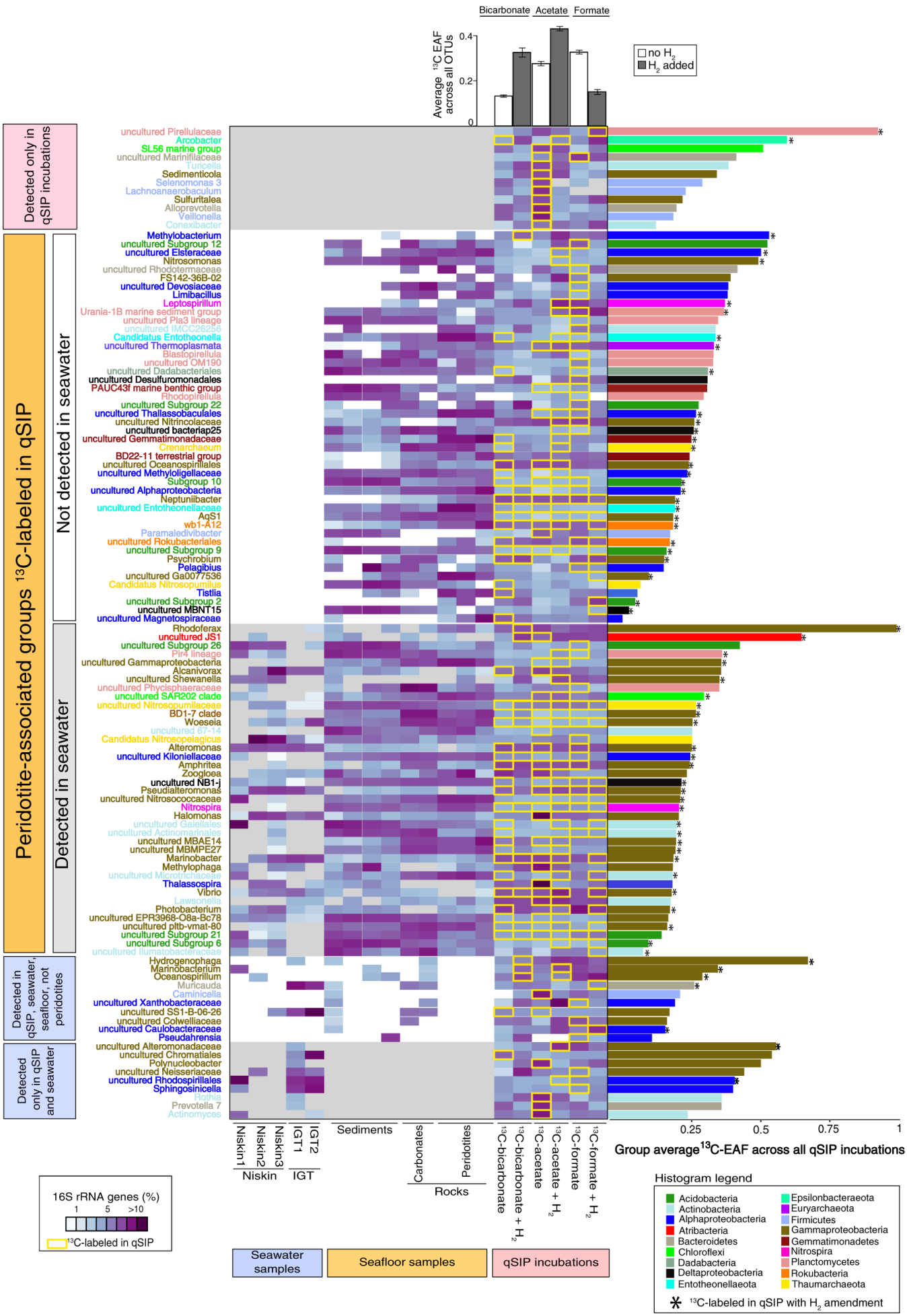
Bicarbonate
Acetate
Formate
Average ¹³C EAF across all OTUs
0.4
0.2
0
no H₂
H₂ added
Detected only in qSIP incubations
Peridotite-associated groups ¹³C-labeled in qSIP
Not detected in seawater
Detected in seawater
Detected in qSIP, seawater, seafloor, not peridotites
Detected only in qSIP and seawater
uncultured Pirellulaceae
Arcobacter
SL56 marine group
uncultured Marinifilaceae
Turicella
Sedimenticola
Selenomonas 3
Lachnoanaerobaculum
Sulfuritalea
Alloprevotella
Veillonella
Conexibacter
Methylobacterium
uncultured Subgroup 12
uncultured Elsteraceae
Nitrosomonas
uncultured Rhodothermaceae
FS142-36B-02
uncultured Devosiaceae
Limibacillus
Leptospirillum
Urania-1B marine sediment group
uncultured Pla3 lineage
uncultured IMCC26256
Candidatus Entotheonella
uncultured Thermoplasmata
Blastopirellula
uncultured OM190
uncultured Dadabacteriales
uncultured Desulfuromonadales
PAUC43f marine benthic group
Rhodopirellula
uncultured Subgroup 22
uncultured Thallassobaculales
uncultured Nitrincolaceae
uncultured bacteriap25
uncultured Gemmatimonadaceae
Crenarchaeum
BD22-11 terrestrial group
uncultured Oceanospirillales
uncultured Methyloligellaceae
Subgroup 10
uncultured Alphaproteobacteria
Neptuniibacter
uncultured Entotheonellaceae
AqS1
wb1-A12
Paramaledivibacter
uncultured Rokubacterales
uncultured Subgroup 9
Psychrobium
Pelagibius
uncultured Ga0077536
Candidatus Nitrosopumilus
Tistlia
uncultured Subgroup 2
uncultured MBNT15
uncultured Magnetospiraceae
Rhodoferax
uncultured JS1
uncultured Subgroup 26
Pir4 lineage
uncultured Gammaproteobacteria
Alcanivorax
uncultured Shewanella
uncultured Phycisphaeraceae
uncultured SAR202 clade
uncultured Nitrosopumilaceae
BD1-7 clade
Woeseia
uncultured 67-14
Candidatus Nitrosopelagicus
Alteromonas
uncultured Kiloniellaceae
Amphritea
Zooglaea
uncultured NB1-j
Pseudidteromonas
uncultured Nitrosococcaceae
Nitrospira
Halomonas
uncultured Gaiellales
uncultured Actinomarinales
uncultured MBAE14
uncultured MBMPE27
Marinobacter
Methylophaga
uncultured Microtrichaceae
Thalassospira
Vibrio
Lawsonella
Photobacterium
uncultured EPR3968-O8a-Bc78
uncultured pltb-vmat-80
uncultured Subgroup 21
uncultured Subgroup 6
uncultured Ilumatobacteraceae
Hydrogenophaga
Marinobacterium
Oceanospirillum
Muricauda
Caminicella
uncultured Xanthobacteraceae
uncultured SS1-B-06-26
uncultured Colwelliaceae
uncultured Caulobacteraceae
Pseudahrensia
uncultured Alteromonadaceae
uncultured Chromatiales
Polynucleobacter
uncultured Neisseriaceae
uncultured Rhodospirillales
Sphingosinicella
Rothia
Prevotella 7
Actinomyces
Niskin1
Niskin2
Niskin3
IGT1
IGT2
Sediments
Carbonates
Peridotites
Niskin
IGT
Rocks
¹³C-bicarbonate
¹³C-bicarbonate + H₂
¹³C-acetate
¹³C-acetate + H₂
¹³C-formate
¹³C-formate + H₂
0.25
0.5
0.75
1
Group average ¹³C-EAF across all qSIP incubations
16S rRNA genes (%)
1
5
>10
¹³C-labeled in qSIP
Seawater samples
Seafloor samples
qSIP incubations
Histogram legend
Acidobacteria
Actinobacteria
Alphaproteobacteria
Atribacteria
Bacteroidetes
Chloroflexi
Dadabacteria
Deltaproteobacteria
Entotheonellaeota
Epsilonbacteraeota
Euryarchaeota
Firmicutes
Gammaproteobacteria
Gemmatimonadetes
Nitrospira
Planctomycetes
Rokubacteria
Thaumarchaeota
¹³C-labeled in qSIP with H₂ amendment

Figure 5: The heatmap shows the relative abundance of 16S rRNA gene sequences per group per sample (purple = more, light blue = less). Within the qSIP incubations (right-hand side), groups that had OTUs with statistically significant ^{13}C-assimilation in qSIP are surrounded by a yellow box. The histograms on the right side of the plot show the average ^{13}C-EAF across all qSIP incubations per group. An asterisk indicates that this group had a significant ^{13}C-EAF within a qSIP incubation with added H_2 (no asterisk means labeling occurred only in qSIP incubations without H_2). The histograms at the top of the heatmap show the average ^{13}C-EAF across all OTUs within each qSIP incubation, error bars represent standard deviations. The analysis shows that the majority of ^{13}C-assimilating groups were rock-associated and that more rock-associated groups became labeled in the presence of H_2 (middle of the heatmap), compared to the seawater-associated groups (at the bottom of the heatmap).

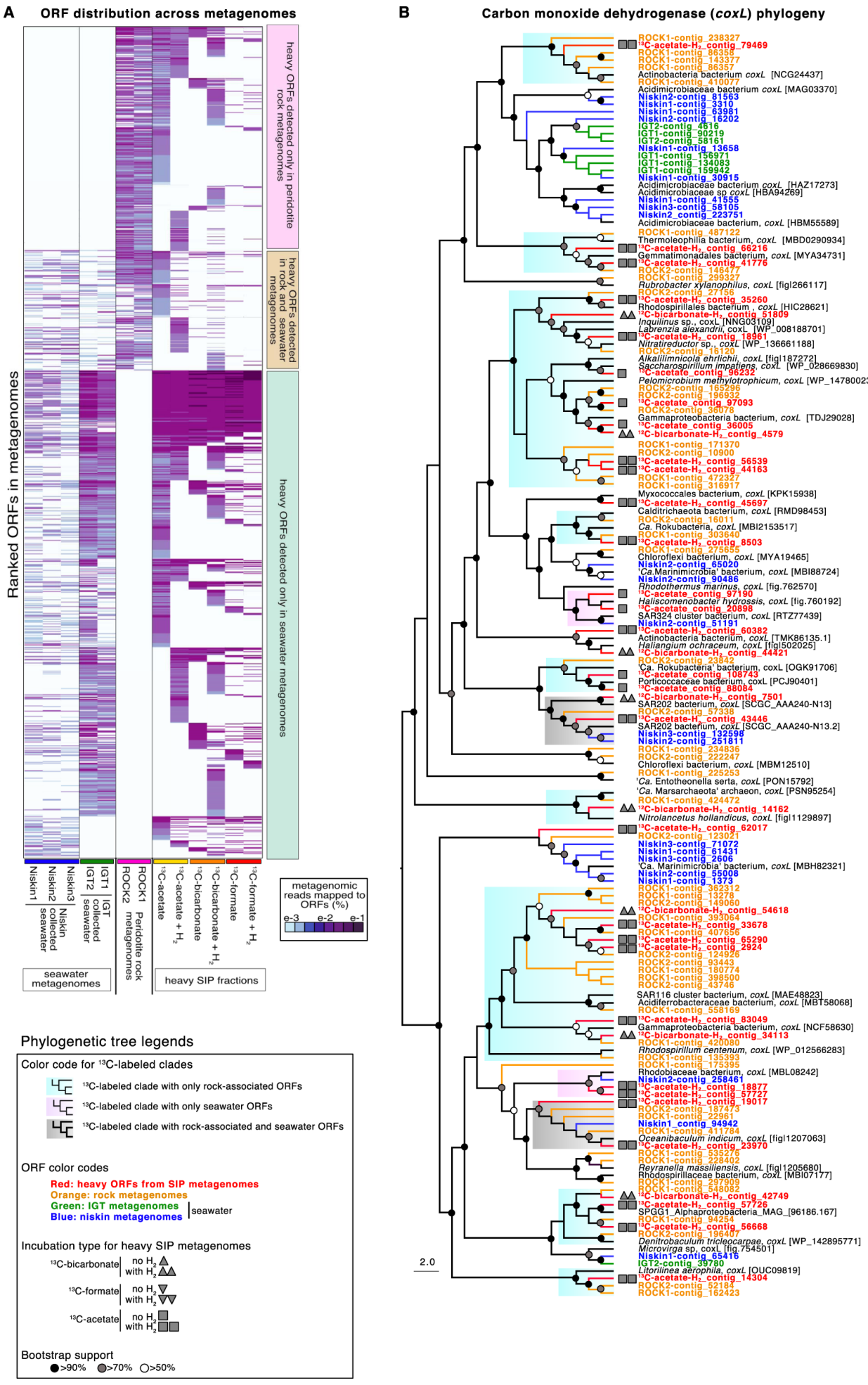
A
ORF distribution across metagenomes
Ranked ORFs in metagenomes
heavy ORFs detected only in peridotite rock metagenomes
heavy ORFs detected in rock and seawater metagenomes
heavy ORFs detected only in seawater metagenomes
Niskin1
Niskin2
Niskin3
IGT1
IGT2
ROCK1
ROCK2
13C-acetate
13C-acetate + H2
13C-bicarbonate
13C-bicarbonate + H2
13C-formate
13C-formate + H2
Niskin collected seawater
IGT collected seawater
Peridotite rock metagenomes
seawater metagenomes
heavy SIP fractions
metagenomic reads mapped to ORFs (%)
e-3
e-2
e-1
B
Carbon monoxide dehydrogenase (coxL) phylogeny
ROCK1-contig_238327
13C-acetate-H2_contig_79469
ROCK1-contig_86358
ROCK1-contig_143377
ROCK1-contig_86357
Actinobacteria bacterium coxL [NCG24437]
ROCK1-contig_410077
Acidimicrobiaceae bacterium coxL [MAG03370]
Niskin2-contig_81563
Niskin1-contig_3310
Niskin1-contig_63981
Niskin2-contig_16202
IGT2-contig_4616
IGT1-contig_90219
IGT2-contig_58161
Niskin1-contig_13658
IGT1-contig_156971
IGT1-contig_134083
IGT1-contig_159942
Niskin1-contig_30915
Acidimicrobiaceae bacterium coxL [HAZ17273]
Acidimicrobiaceae sp coxL [HBA94269]
Niskin1-contig_41555
Niskin3-contig_58105
Niskin2_contig_223751
Acidimicrobiaceae bacterium, coxL [HBM55589]
ROCK1-contig_487122
Thermoleophilia bacterium, coxL [MBD0290934]
13C-acetate-H2_contig_66216
Gemmatimonadales bacterium, coxL [MYA34731]
13C-acetate-H2_contig_41776
ROCK2-contig_146477
ROCK1-contig_29327
Rubrobacter xylanophilus, coxL [figI266117]
ROCK2-contig_27756
13C-acetate-H2_contig_35260
Rhodospirillales bacterium , coxL [HIC28621]
13C-bicarbonate-H2_contig_51809
Inquilinus sp., coxL [NNG03109]
Labrenzia alexandrii, coxL [WP_008188701]
13C-acetate-H2_contig_1861
Nitratireductor sp., coxL [WP_136661188]
ROCK2-contig_16120
Alkaliilimnicola ehrlichii, coxL [figI187272]
Saccharospirillum impatiens, coxL [WP_028669830]
13C-acetate_contig_96232
Pelomicrobium methylotrophicum, coxL [WP_147800236]
ROCK2-contig_165296
ROCK2-contig_196932
13C-acetate_contig_97093
ROCK2-contig_36078
Gammaproteobacteria bacterium, coxL [TDJ29028]
13C-acetate_contig_36005
12C-bicarbonate-H2_contig_4579
ROCK1-contig_171370
ROCK2-contig_10900
13C-acetate-H2_contig_56539
13C-acetate-H2_contig_44163
ROCK1-contig_472327
ROCK1-contig_316917
Myxococcales bacterium, coxL [KPK15938]
13C-acetate-H2_contig_45697
Calditrichaeota bacterium, coxL [RMD98453]
ROCK2-contig_16011
Ca. Rokubacteria, coxL [MBI2153517]
ROCK1-contig_303640
13C-acetate-H2_contig_8503
ROCK1-contig_275655
Chloroflexi bacterium, coxL [MYA19465]
Niskin2-contig_65020
'Ca.Marinimicrobia' bacterium, coxL [MBI88724]
Niskin2-contig_90486
Rhodothermus marinus, coxL [fig.762570]
13C-acetate_contig_97190
Haliscomenobacter hydrossis, coxL [fig.760192]
13C-acetate_contig_20898
SAR324 cluster bacterium, coxL [RTZ77439]
Niskin2-contig_51191
13C-acetate-H2_contig_60382
Actinobacteria bacterium, coxL [TMK86135.1]
Haliangium ochraceum, coxL [figI502025]
12C-bicarbonate-H2_contig_44421
ROCK2-contig_23842
'Ca. Rokubacteria' bacterium, coxL [OGK91706]
13C-acetate_contig_108743
Porticoccaceae bacterium, coxL [PCJ90401]
13C-acetate_contig_88084
12C-bicarbonate-H2_contig_7501
SAR202 bacterium, coxL [SCGC_AAA240-N13]
ROCK2-contig_57338
13C-acetate-H2_contig_43446
SAR202 bacterium, coxL [SCGC_AAA240-N13.2]
Niskin3-contig_132598
Niskin2-contig_251811
ROCK1-contig_234836
ROCK2-contig_222247
Chloroflexi bacterium, coxL [MBM12510]
ROCK1-contig_225253
'Ca. Entotheonella serta, coxL [PON15792]
'Ca. Marsarchaeota' archaeon, coxL [PSN95254]
ROCK1-contig_424472
12C-bicarbonate-H2_contig_14162
Nitrolancetus hollandicus, coxL [figI1129897]
13C-acetate-H2_contig_62017
ROCK2-contig_123021
Niskin3-contig_71072
Niskin1-contig_61431
Niskin3-contig_2606
'Ca. Marinimicrobia' bacterium, coxL [MBH82321]
Niskin2-contig_55008
Niskin1-contig_1373
ROCK1-contig_352312
ROCK1-contig_13278
ROCK2-contig_149060
12C-bicarbonate-H2_contig_54618
ROCK1-contig_393064
13C-acetate-H2_contig_33678
ROCK1-contig_407656
13C-acetate-H2_contig_65290
13C-acetate-H2_contig_2924
ROCK2-contig_124926
ROCK2-contig_93443
ROCK1-contig_180774
ROCK1-contig_398500
ROCK2-contig_43746
SAR116 cluster bacterium, coxL [MAE48823]
Acidiferrobacteraceae bacterium, coxL [MBT58068]
ROCK1-contig_558169
13C-acetate-H2_contig_83049
Gammaproteobacteria bacterium, coxL [NCF58630]
12C-bicarbonate-H2_contig_34113
ROCK1-contig_420080
Rhodospirillum centenum, coxL [WP_012566283]
ROCK1-contig_135393
ROCK1-contig_175395
Rhodobiaceae bacterium, coxL [MBL08242]
Niskin2-contig_258461
13C-acetate-H2_contig_18877
13C-acetate-H2_contig_57727
13C-acetate-H2_contig_19017
ROCK2-contig_187473
ROCK1-contig_22961
Niskin1_contig_94942
ROCK1-contig_411784
Oceanibaculum indicum, coxL [figI1207063]
13C-acetate-H2_contig_23970
ROCK1-contig_535276
ROCK1-contig_228402
Reyranella massiliensis, coxL [figI1205680]
Rhodospirillaceae bacterium, coxL [MBI07177]
ROCK1-contig_297909
ROCK1-contig_548082
12C-bicarbonate-H2_contig_42749
13C-acetate-H2_contig_57726
SPGG1_Alphaproteobacteria_MAG_[96186.167]
ROCK1-contig_94254
13C-acetate-H2_contig_56668
ROCK2-contig_196407
Denitrobaculum tricleocarpae, coxL [WP_142895771]
Microvirga sp, coxL [fig.754501]
Niskin1-contig_65416
IGT2-contig_39780
Litorilinea aerophila, coxL [OUC09819]
13C-acetate-H2_contig_14304
ROCK2-contig_52184
ROCK1-contig_162423
2.0
Phylogenetic tree legends
Color code for 13C-labeled clades
13C-labeled clade with only rock-associated ORFs
13C-labeled clade with only seawater ORFs
13C-labeled clade with rock-associated and seawater ORFs
ORF color codes
Red: heavy ORFs from SIP metagenomes
Orange: rock metagenomes
Green: IGT metagenomes
Blue: niskin metagenomes
seawater
Incubation type for heavy SIP metagenomes
13C-bicarbonate
no H2
with H2
13C-formate
no H2
with H2
13C-acetate
no H2
with H2
Bootstrap support
>90%
>70%
>50%

Figure 6: **A** Heatmap displaying all ORFs detected from heavy SIP metagenomes and the distribution of these heavy ORFs in the rock and seawater metagenomes. Heatmap rows represent predicted proteins from the MetaProt database (Orsi et al. 2020a) having best BLASTp similarity to peptides encoded in ORFs from the metagenomes (columns). Colors represent length normalized read coverage from metagenomes to the ORFs. **B** Phylogenetic analysis (RAxML) of all detected *coxL* ORFs based on an alignment length of 968 amino acids. Note that most of the *coxL* clades were rock-specific and that these also contain the majority of heavy *coxL* ORFs.

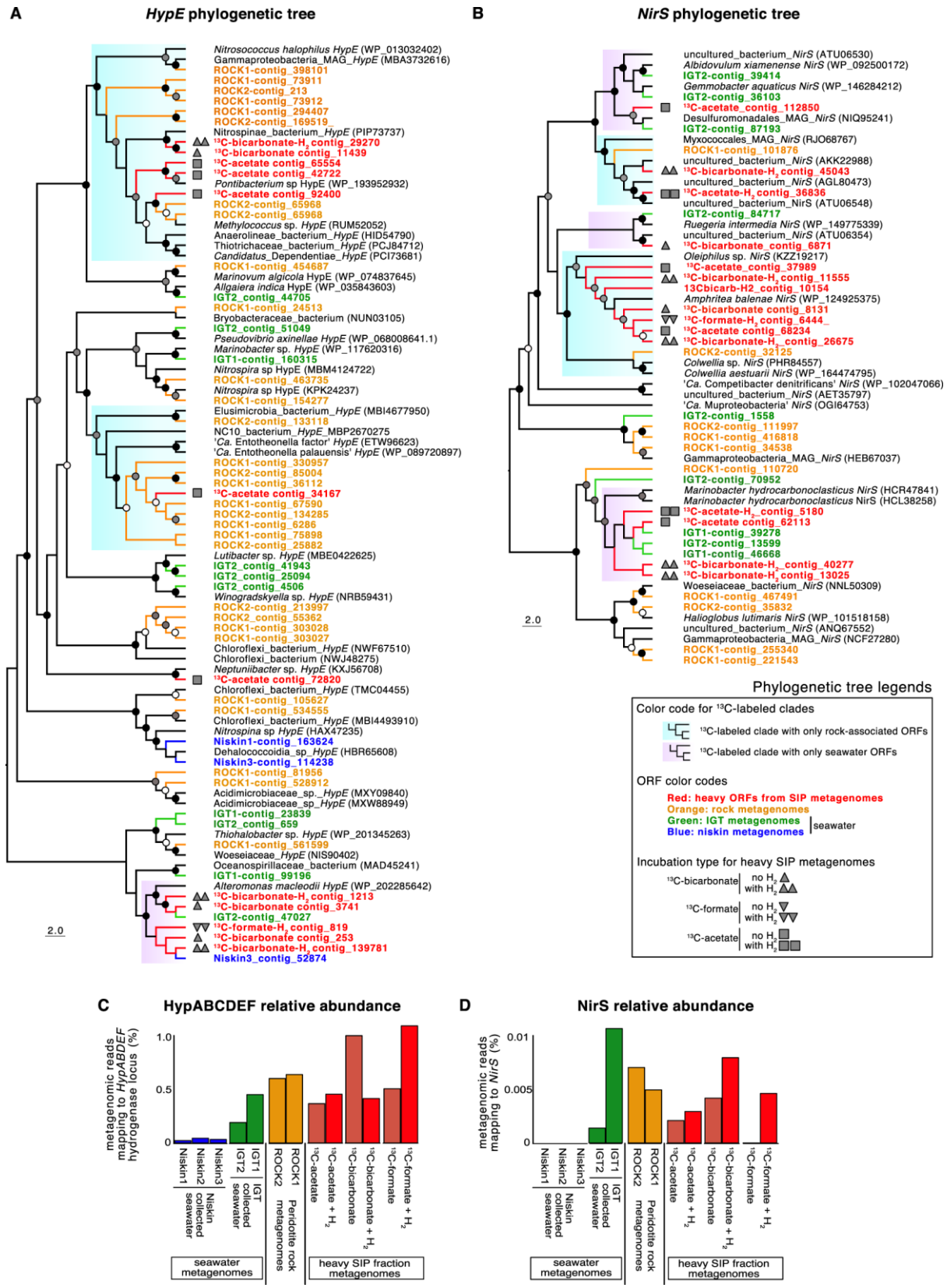

Figure 7: Phylogenetic analyses (RAxML) of all detected *HypE* (**A**) and *nirS* (**B**) ORFs based on alignment lengths of 442 and 638 amino acids, respectively. Note that the separation of seawater (pink highlighted) and rock-associated (light blue highlighted) clades. Panels (**C**) and (**D**) show the relative abundance (% reads mapping, length normalized) within the different metagenomes to ORFs with best BLASTp similarity to the NiFe-hydrogenase assembly locus *HypABCDEF* (**C**) and *nirS* (**D**), respectively. Circles on nodes represent bootstrap values (black > 90%, gray > 70%, white > 50%).

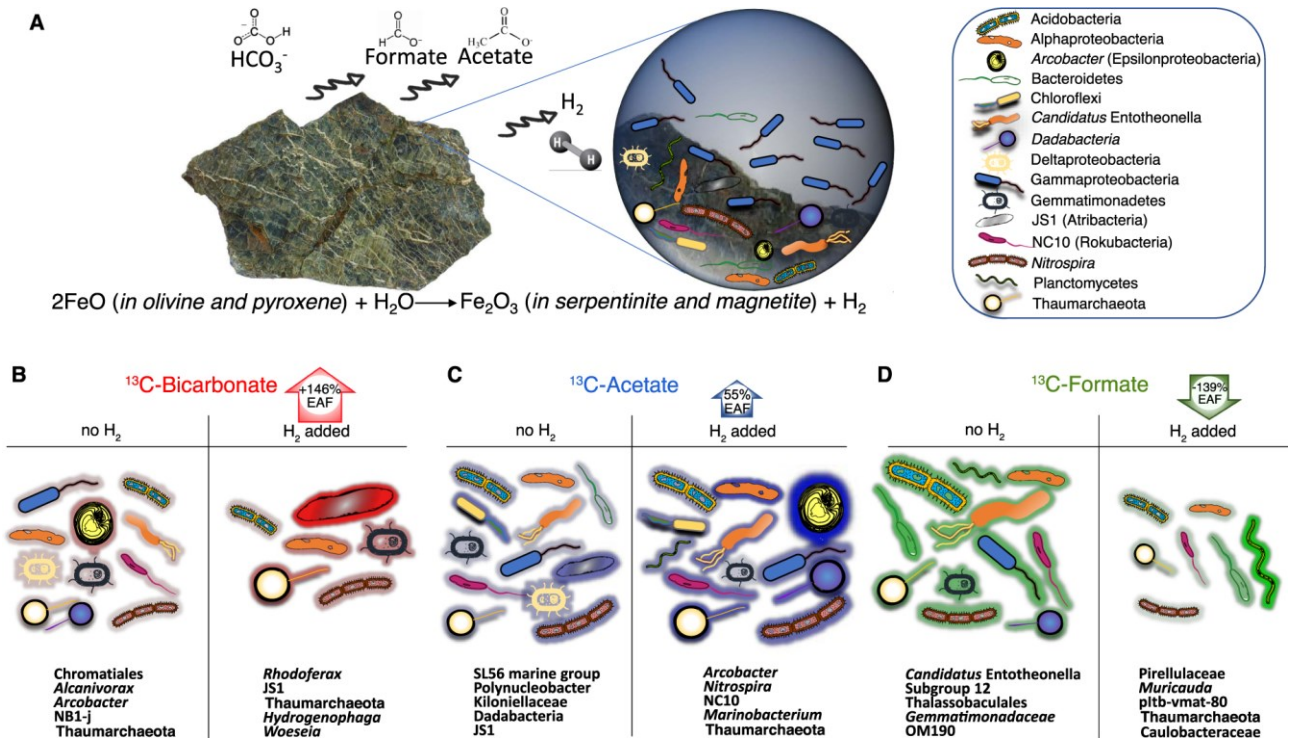

Figure 8: **A** The photograph is a piece of rock from partially serpentinized peridotite that was taken from SPSPA for the qSIP incubations. The cartoon diagram in the upper right shows the corresponding groups that assimilated carbon in the presence (or absence) of H_2. **B–D** The plots below show the main groups that were responsible for carbon assimilation of different substrates with, and without H_2. The extent of red/blue/green shading on the outside of the cells corresponds to ^{13}C-labeling from CO_2/acetate/formate. The percentage number (inside the arrows) indicates the average increase or decrease in ^{13}C-assimilation (EAF) in the community with the addition of H_2.

SUPPLEMANTARY FIGURES

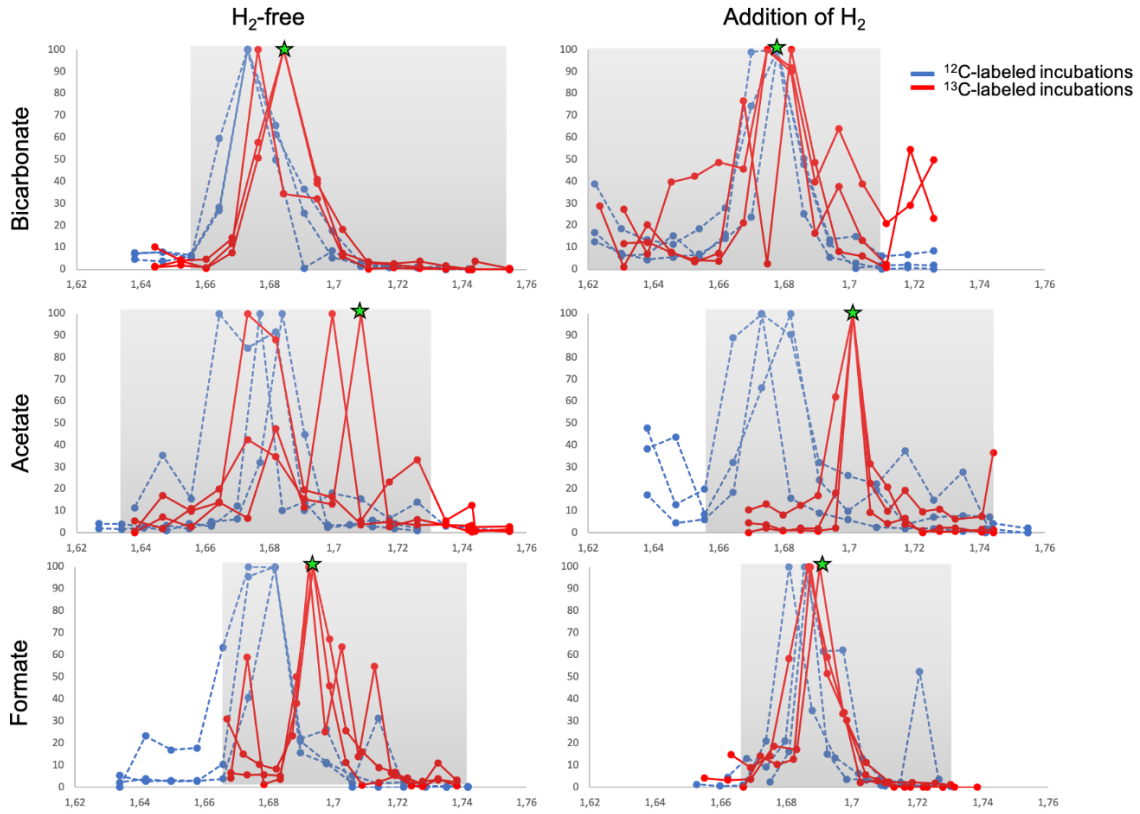

Figure S1: Quantification of 16S rRNA gene copies across CsCl density gradient fractions fractionated from incubations amended with bicarbonate, acetate and formate in the presence or absence of molecular H_2. ^{13}C-substrates are represented by red solid lines and unlabeled replicates (control) are represented by blue dashed lines. The y axis represents the relative abundance of 16S rRNA genes quantified with qPCR, normalized to maximal abundance across all density fractions. The green stars show the fractions that were used for metagenomic library preparation.

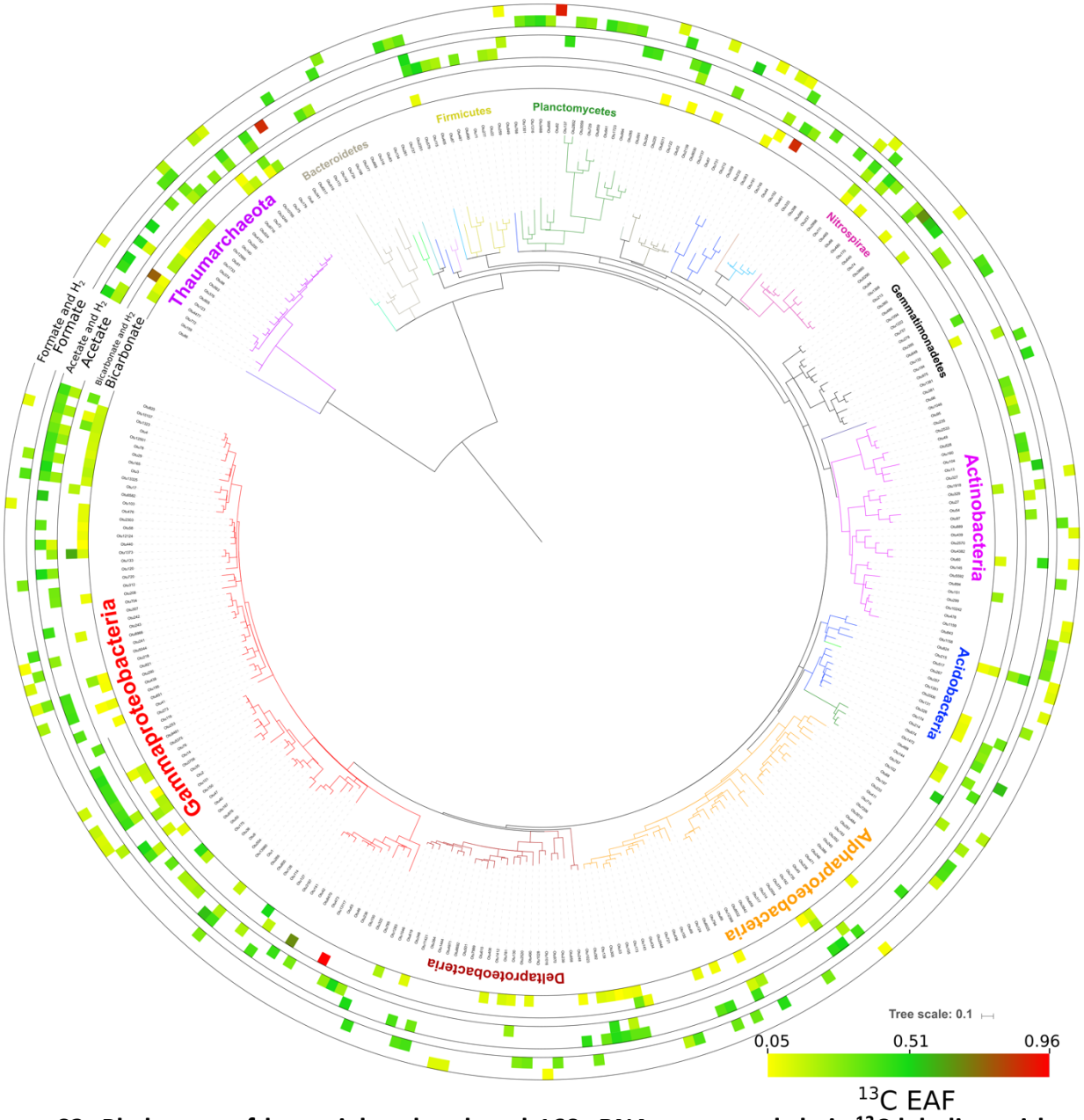

Figure S2: **Phylogeny of bacterial and archaeal 16S rRNA genes and their ^{13}C-labeling with and without hydrogen.** The heat blocks correspond to excess atom fraction (EAF) of ^{13}C-labeled OTUs and represent the following incubations from inner circle to outer: bicarbonate, bicarbonate amended with H_2, acetate, acetate amended with H_2, formate and formate amended with H_2.

Chapter 3

Quantifying population-specific growth in benthic bacterial communities under low oxygen using $H_2{}^{18}O$

Ömer K. Coskun[1], Volkan Özen[1], Scott D. Wankel[2], William D. Orsi[1,3,§]

[1] Department of Earth and Environmental Sciences, Paleontology and Geobiology, Ludwig-Maximilians-Universität München, 80333 Munich, Germany

[2] Department of Marine Chemistry and Geochemistry, Woods Hole Oceanographic Institution, Woods Hole, MA 02543, USA

[3] GeoBio-Center, Ludwig-Maximilians-Universität München, 80333 Munich, Germany

[§]Corresponding author: w.orsi@lrz.uni-muenchen.de

Published in: **The ISME Journal, Nature Publishing Group**

Accepted: 31 January 2019

3.1 Abstract

The benthos in estuarine environments often experiences periods of regularly occurring hypoxic and anoxic conditions, dramatically impacting biogeochemical cycles. How oxygen depletion affects the growth of specific uncultivated microbial populations within these diverse benthic communities, however, remains poorly understood. Here, we applied $H_2{}^{18}O$ quantitative stable isotope probing (qSIP) in order to quantify the growth of diverse, uncultured bacterial populations in response to low oxygen concentrations in estuarine sediments. Over the course of 7- and 28-day incubations with redox conditions spanning from hypoxia to euxinia (sulfidic), ^{18}O labeling of bacterial populations exhibited different patterns consistent with micro-aerophilic, anaerobic, facultative anaerobic, and aerotolerant anaerobic growth. ^{18}O-labeled populations displaying anaerobic growth had a significantly non-random phylogenetic distribution, exhibited by numerous clades currently lacking cultured representatives within the Planctomycetes, Actinobacteria, Latescibacteria, Verrucomicrobia, and Acidobacteria. Genes encoding the beta-subunit of the dissimilatory sulfate reductase (*dsrB*) became ^{18}O labeled only during euxinic conditions. Sequencing of these ^{18}O-labeled *dsrB* genes showed that Acidobacteria were the dominant group of growing sulfate-reducing bacteria, highlighting their importance for sulfur cycling in estuarine sediments. Our findings provide the first experimental constraints on the redox conditions underlying increased growth in several groups of "microbial dark matter", validating hypotheses put forth by earlier metagenomic studies.

3.2 Introduction

Benthic microbial communities living in estuarine ecosystems play an important role in global biogeochemical cycles, because they drive organic matter decomposition, nutrient regeneration, and influence water column dissolved O_2 concentrations (Boynton and Kemp 1985; Nixon 1981). Benthic oxygen depletion is typical in estuarine habitats, where degradation of organic matter is 100–1000 times higher than corresponding values in the water column (Glud 2008). The resulting hypoxia impacts both fisheries by increasing fish mortality (Diaz and Rosenberg 2008), as well as climate by facilitating increased fluxes of the greenhouse gas nitrous oxide (Middelburg et al. 1995).

Estuarine sediments have complex microbial communities composed primarily of uncultured lineages catalyzing aerobic, micro-aerophilic, and anaerobic metabolic pathways that impact carbon, nitrogen, and sulfur cycling (Baker et al. 2015). Quantifying growth of specific bacterial populations is challenging, yet critical for understanding of ecosystem resilience and response to change (Luna et al. 2002). The structure of microbial communities in estuarine habitats can exhibit resistance to environmental perturbation (Bowen et al. 2011), but the levels of activity within populations can change dramatically in response to changing nutrients and oxygen levels, with clear impacts on biogeochemical cycles (Kearns et al. 2016).

The activity of growing microbial populations in environmental samples can be quantified using quantitative DNA-stable isotope probing (qSIP) with $H_2{}^{18}O$ as a passive tracer (Schwartz 2007).

Oxygen atoms from $H_2{}^{18}O$ are incorporated into DNA during genome replication, which when combined with quantitative PCR (qPCR) and high-throughput sequencing of 16S rRNA genes can be used to quantify activity of growing populations within complex microbial communities from environmental samples (Blazewicz et al. 2014; Schwartz et al. 2016). Relative to energy-rich ^{13}C-labeled carbon substrates, labeled water is a passive tracer of cell growth, whereby DNA replication generates a new DNA strand that will contain ^{18}O atoms in the presence of labeled water (Schwartz et al. 2016). The amount of ^{18}O incorporated into the total DNA pool is correlated with growth rates (Blazewicz et al. 2014; Schwartz et al. 2016; Hungate et al. 2015), showing that ^{18}O labeling occurs primarily during growth via DNA replication (Schwartz et al. 2016). The degree of atomic incorporation can then be used as a quantitative proxy for growth (Hungate et al. 2015). qSIP with $H_2{}^{18}O$ has been applied to terrestrial habitats (Woods et al. 2011; Schwartz et al. 2014; Papp et al. 2018), including freshwater sediments (Hayer et al. 2016). But, to our knowledge, $H_2{}^{18}O$ qSIP has not yet been applied to quantify growth in estuarine sediments or under anoxic conditions.

We used $H_2{}^{18}O$ qSIP (Hungate et al. 2015) to quantify for the first time population-specific growth dynamics in benthic bacterial communities in response to changing redox conditions. This allowed us to test hypotheses regarding the potential physiology of several groups of uncultivated microbial groups put forth by earlier metagenomics studies, which suggested an adaptation to low oxygen and anoxic aquatic environments (Baker et al. 2015; Rinke et al. 2013). Our results showed that hypoxia and euxinia selected for specific phylogenetic groups of uncultivated bacteria whose metabolic activity was increased, providing evidence of their optimal redox conditions for growth. Notably, establishment of benthic anoxia coincided with increased growth from numerous uncultivated groups of sulfate-reducing bacteria (SRB) that were dominated by the Acidobacteria, which should thus be more closely considered as an important SRB group impacting sulfur cycling in estuarine sediments. Our experimental findings validate prior hypotheses put forth by metagenomics studies indicating micro-aerophilic and anaerobic lifestyles for many groups of “microbial dark matter (MDM)”.

3.3 Materials and methods

3.3.1 Sampling

Surface sediment samples were collected in July 2016 from 1 m water depth in Sage Lot pond, a coastal lagoon connected as a sub-estuary to Waquoit Bay (Cape Cod, Massachusetts). Sage Lot pond is a small (surface area 0.17 km^2) shallow (ca. 2 m maximum depth) lagoon surrounded by dense vegetation including salt marshes and seagrasses (Valiela et al. 1992; Wang et al. 2016). Sage Lot pond exhibits phytoplankton chlorophyll concentration up to 90 mg L-1 when nitrogen inputs increase (Valiela et al. 1992). These eutrophic conditions lead to frequent benthic anoxic events (Valiela et al. 1992).

3.3.2 Experimental setup

We added sea salts (30 mM $MgCl_2 \cdot 6H_2O$, 16 mM $MgSO_4 \cdot 7H_2O$, 2 mM $NaCO_3$, 10 mM KCl, 9 mM $CaCl_2$, 450 mM NaCl) to 99% $H_2{}^{18}O$ (Sigma-Aldrich, St. Louis, MO, USA) in order to create ^{18}O-labeled artificial seawater (ASW). As a control, ASW was also created using diethyl pyrocarbonate (DEPC)-treated (sterile, nuclease free) water. Both waters were filter sterilized (0.2 µm). One milliliter of either ^{18}O-labeled or -unlabeled (control) ASW was added to 2 g of wet surface sediment from Sage Lot Pond in 20 mL sterile glass vials containing sterile oxygen sensor spots (PreSens Precision Sensing). The oxygen sensor spot was positioned at the sediment-seawater interface to measure benthic O_2 concentrations, and additional sensor spots were placed in the headspace of two flasks to measure gaseous O_2 levels throughout the incubation. Incubations were set up in biological triplicate for each timepoint (7 day and 28 day). The water content of the sediments was 15% (±1%), and thus the final concentration of $H_2{}^{18}O$ in the $H_2{}^{18}O$ incubations was roughly 66%. After addition of labeled and unlabeled ASW, flasks were crimp sealed with gas tight gray butyl rubber stoppers. All flasks contained ca. 15 cm of oxygenated headspace and were incubated in the dark for 7 and 28 days at 8 °C. Dissolved oxygen was measured noninvasively using a fiber optic oxygen sensor (PreSens, Regensburg Germany) ca. 0.5 cm above the sediment-water interface as described previously (Ortega-Arbulú et al. 2019). Oxygen measurements were also performed on autoclaved sediments as a killed control. DNA from the samples was extracted and quantified from the replicate incubations at the beginning (T_0), 7 days, and 28-day timepoints as described previously (Orsi et al. 2018).

3.3.3 Density gradient centrifugation and gradient fraction

DNA samples were prepared for density gradient centrifugation according to previously defined protocol for qSIP (Coskun et al. 2018). In brief, density gradient centrifugations were carried out in a TLN-100 Optima MAX-TL ultracentrifuge (Beckman Coulter, Brea, CA, USA) near-vertical rotor at 18 °C for 72 h at 165,000 × g. In all, 50 µl of DNA spanning from 0.5 to 1.5 µg (Dunford and Neufeld 2010) was added to a solution of cesium chloride (CsCl) and gradient buffer (0.1 M Tris, 0.1 M KCl and 1 mM EDTA) in order to achieve a starting density of 1.70 g mL^{-1} in a 3.3-mL polyallomer OptiSeal tubes (Beckman Coulter, Brea, CA, USA). After ultracentrifugation, the density gradients were fractionated into 15 equal fractions of 200 µl from the bottom of polyallomer OptiSeal tubes by using a syringe pump and fraction recovery system (Beckman Coulter, Brea, CA, USA). The density of these fractions was measured with an AR200 digital refractometer (Reichert Analytical Instruments, Depew, NY, USA). DNA was precipitated from the fractions using two volumes of polyethylene glycol with 2 µl (10 mg mL^{-1}) glycogen and precipitated overnight at room temperature. DNA was pelleted by centrifugation (13,000 × g; 40 min), washed with 70% ethanol, and resuspended with 30 µl molecular-grade (DEPC-treated) water. DNA was quantified fluorometrically using a Qubit 4 fluorometer (Thermo Scientific).

3.3.4 qPCR, 16S rRNA gene, and *dsrB* gene sequencing

Universal primers targeting the V4 hypervariable region of 16S ribosomal RNA (rRNA) genes were used in qPCR to determine density shifts of key genes (16S and *dsrB*) for each incubation. We used a version of the 16S rRNA gene 515F primer with a single-base change (in bold) to increase the

coverage of archaea (515F-Y, 5'-GTGYCAGCMGCC GCGGTAA-3'; (Parada et al. 2016)). All qPCR reactions were carried out as described previously using the Eppendorf EpMotion 5070 pipetting robot that has <5% technical variation (Coskun et al. 2018). Each density fraction was also screened using qPCR for SRB with primer pairs targeting the dissimilatory sulfite reductase β-subunit genes (*dsrB*) according to a previously published assay (Jochum et al. 2017; Rotthauwe et al. 1997; Geets et al. 2006). We chose to focus on the *dsrB* gene because a large database exists for *dsrB* sequences recovered from environmental samples that we could compare our data against (Müller et al. 2015) (www.microbial-ecology.net/download). qPCR standards consisted of 10-fold dilution series of the genes of interest that were PCR amplified from the sample at 40 cycles using the same primers. Prior to creating the dilution series, the correct size of amplified standard was confirmed via gel electrophoresis, gel extracted, and quantified with a Qubit. Reaction efficiencies in all qPCR assays were between 90 and 110% with $r^2 > 0.98$ for the standards. *dsrB* amplicons were cloned and sequenced via sanger sequencing from density fractions at the 28-day incubation timepoint that exhibited ^{18}O labeling, in the density range 1.70–1.71 g mL^{-1}.

Two 16S PCR amplicons from each density fraction (technical replicates to reduce PCR bias) were pooled and sequenced on the Illumina MiniSeq as described previously (Pichler et al. 2018). To account for the influence of contamination, we included barcoded aerosol (laboratory dust) and kit reagents (DNA extraction blanks) samples.

dsrB amplicons were gel extracted and cloned using the TOPO TA cloning kit (Invitrogen, Life Sciences) according to the manufacturer instructions. A total of 132 clones were picked, the insert size confirmed via PCR, and those clones having the correct *dsrB* size (89 clones) were Sanger sequenced bidirectionally. The forward and reverse Sanger reads were used to create *dsrB* contig sequences in CodonCode Aligner version 8.0.2 (CodonCode Corporation, MA, USA).

3.3.5 Bioinformatic analysis

The Illumina reads were quality trimmed and assembled using USEARCH version 10.0.240 with the default parameters (Edgar 2010) resulting in 6.8 million quality checked V4 reads. Reads were then de novo clustered at 97% identity using UPARSE; OTUs represented by a single sequence were discarded (Edgar 2013). Taxonomic assignments were generated by QIIME 1.9.1 (Caporaso et al. 2010) using the implemented BLAST method against the SILVA rRNA gene database release 132 [34]. After that, only operational taxonomic units (OTUs) >12 sequences in total in each replicate for the control and SIP-labeled fractions were selected for further study (Coskun et al. 2018; Orsi et al. 2016). OTUs detected in the contaminant datasets were removed from all downstream analysis if the total number of sequences in the contaminant sample was greater than the experimental sample. Working with this "cleaned" dataset, 598 OTUs and 523 OTUs from 7 days and 28 days incubations were used for downstream analyses.

Observed excess atom ^{18}O fractions (EAFs) were calculated for each taxon as described previously (Hungate et al. 2015) using a qSIP workflow embedded in the HTS-SIP R package (Youngblut et al.

2018a). To calculate the bootstrap confidence intervals (CI) for significant isotopic incorporation, bootstrap replicates (n = 1000) were run with the HTS-SIP R package (Youngblut et al. 2018a); an OTU was considered as having isotopic incorporation (true positive) if the lower CI was >0 (Hungate et al. 2015).

Phylogenetic analyses were performed in SeaView (Gouy et al. 2010) following alignment with MUSCLE (Edgar 2004). Maximum likelihood (ML) with selected substitution model as general time reversable (GTR) was performed with PhyML version 3.0 (Guindon et al. 2010). *dsrB* gene translation was performed using EMBOSS Transeq (Rice et al. 2000). W-IQ-TREE (http://iqtree.cibiv.univie.ac.at) was used to find the best model using Model Finder (Trifinopoulos et al. 2016; Kalyaanamoorthy et al. 2017), which resulted in LG + G4 model. Trees were visualized and edited using iTOL (Letunic and Bork 2016). Statistical analyses and plots were performed using R.Studio Version 3.3.0 (Team and Others 2015). Blomberg'sK (Blomberg et al. 2003) and Pagel's λ (Pagel 1999) tests for significantly nonrandom phylogenetic distributions of growing patterns from qSIP were calculated on all OTUs (labeled and unlabeled) using the phylosignal R package (Keck et al. 2016). Both indices test species' traits under a Brownian motion model (BM) of trait evolution; that is whether or not the distribution of traits across different phylogenetic groups is random or nonrandom. The BM assigns a 0 value to indicate phylogenetic independence (random phylogenetic distribution of traits) and values close to 1 for a strong phylogenetic signal (nonrandom phylogenetic distribution of traits) (Morrissey et al. 2016; Morrissey et al. 2018; Morrissey et al. 2017).

The sizes of the growing and dying fractions of each population, and their rates of change, was calculated using a model developed to determine population growth and mortality rates from ^{18}O-qSIP data (Koch et al. 2018). For all calculations, bootstrap resampling of replicates within each treatment was used to reproduce the uncertainty and 90% CIs were estimated. These calculations were performed in R using the code at https://bitbucket.org/QuantitativeSIP/qsip_repo (Koch et al. 2018). Sequence data were entered in the NCBI Short Read Archive under BioProject ID PRJNA498588.

3.4 Results

3.4.1 Dissolved oxygen measurements

The sediment-water interface was well-oxygenated at the beginning of the incubation (70% atm. saturation), which declined exponentially during the first week until reaching 0% atm. saturation after day 5 (Fig. 1a). This was not observed in the killed control, showing that the rapid drawdown of benthic O_2 was due to respiration. Small fluctuations in the oxygen measurements in the killed control were likely due to temperature fluctuations of the incubator itself (±1 °C), since the non-invasive fiber optic oxygen sensor spots are temperature sensitive (Ortega-Arbulú et al. 2019). By the end of the experiment (28 days), the sediments had turned from a gray-brown color to black, indicating the presence of iron–sulfur minerals (e.g., FeS and FeS_2), and upon opening the vials

sulfide could be smelled. Thus, while the headspace contained oxygen at the beginning of the experiment, the sediments had become anoxic and sulfidic (euxinic) by the end of the incubation period.

3.4.2 qSIP of 16S rRNA genes

^{18}O labeling of 16S rRNA genes was observed at 7 and 28 days, with 16S rRNA genes at 28 days exhibiting a higher degree of labeling compared with 7 days (Figs. 1b, c). The decrease in oxygen (Fig. 1a) was mirrored by a decrease in 16S rRNA gene copies: the total number of 16S rRNA gene copies per gram wet sediment decreased during the first week, from 2.5 (± 0.12) × 10^8 at T_0 to 1.4 (± 0.09) × 10^8 at 7 days, and then decreased further after 28 days to 1.1 (± 0.04) × 10^8 . This indicated net microbial death with a fraction of the community maintaining growth during the incubation.

The composition of microbial populations at 7 and 28 days were markedly different (analysis of variance; $F = 3991$, $p < 0.001$), but dominated by the same phyla in nearly equal proportion (Figure S1). In total, 443 OTUs were detected at both timepoints, whereas 235 OTUs were detected at only a single timepoint (Figure S1). In all, 128 OTUs were ^{18}O labeled after 7 days, which increased to 395 OTUs after 28 days (Figure S1). Of the ^{18}O-labeled OTUs at day 7, Bacteroidetes were the most abundant taxa with 67 OTUs (49.4% of the ^{18}O-labeled OTUs), followed by 39 OTUs affiliated with Proteobacteria (42.1% of the ^{18}O-labeled OTUs) (Fig. 2 and S1). On the other hand, the 395 ^{18}O-labeled OTUs at day 28 were comprised mostly of Proteobacteria (157 OTUs, 61.4% of ^{18}O-labeled OTUs), followed by Bacteroidetes (94 OTUs; 18.1% of ^{18}O-labeled OTUs) and Planctomycetes (53 OTUs; 8.71% of ^{18}O-labeled OTUs) (Fig. 2 and S1).

Although the scope of this study is to determine the growing microorganisms, non-growing cells due to dormancy and or slow growing cells are represented in our results as those OTUs that did not become labeled. Accordingly, a total of 248 OTUs constituted non-growing microbes (unlabeled) in both incubations (Fig. 3). The nongrowing or slow growing bacterial groups were dominated by OTUs affiliated with sulfate-reducing lineages in the Deltaproteobacteria (42 OTUs), Planctomycetes (38 OTUs), Epsilonbacteraeota (7 OTUs), and Spirochaetes (9 OTUs) (Fig. 3).

Growing bacterial OTUs affiliated with MDM (Rinke et al. 2013) candidate phyla Aegiribacteria (1 OTU, 0.08 EAF) and Patescibacteria (1 OTU, 0.04 EAF) were detected only in the 7-day incubations (Fig. 2 and Table 1). Labeled OTUs affiliated with MDM groups after 28 days included Latescibacteria (10 OTUs, 0.24 ± 0.04 EAF) and Calditrichaeota (1 OTU, 0.24 EAF). The only MDM group that was ^{18}O labeled at both 7- and 28-day timepoints was the candidate phylum WPS-2 (Fig. 2 and Table 1).

The change in oxygen concentrations over the course of the experiment allowed us to group OTU growth into five categories based on the pattern of ^{18}O labeling at 7 days (micro-oxic conditions) and 28 days (anoxic conditions) (Fig. 3) [1]. Micro-aerophilic growth was defined as ^{18}O-labeled OTUs detected only at day 7, and not at 28 days [2]. Anaerobic growth was defined as ^{18}O-labeled OTUs detected only after establishment of euxinic conditions at day 28, and not at 7 days [3]. Facultative anaerobic growth was defined as ^{18}O-labeled OTUs overlapping between both timepoints [4].

Aerotolerant anaerobic growth was defined as OTUs detected at both timepoints, but only ^{18}O labeled during anoxic and sulfidic conditions [5]. Dormant or slow growing microorganisms were defined as OTUs that were not ^{18}O labeled at either timepoint.

3.4.3 ^{18}O labeling of *dsrB* genes

Bacterial *dsrB* genes exhibited ^{18}O labeling only after development of euxinic conditions sampled at 28 days of incubation, with peak DNA buoyant density (BD) of 1.71 (±0.008) g mL^{-1}, which was greater than the control where the peak was 1.686 (±0.003) (Fig. 4a). This corresponds to an increase in the atomic enrichment percentage of >20%, which is typically regarded as the threshold for significant isotopic labeling (Lueders 2015). In total, 89 *dsrB* sequences were obtained by molecular cloning from the density fractions that exhibited peak ^{18}O labeling (Fig. 4a). Most of the ^{18}O-labeled *dsrB* sequences were affiliated with novel groups of uncultivated Acidobacteria SRB (61 sequences, 82% of total), whereas the remainder of ^{18}O-labeled *dsrB* sequences (13 sequences, 18% of total) were related to Deltaproteobacteria SRB (Fig. 4b). The ^{18}O-labeled Acidobacteria *dsrB* genes include a clade of four *dsrB* sequences with close relation to a novel clade of SRB originally described as "novel dsrB Group IV" from the Guaymas hydrothermal vent (Dhillon et al. 2003), raising the possibility that this group of Acidobacteria contains both thermophilic and mesophilic SRB.

3.4.4 Growth and death dynamics of ^{18}O-labeled populations

After 7 days, most genera exhibited gross reproduction and three OTUs exhibited significant net production (defined as 90% CI in the growth/death model not overlapping 0), affiliated with Sva0081 sediment group (Desulfobacteraceae), *Desulfobacterium catecholicum*, and SB-5 family of Bacteroidetes (Fig. 5). The rate of mortality per genus was higher at day 28 than day 7, indicating that establishment of euxinic conditions caused the majority of cells per genus to die faster than they grew (Fig. 5). However, despite the higher net mortality rates, many exhibited relatively low positive gross reproduction rates (Fig. 5) indicating that a smaller proportion of individuals per population were actively growing. This is consistent with the result that most of the OTUs were ^{18}O labeled at this timepoint. We also calculated the whole-assemblage turnover estimated via qSIP using the developed model of Koch *et al.* (Koch et al. 2018). The seven-day incubation had an average community turnover value of 0.28 d^{-1} (90% CI: 0.219–0.36 d^{-1}), whereas 28 days of incubation had an average community turnover value of 0.371 d^{-1} (90% CI: 0.315–0.476 d^{-1}).

3.5 Discussion

Dissolved oxygen has declined in ocean water in the past five decades due to the increase in global temperature (Schmidtko et al. 2017), resulting in the expansion of oxygen minimum zones (OMZs) in the oceans (Wright et al. 2012). In coastal settings, increased human activity such as high fertilizer use has caused widespread eutrophication and recurrent bottom water anoxia that influences the benthos (Valiela et al. 1992; D'Avanzo and Kremer 1994; Kemp et al. 2005). The effects of such benthic anoxia on the growth of diverse bacterial populations driving elemental cycles is poorly understood. We used ^{18}O-qSIP to quantify for the first time to quantify the growing bacterial

populations in response to benthic oxygen depletion, including many groups for which there currently exists no cultured representatives.

3.5.1 Assessing effects of incubation conditions

Although the sediment surface became oxygen depleted after 5 days of incubation, there was an oxygenated headspace, and O_2 measurements of the headspace confirmed oxygen throughout the 28-day incubations at concentrations of 90–80% atmospheric saturation (data not shown). The gradual depletion of oxygen at the benthic interface during the first week thus indicates a shoaling of the oxic–anoxic transition zone within the sediments into the overlying ASW. Benthic anoxia is a common feature of the sampled environment in Waquoit Bay (Cape Cod, USA), where increased nitrogen input to the watershed through atmospheric deposition, fertilizer, and wastewater has led to an increase in primary productivity and recurrent bottom water anoxia (Valiela et al. 1992; D'Avanzo and Kremer 1994). This phenomenon is also known to occur in the marine environment, for example, in the Benguela upwelling system where summer time water column stratification results in a shoaling of the sediment oxic–anoxic transition zone several meters upwards into the bottom waters and where sulfide accumulates to high levels on the continental shelf (Lavik et al. 2009). Thus, our experimental conditions are relevant to naturally occurring benthic habitats in estuaries and continental shelf settings that are especially prone to the development of anoxia. Dormancy by anaerobic bacteria during periods of oxygenation at the sediment surface may explain how they survive until favorable anoxic conditions are re-established, for example, after burial deep below the subseafloor in anoxic sediments (Orsi 2018).

Given the detection limit of the fiber optic oxygen measurements (ca. 0.5 % atmospheric saturation), we cannot rule out the presence of trace amounts of dissolved oxygen within the overlying seawater or sediment. Nevertheless, the appearance of black color throughout the sediments and the strong smell of sulfide at the end of the 28-day incubation strongly indicated anoxic conditions in the sediments by the end of the experiment. The strong smell of sulfide suggests that the black color reflected formation of amorphous iron–sulfur compounds, caused by a reaction between oxidized Fe (III) with HS^- (Rickard and Luther 2007). As we sampled the entire sediment slurry for our qSIP analysis, we likely sampled a mixture of both anoxic and micro-aerophilic habitats that were present as a steep redox gradient within the flasks. Therefore, the active microbes detected at 7 days probably represent microaerophilic bacteria, whereas active microbes sampled at 28 days were living under predominantly anoxic and sulfidic conditions.

It is likely that anoxic microsites likely developed within the sediment in the first 7 days, potentially complicating the categorization of aerobic, facultatively anaerobic, and aerotolerant growth in OTUs detected at this timepoint. Anaerobic SRB can remain active in oxidized marine sediments within anoxic microniches (Jørgensen 1977), but some SRB are aerotolerant since they can grow (albeit slightly) in the presence of oxygen [reviewed in (Rabus et al. 2015)]. The total area occupied by anoxic microsites should be much smaller compared with the rest of the bulk sediment sampled that experienced oxygen during the first 7 days. Thus, the dominant OTUs detected at day 7 are unlikely

to be those living in anoxic microsites. But, it is possible that some strictly anaerobic populations survived at low abundance under oxygen exposure during the first 7 days within anoxic microsites.

It is also likely that after the 28 days of incubation the label turned over, and a second generation of microbial cells became labeled not only from ^{18}O water but also from ^{18}O-labeled organic compounds that formed earlier. In this case, some of the labeling detected at the 28-day timepoint could have been due to assimilation of ^{18}O-labeled organic compounds. However, the concentration of any ^{18}O transferred to organic matter would be diluted within the much larger (unlabeled) dissolved organic matter pool. This would then be further diluted several orders of magnitude by the ^{18}O label in the water that was present at a molar concentration. Thus, the potential assimilation of ^{18}O-labeled organic compounds is unlikely to affect the conclusion that the degree of ^{18}O labeling is a measure of assimilation of ^{18}O from water, and thus activity, in growing populations.

3.5.2 Phylogenetic grouping of redox-specific activities

The oxygenated concentrations during the first week and development of anoxic and sulfidic conditions at 28 days allowed us classify ^{18}O-labeled OTUs detected between these two timepoints into four categories of growth (Fig. 3) [1]; micro-aerophilic growth [2], facultative anaerobic growth [3], anaerobic growth, and [4] aerotolerant anaerobic growth (see Results for category definitions). The non-growing microorganisms were also considered as an additional category [5]: dormant or slow-growers. We recognize that because oxygen was present in the headspace throughout the incubation, strict anaerobic growth cannot be unequivocally assigned to the OTUs. But, given the increase in their growth later in the incubation after the onset of euxinic conditions at the sediment-water interface were established, we interpret this as an indicator of anaerobic growth. We also recognize that our designation of facultative versus aerotolerant anaerobic growth is arbitrary, but is used here to differentiate between those OTUs labeled at day 28 present also at day 7 that were, or were not, ^{18}O labeled at day 7.

OTUs exhibiting micro-aerophilic growth had a relatively weak phylogenetic distribution across the phylogeny ($\lambda = 0.38$) (Fig. 3). In contrast, ^{18}O-labeled OTUs exhibiting anaerobic growth corresponded to non-random phylogenetic groupings ($\lambda = 0.9$ and 0.87, respectively), implying that traits conferring anaerobic growth were conserved in the sampled communities. ^{18}O-labeled organisms detected at both timepoints (facultative anaerobes) did not display a significant phylogenetic pattern ($\lambda = 0.16$), suggesting that facultative anaerobic growth was not a conserved trait in our sampled communities.

3.5.3 Populations exhibiting micro-aerophilic growth

A total of 47 OTUs affiliated with orders Flavobacteriales and Chitinophagales within the phylum Bacteroidetes were the most active growing bacteria after 7 days, maintaining metabolic activity under suboxic conditions. Similarly, seven OTUs affiliated with order Anaerolineae (Chloroflexi) were ^{18}O labeled at day 7 (0.08 ± 0.008 EAF). Furthermore, 26 OTUs affiliated with Gammaproteobacteria

(mainly orders Cellvibrionales and Thiotrichales) were labeled at day 7, and demonstrated relatively high EAF values (0.102 ± 0.031) indicating micro-aerophilic growth (Fig. 3).

^{18}O-labeled OTUs affiliated with candidate class Gracilibacteria were observed solely at day 7, consistent with a micro-aerophilic growth (Table 1). Gracilibacteria have a cytochrome/quinol oxidase (Rinke et al. 2013), most specifically cytochrome bd, which is implicated in ameliorating oxidative stress effects [reviewed in (Giuffrè et al. 2014)]. Cytochrome *bd* could thus help to explain the higher growth of Gracilibacteria under low oxygen conditions.

3.5.4 Populations exhibiting anaerobic growth

There were 256 OTUs that exhibited a pattern of ^{18}O labeling consistent with aerotolerant anaerobic growth (Fig. 3). They are apparently capable of surviving in the presence of oxygen during the beginning of the incubation, but their growth was maximized under anoxic conditions. The majority of these OTUs were affiliated with the Gammaproteobacteria (69 OTUs; 0.18 ± 0.06 EAF) and Deltaproteobacteria (19 OTUs; 0.29 ± 0.02 EAF). The highest ^{18}O-labeled OTU was affiliated with genus Zhongshania that contains the facultative anaerobic heterotrophic species Zhongshania aliphaticivorans SM-2^{T} (Jia et al. 2016). In addition, one of the ^{18}O-labeled Gammaproteobacteria OTUs was affiliated with the JTB255/Woesiaceae clade, which have been identified as the most dominant dark carbon-fixing microbes with a capacity to oxidize reduced sulfur compounds in anoxic and suboxic coastal sediments (Dyksma et al. 2016). The genus Sandaracinus in Deltaproteobacteria known to degrade complex polysaccharides (Garcia and Müller 2014), also exhibited aerotolerant anaerobic growth. At day 28 after the onset of euxinic conditions, 10 OTUs affiliated with the Latescibacteria were detected that grew anaerobically (Table 1). This is consistent with their proposed fermentative mode of metabolism in anoxic sediment and water columns (Rinke et al. 2013; Youssef et al. 2015).

OTUs affiliated with the known SRB genera (Wasmund et al. 2017) *Desulforhopalus, Desulfosarcina, Desulfobulbus, Desulfopila, Desulfobacter, Desulfotignum,* and *Desulfatitalea* were well-represented comprising 9% (42 OTUs) and 8% (26 OTUs) of the total sequences at days 7 and 28, respectively. However, only one SRB OTU was ^{18}O labeled, which occurred at day 7 and was affiliated with the SRB genus *Desulfobulbus* (0.10 EAF). The relatively small number of growing Deltaproteobacteria SRB is low compared with the more numerous populations of sulfate-reducing Acidobacteria that have higher ^{18}O EAF values (Figs. 3, 4). This indicates that these anaerobic Acidobacteria SRB were growing faster compared with the Deltaproteobacteria SRB.

Acidobacteria belong to several newly discovered groups of SRB, showing that dissimilatory sulfur metabolism is more widespread than previously thought (Müller et al. 2015; Anantharaman et al. 2018). For example, Acidobacteria with a dissimilatory sulfur metabolism have been recently identified in acidic peatland (Anantharaman et al. 2018; Hausmann et al. 2018) and a DNA-SIP study (Pester et al. 2010) showed activity of *dsrAB*-containing organisms derived from Acidobacteria (Hausmann et al. 2018). Our study shows that in addition to acidic peatland, *dsrB* carrying Acidobacteria grow in anoxic estuarine sediments with a relatively fast rate. Their increased growth

rate and activity compared to Deltaproteobacteria SRB shown here implies that they should have a large impact on dissimilatory sulfur cycling under anoxic conditions.

Our finding that the majority of deltaproteobacterial sulfate reducers had minimal growth is in line with the previous reports that their mean in situ doubling times are on the order of months to years (Hoehler and Jørgensen 2013). Metabolic activity (e.g., rRNA synthesis) in natural microbial communities is typically followed by cell division (Papp et al. 2018), but metabolic activity of non-growing organisms can also influence biogeochemical cycles (Hoehler and Jørgensen 2013). For example, the increase in activity of SRB Candidatus Desulfosporosinus infrequens can occur independent of cell growth-associated processes (Hausmann et al. 2019). Thus, the low degree of ^{18}O labeling in abundant deltaproteobacteria SRB seen in our study (Fig. 3) may relate to a different ecophysiological strategy (e.g., slow growth) compared with the faster growing Acidobacteria SRB.

Within the Planctomycetes, members of the uncultured OM190 clade were abundant (44% total Planctomycetes) and only became ^{18}O labeled at day 28 (Fig. 3), indicating anaerobic growth. Representatives of the OM190 clade closely related to anaerobic ammonia oxidizing bacteria (anammox) were also detected in hypoxic estuarine surface sediments in the East China Sea (Ye et al. 2016). The anaerobic growth of OM190 clade organisms seen here is consistent with a potential anammox metabolism.

The ^{18}O-labeled Actinobacteria were dominated by OTUs most closely related to the enigmatic Sva0996 actinobacterial clade first described from marine sediments (Ravenschlag et al. 1999), the "*Candidatus* Actinomarinales" (Ghai et al. 2013), and *Rhodococcus*. While aerobic growth of *Rhodococcus* is well known as it relates to hydrocarbon degradation (Rosenberg 2006), our results showing facultative anaerobic growth indicate that Rhodococcus has potential to degrade hydrocarbons also under anoxic conditions in sediments. A facultative anaerobic lifestyle also explains why *Rhodococcus* are often found in deep subseafloor anoxic marine sediments (Inagaki et al. 2003).

The ^{18}O-labeled Verrucomicrobia were dominated by OTUs affiliated with the uncultured DEV007 clade, first reported from the Elbe River in Germany (unpublished data, accession number: AJ401107). ^{18}O-labeled OTUs affiliated with DEV007 were labeled at 7 days and became increasingly labeled after 28 days and the establishment of anoxic conditions (Fig. 2). This is consistent with biogeographic surveys that have detected this group in anoxic estuarine sediments (unpublished data, accession number: JN672646), OMZs (unpublished data, accession number: MG875625), and marine sediments (Cornall et al. 2016). However, the DEV007 clade is also found in oxic seawater attached to particles (Orsi et al. 2016). Our ^{18}O labeling results showing a facultative anaerobic growth of the DEV007 clade explains this wide biogeographic range.

An OTU affiliated with the WPS-2 (Writtenberg Polluted Soil) clade was the only MDM group exhibiting facultative anaerobic growth (Fig. 2). The WPS clade was first described in a study of polychlorinated biphenyl-polluted soil in Germany (Nogales et al. 2001) and was since detected in a wide range of oxic and anoxic environments (Camanocha and Dewhirst 2014). The facultatively

anaerobic growth shown here could potentially explain the ability of the WPS-2 group to survive in a large number of habitats with widely varying redox states.

3.5.5 Growth and death dynamics of ^{18}O-labeled populations

Although total microbial abundance decreased over the incubation by nearly an order of magnitude, 16S rRNA genes became increasingly enriched in ^{18}O (Fig. 1c). This raised the possibility that within populations, a high number of cells were dying while a smaller number were growing. In order to investigate this possibility further, we applied a model (Koch et al. 2018) that uses the ^{18}O-qSIP data to calculate the number of ^{18}O-labeled and -unlabeled 16S rRNA genes per OTU and the changes in their ratio over time to estimate rates of gross reproduction, mortality, and net production of individual OTUs (Fig. 5). After seven days, only three OTUs exhibited net production (defined as net production 90% CI not overlapping zero), which were affiliated with the Sva0081 sediment group (Desulfobacteraceae), *Desulfobacterium catecholicum*, and SB-5 family of Bacteroidetes. Our analysis suggests that the Sva0081 marine benthic group (MBG), a putative group of SRB that are an important sink of acetate (Dyksma et al. 2018a) and H_2 (Dyksma et al. 2018b) in coastal marine sediments, was one of the fastest growing populations under micro-aerophilic conditions at day seven (Fig. 5). The increased micro-aerophilic growth of Sva0081-MBG individuals is consistent with their higher acetate uptake rates in oxic–suboxic surface layer sediment slurries [82]. As Sva0081-MBG are H_2 oxidizers (Dyksma et al. 2018b), it is possible that the fast growing Sva0081- MBG individuals at the oxic–anoxic interface were also utilizing fermentation-derived H_2 diffusing upwards from the deeper anoxic sediments. *Desulfobacterium catecholicum*, which exhibited net production at day seven (Fig. 5), is a mesophilic SRB that can also perform dissimilatory reduction of nitrate to ammonium (Szewzyk and Pfennig 1987). This would explain its higher growth rate under the micro-aerophilic conditions at day seven during which nitrate was possibly still present. The SB-5 group of Bacteroidetes belongs to the Cytophagales and was previously detected in a benzene degrading, sulfate-reducing consortium (Phelps et al. 1998). The high net production under micro-aerophilic conditions indicates this group was growing faster compared with most other OTUs (Fig. 5). After 28 days, most of the OTUs were ^{18}O labeled (Fig 2). However, the rate of mortality per genus was higher at day 28 than day 7, indicating that establishment of euxinic conditions caused the majority of cells per genus to die faster than they grew (Fig. 5). However, despite the higher the net mortality rates, many exhibited relatively low positive gross reproduction rates. This indicates that a smaller proportion of individuals within each OTU were actively growing, while the majority of individuals were dying. This small fraction of active cells per population explains how nearly all OTUs became ^{18}O labeled by day 28, despite of the increase in total microbial mortality. Larger mortality compared with production at the end of the 28-day incubation could be partly explained by a decrease in electron donors (e.g., organic matter) and acceptors (e.g., nitrate, Fe(III), and sulfate). Indeed, under normal conditions organic matter and dissolved ions from seawater (e.g., sulfate) would be slowly but continuously entering the sediment to fuel new microbial growth. In our incubations, however, nutrients were constantly being depleted without replacement. Some of the inactive populations could also be explained by an increase in dormant cells due to unfavorable environmental conditions (Kearns et al. 2016).

3.6 Conclusions

Our findings provide the first experimental evidence demonstrating the redox conditions promoting growth in several groups of uncultured “microbial dark matter”, validating hypotheses put forth by earlier metagenomics studies. The data help to explain previously observed biogeographic patterns for many uncultivated groups of bacteria that tend to correlate with anoxic or low oxygen conditions in aquatic habitats. This information could be helpful to guide future cultivation efforts for groups of ubiquitous, yet uncultured, bacterial taxa.

Acknowledgements

This work was supported by a grant OR 417/1-1 from the Deutsche Forschungsgemeinschaft, and a Junior Researcher Fund grant from LMU Munich to WDO. This work was performed in part, through the Master’s Program in Geobiology and Paleontology (MGAP) at LMU Munich.

Figures

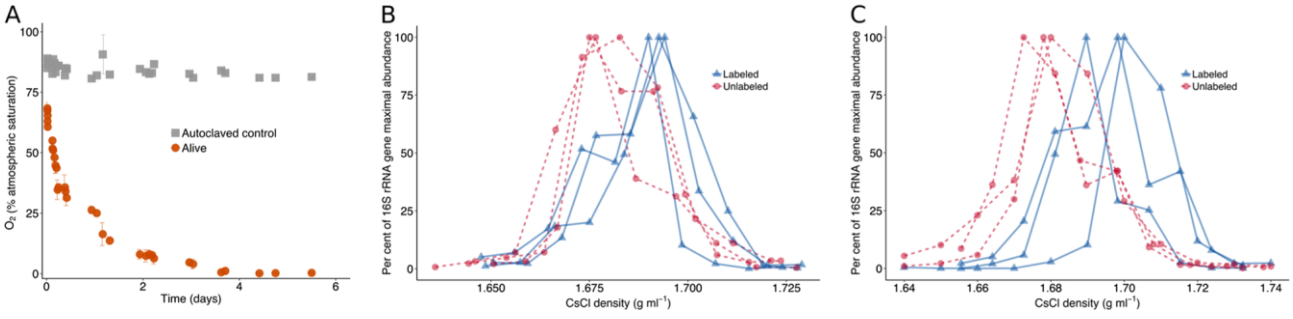

Fig. 1. a Benthic O_2 concentrations during the incubation and killed (autoclaved) control. **b, c** Quantification of 16S rRNA gene copies across CsCl density gradient fractions after 7 (**b**) and 28 days (**c**). ^{18}O water replicates are represented by blue solid lines with triangles and unlabeled replicates (control) are represented by red dashed lines with circles. The y axis represents the relative abundance of 16S rRNA genes quantified with qPCR, normalized to maximal abundance across all density fractions.

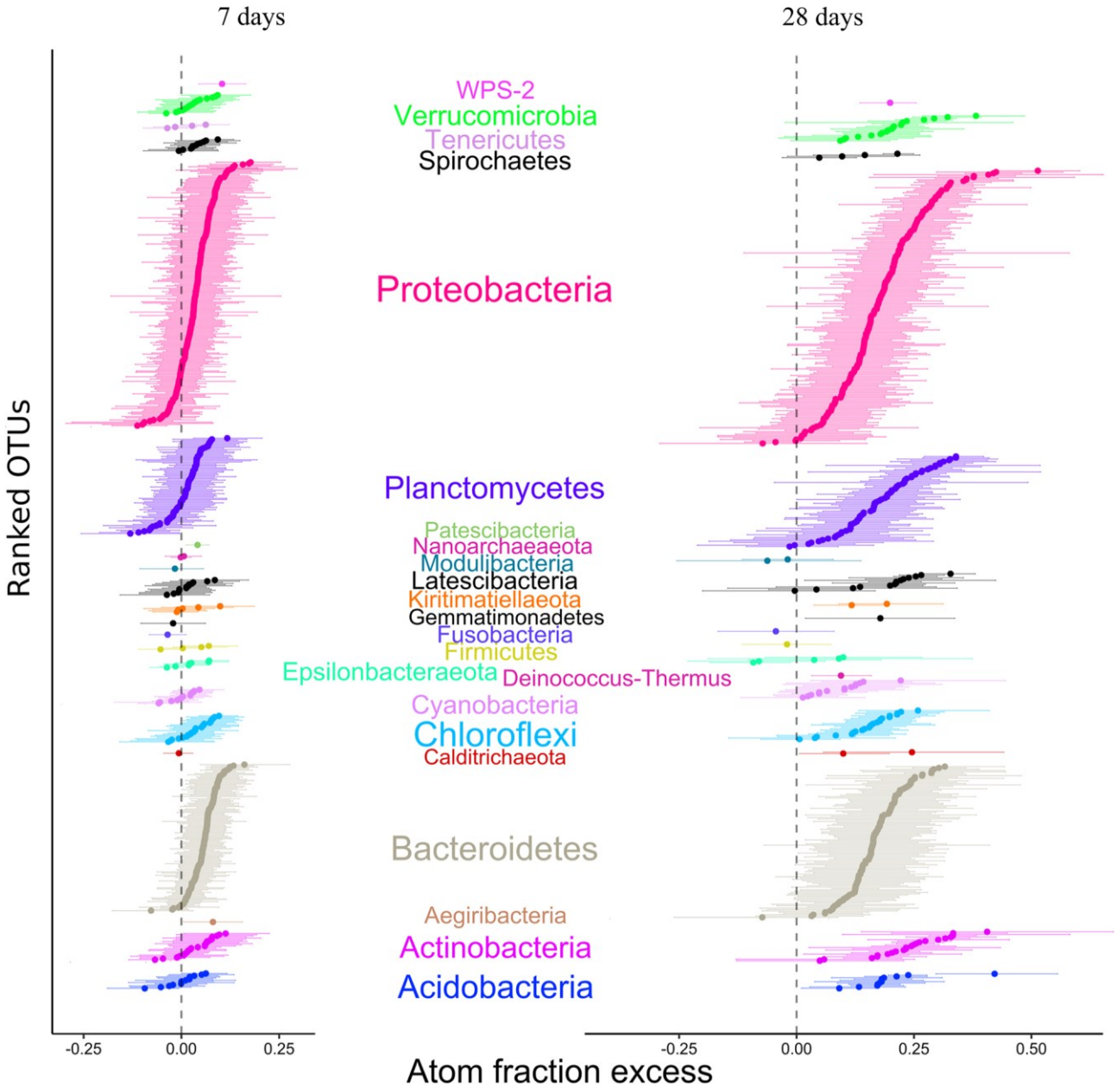

Fig. 2. OTU-specific shifts in the median atom fraction excess (^{18}O) of OTUs with 90% confidence interval (CI). OTUs were colored by phylum. OTUs that do not have a 90% CI overlapping with 0 are considered to be ^{18}O labeled.

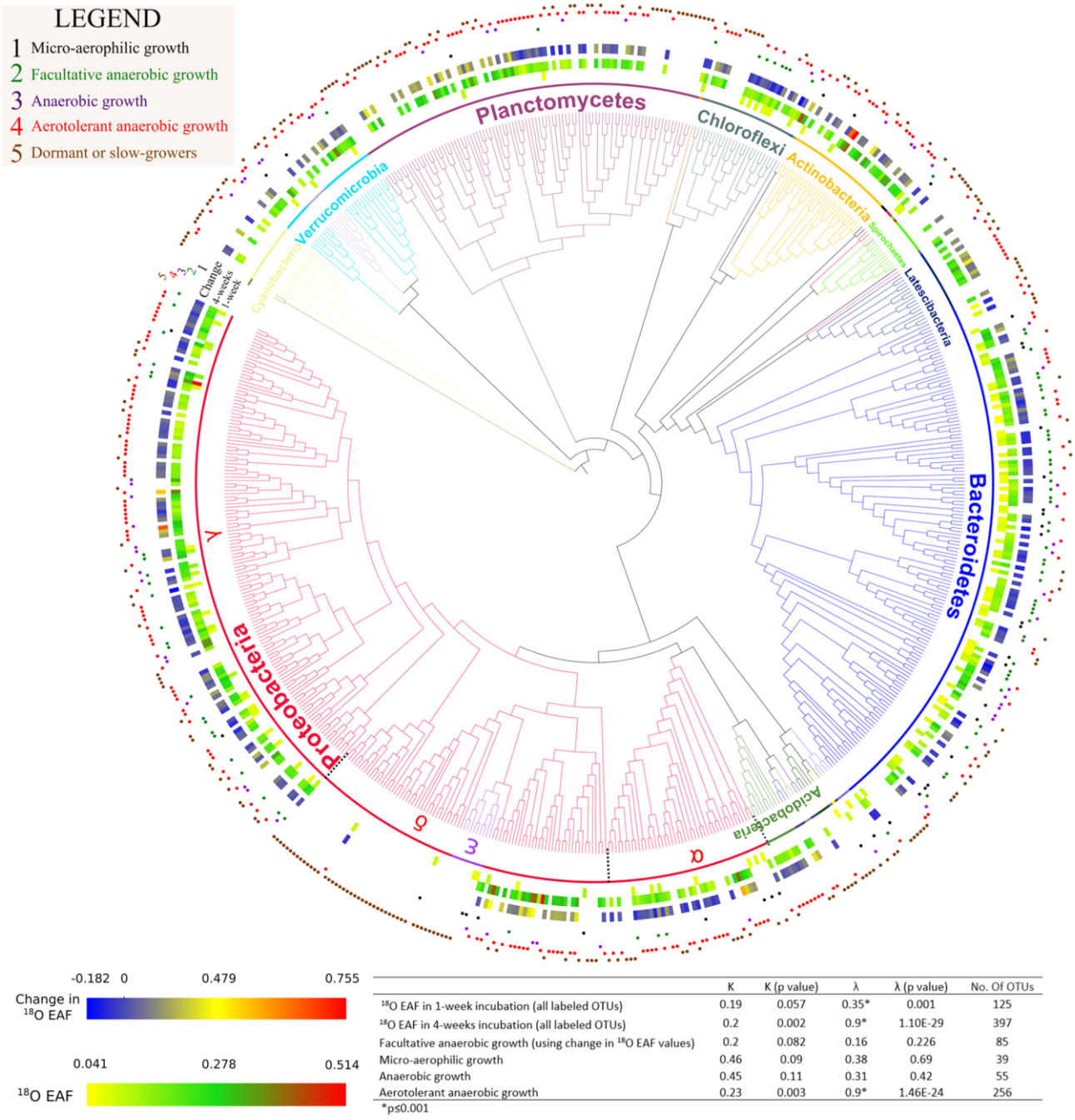

	K	K (p value)	λ	λ (p value)	No. Of OTUs
^{18}O EAF in 1-week incubation (all labeled OTUs)	0.19	0.057	0.35*	0.001	125
^{18}O EAF in 4-weeks incubation (all labeled OTUs)	0.2	0.002	0.9*	1.10E-29	397
Facultative anaerobic growth (using change in ^{18}O EAF values)	0.2	0.082	0.16	0.226	85
Micro-aerophilic growth	0.46	0.09	0.38	0.69	39
Anaerobic growth	0.45	0.11	0.31	0.42	55
Aerotolerant anaerobic growth	0.23	0.003	0.9*	1.46E-24	256

*p≤0.001

Fig. 3. Phylogeny of bacterial taxa detected and their extent of ^{18}O labeling at 7 and 28 days. The inner circles correspond to excess atom fraction (EAF) ^{18}O values of labeled taxa after 7 and 28 days of incubation. The outer ring of the heatmap represents the EAF change between the timepoints. The numbered and colored circles represent the growth mode of the OTUs and the legend defines the growth mode of categories explained in result section. Bottom panel shows phylogenetic signal tests (Blomberg's K and Pagel's λ) and corresponding p-values for labeled taxa and growth mode categories

Group	Growth mode	EAF values (number of OTUs)	*r*-Value (net population growth rate)	*b*-Value (rates of reproduction)	*d*-Value[a] (mortality rate)
Aegiribacteria	Micro-aerophilic	0.08 (*n* = 1)	-0.202	0.081	-0.288
Latescibacteria	Aerotolerant anaerobic	0.013 ± 0.008 (*n* = 10)	-0.227	-0.038	-0.191
Gracilibacteria	Micro-aerophilic	0.04 (*n* = 1)[b]	-0.172	-0.041	-0.136
Calditrichaceae	Aerotolerant anaerobic	-0.007 (*n* = 1)	-0.214	-0.018	-0.197
WPS-2	Facultative anaerobic	0.1 (*n* = 1)[b]	-0.339	0.079	-0.421
28 days of incubation					
Gracilibacteria	Aerotolerant anaerobic	0.17 ± 0.073 (*n* = 2)[b]	-0.136	0.023	-0.171
Latescibacteria	Aerotolerant anaerobic	0.19 ± 0.023 (*n* = 14)[c]	-0.373	0.019	-0.392
WPS-2	Facultative anaerobic	0.2 (*n* = 1)[b]	-0.422	0.014	-0.436

[a]*r*, *b*, and *d* values correspond to the rates per day (d^{-1})

[b]Significantly growing microorganisms based on qSIP (i.e., lower boundary of bootstrap is >0)

[c]Most of the Latescibacteria grew (10 OTUs out of 14)

Table 1. A summary of growth by uncultivated taxa, previously designated as “microbial dark matter”, under various redox conditions

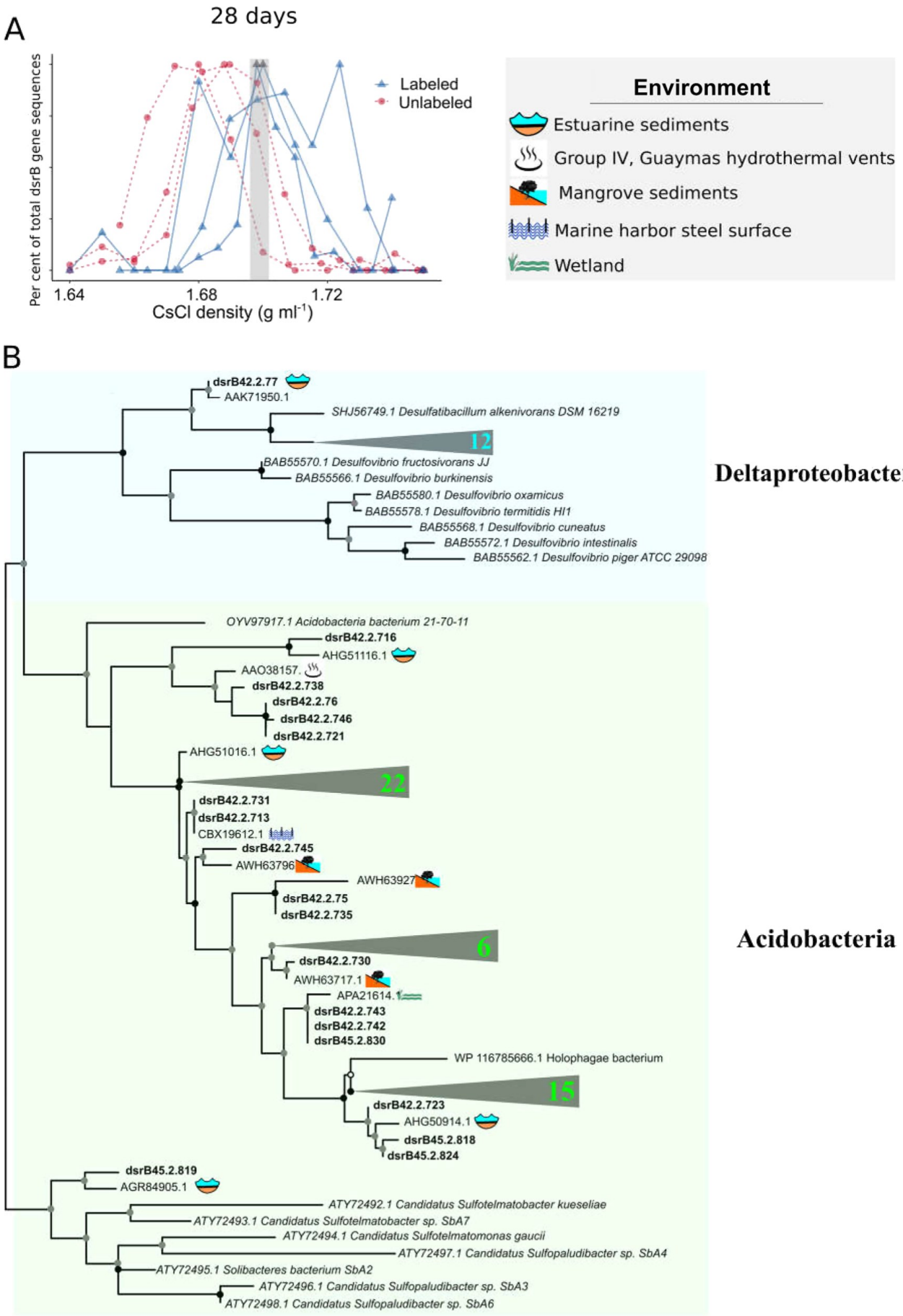
A
28 days
Per cent of total dsrB gene sequences
1.64
1.68
1.72
CsCl density (g ml-1)
Labeled
Unlabeled
Environment
Estuarine sediments
Group IV, Guaymas hydrothermal vents
Mangrove sediments
Marine harbor steel surface
Wetland
B
dsrB42.2.77
AAK71950.1
SHJ56749.1 Desulfatibacillum alkenivorans DSM 16219
12
BAB55570.1 Desulfovibrio fructosivorans JJ
BAB55566.1 Desulfovibrio burkinensis
BAB55580.1 Desulfovibrio oxamicus
BAB55578.1 Desulfovibrio termitidis HI1
BAB55568.1 Desulfovibrio cuneatus
BAB55572.1 Desulfovibrio intestinalis
BAB55562.1 Desulfovibrio piger ATCC 29098
Deltaproteobacteria
OYV97917.1 Acidobacteria bacterium 21-70-11
dsrB42.2.716
AHG51116.1
AAO38157.
dsrB42.2.738
dsrB42.2.76
dsrB42.2.746
dsrB42.2.721
AHG51016.1
22
dsrB42.2.731
dsrB42.2.713
CBX19612.1
dsrB42.2.745
AWH63796
AWH63927
dsrB42.2.75
dsrB42.2.735
6
dsrB42.2.730
AWH63717.1
APA21614.1
dsrB42.2.743
dsrB42.2.742
dsrB45.2.830
WP 116785666.1 Holophagae bacterium
15
dsrB42.2.723
AHG50914.1
dsrB45.2.818
dsrB45.2.824
Acidobacteria
dsrB45.2.819
AGR84905.1
ATY72492.1 Candidatus Sulfotelmatobacter kueseliae
ATY72493.1 Candidatus Sulfotelmatobacter sp. SbA7
ATY72494.1 Candidatus Sulfotelmatomonas gaucii
ATY72497.1 Candidatus Sulfopaludibacter sp. SbA4
ATY72495.1 Solibacteres bacterium SbA2
ATY72496.1 Candidatus Sulfopaludibacter sp. SbA3
ATY72498.1 Candidatus Sulfopaludibacter sp. SbA6

Fig. 4. Quantification of *dsrB* gene copies across CsCl density gradient fractions after 28 days. ^{18}O water replicates are represented by blue solid lines with triangles and unlabeled replicates (control) are represented by red dashed lines with circles. The y axis represents the relative abundance of *dsrB* genes quantified with qPCR normalized to maximal abundance across all density fractions. b Phylogenetic tree of ^{18}O-labeled *dsrB* genes including their most similar sequences from the NCBI nr database, bold sequences indicate those from this study. Collapsed clades (triangles) show the number of ^{18}O-labeled *dsrB* gene sequences contained within the clade. Black circles at nodes represent bootstrap support of 90%, gray circles represent bootstrap support from 70 to 90%, and white circles represent bootstrap support from 70 to 50%.

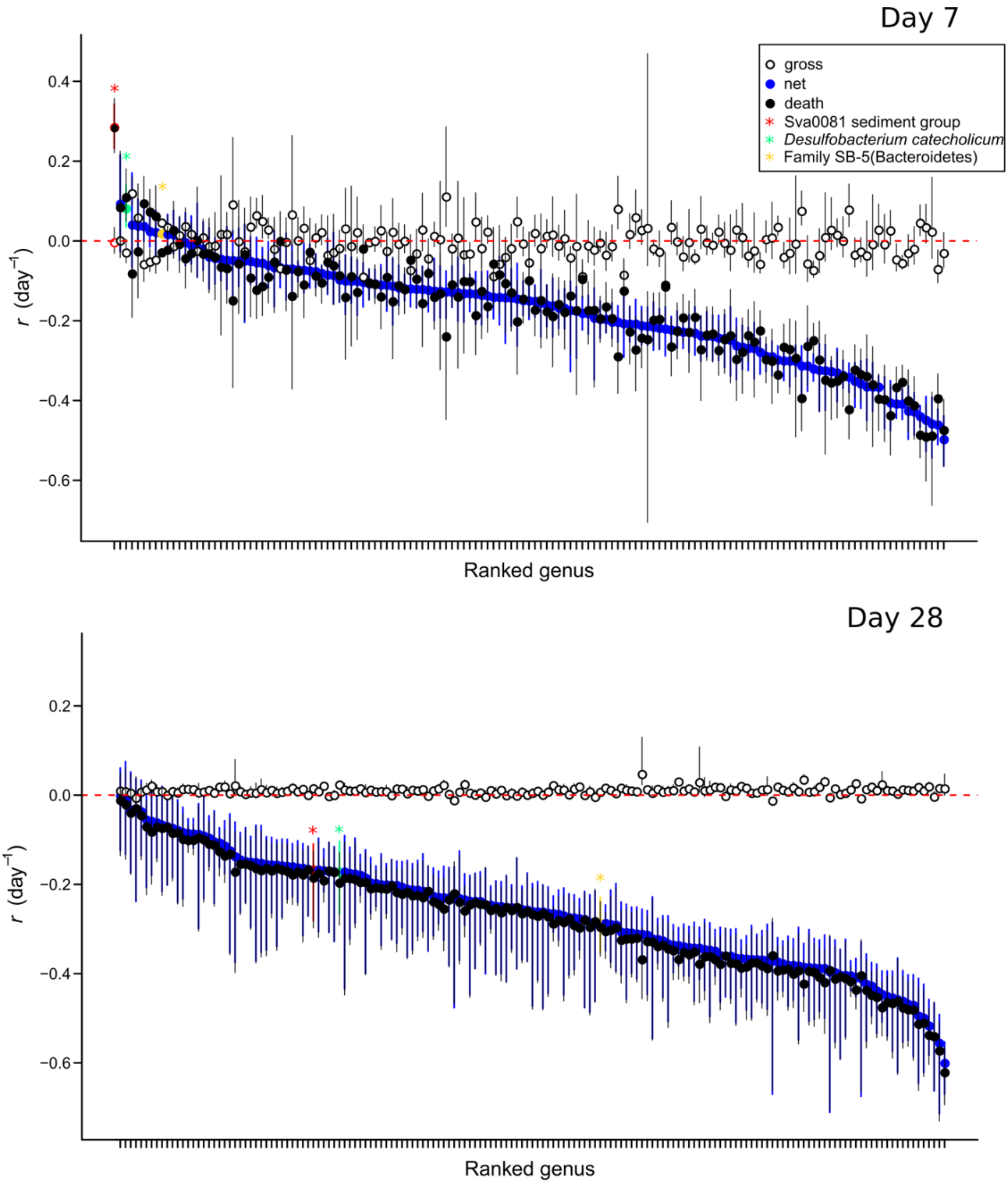

Fig. 5. Population growth rates (r) at 7 and 28 day timepoints. After 28 days, all taxa exhibited mortality rates greater than reproduction rates. Points indicate bootstrapped medians and bars show 90% confidence intervals for each OTU. The positive net production rates here are considered as statistically significant increase in the populations if the bootstraps are not crossing the zero. Open circles: rates of reproduction, black filled circles: mortality rates, blue filled circles: net reproduction rates. The only groups that exhibiting significant net production at day 7 are indicated with asterisks (see legend).

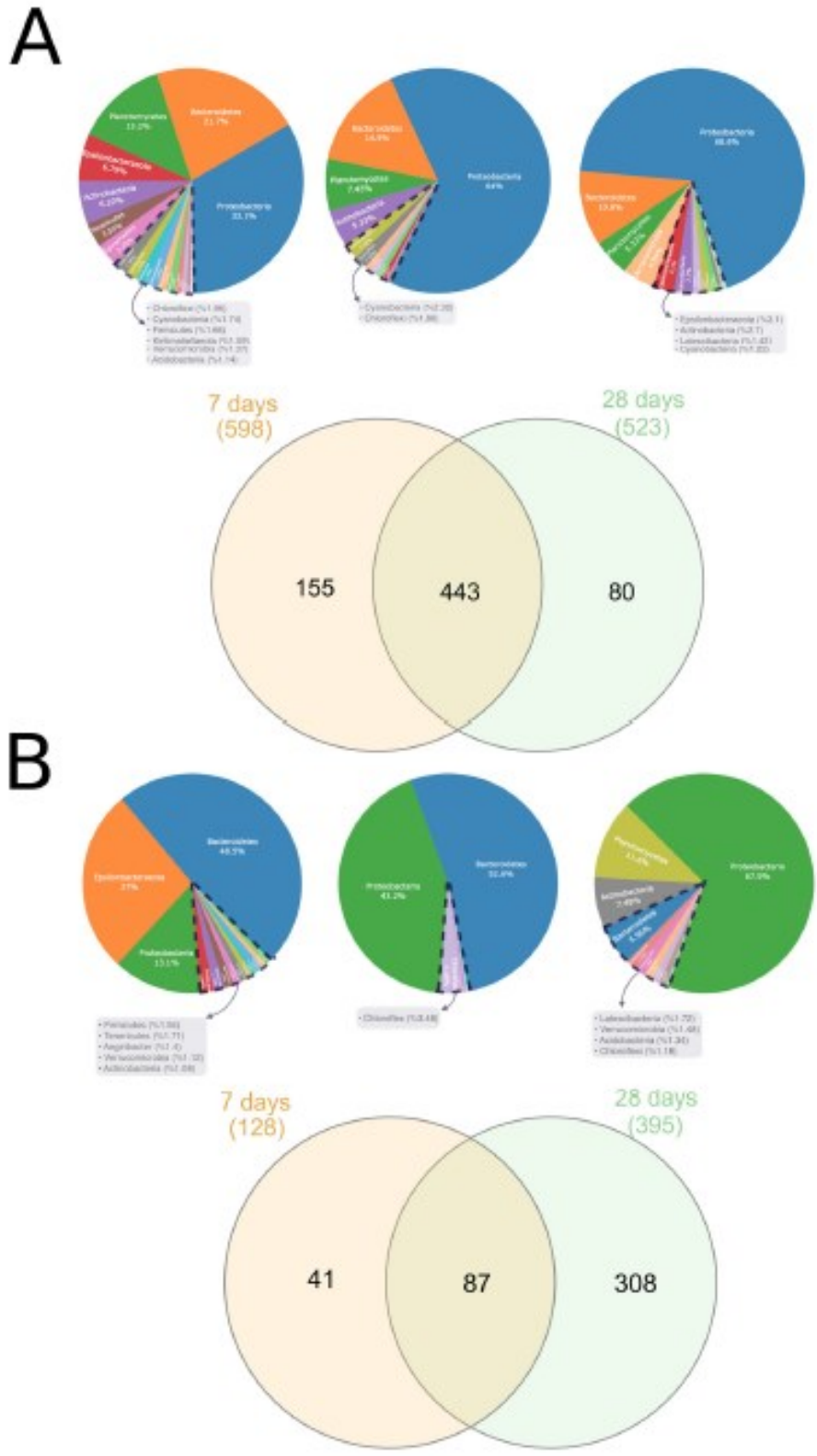

Figure S1: Pie charts displaying the proportions (%) and phylum-level composition of total (A) and labeled (B) 16S rRNA gene sequences together with corresponding number of overlapping and non-overlapping OTUs between the experimental timepoints.

Chapter 4

Primary production by mixotrophic bacteria in a deep subsurface hydrothermal ecosystem

Ömer K. Coskun[1], Murat Beren[3], Doğacan Özcan[3], Suna D. Günay[1], Viktor Elkin[1], Hakan Hoşgörmez[3], Florian Einsiedl[4], Wolfgang Eisenreich[5] and William D. Orsi[1,2,§]

[1]Department of Earth and Environmental Sciences, Ludwig-Maximilians-Universität, 80333 Munich, Germany

[2]GeoBio-Center[LMU], Ludwig-Maximilians-Universität München, 80333 Munich, Germany

[3] Department of Geological Engineering, Istanbul University - Cerrahpasa, Istanbul, Turkey

[4] Chair of Hydrogeology, School of Engineering and Design, Technical University Munich, 80333 Munich, Germany

[5] Lehrstuhl für Biochemie, Department Chemie, Technische Universität München, Lichtenbergstraße 85748 Garching, Germany

[§]Corresponding author: w.orsi@lrz.uni-muenchen.de

Submitted to PNAS

02 October 2022

4.1 Abstract

Deep subsurface hydrothermal environments house enigmatic microbial communities that perform primary production in the absence of sunlight, helping to sustain subsurface ecosystems. Compared to autotrophs however, the contribution of primary production from mixotrophic taxa remains unquantified in deep hydrothermal ecosystems. Here, we used quantitative stable isotope probing to link ^{13}C carbon fixation rates at different $H^{13}CO_3^-$ concentrations (1 mM, 5 mM, 10 mM) to metagenome assembled genomes (MAGs) in hydrothermal fluids from a deep (750 m below surface) subsurface aquifer. Across all three ^{13}C-bicarbonate concentrations tested, a significant positive correlation (*P*=0.002) between ^{13}C-fixation and the number of ABC transporters for organic substrates per MAG was observed. Most of the highest carbon fixation rates observed were associated with mixotrophic metabolism in nitrate-reducing, sulfur-oxidizing Gammaproteobacteria taxa encoding the Calvin-Benson-Bassham (CBB) carbon fixation pathway. The total amount of ^{13}C-bicarbonate that was assimilated by these mixotrophic sulfide-oxidizers into biomass was higher compared to chemoautotrophs (primarily Aquificae) encoding the reverse TCA carbon fixation cycle. The relatively large contribution by mixotrophic bacteria to primary production from ^{13}C-bicarbonate could be traced into ^{13}C-labeled bacterial MAGs that did not contain carbon fixation pathways, indicating a substantial amount of secondary production by heterotrophs is derived from mixotrophic primary-producers. Our data provide the first quantitative estimates on primary production by potential mixotrophic bacteria in a subsurface ecosystem, and indicate mixotrophy may be a previously underestimated source of primary production in these settings.

4.2 Significance

Deep hydrothermal fluids host vast number of microbes driving a broad range of biogeochemical cycles in conditions mostly devoid of photosynthesis, but the community-wide trophic networks, especially the carbon flow from chemolithoautotrophs to heterotrophs, are still poorly understood. By tracking the carbon in metabolically versatile microbes under oligotrophic conditions, we show that dominant nitrate-reducing, sulfur-oxidizing mixotrophic taxa play a crucial role in carbon turnover by employing the Calvin-Benson-Bassham cycle for carbon fixation and genes necessary for utilizing wide range of organic carbon substrates. This study shows that metabolically diverse mixotrophs are a key source of primary production sustaining a subsurface hydrothermal ecosystem, allowing for the survival of the deep subsurface microbial hydrothermal ecosystem.

4.3 Introduction

Deep subsurface environments are the largest ecosystems in terms of size for prokaryotes whose biomass was estimated to be 23 to 31 petagrams of carbon (PgC) with 2 to 6 x 10^{29} cells (Magnabosco et al. 2018). The deep-subsurface biosphere drives a diverse range of biogeochemical cycles such as carbon and important nutrients for life (Magnabosco et al. 2018; Merino et al. 2019; Fullerton et al. 2021).The primary production in terrestrial deep subsurface is based on chemolithotrophy because no sunlight is available for the prokaryotes (Stevens 1997). Since photosynthetically derived organic carbon is often a limited nutrient for heterotrophs in deep subsurface (Pedersen 2000), *in situ* production of dissolved organic carbon (DOC) by chemolithoautotrophs supports the microbial communities (Probst et al. 2020; Magnabosco et al. 2016; Lau et al. 2016; Momper et al. 2017; Osburn et al. 2014; Emerson et al. 2016). Chemolithoautotrophic communities have been shown to be related to availability of dissolved inorganic carbon (DIC) in the deep-subsurface biosphere (Fullerton et al. 2021) which was predicted to have a dominant role in these communities (Stevens and McKinley 1995; Pedersen 1997). Specifically, dissolved inorganic and organic carbon concentrations in hot springs in Costa Rican convergent margin have been shown to have positive correlation with reductive tricarboxylic acid cycle-utilizing (rTCA) microbes, suggesting higher DIC derived from the subducting slab may help sustain chemolithoautotrophic-based ecosystems (Fullerton et al. 2021).

Depending on the environmental conditions, availability of energy sources and fluid composition, microbial carbon fixation pathways may differ as the dominant source of carbon fixation (Fullerton et al. 2021; Momper et al. 2017; Lau et al. 2016; Probst et al. 2017). In addition to autotrophs, mixotrophic microorganisms have been also shown to contribute to the carbon cycle in groundwater (Taubert et al. 2022). Although the potential carbon acquisition pathways of the microbes are predicted from mostly metagenome-based studies in diverse subsurface environments (Fullerton et al. 2021; Momper et al. 2017; Lau et al. 2016; Probst et al. 2017; Taubert et al. 2022), quantitative experimental data on the mechanisms of primary production that sustain microbial life in deep subsurface hydrothermal ecosystems is lacking.

To investigate the carbon flow from primary producers to secondary utilizers under different DIC concentrations in a deep (750 meters below surface) hydrothermal aquifer system (Biga Peninsula, Turkey), we used $H^{13}CO_3^-$ as an isotope tracer to quantify microbial carbon assimilation by specific operational taxonomic units (OTUs) using the qSIP method (Hungate et al. 2015). We linked metagenome-assembled-genomes (MAGs) to ^{13}C-labeled OTUs using a phylogenetic approach, to directly link genomic potential with carbon assimilation rates by specific taxa. The results show that bacterial mixotrophs dominated primary production across bicarbonate concentrations spanning the natural range present in the tested ecosystem (1-10 mM), and therefore are implicated as important microbial primary producers that support this deep subsurface hydrothermal ecosystem.

4.4 Results and Discussion

4.4.1 Biogeochemical setting.

The reservoir bedrock of the Bardakçılar geothermal field is metamorphically altered carbonate rocks (marble) embedded in Kazdağ massif (Yalcin 2007) (*SI Appendix,* Figure S2). Alkaline hydrothermal fluids from this carbonate aquifer become Na- and SO_4-enriched while rising through the Upper Oligocene-Lower Miocene volcanic rocks (Akkuş et al. 2005), and were found to be depleted in NO_3^- and NO_2^- (Dataset S1) which is in line with previous reports (Yalcin 2007). The fluids had a constant temperature of 73 °C and are alkaline (pH: 8.27), with 91.5 mg/l DIC (*SI Appendix*, Figure S1-B) and 0.8 mg/l dissolved organic carbon (DOC) (Dataset S1). The concentration of DOC is approximately an order of magnitude lower compared to other surface-influenced continental subsurface aquifers (Lopez-Fernandez et al. 2018), indicating an oligotrophic ecosystem where biological production is relatively limited. Oxidation-reduction potential (ORP) of the fluid was measured as +4 mV and hydrogen sulfide could be smelled, indicating anoxic fluids with a relatively low redox potential. Methane was detectable in the fluids, albeit at relatively low concentration of 0.079 (mg/l), and the $\delta^{13}CH_4$ was measured to be -10.4 ‰ (Dataset S1) indicating that the CH_4 in the fluids is likely not of a biological source but rather primarily derived from thermogenic pyrolysis of organic matter (Schoell 1988).

δ^2H and $\delta^{18}O$ composition of water in the fluids falls between the global meteoric water (GMWL)(Craig 1961) and East Mediterranean meteoric water lines (EMMWL)(Gat and Carmi 1970) (*SI Appendix*, Figure S1-A). Moreover, the $\delta^{18}O$ values of the subsurface water are within the range of annual average $\delta^{18}O$ values of precipitation and groundwater (-6 to -9‰) from nearby sites in Turkey (Jasechko 2019). This suggests that the origin of the subsurface hydrothermal fluids in our tested ecosystem is modern meteoric water, consistent with prior studies of hydrothermal fluids of Biga Peninsula (Yalcin 2007).

4.4.2 Microbial community and experimental setup

Over a three-year period (2019, 2020 and 2021), we sampled a 750-meter-deep borehole penetrating a deep subsurface hydrothermal aquifer from the Bardakçılar geothermal field (Biga Peninsula, Turkey) (*SI Appendix*, Figure S2). Untreated, pristine alkaline hydrothermal fluid samples were collected directly from the borehole (*SI Appendix*, Figure S3) allowing us to measure geochemical parameters and access to the microbial community inhabiting this deep hydrothermal aquifer system. The microbial 16S rRNA gene concentrations in the alkaline hydrothermal fluids from the 750-meter aquifer were relatively low, 1.8×10^2 ($\pm 3.3 \times 10^1$) copies per mL (*SI Appendix*, Figure S4). For a comparison, we also sampled fluids from a shallower, 75-meter-deep well at the same site which had 1.4×10^3 ($\pm 1.3 \times 10^1$) 16S rRNA gene copies per mL. Our results are in line with previous continental subsurface studies from 500 – 800 meters depth where similarly low 16S rRNA gene copy concentrations (10^1 – 10^4 copies per mL) were detected (Lavalleur and Colwell 2013; Bomberg et al. 2016; Magnabosco et al. 2018). The 16S rRNA gene concentrations measured were

consistently higher than our detection limit of 10^2 total 16S copies per DNA extraction blank (Coskun et al. 2021), showing that we detected the natural microbial community emanating from the 750m deep hydrothermal aquifer with a minimal influence of contamination. The low microbial biomass can be explained by the ca. 10 fold lower concentration of DOC (Dataset S1) compared to other surface-influenced continental subsurface aquifers (Lopez-Fernandez et al. 2018), because DOC availability is known to shape microbial communities in continental subsurface crustal ecosystems (Lopez-Fernandez et al. 2018; Westmeijer et al. 2022). Over the three years (2019, 2020, 2021), the microbial community was dominated by operational taxonomic units (OTUs) affiliated with known thermophilic groups such as Aquificae, Deinococcus-Thermus, *Thermodesulfovibrio*, and groups typical of subsurface habitats such as the Hadesarchaeaeota (Baker et al. 2016) and Chloroflexi (Orsi 2018) (*SI Appendix*, Figure S5). The prevalence of these microbial groups bears resemblance to other alkaline hot springs of the Tibetan Plateau (Wang et al. 2013), Yellowstone national park (Schubotz et al. 2015), Costa Rican convergent margin (Fullerton et al. 2021) and deep-subsurface aquifers (Spanevello and Patel 2004).

In 2021, we performed a quantitative DNA stable isotope probing experiment with ^{13}C-bicarbonate at three different concentrations (1 mM, 5 mM, 10 mM) to reflect the range of natural bicarbonate concentrations that exists within the greater Bardakçılar hydrothermal aquifer system (Figure S3) (*SI Appendix,* Fig. S1) (Yalcin 2007). Therefore, by adding the $H^{13}CO_3^-$ at these concentrations we were testing the naturally available range of bicarbonate concentrations that the microbial communities are exposed to as they are transported through the subsurface aquifer. After five days, 16S rRNA gene copies in all incubations increased roughly 10-fold (*SI Appendix*, Figure S4) and ^{13}C-labeling of 16S rRNA genes was observed (*SI Appendix*, Figure S6). Quantitative stable isotope probing analysis (qSIP) revealed which OTUs were significantly labeled across the three bicarbonate concentrations (Figure S7). ^{13}C-assimilation is measured in the qSIP method via excess atom fraction (EAF) ^{13}C in the 16S rRNA genes of OTUs, whereby ^{13}C-EAF values are reported on a scale between 0 - 1.0 with 1.0 representing 100% labeling of carbon atoms in the 16S rRNA gene (Hungate et al. 2015). This information was then linked to metagenome assembled genomes (MAG) from the same samples to decipher how much ^{13}C-bicarbonate was assimilated per MAG.

4.4.3 Linking ^{13}C-labeled OTUs to MAGs

We linked the ^{13}C-labeled OTUs to MAGs using phylogenetic analyses (*SI Appendix*, Figure S8). MAGs were grouped into two categories (1) those encoding a binned 16S rRNA gene, and (2) those not encoding a 16S rRNA gene. For those MAGs encoding a binned 16S rRNA, we were able to directly link the identity of the MAG to its corresponding 16S rRNA gene within the qSIP dataset using 16S rRNA gene phylogenies (*SI Appendix*, Figure S8A). For all MAGs that contained a 16S rRNA gene (n=11), a ^{13}C-labeled 16S OTU detected in qSIP could be directly linked to the MAG, by its relatively short phylogenetic distance in the tree (*SI Appendix*, Figure S8A).

For those MAGs that did not contain a binned 16S rRNA gene (n=12), we indirectly linked

the identity of the MAG to its corresponding ^{13}C-labeled 16S rRNA gene OTU. This was done by comparing the MAG ribosomal protein phylogeny to a 16S rRNA gene phylogeny of the same affiliated named species and '*Candidatus'* organisms (*SI Appendix*, Figure S8C). This allowed us to indirectly link MAGs lacking a 16S rRNA gene with their most likely ^{13}C-labeled labeled OTUs in the qSIP dataset (*SI Appendix*, Figure S8B-S8C). Once all MAGs (n=24) were linked (either directly or indirectly) to the labeled OTUs, we were able to compare the gene content of the MAGs with their ^{13}C-assimilation across the three tested bicarbonate concentrations (Figure 1).

4.4.4 Carbon fixation potential of ^{13}C-labeled MAGs

After identifying the ^{13}C-labeled MAGs, functional characterization of MAGs made it possible to group them into three distinct lifestyles based on carbon acquisition strategy predicted from the encoded gene content. Fifteen of the ^{13}C-labeled MAGs were found to have genomic capability to fix carbon dioxide/bicarbonate, indicating their potential to contribute to primary production (Figure 1). The Calvin-Benson-Bassham (CBB) cycle and Wood-Ljungdahl Pathway (WLP) were the most common carbon fixation pathways detected (Figure 1). A relatively smaller number of MAGs was found to encode the rTCA carbon fixation cycle and components of the 3-Hydroxypropionate bicycle (3-HP bicycle) (Figure 1). Nine of the ^{13}C-labeled MAGs lacked any of genes encoding one of the carbon fixation pathways and therefore display the potential for a heterotrophic lifestyle. Here we do not exclude the anaplerotic carbon fixation reactions in heterotrophs that can account for 2-8% of cell carbon (Roslev et al. 2004; Spona-Friedl et al. 2020) and indeed most MAGs encode this potential. However, deep subsurface environments are considered as energy limited areas where photosynthetically derived organic carbon sources are limited (Pedersen 2000) and heterotrophs are directly dependent on the *in situ* production of organic matter from primary producers.

There are seven carbon fixation pathways known to exist (Hügler and Sievert 2011; Sánchez-Andrea et al. 2020) and some of these pathways may harbor oxygen-sensitive enzymes (Hügler and Sievert 2011). WLP, rTCA cycle, dicarboxylate/4-hydroxybutyrate (DC/4-HB) cycle and recently-discovered reductive glycine pathway are performed by anaerobic and microaerophilic organisms while CBB cycle, 3-HP bicycle and 3-hydroxypropionate/4-hydroxybutyrate (3-HP/4-HB) cycle can function in fully-oxygenated environments (Hügler and Sievert 2011). The presence of four very different carbon fixation pathways (CBB, WLP, rTCA, 3-HP bicycle) in our sampled fluids indicates a variety of redox environments within the aquifer system and in the experimental incubations. It is possible that the sampled fluids derive from a mixture of different fluid sources of varying redox states (Probst et al. 2018), and the detected pathways (WLP, CBB, rTCA, 3-HP bicycle) probably vary in terms of importance for primary production at different depths, redox zones, and O_2 concentrations in the subsurface aquifer. Under our tested conditions, the overall redox state of the sampled fluid for our SIP incubations was relatively low (+4 mV), and O_2 concentrations at the end of the incubations were in the sub-hypoxic range (33 µM, +/- 3) (Supplementary Dataset 1). These reduced conditions should favor microbial dissimilatory nitrate reduction as the most favorable terminal electron accepting process (as opposed to aerobic respiration) (Hügler and Sievert 2011).

Indeed, many of the MAGs that assimilated ^{13}C had the genomic capacity for utilizing nitrate as a terminal electron acceptor for anaerobic respiration (Figure 1), which was consistent with the depletion of dissolved nitrate in the hydrothermal fluids (Supplementary Dataset 1). This indicates that dissimilatory nitrate reduction was a dominant energetic pathway in the sampled fluids and our SIP experiment.

Potentially mixotrophic ^{13}C-labeled MAGs were identified based on the genomic capability for both CO_2 fixation and uptake of carbon containing organic matter via genes encoding ABC-transport proteins (Figure 1). Out of 15 MAGs that encode carbon fixation pathways, 10 of them also contained relatively higher numbers of ABC-type transporters for classes of organic molecules (Figure 1), suggesting a mixotrophic lifestyle whereby they can supplement their cellular carbon sources from CO_2 with organic carbon from the environment. All of the MAGs encoding CBB cycle, most of the MAGs encoding WLP cycle and one MAG encoding 3-HP bicycle display a genomic potential for such a mixotrophic lifestyle, potentially providing them an increased fitness in hydrothermal oligotrophic conditions where they can switch between autotrophy and heterotrophy as new organic matter becomes available. Such a mixotrophic metabolic lifestyle was also shown to be important in microbial survival in oligotrophic groundwater ecosystems (Taubert et al. 2022). On the other hand, MAGs with the rTCA cycle (exlusive Aquificae) were able to fix carbon while having a relatively reduced suite of ABC-transporters for organic molecules (Figure 1) with the exception of an incomplete ABC-type phospholipid transporter system (MlaABCDEF). This transporter has an important role in maintaining outer membrane lipid asymmetry (Chong et al. 2015), survival in infection (Suzuki et al. 1994) and phospholipid-trafficking between outer and inner membrane (Hughes et al. 2019), suggesting that this transporter plays a role in maintaining the integrity of the cell membrane as opposed to uptake of lipids as a carbon source from the environment. The highest number of ABC-transporters in ^{13}C-labeled MAGs encoded the 3-HP bicycle (11 complete and incomplete ABC-type transporters) and CBB cycle (5 ABC-type transporters on average) (Figure 1). ^{13}C-labeled MAG encoding 3-HP bicycle was taxonomically affiliated to *Chloroflexus aurantiacus*, whereas the MAGs with CBB cycle were closely related to order Burkholderiales (mainly genus *Tepidomonas*) and phylum Deinococcus-Thermus (Dataset 2). The single detected ABC-transporter in the rTCA encoding Aquificae MAGs (Figure 1) indicates that they were fixing ^{13}C-bicarbonate primarily via an autotrophic metabolism, whereas the CBB, WLP, and 3-HP encoding MAGs that also contain higher number of ABC-transporters were likely fixing ^{13}C-bicarbonate via a mixotrophic metabolism.

4.4.5 Energy conservation by ^{13}C-labeled MAGs

The genome content of the MAGs indicate reduced sulfur compounds were an important source of electron donors, and that nitrate is an important terminal electron acceptor in anaerobic respiration for most MAGs (Figure 1). Sulfide oxidation (H_2S/HS^- à S^0) was found to be a dominant potential energy conservation mechanism for most of the detected ^{13}C-labeled MAGs (15 out of 24 MAGs) mostly through Sulfide:quinine reductase (Sqr) and/or flavocytochrome c (fccAB). Sulfur oxidation through Sox system and thiosulfate oxidation using tdsA was also fully encoded by two

Deinococcus-thermus (MAGSIPTR4 and MAGSIPTR19), a Nitrospirae MAG (MAGSIPTR4), and a MAG affiliated with the thermophile *Schleiferia thermophila* (MAGSIPTR25), respectively (Figure 1, Figure S8). Among the MAGs with capacity to use reduced sulfur compounds as an electron donor, seven are putative mixotrophs including all five MAGs encoding CBB cycle.

These ^{13}C-labeled CBB-encoding MAGs were affiliated to Deinococcus-Thermus (genera of *Thermus* and *Meiothermus*) and Gammaproteobacterial genera *Sulfuritortus* and *Tepidomonas.* These CBB-encoding organisms are known to obtain energy by sulfur oxidation coupling with reducing O_2 or NO_3^-/NO_2^- as electron acceptors (Bjornsdottir et al. 2009; Kojima et al. 2017). Their ability to use nitrate as terminal electron acceptor is the likely reason why their activity was favored under the sub-hypoxic conditions of our SIP-incubations (33 µM O_2, +4 mV). Our findings indicating an anaerobic, mixotrophic lifestyle for these subsurface microbes are in line with pure culture studies showing mixotrophic growth of CBB-encoding microbes, that are nitrate reducing sulfur oxidizers such as '*Candidatus* Desulfobacillus denitrificans' (Okubo and Takami 2021) and *Sulfuritortus calidifontis* (Kojima et al. 2017). Our results are furthermore in line with other deep subsurface oligotrophic environments that often favor a sulfur-oxidizing, denitrifying bacterial community (Lau et al. 2016).

In our setting, more than half of the sulfur-oxidizing microbial community displays putative mixotrophy (Figure 1). We therefore sought to use the linked qSIP and metagenomic data quantify the contribution of mixotrophy to primary production in the studied system.

4.4.6 Mixotrophic potential correlates with bicarbonate assimilation.

A positive correlation was observed between the number of ABC-transporters for organic molecules and EAF values of ^{13}C-labeled MAGs (Figure 1), encoding CBB cycle, WLP and 3-HP bicycle ($P = 0.002$, $r^2 = 0.3$, Figure 2). Therefore, the amount of carbon assimilation from bicarbonate increased as a function of potential for uptake of organic molecules (mixotrophic potential) from CBB cycle, WLP and 3-HP bicycle encoding organisms. As a result, they are likely being labeled by a combination of organic matter utilization and the C-fixation routes, and the correlation suggests that the ability to supplement carbon demand with organic matter can increase carbon fixation from bicarbonate in these thermophilic bacteria. Mixotrophic capabilities have been observed in pure cultures of *Chloroflexus aurantiacus* (Pierson and Castenholz 1974), *Thermus islandicus* (Bjornsdottir et al. 2009), and *Thermodesulfovibrio* sp. (Thiel et al. 2017), which are all close affiliates of many of the ^{13}C-labeled MAGs detected in our SIP experiments (Figure 1, Figure S8). However, the mixotrophic activity of *Tepidimonas* sp shown here (Figure 1) is to the best of our knowledge the first evidence for mixotrophic growth by subsurface thermophilic *Tepidimonas*.

In contrast, MAGs encoding rTCA (affiliated to *Thermocrinis minervae* and *Sulfurihydrogenibium azorense*; Aquificae) had a some of the highest amount of bicarbonate assimilation compared to all MAGs (EAF = 22,45% +/- 2,23) but this did not correlate with higher numbers of ABC-transporters (Figure 2). This indicates that the rTCA encoding Aquificae MAGs were acting as autotrophs. This is in line with a study that suggested rTCA-based chemolithoautotrophy is important for the primary production in the Costa Rican convergent margin (Fullerton et al. 2021). Most members of Aquificae species are obligate chemolithoautotrophs (Gupta 2014), which is

consistent with our findings showing that rTCA encoding Aquificae were acting as autotrophs using inorganic carbon from ^{13}C-bicarbonate as a main carbon source (Figure 1).

Interestingly, the assimilation of ^{13}C-bicarbonate by the rTCA encoding Aquificae increased with increasing bicarbonate concentrations (Figure 3) as predicted in a previous study (Fullerton et al. 2021). One of the main Aquificae assimilators of ^{13}C-bicarbonate was closely affiliated with *Sulfurihydrogenibium azorense* setting, that encodes the most active α-carbonic anhydrase known to date for the CO_2 hydration reaction (De Simone et al. 2015). This high activity of carbonic anhydrase (responsible for converting bicarbonate to carbon dioxide), could explain why a higher DIC concentration resulted in more carbon fixation at higher DIC concentrations for this organism.

4.4.7 Tracing carbon flows between autotrophs, mixotrophs, and heterotrophs

In order to trace carbon flows between different functional groups in the qSIP experiments, we grouped ^{13}C-labeled MAGs into autotrophs, mixotrophs, and heterotrophs based on defined criteria. First, ^{13}C-labeled MAGs with a carbon fixation pathway >80% completeness but depleted in ABC-transporters for utilization of organic matter were grouped as likely autotrophs. The ^{13}C-labeled MAGs grouped as autotrophs (n=2) consisted exclusively of rTCA encoding Aquificae (Figure 1). Second, ^{13}C-labeled MAGs with a carbon fixation pathway >80% completeness but encoding relatively higher numbers of ABC-transporters for utilization of organic matter were grouped as likely mixotrophs. The ^{13}C-labeled MAGs grouped as mixotrophs (n=11) consisted of CBB, WLP, and 3-HP encoding MAGs (Figure 1). Third, ^{13}C-labeled MAGs that did not encode a carbon fixation pathway, or encoding <20% of a carbon fixation pathway were grouped as likely heterotrophs. This comprised the majority of remaining MAGs (n=12) (Figure 1) and we could group all ^{13}C-labeled MAGs into one of these three categories according to these criteria.

Next, we estimated the absolute ^{13}C-assimilation from bicarbonate into biomass by the MAGs, by normalizing MAG-specific ^{13}C-EAF values against the absolute abundance of the MAG 16S rRNA gene from qPCR (fractional 16S rRNA gene sequence %, as proportion of total 16S rRNA genes). The ^{13}C-assimilation normalized to absolute MAG abundance relates to the total amount of carbon assimilated by a MAG in the qSIP experiments. Across all three concentrations of bicarbonate tested, MAGs with mixotrophic potential encoding the CBB cycle contributed overwhelmingly to the total carbon flux and were responsible for the 82.2%, 95.2% and 77% of the ^{13}C-labeled carbon turnover in the 1 mM, 5 mM and 10 mM bicarbonate incubations, respectively (Figure 3). The mixotrophic production by these bacteria was at least 8.8 times higher than the absolute amount of carbon fixation by the autotrophic rTCA encoding Aquificae (Figure 3). We acknowledge that these results are only tested under a limited set of conditions and cannot speculate as to how widespread this dominance of carbon fixation by mixotrophic bacteria might be in other subsurface hydrothermal ecosystems. Nevertheless, to our knowledge these are the first quantitative measurements of primary production by mixotrophic bacteria in a deep subsurface hydrothermal environment and show that this should be considered as an important mechanism supporting deep thermophilic microbial ecosystems. Our results are also supported by another SIP-study that has also shown the importance of mixotrophs in oligotrophic groundwater (Taubert et al. 2022). Therefore, primary

production by mixotrophic bacteria might be an important, yet understudied mechanism that helps microbial ecosystems to survive under extremely oligotrophic conditions.

There are benefits to being a in the oligotrophic deep subsurface hydrothermal aquifer system. Mixotrophs have the potential to adjust how they meet their anabolic needs depending on the availability and changing concentrations of carbon (inorganic and organic) that are accessible as they are transported through the subsurface aquifer system. Our findings show that mixotrophic lifestyle can confer fitness on the bacteria under the tested conditions, and that mixotrophy may be especially important in oligotrophic hydrogeologically isolated systems where the concentrations of carbon substrates are extremely low and fluctuate over time (Moser et al. 2005; Taubert et al. 2022; Magnabosco et al. 2016).

4.5 Concluding Remarks

Our qSIP study coupled with metagenomics and phylogenetic approaches permitted us to unravel the carbon flow among microbial groups displaying distinct metabolic pathways and lifestyle characteristics. It is demonstrated that mixotrophic bacteria can contribute to the primary production across a range of bicarbonate concentrations as a key player in deep subsurface hydrothermal ecosystems. These mixotrophs exhibit a broad range of potential metabolic capacity to obtain their carbon needs through CO_2-fixation and organic carbon utilization, allowing them to dominante in an oligotrophic, hydrothermal aquifer system. The resulting carbon fixation is acquired relatively quickly by heterotrophic bacteria indicating that primary production via mixotrophy plays a quantitatively important role in sustaining the larger microbial community in this oligotrophic, deep hydrothermal ecosystem.

4.6 Material and Methods.

4.6.1 Sampling for microbial biomass and geochemistry analyses.

Alkaline hydrothermal fluids were collected in summertime of the years between 2019 and 2021 from 75- and 750-meter wells owned by a private hotel (Kaz Mountain Thermal Hotel) in Bardakçılar Village, Biga peninsula (Figure S1). Electrical conductivity (Ec) (WTW, Cond 3110 Set 1, Weilheim, Germany), temperature, salinity (WTW, Cond 3110 Set 1, Weilheim, Germany), pH (WTW, pH 3110 Set 2, Weilheim, Germany), dissolved oxygen (WTW Oxi 3310, Weilheim, Germany) and total dissolved solids (TDS) were measured in the field using handheld probes. 10 to 20 liters of water directly from borehole were filtered through 0.22 µm hydrophilic polyethersulfone (PES) filters (Millipore Express, Merck, Darmstadt, Germany) for 20 minutes at a medium speed using a peristaltic pump (Masterflex E/S 07571-05, Cole Parmer, USA). 4 replicates were collected for the filters. Collected samples were immediately placed into dry ice supplied by a local company in Turkey.

The detailed information on the laboratory-based measurements can be found in previously published article (Einsiedl et al. 2020). Briefly, samples for laboratory-based measurements of major anion and cation concentrations and water isotopes ($\delta^{2}H$ and $\delta^{18}O$) were collected in 1.5 ml tubes after filtering with 0.2 µm PES filters. Samples for analysis of DOC (dissolved organic carbon) concentrations were collected in 50 mL glass bottles after filtering through 0.45 µm PVDF filters. Samples for the concentrations and isotope analysis of methane ($\delta^{13}C$) were transferred into 200 mL glass vials without headspace and sealed with crimped butyl stoppers. Samples for dissolved organic matter (DOC) measurements were collected in a 100 mL glass vials and sealed with crimped butyl stoppers. All samples were stored in the dry ice. Laboratory measurements were done in hydrogeology department of Technical University of Munich (TUM).

4.6.2 Regional geology of Bardakçılar thermal field and additional information about the hotel

The Biga Peninsula is in the north-west of Turkey and is surrounded by the sea of Marmara in the north and Aegean Sea in the west and south (Figure S1) and historically known as Troas or Troad after the ancient city Troy. Biga peninsula is the west part of the Sakarya Continent and the eastern part of the Rhodope belt which formed tectonically by the collision of Gondwana and Laurasia (Okay et al. 1991). Therefore, the regional geology of the Biga peninsula has a complicated geologic and tectonic history. The detailed regional geology can be found in (Okay et al. 1991).
Kazdagi Thermal Resort and SPA hotel is in Bardakçılar village in the Kaz Mountain, Biga peninsula, Turkey (Mount Ida) (Figure S1). The hotel facility sits on the Middle Miocene İlyasbaşı formation (Figure S1). The reservoir bedrock of the Bardakçılar geothermal field is carbonate rocks in Permo-Triassic Kazdag massif. The fluids rise through Upper Oligocene-Lower Miocene Hallaçlar volcanic rocks (Toh) which consists of andesite, volcanic tuff, dacite, rhyodacite and anglomerate (Akkuş et al. 2005). Granodioritic intrusions due to Oligocene-Miocene volcanic activity are outcropped in the studied area (Sarp et al. 1998) and may constitute the source of the heat. North-east-south-west trended faults in Bardakçılar geothermal field as well as in nearby geothermal fields in Can and Etili are the main source of the heat transfer (Figure S1). Before the drilling of 750 meter-deep-borehole, the Bardakçılar hot spring has been reported to have a temperature of 59 °C (Sarp et al. 1998). The nearest borehole in the region, Can-Etili borehole, also carries 59 °C geothermal water at a depth of 450 meters and the geological units which were crossed in the borehole drilling consisted of andesite and volcanic tuffs. The hotel uses 4 different pumps, but only two of them are being actively used at different times of the year due to the difference in the temperature. Although the pumps are located 60 meters below the ground for these two wells (Personal communication with hotel owner), water temperatures are 56.7 °C and 73 °C for 75 meter-deep well and 750 meter-deep well, respectively. Hotel owner also informed us that the 750-meter deep well was drilled by a private gold company to seek commercially extractable gold in the field. The drilling ended up with 73 °C water which was then rented by the hotel owners and the construction of the hotel was subsequently completed. The deep well is only being used in the winter times when the winter conditions prevail in this mountainous area and therefore, it was at least 6-month-long inactive in 2021. Upon opening the

valve, the temperature of the well was measured as 58 °C. Water temperature increased to 62 °C after 20 minutes.

4.6.3 Experimental setup for SIP incubations and DNA extraction.

For incubation experiments, 5-liter borosilicate bottles (VWR, Germany) were filled with 62 °C geothermal water until 5% - 10% headspace left (Figure S2-b and c). Each bottle was amended with either ^{13}C-labeled 1, 5 and 10 mM sodium-bicarbonate (99% ^{13}C-content, Sigma-Aldrich, Darmstadt, Germany) (Figure S2-C). No additional electron donors/acceptors were added to the incubations except the atmospheric O_2 which was introduced to the incubations prior to addition of bicarbonate. We did not flush the bottles with any noble gas to purge the introduced O_2 but initial O_2 concentration of the hydrothermal fluid already contained a certain amount of O_2 (Table S1). As is common practice for all DNA-SIP studies, control vials were also prepared with the same unlabeled (^{12}C-containing) carbon sources to compare the extent of ^{13}C-labeling. Each bottle was sealed with rubber stoppers prior to tightly screwing the caps (Figure S2-c). The experiments were incubated at 58 °C and terminated after 135 hours (5 days and 15 hours). The pH, Ec, salinity and dissolved O_2 measurements were conducted before and after the incubation. The experiments were filtered onto 0.22 µm filters using a peristaltic pump (Figure S2-d) and kept in dry ice in the field until being stored at -20 °C. Samples were shipped to our laboratory in Germany in dry ice.
After the samples reached our laboratory, DNA was extracted from (t_0) and Stable Isotope Probing experiments (SIP) as described previously (Orsi et al. 2015). In brief, four of 2 mL Lysing Matrix E tubes (MP Biomedicals, Solon, OH, USA) were poured into each 15 mL falcon tube containing the filters. 4 mL of a sterile-filtered sucrose ethylene-diaminetetraacetic lysis buffer (0.75 M sucrose, 0.05 M Tris-Base, 0.02 M ethylenediaminetetraacetic, 0.4 M NaCl, 4 mL 10% sodium dodecyl and pH 9.0) were added to the tubes and then, beat beating was performed for 40 sec using a Fast-Prep 5G homogenizer (MP Biomedicals, OH, USA) at a speed of 4 m / sec. Samples were subsequently heated for 2 min at 99 °C. After heating, 25 mL of 20 mg mL^{-1} proteinase K was added, and tubes were incubated at 55 °C overnight. DNA was extracted and purified from the lysate using the DNeasy Blood and Tissue Kit (Qiagen). DNA was suspended with 200 µl (DEPC)-treated (sterile, nuclease free) water. Extracted DNA was quantified fluorometrically using Qubit 3.0 fluorometer (Invitrogen, Eugene, OR, USA).

4.6.4 Experimental considerations.

Hydrothermal fluid is directly collected from the pipe system before it enters to the water tank (Figure SX). The atmospheric air is introduced to the bottles and we did not flush the bottles with "N_2" gas to create O_2 concentration similar to the initial conditions (Dataset 1). Therefore, the redox potential is likely to be altered to certain degree. Although we did not have any killed control experimental setup to test if the decline in dissolved O_2 measurements was associated with the microbial respiration, we speculate that microbial respiration was the main driver in this drawdown in the gas-tight SIP incubations (Dataset 1), supported by previous report in a $H_2{}^{18}O$ qSIP study.

Apart from oxygen, pH values also dropped by 1 in the incubations amended with 10 mM sodium-bicarbonate, meaning that the increase in the bicarbonate concentration favored more dissolved CO_2 (aq) speciation as it is a similar effect in ocean acidification event (Turley et al. 2010). The fluid chemistry after the termination of SIP-experiments also showed 10 mM addition of sodium bicarbonate increased Ec, salinity and sodium concentrations compared to 5 mM sodium-bicarbonate. Hence, the conditions in the incubations were slightly different from each other due to addition of different amounts of bicarbonate.

4.6.5 Density gradient centrifugation and gradient fraction.

DNA samples were prepared for density gradient centrifugation according to previously defined protocols for quantitative SIP (qSIP) (Coskun et al. 2018; Hungate et al. 2015) with minor modifications. In brief, density gradient centrifugations were carried out in a TLN-100 Optima MAX-TL ultracentrifuge (Beckman Coulter, Brea, CA, USA) near-vertical rotor at 18 °C for 72 h at 165,000 × g. 50 µl of DNA was added to a solution of cesium chloride (CsCl) and gradient buffer (0.1 M Tris, 0.1 M KCl and 1 mM EDTA) in order to achieve a starting density of 1.705 - 1.715 g mL^{-1} in a 3.3-mL polyallomer OptiSeal tubes (Beckman Coulter, Brea, CA, USA). For the triplicate ultracentrifuge runs from the same experiments, we used three sets of 50 µl of extracted DNA. After ultracentrifugation, the density gradients were fractionated into 20 equal fractions of 165 µl from the bottom of polyallomer OptiSeal tubes by using a syringe pump and fraction recovery system (Beckman Coulter, Brea, CA, USA). The density of these fractions was measured with an AR200 digital refractometer (Reichert Analytical Instruments, Depew, NY, USA). DNA was precipitated from the fractions using two volumes of polyethylene glycol with 2 µl (10 mg mL^{-1}) glycogen and precipitated overnight at room temperature. DNA was pelleted by centrifugation (13,000 × g; 40 min), washed with 70% ethanol, and resuspended with 30 µl molecular-grade (DEPC-treated) water. DNA was quantified fluorometrically using a Qubit 3.0 fluorometer (Thermo Scientific).

4.6.6 qPCR of 16S rRNA gene copies.

Universal primers targeting the V4 hypervariable region of 16S ribosomal RNA (rRNA) genes were used in quantitative PCR (qPCR) to determine density shifts in the peak DNA of buoyant density (BD) for each incubation. We used a version of the 515F primer with a single-base change (in bold) to increase the coverage of certain taxonomic groups (515F-Y, 5′-GTGYCAGCMGCCGCGGTAA; (Parada et al. 2016)). qPCR reactions were carried out as described previously (Coskun et al. 2019). The quantified 16S rRNA genes of the density fractions were plotted against their corresponding densities and 10-12 fractions (on average) from each replicate set were selected for sequencing (Figure S3-A, S3-B, S3-C; gray shaded area). Two 16S PCR amplicons from each density fraction (technical replicates to reduce PCR bias) were pooled and subjected to dual-indexed barcoded sequencing of 16S rRNA gene amplicons on the Illumina MiniSeq as described previously (Pichler et al. 2018).

4.6.7 Bioinformatic and qSIP Analysis.

The MiniSeq reads from fractionated SIP incubations, t_0 and previously sequenced common laboratory contaminants (Pichler et al. 2018) were quality trimmed and assembled using USEARCH version 11.0.667 with the default parameters (Edgar 2010) resulting in 28.4 million quality checked 16S rRNA V4 reads. Reads were then de novo clustered at 97% identity using UPARSE; Operational Taxonomic Units (OTUs) represented by a single sequence were discarded (Edgar 2013). Taxonomic assignments were generated by QIIME 1.9.1 (Caporaso et al. 2010) using the implemented BLAST method against the SILVA rRNA gene database release 132 (Quast et al. 2013). The level of contamination in each density fraction for qSIP analysis was determined using DNA sequences of the dust samples collected from three different laboratories in our building. The common contaminant genera such as *Pseudomonas*, *Ralstonia*, *Variovorax* or *Streptococcus* were also removed as these are common contaminants of molecular reagent kits (Salter et al. 2014). Next, only OTUs greater than 10 sequences in total in each replicate for the control and SIP-labeled fractions were selected for further study (Orsi et al. 2016; Coskun et al. 2018) since low abundance taxa may cause large variations in qSIP calculations (Morrissey et al. 2016).
The excess atom ^{13}C fractions (EAF) values were calculated for the 16S rRNA genes corresponding to OTUs according to previously described study (Hungate et al. 2015) using a qSIP workflow embedded in the HTS-SIP R package (Youngblut et al. 2018a). An OTU was considered as an ^{13}C-incorporator if the lower CI was greater than zero (Hungate et al. 2015). Statistical analyses and plots were performed using RStudio Version 3.3.0 (Team 2015). The 16S sequence data were entered in the NCBI Short Read Archive under BioProject ID PRJNA837050.

4.6.8 Metagenomic analysis of ^{13}C-labeled fractions.

Based on the shift in DNA buoyant density of 16S rRNA genes between the experimental treatments (which indicate ^{13}C-labeling of DNA), ^{13}C-labeled stable isotope probing (SIP) fractions resulting from the density gradient ultracentrifugation were selected for metagenomic shotgun sequencing (Figure S6D). Metagenomic libraries were prepared using Nextera XT DNA Library Prep Kit (Illumina) and following the manual provided by the manufacturer. Quality control and quantification of the metagenomics libraries were done on an Agilent 2100 Bioanalyzer System using high sensitivity DNA reagents and DNA chips (Agilent Genomics). Metagenomic libraries were diluted to 1 nM and pooled together to sequence on Illumina MiniSeq platform. SqueezeMeta (Tamames and Puente-Sánchez 2018) and Anvi'o snakemake workflow (Köster and Rahmann 2012; Eren et al. 2015) were used for downstream analysis using co-assembly mode with default settings. In short, SqueezeMeta workflow deployed Trimmomatic for adapter removing, trimming and quality filtering by setting the parameters: leading = 8, trailing = 8, slidingwindow = 10:15, and minimum length = 30 (Bolger et al. 2014). Contigs were assembled using Megahit assembler using minimum length 200 nucleotides (Li et al. 2015). Open reading frames (genes and rRNAs; ORFs) were called using Prodigal (Hyatt et al. 2010), rRNAs genes were determined by barrnap (Seemann 2013). Diamond software (Buchfink et al. 2015) was deployed to search for gene homologies against the databases Genbank nr database

for taxonomic assignment, eggNOG v4.5 (Huerta-Cepas et al. 2016) and KEGG database (Kanehisa and Goto 2000). Cutoff values for assigning hits to specific taxa were performed at e value as e^{-3}, and a minimum amino acid similarity of 40 for taxa and 30 for functional assignment which were default settings of SqueezeMeta. Bowtie2 (Langmead and Salzberg 2012) was used to map the read onto contigs and genes. Anvi'o snakemake workflow (anvi'o v7) was used to bin and to refine the Metagenome assembled genomes (MAGs). MaxBin (Wu et al. 2016), concoct (Alneberg et al. 2014) and Metabat2 (Kang et al. 2019) were deployed for the binning and DAS Tool (Sieber et al. 2018) was deployed to choose the best bin for each population. The completeness and contamination of the bins were checked in anvi'o v7. The metagenomic sequence data will be entered in the NCBI Short Read Archive under BioProject ID PRJNA837050. Metagenomic dataset and intermediate files to produce qSIP results were deposited under https://figshare.com/authors/_mer_Coskun/9725927.

4.6.9 Phylogenetic tree construction

16S rRNA gene phylogenetic trees (*SI Appendix*, Figure S8A and S8B) was constructed using GTR algorithm with 100 bootstraps in Seaview (Gouy et al. 2010). In brief, rRNA and single copy genes were extracted from the MAGs using hidden markov model (HMM) sources of barnapp (Seemann 2013) and 'Bacteria_71' (a modified version of (Lee 2019)) in anvio's 'anvi-run-hmms' command (Eren et al. 2015), respectively. Ribosomal phylogenetic tree (*SI Appendix*, Figure S8C) was constructed using Seaview (Gouy et al., 2010) with 5 concatenated ribosomal proteins (L18, L3, L4, S11, S3) extracted from metagenome assembled genomes and closest complete or incomplete genomes to our MAGs determined by a BLAST search (Altschul et al. 1990).

4.6.10 Calculating Absolute ^{13}C-labeled carbon of MAGs linked with ^{13}C-labeled OTUs

The absolute ^{13}C-labeling in MAGs were calculated after associating them with a ^{13}C-labeled OTU. In brief, by multiplying the relative abundance of each linked OTUs (determined from sequencing from the fractions) to total 16S rRNA gene copy number per mL (obtained from qPCR) in each bicarbonate concentration tested in this study, we calculated the absolute 16S rRNA gene copy number of each linked OTU. We assumed that each MAG contains one copy of 16S rRNA gene in their putative complete to incomplete genome. Also, we confirmed that our MAGs linked to ^{13}C-labeled OTUs did contain one copy of 16S rRNA in their genome. Absolute 16S rRNA gene per OTU were multiplied by corresponding EAFs calculated in qSIP (Hungate et al. 2015) to obtain absolute ^{13}C-labeling of each OTU. Since each OTU is linked to a representative high-quality MAG in this study, those absolute ^{13}C-labelings also belong to corresponding ^{13}C-labeled MAGs.

4.7 Acknowledgements

This work was supported by the Deutsche Forschungsgemeinschaft (DFG, German Research Foundation)—Project-ID 364653263—TRR 235 to WDO and WE, and under Germany's Excellence Strategy—EXC 2077-390741603. We are grateful for the support of the management and the staff

of Kazdagi Thermal Resort & Spa. We also thank to Mustafa Coskun and Halil Gültekin who participated a part of field campaign in 2019 and 2020.

FIGURES AND TABLES

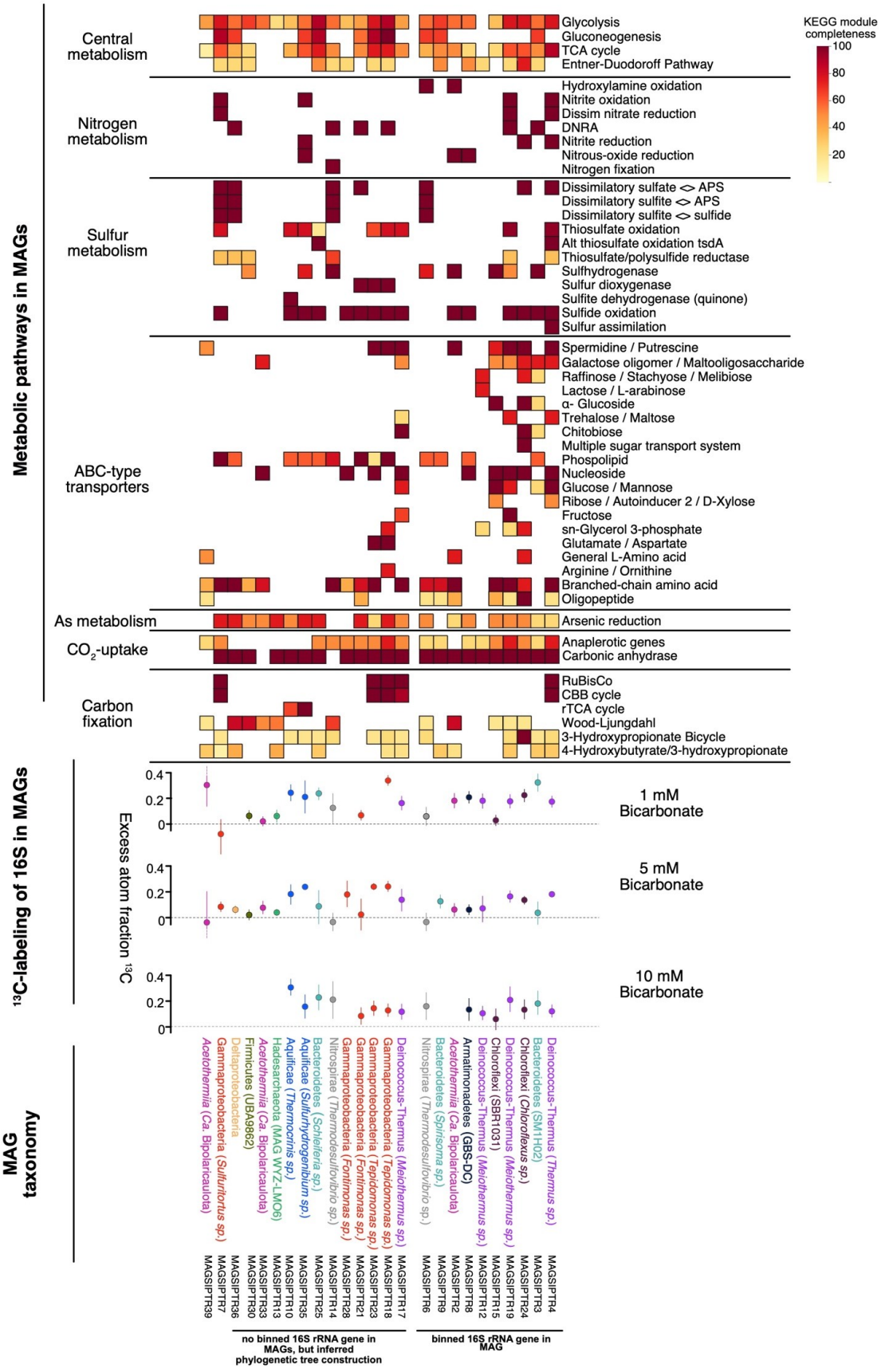

Figure 1: Top panel: KEGG decoder heatmap (Graham et al. 2018) showing the metabolic pathway completeness of each MAG assembled in this study. MAGs are sorted based on number of transporters they have and grouped into two categories: right column shows the MAGs that have a binned 16S rRNA, whereas left column represents the MAGs that do not have binned 16S rRNA. The linkage between ^{13}C-labeled OTUs and MAGs are briefly explained the main text and the materials and methods section. **Middle panel**: Quantitative assimilation of ^{13}C from $H^{13}CO_3^-$ by OTUs at three different concentrations (1mM, 5 mM, 10 mM). Individual points represent excess atom fraction (EAF) values of specific OTUs, which are colored by Phylum for qSIP incubations that received different bicarbonate concentrations. The error bars correspond to 90% CI across three biological replicates. OTUs that do not have a 90% CI overlapping with 0 are considered to be ^{13}C-labeled. The x-axis EAF values indicate the quantitative ^{13}C-enrichment of OTU 16S rRNA genes (e.g., an EAF value of 0.5 relates to 50% of carbon atoms in an OTU being ^{13}C-labeled). **Bottom panel:** Taxonomy of the MAGs. Taxonomical classification of MAGs represents the classification of OTUs against SILVA v132 database and single copy gene taxonomy of the MAGs determined in anvi'o (Eren et al. 2015).

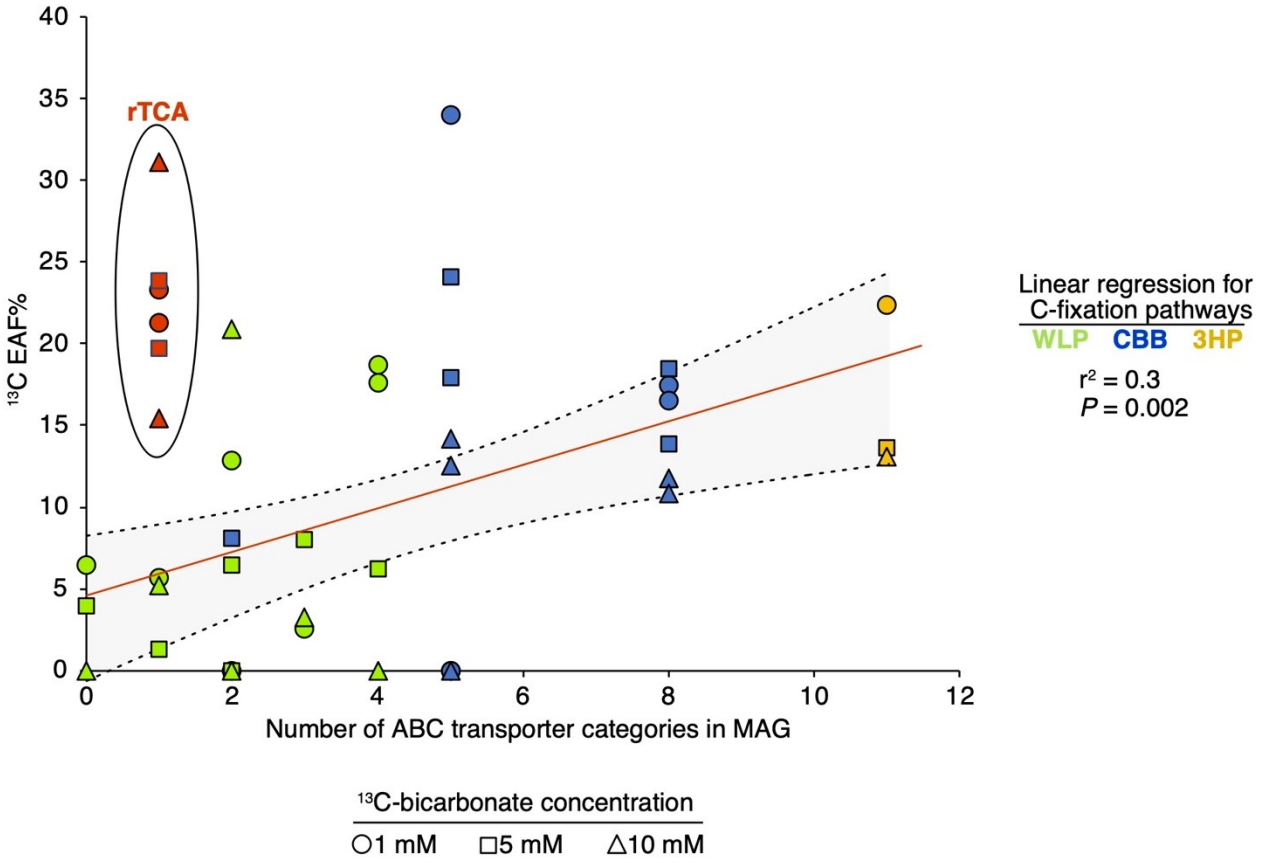

Figure 2: Correlation between MAG ^{13}C-bicarbonate assimilation at three different bicarbonate concentrations and the number of ABC transporters encoded per MAG. Colors indicate which carbon fixation pathway is encoded by the MAG, symbols show which bicarbonate concentration the EAF value is derived from.

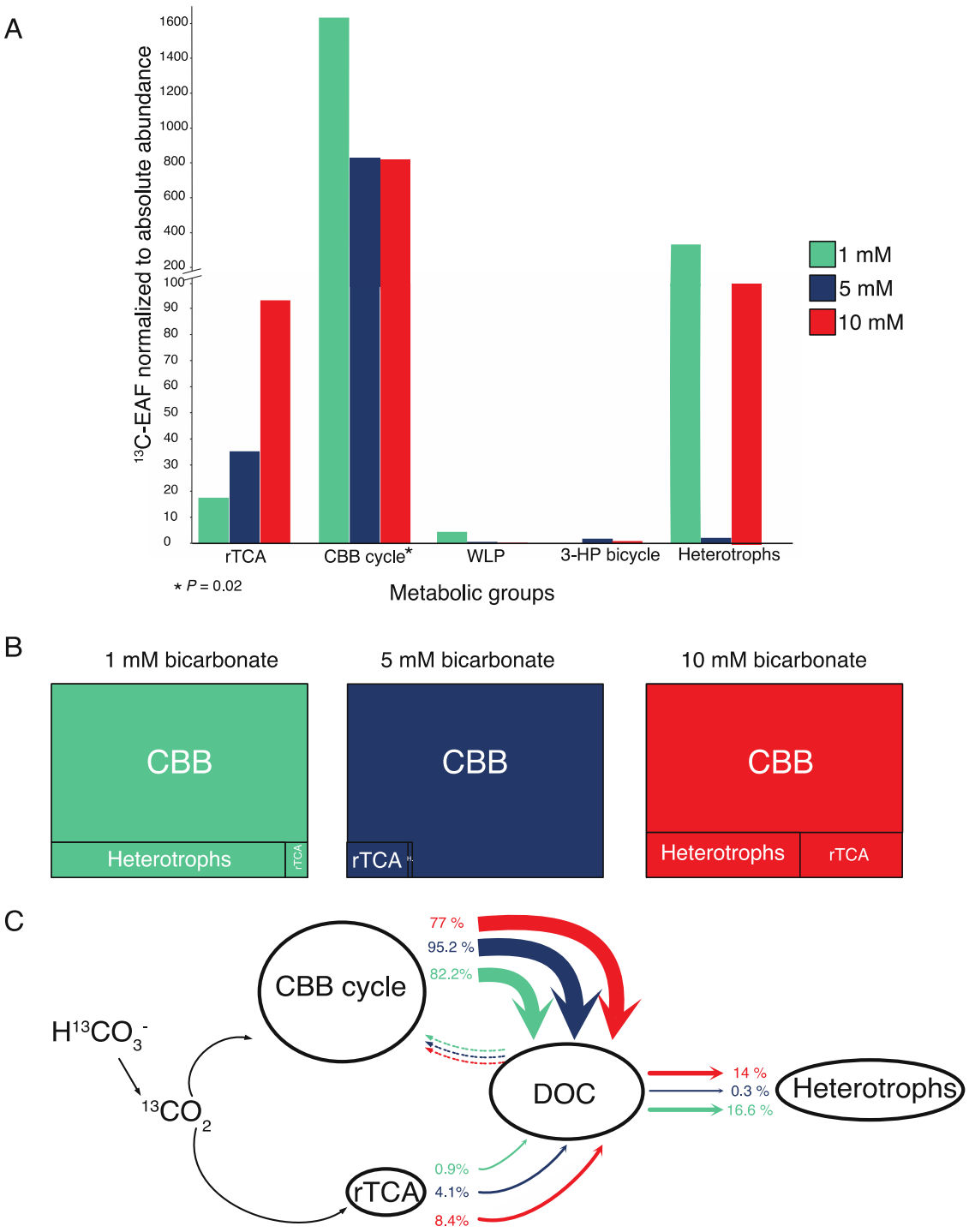

Figure 3: Panel A: Quantitative carbon assimilation from bicarbonate or secondarily produced ^{13}C-DOC across three different concentrations, summarized for MAGs encoding carbon fixation pathways as well as MAGs defined as heterotrophs (no C-fixation pathway detected). The y-axis depicts the average MAG specific carbon assimilation (EAF), normalized against the absolute abundance of each MAG in the hydrothermal fluids determined via 16S qPCR and high-throughput sequencing. **Panel B:** Distribution of ^{13}C-labeled carbon across MAGs encoding carbon fixation pathway as well as heterotrophic MAGs in a rectangular graph. The areas that each category holds in rectangles are proportional to ^{13}C-labeled carbon incorporation of microbial populations grouped by carbon fixation pathways (% in each bicarbonate concentration). Note that the highest

total amount of carbon assimilation was seen in the CBB encoding MAGs, which is due in large part to the higher absolute abundance of these organisms in the fluids as determined by qPCR. **Panel C:** Schematic representation of carbon flow from autotrophs to heterotrophs. The percentages represent the ^{13}C-labeled carbon incorporation across carbon fixation pathways (and heterotrophs) and are obtained from Panel A and used in Panel B.

Supplementary Figures

Dataset 1. **Water chemistry and information of the sampling sites.** Note that we also provided the water chemistry of the closest geothermal fields to our sampling site in Biga Peninsula, Turkey.

Name of the geothermal field/well	Depth of the fluid	Temperature (°C)	pH	Ec (uS/sn)	Oxygen (mg/L) @T	Salinity (ppm or mg/L)	Carbonate hardness (mmol/L)	Bicarbonate (ppm) Yalcin, 2007	Bicarbonate (mg/L)	Bicarbonate in mM
Can	60 m	45,6	6,92	2200	0,49 @44	1,1 ppm	4,5 mmol/lt - 12.4 od	268,4	274,59	4,5
Hidirlar	Hot spring	78,5	8,13	889	1,38 @45	0,4	2,2 mmol/lt - 6 od	128,1	134,244	2,2
Bardakcilar geothermal field*	750 m	61.7**	8,27	1514	1,64 @47	0,8 mg/L	1,5 mmol/lt - 4od		91,53	1,5
Bardakcilar geothermal field	75 m	56.7	8,28	1340	0,99 @47	680 ppm	2 mmol/lt - 5.5 od		122,04	2,0

anions												DOC	methane		
Phosphate (mg/L)	Bromid (mg/L)	Chloride (mg/L)	Nitrate (mg/L)	Nitrite (mg/L)	Sulfat mg/L	Type	Na (mg/L)	NH_4 (mg/L)	K (mg/L)	Mg (mg/L)	Ca (mg/L)	NPOC (mg/L)	CH_4 (mg/L)	$d^{13}C$-CH_4	$d^{13}C$-CH_4
														d ^{13}C	std dev
n.a.	n.a.	170,9585173	n.a.	n.a.	1116,240992	Type-1 (Sulfate-dominant waters)	444,06	n.a.	21,48	8,63	218,18	0,9+-0,06%	0,0091		
n.a.	n.a.	8,37796944	n.a.	n.a.	204,6407377	Type-4 (No dominant species)	181,54	n.a.	5,75	n.a.	6,83	0,7+-0,03%	0,0018		
n.a.	n.a.	18,0157599	n.a.	n.a.	556,0052322	Type-1 (Sulfate-dominant waters)	244,05	n.a.	5,71	n.a.	74,23	0,8+-1,99%	0,0079	-10,43	
n.a.	n.a.	20,6054583	n.a.	n.a.	637,3433528	Type-1 (Sulfate-dominant waters)	238,03	n.a.	5,96	n.a.	76,62				

Dataset 2. **Summary of metagenome-assembled-genomes with their putative taxonomy assigned by anvi'o v7.**

MAG sample names	Related OTU	Total length	Num contigs	N50	GC content	Completion (%)	Redundancy (%)	Domain	Phylum	Class	Order	Family	genus	Species
MAGSIPTR10	OTU259	1663680	102	23118	38,84	91,54	0	Bacteria	Aquificota	Aquificae	Aquificales	Aquificaceae	Thermocrinis	Thermocrinis minervae
MAGSIPTR12	OTU9	706529	187	5556	62,47	0	0	Bacteria	Deinococcota	Deinococci	Deinococcales	Thermaceae	Meiothermus	
MAGSIPTR13	OTU151	1032973	292	4603	64,02	92,10	5,26	Archaea	Hadarchaeota	Hadarchaeia	Hadarchaeales	WYZ-LMO6	WYZ-LMO6	WYZ-LMO6 sp004347925
MAGSIPTR14	OTU425	1845029	34	84044	35,71	95,77	1,41	Bacteria	Nitrospirota	Thermodesulfovibrionia	Thermodesulfovibrionales	Thermodesulfovibrionaceae	Thermodesulfovibrio	Thermodesulfovibrio yellowstonii
MAGSIPTR15	OTU45	2403728	489	5181	62,92	74,65	5,63							
MAGSIPTR17	OTU1743	1960805	657	3840	61,79	81,69	4,23	Bacteria	Deinococcota	Deinococci	Deinococcales	Thermaceae	Meiothermus	Meiothermus cerbereus
MAGSIPTR18	OTU2	1813843	69	41332	69,38	42,25	5,63	Bacteria	Proteobacteria	Gammaproteobacteria	Burkholderiales	Burkholderiaceae	Tepidimonas	Tepidimonas ignava
MAGSIPTR19	OTU69	2908268	496	9566	60,98	84,51	0	Bacteria	Deinococcota	Deinococci	Deinococcales	Thermaceae	Meiothermus	Meiothermus hypogaeus
MAGSIPTR2	OTU56	1715316	119	21351	56,35	90,14	0							
MAGSIPTR23	OTU3132	1634774	52	47611	68,08	80,28	2,82	Bacteria	Proteobacteria	Gammaproteobacteria	Burkholderiales	Burkholderiaceae	Tepidimonas	
MAGSIPTR24	OTU24	4777522	251	29934	56,88	94,37	4,23	Bacteria	Chloroflexota	Chloroflexia	Chloroflexales	Chloroflexaceae	Chloroflexus	Chloroflexus aurantiacus
MAGSIPTR25	OTU19	2568817	38	142546	43,27	98,59	0	Bacteria	Bacteroidota	Bacteroidia	Flavobacteriales	Schleiferiaceae	Schleiferia	Schleiferia thermophila
MAGSIPTR28	OTU36	1921569	17	356240	65,94	66,2	0	Bacteria	Proteobacteria	Gammaproteobacteria	Nevskiales	Nevskiaceae	Fontimonas	Fontimonas thermophila
MAGSIPTR3	OTU16	2466952	271	12431	32,22	90,14	5,63							
MAGSIPTR30	OTU49	2119855	154	23185	48,82	84,51	1,41	Bacteria	Firmicutes	Dethiobacteria	DTU022	UBA8154	UBA9862	UBA9862 sp003444595
MAGSIPTR33	OTU100	1495287	474	4108	62,62	92,96	8,45							
MAGSIPTR35	OTU57	1591738	136	18555	32,26	95,78	1,41	Bacteria	Aquificota	Aquificae	Hydrogenothermales	Hydrogenothermaceae	Sulfurihydrogenibium	Sulfurihydrogenibium azorense
MAGSIPTR36	OTU220	2068330	750	3377	45,04	90,14	8,45							
MAGSIPTR39	OTU76	1043573	499	2221	56,02	83,1	4,23							

MAGSIPTR4	OTU1	2395327	366	11275	64,96	87,32	9,86	Bacteria	Deinococcota	Deinococci	Deinococcales	Thermaceae	Thermus	
MAGSIPTR6	OTU6	2137166	127	25177	39,36	92,96	0							
MAGSIPTR7	OTU46	2576370	236	18126	65,65	100	7,04	Bacteria	Proteobacteria	Gammaproteobacteria	Burkholderiales			
MAGSIPTR8	OTU125	3178920	446	11557	57,3	95,77	8,45	Bacteria	Armatimonadota	Fimbriimonadia	OS-L	GBS-DC	GBS-DC	GBS-DC sp001442985

Dataset 3. **Predicted metabolism of each metagenome-assembled-genomes (MAGs) generated in anvi'o v7.** (Dataset 3 can be found in https://figshare.com/authors/_mer_Coskun/9725927)

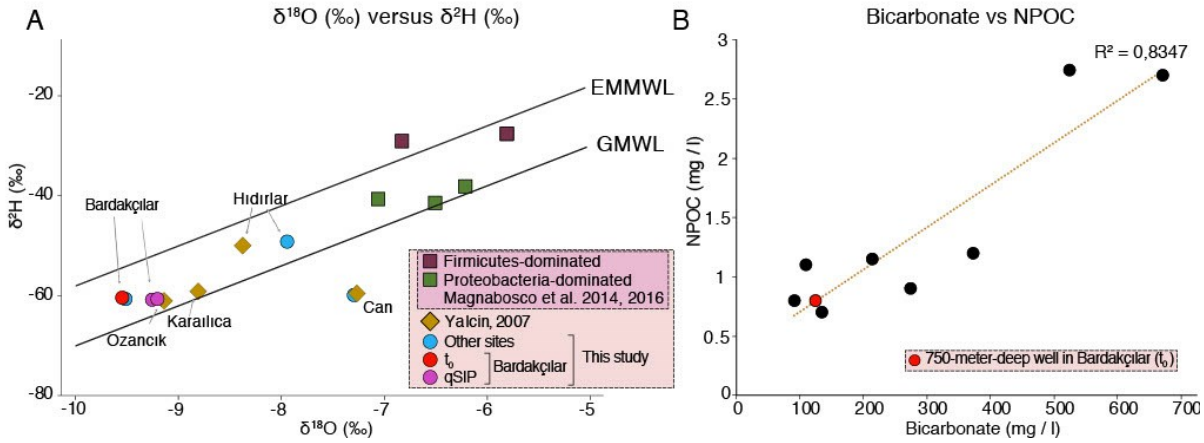

Figure S1: A) The δ^2H (‰) and $\delta^{18}O$ (‰) plot of thermal waters obtained in study (blue and red), and the other studies (Magnabosco et al. 2016; Yalcin 2007). The GMWL and EMMWL stand for Global Meteoric Water Line (Craig 1961) and East Mediterranean Water Line (Gat and Carmi 1970). B) Concentrations of NPOC (non-purgeable organic carbon; in other words, DOC) and Bicarbonate (in other words, DIC) across the sampled sites in Biga Peninsula (r^2 = 0.835). The bicarbonate concentrations were calculated from the values obtained from carbonate hardness test (Dataset 1).

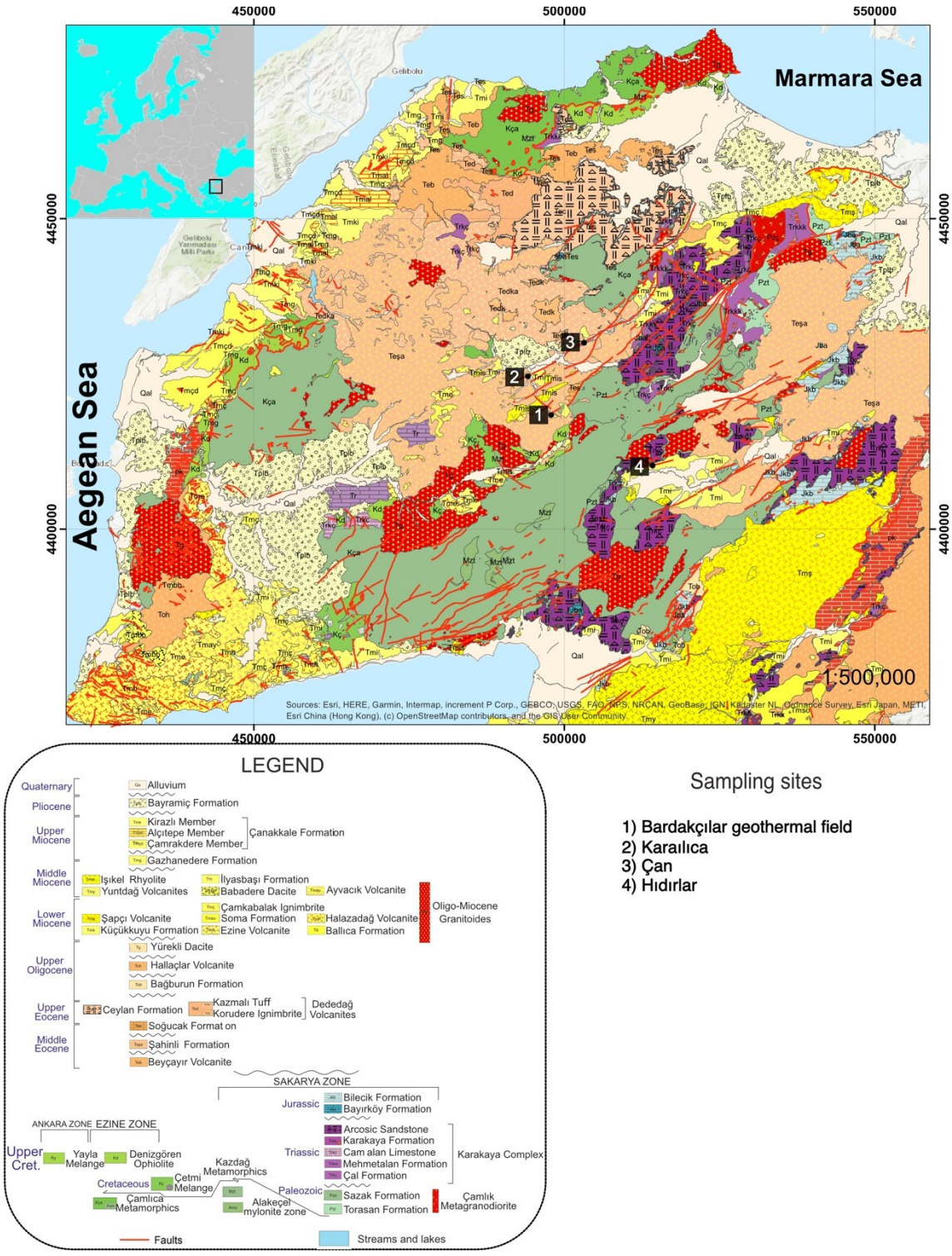

Figure S2: The geology map of Biga peninsula. The geological map is modified after Duru et al., 2007 which can be found online in provided by General Directorate of Mineral Research and Exploration of Turkey (MTA) (https://www.mta.gov.tr/en/). The sampling points were shown with corresponding numbers.

Figure S3: Photographs of the fluid sampling from the 750m deep aquifer and experimental setup, at the private hotel in Bardakçılar village (Biga Peninsula, Turkey). A) Pristine alkaline hydrothermal fluids that were collected, before the geothermal water enters the hotel plumbing system. Arrow shows the fluids that were sampled. The bottles were filled with fluid and incubated at high temperature with the labeled or unlabeled bicarbonate in the square shaped water collector. The bottles were secured in the water collector using fish nets (panel B). C) Incubations with added sodium-bicarbonate. D) Termination of the incubations. A field pump was used to filter the incubated alkaline hydrothermal fluids after the 135 hours of incubation.

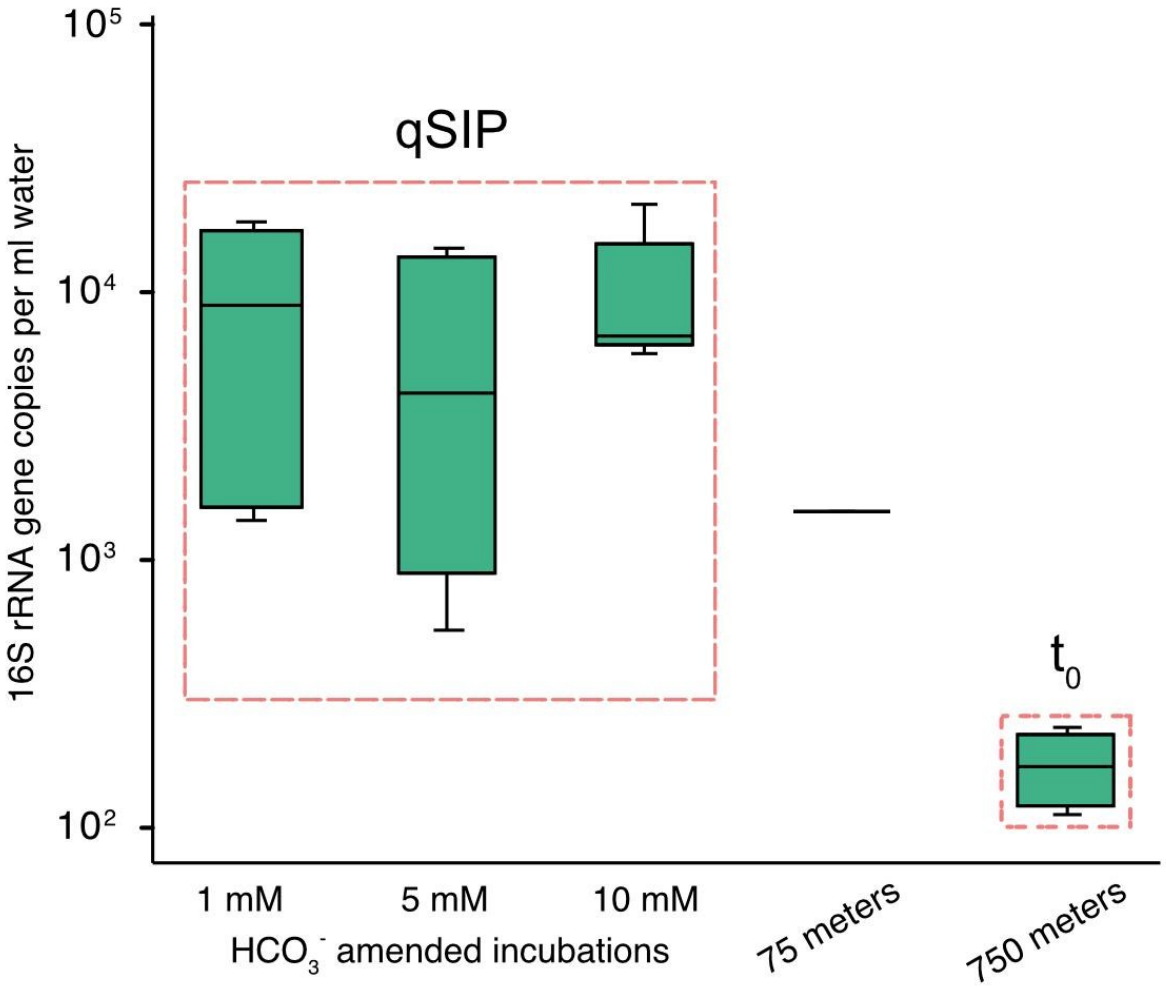

Figure S4: Concentration of 16S rRNA genes from the terminated qSIP experiments, 75-meter-deep well and 750-meter-deep well in Bardakçılar geothermal field. Concentrations are normalized to per mL for seawater samples. The detection limit for our DNA extraction and qPCR assay is 100 total copies of 16S rRNA genes per extractions and therefore all of the samples analyzed were above our detection limit (albeit still very low biomass).

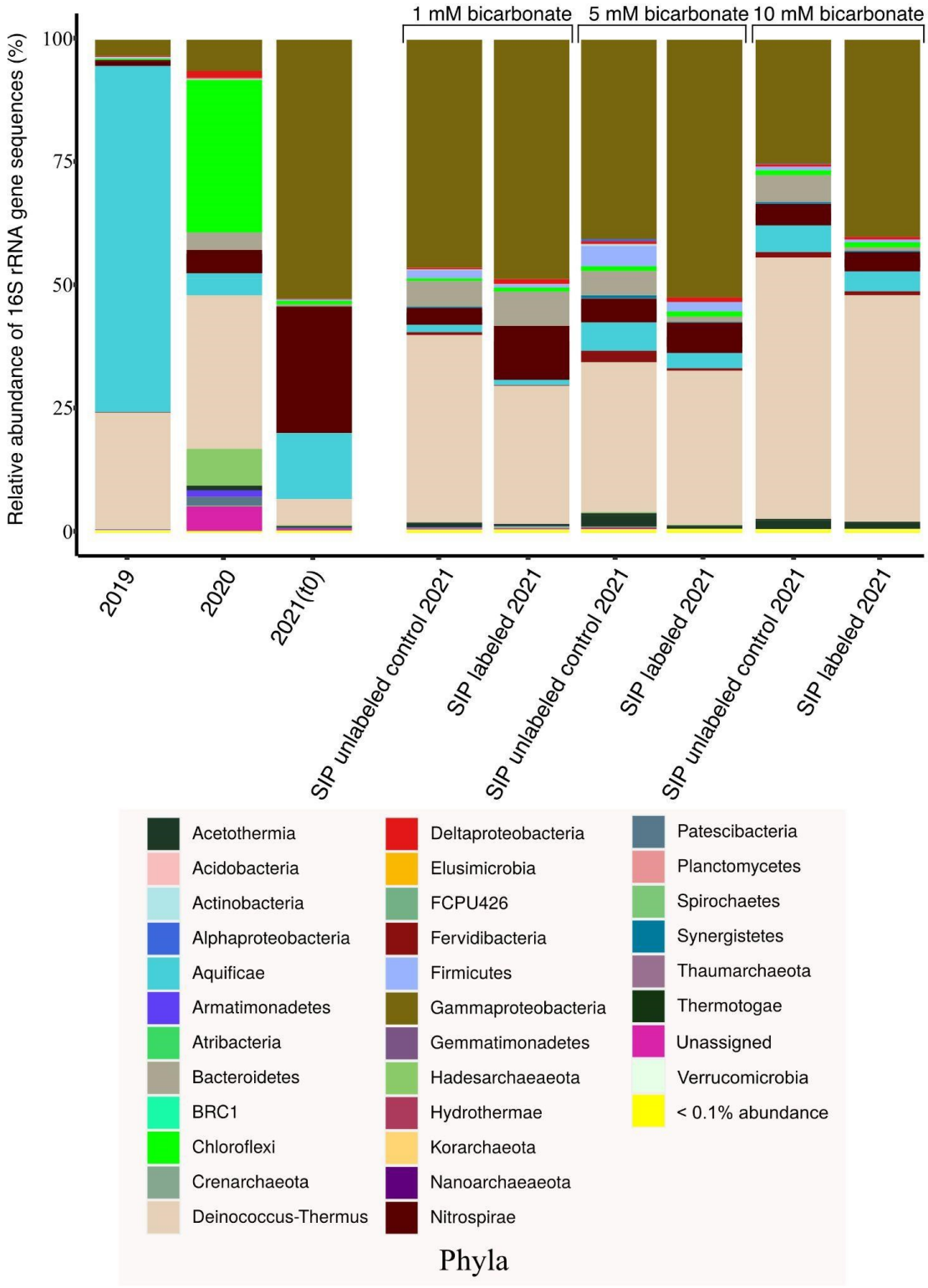

Figure S5: Stacked bar plots display the phylum-level microbial composition of 16S rRNA gene sequences.

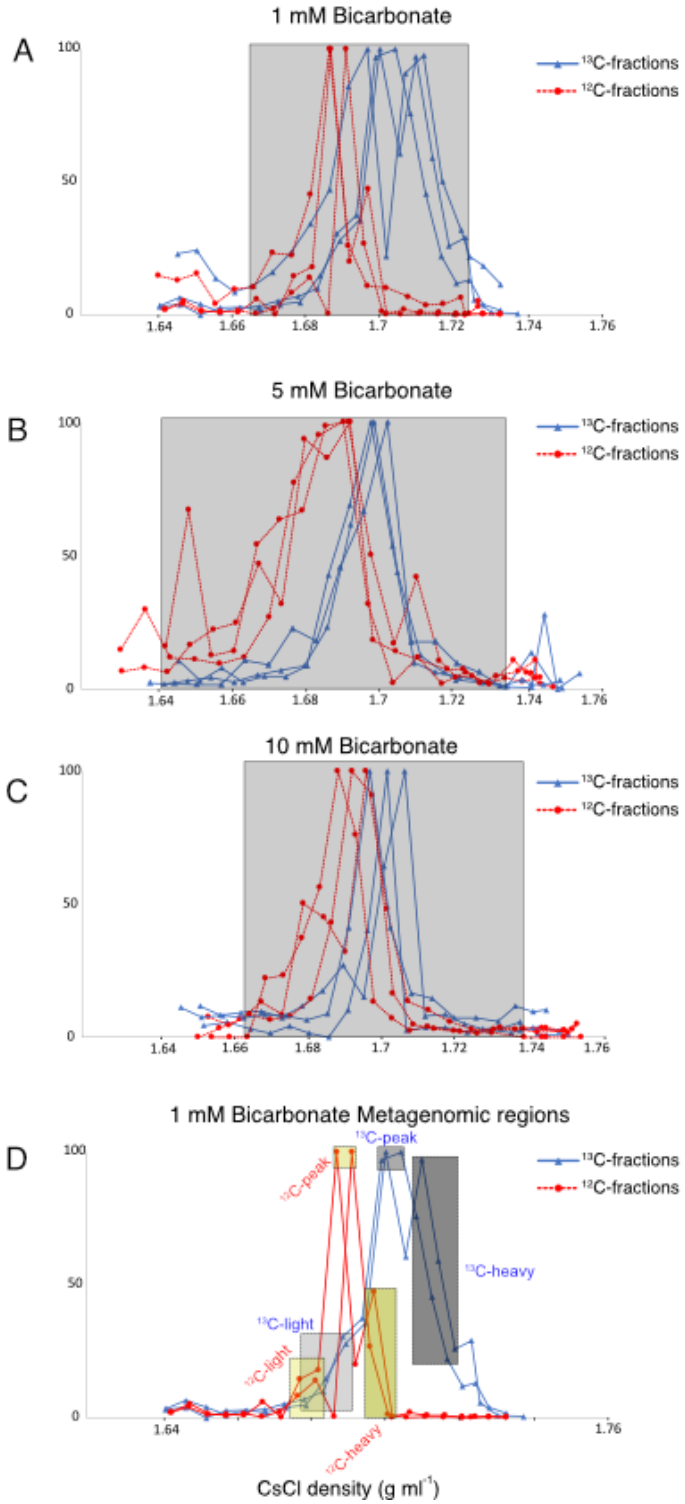

Figure S6: Quantification of 16S rRNA gene copies across CsCl density gradient fractions fractionated from incubations amended with (A) 1 mM, (B) 5 mM, and (C) 10 mM sodium-bicarbonate. ^{13}C-substrates are represented by blue solid lines and unlabeled replicates (control) are represented by red dashed lines. The y axis represents the relative abundance of 16S rRNA genes quantified with qPCR, normalized to maximal abundance across all density fractions. D) Selected fractions for light, peak and heavy regions that were used for metagenomic library preparation.

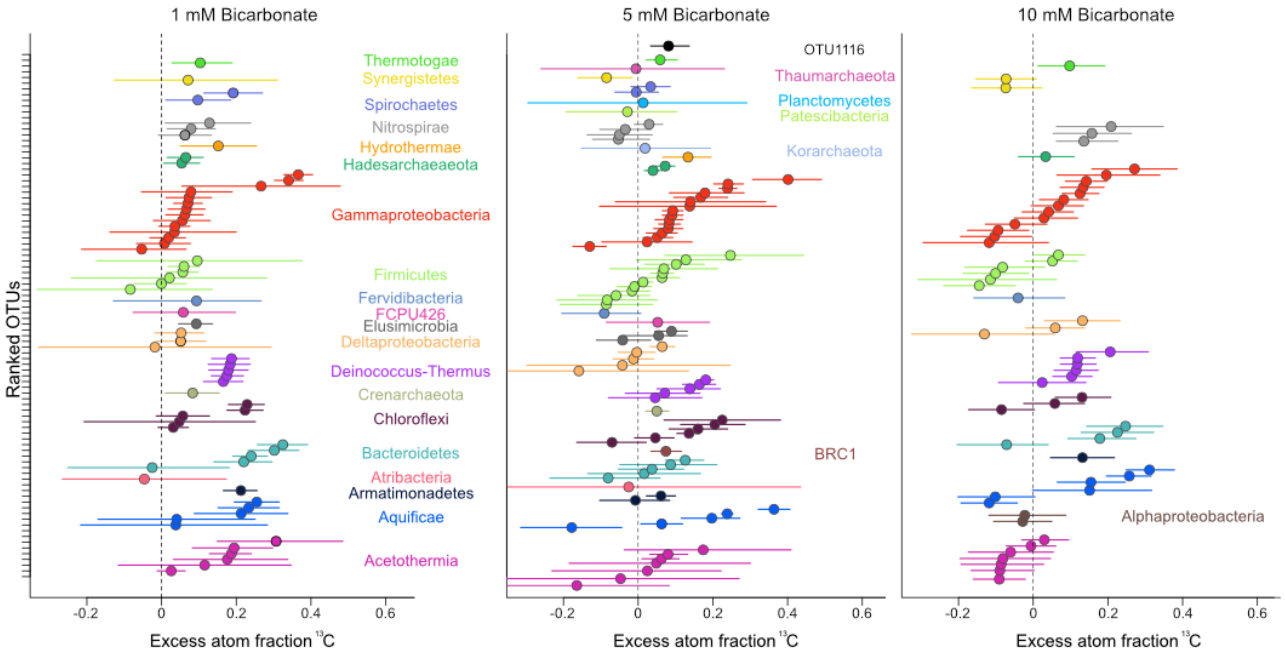

Figure S7: Quantitative assimilation of ^{13}C from $H^{13}CO_3^-$ by OTUs at three different concentrations (1mM, 5 mM, 10 mM). Individual points represent excess atom fraction (EAF) values of specific OTUs, which are colored by Phylum for qSIP incubations that received different bicarbonate concentrations. The error bars correspond to 90% CI across three biological replicates. OTUs that do not have a 90% CI overlapping with 0 are considered to be ^{13}C labeled. The x-axis EAF values indicate the quantitative ^{13}C enrichment of OTU 16S rRNA genes (e.g., an EAF value of 0.5 relates to 50% of carbon atoms in an OTU being ^{13}C-labeled).

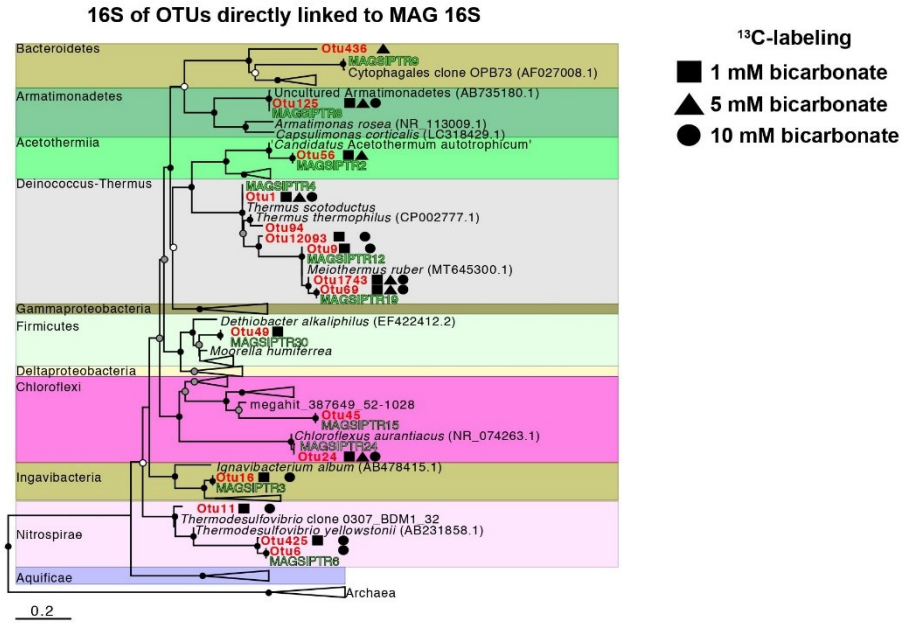

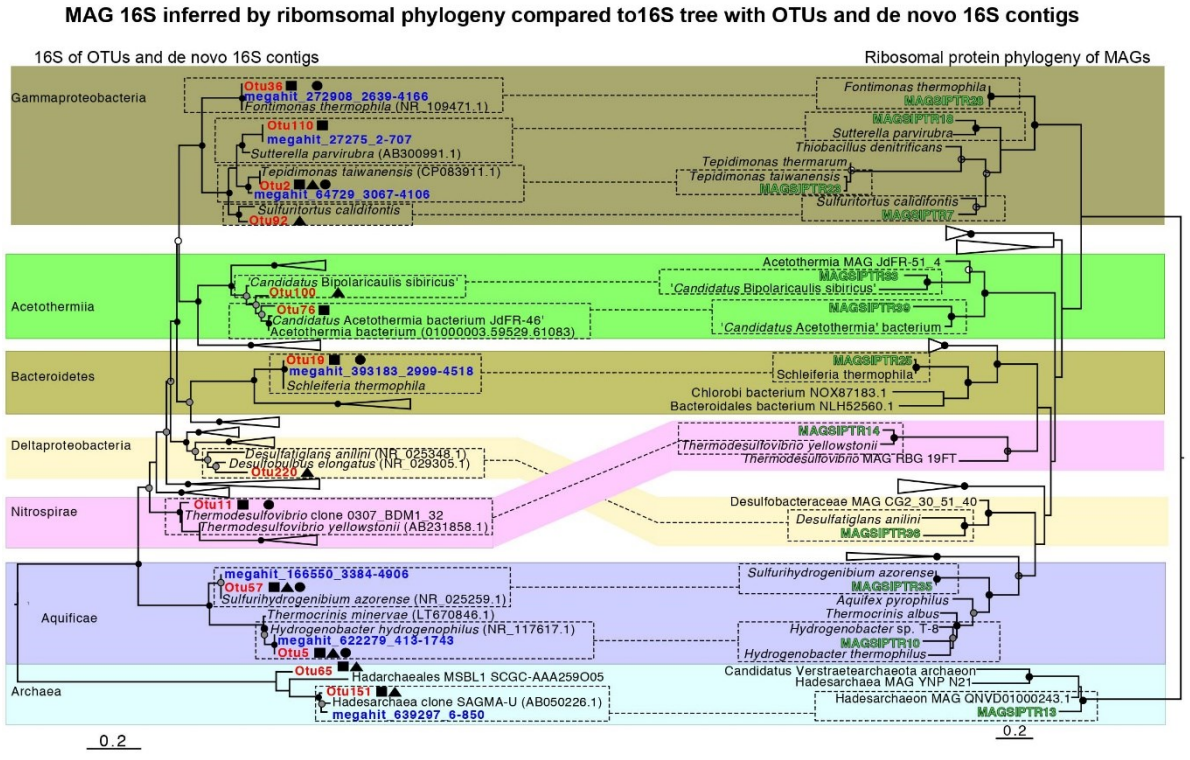

Figure S8: Top Panel (A): Phylogenetic tree of 16S rRNA gene of ^{13}C-labeled OTUs including their most similar sequences from the NCBI database and MAGs that have a binned 16S rRNA gene. **Bottom Panel Left (B):** Phylogenetic tree of 16S rRNA gene of ^{13}C-labeled OTUs together with 16S rRNA gene of closely related genomes to the MAGs that does not have a binned 16S rRNA gene. Blue colored texts represent the 16S rRNA gene that could not be binned but present in the contigs (determined by SqueezeMeta workflow). **Bottom Panel Left (C):** Phylogenetic tree of 5 ribosomal proteins (L18, L3, L4, S11, S3) extracted from metagenome assembled genomes and closest complete or incomplete genomes to our MAGs determined by a BLAST search. Black circles at nodes

represent bootstrap support of 90%, gray circles represent bootstrap support from 70 to 90%, and white circles represent bootstrap support from 70 to 50%

Chapter 5

Wood-Ljungdahl pathway in *Candidatus* Bipolaricaulota thriving in thermal waters in Biga Peninsula, Turkey

Ömer K. Coskun[1], Murat Beren[3], Doğacan Özcan[3], Hakan Hoşgörmez[3], Florian Einsiedl[4] and William D. Orsi[1,2,§]

[1]Department of Earth and Environmental Sciences, Ludwig-Maximilians-Universität, 80333 Munich, Germany.

[2]GeoBio-Center[LMU], Ludwig-Maximilians-Universität München, 80333 Munich, Germany

[3] Department of Geological Engineering, Istanbul University - Cerrahpasa, Istanbul, Turkey

[4] Chair of Hydrogeology, Technical University of Munich, TUM Department of Civil, Geo and Environmental Engineering, Arcisstrasse 21, 80333 Munich, Germany

[§]Corresponding author: w.orsi@lrz.uni-muenchen.de

Keywords: stable isotope probing, qSIP, carbon cycling, *Candidatus* Bipolaricaulota, hypersaline geothermal springs

5.1 Abstract

The Wood-Ljungdahl pathway (WL) has been proposed as one of the ancient metabolic carbon fixation pathways where the last common ancestor of all organisms (LUCA) might have used to fix carbon in anaerobic hydrothermal settings in the Early Earth. Therefore, the microorganisms thriving in modern deep terrestrial subsurface hydrothermal aquifers and hot springs have become a focal point of origin-of-life-based studies to seek primordial roots of carbon metabolism, yet these settings have been relatively understudied. To determine the biogeographical distribution of chemoautotrophs, we collected samples from deep hydrothermal aquifers and hot springs in tectonically active Biga Peninsula and vicinity of Edremit, Turkey. A total of 137 metagenome-assembled-genomes (MAGs) was reconstructed using metagenomic binning techniques and 4 of them were found to be affiliated with *Candidatus* Bipolaricaulota. WL pathway was shown to be ubiquitous in this phylum, yet the functionality was mainly attributed to heterotrophic processes. Additionally, to elucidate the genomic capacity of the MAGs reconstructed from deeply sourced hot springs and hydrothermal aquifers, we compared them to 19 publicly available incomplete to complete genomes of *Ca.* Bipolaricaulota. Our results showed that more than half of the genomes used in this study possessed a nearly complete/complete WLP pathway with a potential capacity to fix carbon and homoacetogenic fermentation. Complete to nearly complete ATPases were found in 12 MAGs which have genes encoding WL pathway, but ATP-citrate lyase, a key enzyme in reverse TCA to prove carbon fixation with WL pathway, was not found in those MAGs. However, the ^{13}C-labeled OTUs affiliated with *Ca.* Bipolaricaulota in the incubation amended with 1 mM sodium-bicarbonate were widespread in nearly all the hydrothermal spots, suggesting that carbon fixation with WL pathway in this phylum is already achieved. All in all, our results may shed light on the primordial carbon metabolism as biological, geological, and chemical requirements were met in this study, simply put, thermophilic and deeply branching *Ca.* Bipolaricaulota (Biology) living in hot springs and deep terrestrial aquifers (Geology) actively fixes carbon using with WL pathway (Chemistry).

5.2 Introduction

All life on Earth builds itself from CO_2 (Fuchs 2011), and we agree with the argument that this was no different at the emergence of life (Martin et al. 2008; Russell et al. 2014). The evolutionary metabolic analysis of all available genomic data indicates the last universal common ancestor (LUCA) was likely an H_2- and CO_2- utilizing autotroph (Wimmer et al. 2021). Two of carbon fixation pathways, the reductive tricarboxylic acid (rTCA) and pathways Wood-Ljungdahl pathway (WLP, also known as reductive acetyl-CoA pathway), are present in modern hydrothermal microbes and thought to be the most ancient primordial metabolism (Wächtershäuser 1990; Smith and Morowitz 2004; Braakman and Smith 2012, 2013).

Candidatus Bipolaricaulota (Hao et al. 2018), formerly known as OP1 (Hugenholtz et al. 1998) and *Candidatus* Acetothermia (Takami et al. 2012), has been detected in several environments, including

hot springs (Hugenholtz et al. 1998; Tobler and Benning 2011), deep-sea hydrothermal environments (Teske et al. 2002; Stott et al. 2008), subsurface thermophilic mat community (Takami et al. 2012), oil fields (Hu et al. 2016), sediment of hypersaline laguna (Fernandez et al. 2016) and anaerobic bioreactor (Hao et al. 2018). *Acetothermium Autotrophicum* (Takami et al. 2012) has been shown phylogenetically to be one of the deep branches of Bacteria domain with members capable of fixing carbon autotrophically (Takami et al. 2012). A recent metagenomic study has reported that WL pathway is widespread in this phylum (Youssef et al. 2019), yet existence of WL pathway is not solely adequate to show in which mode WL pathway is functioning. As opposed to Takami et al. (Takami et al. 2012), *Acetothermium Autotrophicum* was predicted to use WL pathway in homoacetogenic fermentation metabolism as an electron sink (Youssef et al. 2019)

Turkey is one of important geothermal fields with more than 2000 geothermal sources and 460 geothermal fields (Mertoglu et al. 2020), to our knowledge, microbial community studies from hot springs and boreholes in Turkey are limited and focus mainly on isolates with usually conventional sequencing techniques targeting 16S rRNA genes (Çelikoğlu et al. 2016; Belduz et al. 2003; Guven et al. 2018). Furthermore, isolates in these studies were mostly detecting members of Family Bacillaceae, underlining the fact that studies on microbial isolation underestimate the microbial composition due to the fastidious nature of microbes to cultivation. Here, we collected samples from 11 different thermal waters in Biga Peninsula and around the vicinity of Edremit to explore the microbial diversity using culture independent techniques targeting 16S rRNA gene and environmental metagenomes. We also linked carbon fixing OTUs in 750-meter-deep well (Chapter 4; Kaz Mountain Hotel) to geochemically distinct thermal settings to uncover biogeographic distribution of active carbon fixers revealed by quantitative isotope probing (qSIP). We focus on 5 metagenome-assembled-genomes (MAGs) associated with *Candidatus* Bipolaricaulota and present a detailed analysis of possible functional capacity in their genome.

5.3 Materials and Methods

5.3.1 Sampling.

Soil, sediment, microbial mat and water samples were collected in summertime of the year between 2019 and 2021 from geothermal springs and boreholes in Biga peninsula and in the vicinity of Edremit Town (Balikesir, Turkey) (Figure S1). Electrical conductivity (Ec) (WTW, Cond 3110 Set 1, Weilheim, Germany), temperature, salinity (WTW, Cond 3110 Set 1, Weilheim, Germany), pH (WTW, pH 3110 Set 2, Weilheim, Germany), dissolved oxygen (WTW Oxi 3310, Weilheim, Germany) and total dissolved solids (TDS) were measured in the field using handheld probes. 10 to 20 liters of water directly from each geothermal spot by throwing a pump tube into the spring were filtered through 0.22 µm hydrophilic polyethersulfone (PES) filters (Millipore Express, Merck, Darmstadt, Germany) for 20 minutes at a medium speed using a peristaltic pump (Masterflex E/S 07571-05, Cole Parmer, USA). 4 replicates were collected for the filters. Collected samples were immediately placed into dry ice supplied by a local company in Turkey.

The detailed information on the laboratory-based measurements can be found in previously published article (Einsiedl et al. 2020). Briefly, samples for laboratory-based measurements of major anion and cation concentrations and water isotopes (δ^2H and $\delta^{18}O$) were collected in 1.5 ml tubes after filtering with 0.2 µm PES filters. Samples for analysis of DOC (dissolved organic carbon) concentrations were collected in 50 mL glass bottles after filtering through 0.45 µm PVDF filters. Samples for the concentrations and isotope analysis of methane ($\delta^{13}C$) were transferred into 200 mL glass vials without headspace and sealed with crimped butyl stoppers. Samples for dissolved organic matter (DOC) measurements were collected in a 100 mL glass vials and sealed with crimped butyl stoppers. All samples were stored in the dry ice. Laboratory measurements were done in hydrogeology department of Technical University of Munich (TUM).

5.3.2 DNA extraction

After the samples reached our laboratory, DNA was extracted as described previously for filters (Orsi et al. 2015) and for the sediments (Coskun et al. 2018). In brief, four of 2 ml Lysing Matrix E tubes (MP Biomedicals, Solon, OH, USA) were poured into each 15 ml falcon tube containing the filters. 4 ml of a sterile-filtered sucrose ethylene-diaminetetraacetic lysis buffer (0.75 M sucrose, 0.05 M Tris-Base, 0.02 M ethylenediaminetetraacetic, 0.4 M NaCl, 4 ml 10% sodium dodecyl and pH 9.0) were added to the tubes and then, beat beating was performed for 40 sec using a Fast-Prep 5G homogenizer (MP Biomedicals, OH, USA) at a speed of 4 m / sec. Samples were subsequently heated for 2 min at 99 ^oC. After heating, 25 ml of 20 mg ml^{-1} proteinase K was added, and tubes were incubated at 55 ^oC overnight. DNA was extracted and purified from the lysate using the DNeasy Blood and Tissue Kit (Qiagen). Extracted DNA was quantified fluorometrically using Qubit 3.0 fluorometer (Invitrogen, Eugene, OR, USA).

5.3.3 qPCR of 16S rRNA gene copies

Universal primers targeting the V4 hypervariable region of 16S ribosomal RNA (rRNA) genes were used in quantitative PCR (qPCR). We used a version of the 515F primer with a single-base change (in bold) to increase the coverage of certain taxonomic groups (515F-Y, 5'-GTG**Y**CAGCMGCCGCGGTAA; (Parada et al. 2016)). qPCR reactions were carried out as described previously (Coskun et al. 2019). The 16S rRNA genes were subjected to dual-indexed barcoded sequencing of 16S rRNA gene amplicons on the Illumina MiniSeq as described previously (Pichler et al. 2018).

5.3.4 Bioinformatic and qSIP Analysis

The MiniSeq reads from fractionated SIP incubations (Chapter 4), T_0 (untreated samples) and previously sequenced common laboratory contaminants (Pichler et al. 2018) were quality trimmed and assembled using USEARCH version 11.0.667 with the default parameters (Edgar 2010) resulting in 28.4 million quality checked V4 reads. Reads were then de novo clustered at 97% identity using UPARSE; Operational Taxonomic Units (OTUs) represented by a single sequence were discarded

(Edgar 2013). Taxonomic assignments were generated by QIIME 1.9.1 (Caporaso et al. 2010) using the implemented BLAST method against the SILVA rRNA gene database release 132 (Quast et al. 2013). The common contaminant genera such as *Pseudomonas*, *Ralstonia*, *Variovorax* or *Streptococcus* were also removed as these are common contaminants of molecular reagent kits (Salter et al. 2014). Statistical analyses and plots were performed using R.Studio Version 3.3.0 (Team and Others 2015). The 16S sequence data will be entered in the NCBI Short Read Archive under BioProject ID PRJNAXXXXXX.

5.3.5 Metagenomic analysis.

Most of the samples were selected for metagenomic shotgun sequencing (see Figure S3). Metagenomic libraries were prepared using Nextera XT DNA Library Prep Kit (Illumina) and following the manual provided by the manufacturer with some modifications. The starting concentration of genomic DNA could not be set to 0.2 ng as suggested by the manufacturer's manual due to low DNA content in some samples. Instead, the PCR program in the amplification step of the tagmented DNA was modified from 12 to 15 cycles. Quality control and quantification of the metagenomics libraries were done on an Agilent 2100 Bioanalyzer System using high sensitivity DNA reagents and DNA chips (Agilent Genomics). Metagenomic libraries were diluted to 1 nM and pooled together to sequence on Illumina MiniSeq platform. SqueezeMeta (Tamames and Puente-Sánchez 2018) and Anvi'o snakemake workflow (Köster and Rahmann 2012; Eren et al. 2015) were used for downstream analysis using co-assembly mode with default settings. In short, SqueezeMeta workflow deployed Trimmomatic for adapter removing, trimming and quality filtering by setting the parameters: leading = 8, trailing = 8, slidingwindow = 10:15, and minimum length = 30 (Bolger et al. 2014). Contigs were assembled using Megahit assembler using minimum length 200 nucleotides (Li et al. 2015). Open reading frames (genes and rRNAs; ORFs) were called using Prodigal (Hyatt et al. 2010), rRNAs genes were determined by barrnap (Seemann 2013). Diamond software (Buchfink et al. 2015) was deployed to search for gene homologies against the databases Genbank nr database for taxonomic assignment, eggNOG v4.5 (Huerta-Cepas et al. 2016) and KEGG database (Kanehisa and Goto 2000). Cutoff values for assigning hits to specific taxa were performed at e value as $1 \times e^{-3}$, and a minimum amino acid similarity of 40 for taxa and 30 for functional assignment which were default settings of SqueezeMeta. Bowtie2 (Langmead and Salzberg 2012) was used to map the read onto contigs and genes. Anvi'o snakemake workflow (anvi'o v7) was used to bin and to refine the Metagenome assembled genomes (MAGs). MaxBin (Wu et al. 2016), concoct (Alneberg et al. 2014) and Metabat2 (Kang et al. 2019) were deployed for the binning and DAS Tool (Sieber et al. 2018) was deployed to choose the best bin for each population. The completeness and contamination of the bins were checked in anvi'o v7. The metagenomic sequence data will be entered in the NCBI Short Read Archive under BioProject ID PRJNAXXXXXX.

5.4 Results

5.4.1 Fluid geochemistry and the origin of thermal waters in Biga Peninsula

The origin of geothermal waters in Biga peninsula was determined using stable isotopic composition, δ^2H and $\delta^{18}O$, of the thermal waters. The results showed that isotopic composition of samples, except Kestanbol, Tuzla and Can, fell between global meteoric water line (GMWL, (Craig 1961)) and East Mediterranean meteoric water line (EMMWL, (Gat and Carmi 1970)). δ^2H - $\delta^{18}O$ graph displays those thermal waters existing in Tuzla and Kestanbol have been affected from a salt-concentrated water source, as they fell onto a mixing line (Figure 1). Thermal waters from Can exhibited $\delta^{18}O$-shift towards the right side of the graph. Tuzla and Kestanbol sites were enriched with high NaCl concentrations whereas the other spots were dominated with $NaSO_4$-enriched waters.

5.4.2 Abundance of *Ca.* Bipolaricaulota in thermal waters

31 OTUs affiliated with *Ca.* Bipolaricaulota were identified across the samples taken from Biga peninsula determined by V4 region of 16S rRNA gene sequences (Figure 2). The highest abundance of *Ca*. Bipolaricaulota (63% of the total reads) was found in a hypersaline Tuzla sample. The 16S rRNA phylogeny has highlighted that 22 of them were closely related to 16S rRNA gene sequences obtained from the hydrothermal and subsurface settings (Figure 2). Further analysis on ^{13}C-labeled OTUs identified in "Chapter 4" in this thesis (OTU22, OTU20, OTU76, OTU56, OTU100) to show the distribution of *Ca*. Bipolaricaulota was performed (Figure 3). It highlights that 3 of the ^{13}C-labeled OTUs affiliated with *Ca*. Bipolaricaulota were matching with the same OTUs dominating Tuzla Samples, namely OTU22, OTU20, OTU76. It has revealed that carbon-fixing *Ca*. Bipolaricaulota members in Tuzla samples were thriving in most of the sampling sites except Entur, Buyukilica (Figure 3).

5.4.3 Metagenome-assembled genome quality and taxonomic identification.

137 metagenome-assembled-genomes (MAGs) (Table S2) were assembled from 11 thermal spots across the Biga peninsula and close vicinity of Edremit region, Turkey (Figure S1) using 34 metagenomic library generated from fractionated SIP samples (n = 14), unfractionated SIP samples (n = 3), 0.22 µm filtered water (n = 14), and sediments (n =3). Two of the MAGs were taxonomically assigned to *Ca.* Bipolaricaulaota with 90.1% (0% redundancy) and 60% (0% redundancy) completeness by anvi'o and our further phylogenetic tree investigations have revealed that MAGSIPTR38 and MAGSIPTR2 were taxonomically assigned to *Ca.* Bipolaricaulaota with completeness of 83.1% (4.2% redundancy) and 90.1% (0% redundancy).

5.4.4 Comparison of MAGs with the MAGs found in the other studies.

In order to compare the MAGs reconstructed in this study to the published MAGs, we followed a pangenomic analysis in anvi'o using *Ca. Bipolaricaulis anaerobius* Ran1 (Hao et al. 2018), Ca_Bipolaricaulis_sibiricus_Ch78 (Kadnikov et al. 2019), Ca_Bipolaricaulis_sp_Go_SlDig_bin_182 (Schneider et al. 2021), *Ca.* Bipolaricaulota AUK024, *Ca.* Bipolaricaulota 0786_k87 (Youssef et al.

2019), *Ca.* Bipolaricaulota bin446 (Wang et al. 2021), *Ca.* Bipolaricaulota GSL_GSL3510, *Ca.* Bipolaricaulota MAG23 (Liu et al. 2020), *Ca.* Bipolaricaulota MAG24 (Liu et al. 2020), *Ca.* Bipolaricaulota MAG1260 (Liu et al. 2020), *Ca.* Bipolaricaulota S141 (Reysenbach et al. 2020), *Ca.* Bipolaricaulota SZUA1496 (Zhou et al. 2020), *Ca.* Bipolaricaulota UWMA_0174, *Acetothermium Autotrophicum (Takami et al. 2012)*, Acetothermia UBA3560 (Parks et al. 2017), Acetothermia UBA3574 (Parks et al. 2017), Acetothermia_JdFRolivine_4 (Smith et al. 2019), Acetothermia JdFR 48 (Jungbluth et al. 2017), Acetothermia_JdFR_52 (Jungbluth et al. 2017). We named our MAGs as Acetothermia_TUZ33, Acetothermia_CK84, Acetothermia_CK101, UBA3571_sp_HID15. The pangenome analysis has uncovered that pairwise average nucleotide identities were spanning from nearly 65% to 99.9% between MAGs. The closest strain to *Acetothermium Autotrophicum* has been found to be CK101 reconstructed in this study.

5.5 Discussion

5.5.1 The origin of the thermal waters

The origin of geothermal waters in Biga peninsula was determined using stable isotopic composition, δ^2H and $\delta^{18}O$, of the thermal waters (Figure 1). The results showed that isotopic composition of samples, except Kestanbol, Tuzla and Can, fell between global meteoric water line (GMWL, (Craig 1961)) and East Mediterranean meteoric water line (EMMWL, (Gat and Carmi 1970)), suggesting that the subsurface hydrothermal water had been replenished by modern meteoric water (Figure 1). These results were also in line with the findings published by Yalcin, 2007 (Yalcin 2007). Samples taken from Kestanbol and Tuzla contain high amounts of sodium and chloride, that is why they have been classified as NaCl-dominated waters (Yalcin 2007). Stable isotopic composition of the thermal waters in these areas, δ^2H and $\delta^{18}O$, fell onto a mixing line between meteoric waters and deep-seated hot brine waters whose origin is not known, consistent with the previous study (Yalcin 2007). It has been proposed that the origin of water could be the fossil water trapped in Miocene sediments (Mützenberg 1997; Balderer 1997), whereas another study stressed that hypersalinity in these waters could be resulted from dissolution of salt deposits (Vengosh et al. 2002). Thermal waters from Can, exhibiting $\delta^{18}O$-shift, may be explained by CO_2 input from a geological source, which was also suggested by the previous study that investigated thermal waters in Biga Peninsula (Yalcin 2007).

5.5.2 The carbon fixation by *Ca.* Bipolaricaulota in qSIP samples

Our qSIP experiments to unravel the diversity of microbes fixing inorganic carbon into biomass are explained in detail in chapter 4, highlighting that 5 OTUs affiliated to *Ca.* Bipolaricaulota assimilated the sodium bicarbonate. Thus, we wanted to further investigate its distribution and functional capacity in hot springs and deep hydrothermal wells in this chapter because (1) *Ca.* Bipolaricaulota has been shown that a member of this phylum is deeply-branching (Takami et al. 2012), (2) WL-pathway is widespread within this phylum (Youssef et al. 2019), (3) the members of this phylum

actively fixes carbon in deep hydrothermal aquifers in Turkey (chapter 4), and lastly (4), three recovered MAGs (out of 4) have genomic capability to fix carbon using WL pathway.

5.5.3 Pangenome of investigated Ca. Bipolaricaulota

We have downloaded publicly available 19 MAGs related to *Ca.* Bipolaricaulota from NCBI (https://www.ncbi.nlm.nih.gov/) with completeness levels ranging from 77% to 95% except 50% complete *Acetothermium Autotrophicum* (Takami et al. 2012) and compared to our newly reconstructed MAGs in study. Our results have revealed that average nucleotide identity values were on average 72%, underlining the possibility that (1) the members have undergone evolution in different ecological and biogeographical settings (Konstantinidis and Tiedje 2005) or (2) that not having a cultured strain of *Ca.* Bipolaricaulota is hindering a phylogenetic congruence because assessing the quality of metagenomic-assembled-genomes without a reference genome from cultivated strains can be challenging (Bowers et al. 2017).

The pangenome analysis concluded on just a single gene existing in 24 samples and 15 genes in 23 samples. Thus, more complete, and reliable genomes are still needed to resolve the core genome of this highly interesting taxa, which are ubiquitous in hypersaline Tuzla samples and biogeographically widespread in Biga Peninsula. We leave further investigation on the core genomic part for the future studies when, hopefully, complete *Ca.* Bipolaricaulota genomes are high in number.

5.5.4 WL Pathway within Ca. Bipolaricaulota obtained from pangenome analysis

WL pathway was found to be widespread in MAGs of *Ca.* Bipolaricaulota in a similar study which used 14 MAGs (Youssef et al. 2019), of which 5 MAGs were identical between the studies, namely Bin Zgenome_0786 (named as Ca_Bipolaricaulota_0786_k87 in this study) (Youssef et al. 2019), Candidatus *Acetothermum autotrophicum* (Takami et al. 2012), Ca. *Bipolaricaulis anaerobius* Ran1 (Hao et al. 2018), *Candidatus* Acetothermia bacterium JdFR-52 and jdsFR-48 (Jungbluth et al. 2017) (Figure 4). Youssef et al. (Youssef et al. 2019) have concluded that the WL pathway is versatile in 14 *Ca.* Bipolaricaulota MAGs they investigated. The WL pathway may be involved in homoacetogenic fermentative process by reducing pyruvate to CO_2 and subsequent use of CO_2 in WL pathway as a function for electron sink (Schuchmann and Müller 2016), in autotrophy to fix CO_2 into biomass (Fuchs 2011), and lastly in syntrophic oxidation of acetate (SAO) to use WL pathway in reverse direction, producing CO_2 and H_2 as end products (Müller et al. 2013).

The identification of WL pathway in a genome, as mentioned above, is not adequate evidence that the organism is fixing inorganic carbon. However, functional capabilities may be indicative of which way WL pathway is functioning as discussed in (Schuchmann and Müller 2016). Likewise, SIP studies are powerful techniques to track the labeled substrate (Hungate et al. 2015), thereby a simple link between an organism and tested substrate (Here $NaH^{13}CO_3$) can be established if the labeling occurs. As such, sodium-bicarbonate utilization by an OTU/MAG resulting from qSIP study will most likely represent that carbon fixation is achieved by that organism.

The existence of core WL pathway in acetogens is a requirement, which is defined as the reactions that lead from 2 molecules of CO_2 to acetyl-CoA (Schuchmann and Müller 2016). When 5 common MAGs between this study and Youssef et al. were compared, our regular workflow in anvi'o v7 (Eren et al. 2015) (See materials and methods) failed to recognize WL involving genes in Ca. *Bipolaricaulis anaerobius* Ran1 and in the bin named as Zgenome_0786 using COG (Galperin et al. 2021) and KEGG databases (Kanehisa and Goto 2000). However, we found *acsB* (K14138), *cdhD* (K00194) and *cdhE* (K00197) for the latter MAG, but the other necessary genes for the WL pathway were missing. This might be related to differences in methodology, on the other hand, our workflow has identified the WL pathway involving genes in the bins of JdFR 48, JdFR 52 and *Acetothermium Autotrophicum* as it was also shown in paper published by Youssef et al. (Youssef et al. 2019). Opposite to their finding, 10 MAGs used in this study did not carry most of the genes encoding WL pathway, but more than half of the MAGs possessed the key genes for WL pathway, including bins reconstructed in this study, named as UBA3571 sp HID15, CK101 and CK84. Therefore, we conclude that the WL pathway is ubiquitous in *Ca.* Bipolaricaulota, but not phylum-wide distributed. Still, this does not mask the importance of *Ca.* Bipolaricaulota in microbial ecology, since the deeply branching phylogenetic support and existence of WL pathway in the genome should place the members of *Ca.* Bipolaricaulota species into the center of studies investigating the traces of ancient genes.

5.5.5 Autotrophic growth using WL pathway

ATPase complex is necessary for organisms to grow chemolithoautotrophically using WL pathway (Müller 2003). It was postulated that a gluconeogenic pathway, acetyl-CoA conversion to pyruvate, and a TCA cycle reversal to consume acetyl-CoA into central metabolism (Youssef et al. 2019).
In consistent with (Youssef et al. 2019), all MAGs analyzed in this study contained genes encoding pyruvate, water dikinase [EC:2.7.9.2] (CK84, CK101 and *Acetothermium Autotrophicum*) and pyruvate, orthophosphate dikinase [EC:2.7.9.1] (all the other MAGs). Key enzyme involved in reverse TCA, ATP-citrate lyase, was found in only 7 MAGs, which we could not retrieve many components of WL pathway in their genome, namely S141, MAG24, MAG23, AUK024, k0786_k87, Go_SIDig_bin182, and *Bipolaricaulis anaerobius* Ran1. The citrate synthase, which was shown to fix carbon when reversed in TCA cycle (Mall et al. 2018), was found in the genomes of Acetothermium *Autotrophicum*, CK101 and S141. Since CK101 had ^{13}C-labeling in the incubations amended with sodium-bicarbonate (Chapter 4), it may show that the reversibility of TCA to fix carbon may be taking place in the natural environment, together with WL pathway. Complete to incomplete V- and F-type ATPases could be detected in all the MAGs except *Bipolaricaulis anaerobius* Ran1 and Go_SIDig_bin182, consistent with (Youssef et al. 2019). All in all, these results show that WL pathway containing MAGs can fix carbon, including the MAGs reconstructed in this study, namely CK101, CK84 and HID15 (Figure 4).

5.5.6 Homoacetogenic fermentative process.

The utilization of a wide range of sugar and amino acids to pyruvate is a prerequisite for an organism conducting homoacetogenic fermentation, also known as homoacetogenesis (Schuchmann and Müller 2016). 2 Acetyl-coA, 2 CO_2 and 2 ferredoxin are produced from 2 pyruvates by the enzyme pyruvate:ferredoxin oxidoreductase (PFO) (Ragsdale 2003; Schuchmann and Müller 2016). Then, the produced 2 CO_2 and 1 ferredoxin take part in the WL pathway. Also, H_2 needs to be produced from the remaining ferredoxin to involve in WL pathway; therefore Rnf complex and an electron-bifurcating hydrogenase are necessary (Schuchmann and Müller 2012). Pyruvate:ferredoxin oxidoreductases were found in 17 MAGs, 12 of which have complete/incomplete genes encoding WL pathway components (CK101, CK84, jdFR48, jdFR52, Olivine4, UBA3560, UBA3574, Acetothermium Autotrophicum, GSL_GSL3510, SZUA1496, UMWA_0174, and HID15). 12 MAGs encode membrane-bound hydrogenases (alpha, beta and mbhJ were observed) [EC:1.12.7.2]. In addition, 10 WLP encoding MAGs had subunits of heterodisulfide reductase (Buckel and Thauer 2018). These findings highlight the genomic capacity of MAGs under *Ca.* Bipolaricaulota as they can switch between autotrophy and heterotrophy using WL pathway in these hydrothermal springs and deep subsurface aquifers.

In line with our analysis, it has been reported that the Tuzla sample contains nearly twice the amount of the salt concentration compared to the same concentrations in seawater as sodium and chloride concentrations reaching 16,963 mg/l and 68,256 mg/l, respectively (Baba et al. 2009). 3 OTUs associated with *Ca.* Bipolaricaulota, which assimilated sodium-bicarbonate only in 1 mM incubations (Figure 3), were found to be dominant taxa in this hypersaline environment.

Interestingly, phylum OP1/KB1 (now, *Ca.* Bipolaricaulota) has been found in hypersaline waters such as in Orca Basin (the largest hypersaline seafloor brine basin in the Gulf of Mexico) (Nigro et al. 2016), Hephaestus and Kryos basins (Fisher et al. 2021), hypersaline stratified layers of Ursu Lake (Baricz et al. 2021), saline pan sediments in the Kalahari Desert of southern Africa (Genderjahn et al. 2018), and in surface sediments of salty Siberian soda lakes (Vavourakis et al. 2018). We propose that carbon-fixing *Ca.* Bipolaricaulota are halotolerant as they were found in the other hydrothermal spots in Biga Peninsula, mainly dominated by $NaSO_4$. In agreement with carbon metabolism of *Ca.* Bipolaricaulota, this taxa, comprising 12-44% of total microbial community in anoxic, hypersaline layers of Witpan in South Africa (Genderjahn et al. 2018), was correlated to acetate concentrations, suggesting their acetogenic activity. Glycine betaine uptake was reported in the genome of KB1 to involve “salt out” (Oren 2008) strategy in a response to osmotic pressure (Nigro et al. 2016). We searched for homologous genes, but we only identified these genes related to osmotic pressure in GSl_GSL3510 bin. On the other hand, the other MAGs contained K^+ uptake protein (*trk*), which was reported to be 10 times faster than the *Kup* transporters (Johnson Hope et al. 2009). Therefore, it is most likely that *Ca.* Bipolaricaulota is a “salt-in” strategist which accumulates potassium salts (Oren 2008), explaining their majority in hypersaline environments.

5.5.7 Dissolved Oxygen in the incubations

The dissolved O_2 in our incubations were between 0.75-1.35 mg/l, where the O_2 levels declined after 135 hours of incubation period (Table S1). Tuzla samples were also oxygenated as the measurement was 1.46 mg/l. The presence of O_2 and carbon fixation by WL pathway are contradicting evidence, although the measurements are categorized as severe to moderate dsyoxic levels (Tyson and Pearson 1991). We propose that complete absence of O_2 must be present in these hot springs and deep subsurface wells, but our measurements were done after cooling the water to certain degrees not to harm the equipment. These may show O_2 values a little bit higher than its actual value. Successful labeling of *Ca.* Bipolaricaulota members can also support this because genes encoding WL pathway components are sensitive to oxygen (Lu and Imlay 2021).

5.6 Conclusion

To sum up, the results show that the WL pathway is a widespread mechanism to fix the CO_2 in *Ca.* Bipolaricaulota, although nearly 40% of them did not possess complete/nearly complete genes encoding WL pathway components. Newly reconstructed MAGs also possess WL pathway, which was shown to be used to fix CO_2 by qSIP study in chapter 4. In addition, the potential for homoacetogenic fermentation existed in most of the MAGs. Lastly, *Ca.* Bipolaricaulota was proposed as “salt-in” strategist and its spatial distribution across the hydrothermal spots in Biga Peninsula demonstrated the halotolerant ecophysiology. All in all, all aspects *Ca.* Bipolaricaulota should be studied in detail because the genome of *Ca.* Bipolaricaulota may provide clues for primordial metabolism of last universal common ancestor (LUCA).

Figures

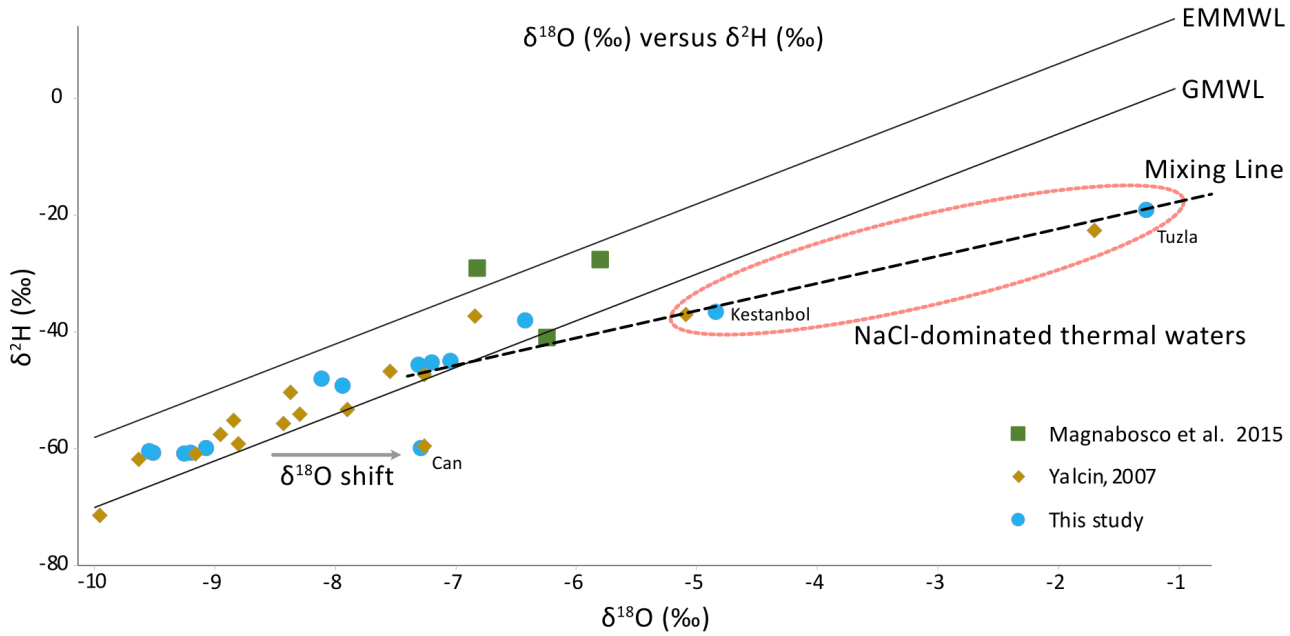

Figure 1: A) The $\delta^{2}H$ (‰) and $\delta^{18}O$ (‰) plot of thermal waters obtained in study (blue), and the other studies (Yalcin 2007, Magnabosco et al. 2016). The GMWL and EMMWL stand for Global Meteoric Water Line (Craig 1961) and East Mediterranean Water Line (Gat and Carmi 1970).

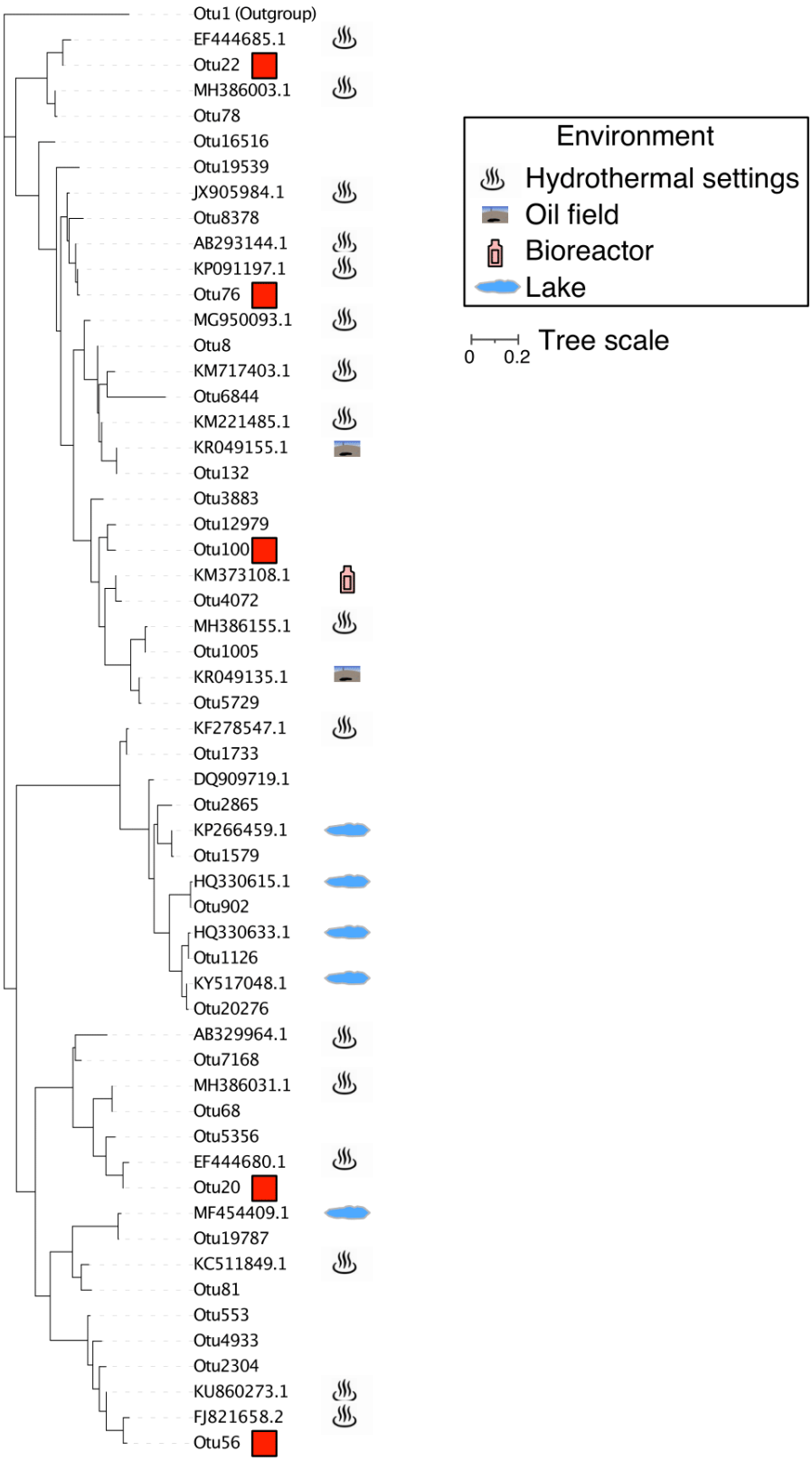

Figure 2: Phylogenetic tree of 16S rRNA genes of OTUs affiliated with *Ca.* Bipolaricaulota including their most similar sequences from the NCBI nr database (accession numbers shown), branches starting with 'OTU' indicate those from this study. Red squares represent ^{13}C-labeled OTUs with sodium-bicarbonate determined from qSIP study in chapter 4. The distinct shapes showing the information of environmental setting were aligned with the sequences downloaded from NCBI.

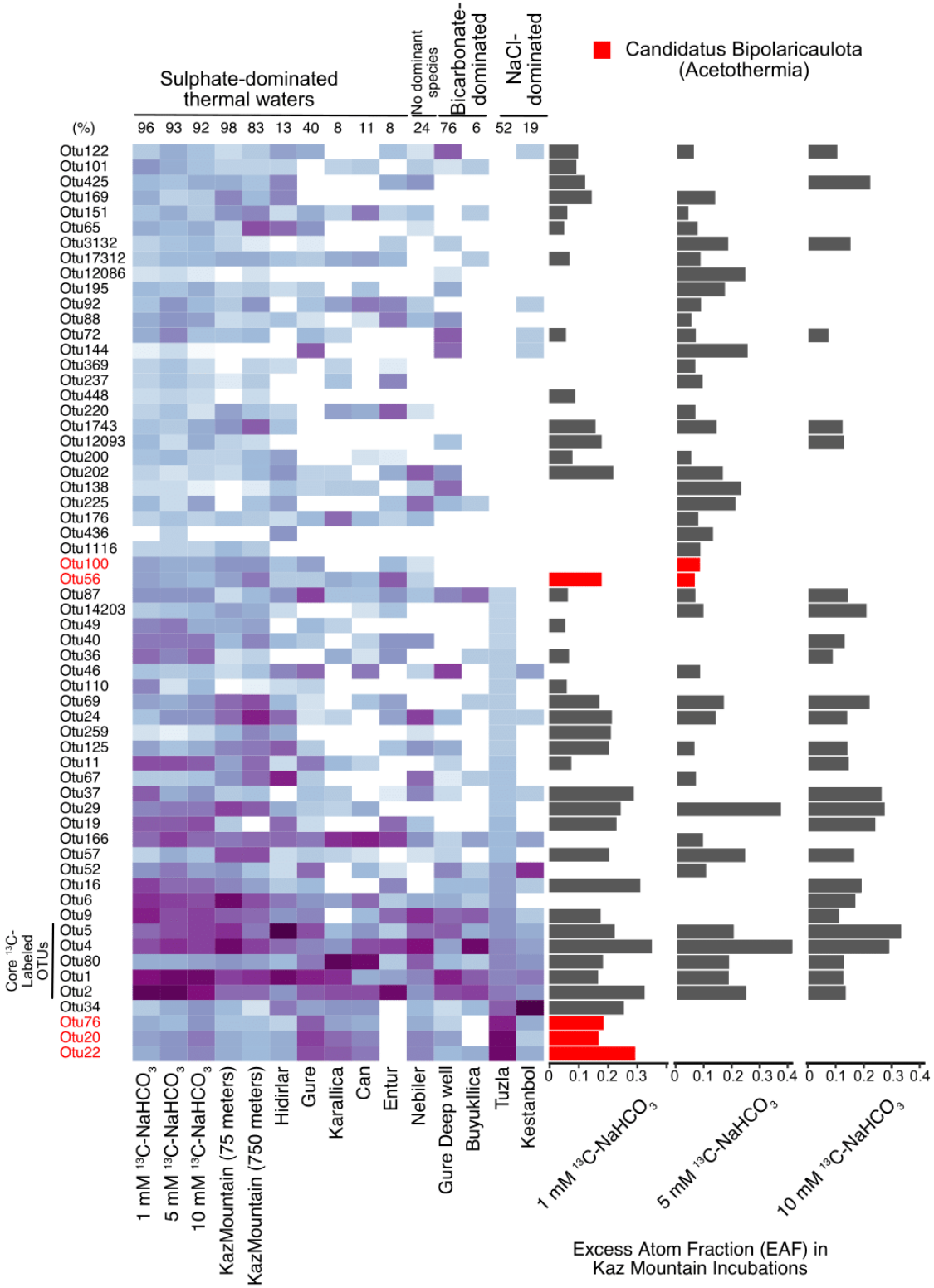

Figure 3: The heatmap shows the relative abundance of 16S rRNA gene sequences per labeled OTU per samples. Differential bicarbonate incubations on the left-hand side (1 mM, 5 mM and 10 mM sodium bicarbonate incubations; Chapter 4) and followed by T_0 samples collected from different hydrothermal hotspots in Biga Peninsula in 2019, 2020 and 2021 (purple = more, light blue = less). The histograms on the right side of the plot show the average ^{13}C-EAF across all qSIP incubations

per OTU. The heatmap focuses on the OTUs affiliated with *Ca.* Bipolaricaulota which are shown with red color. Note that sample named as Tuzla had 50% relative abundance of ^{13}C-labeled *Ca.* Bipolaricaulota

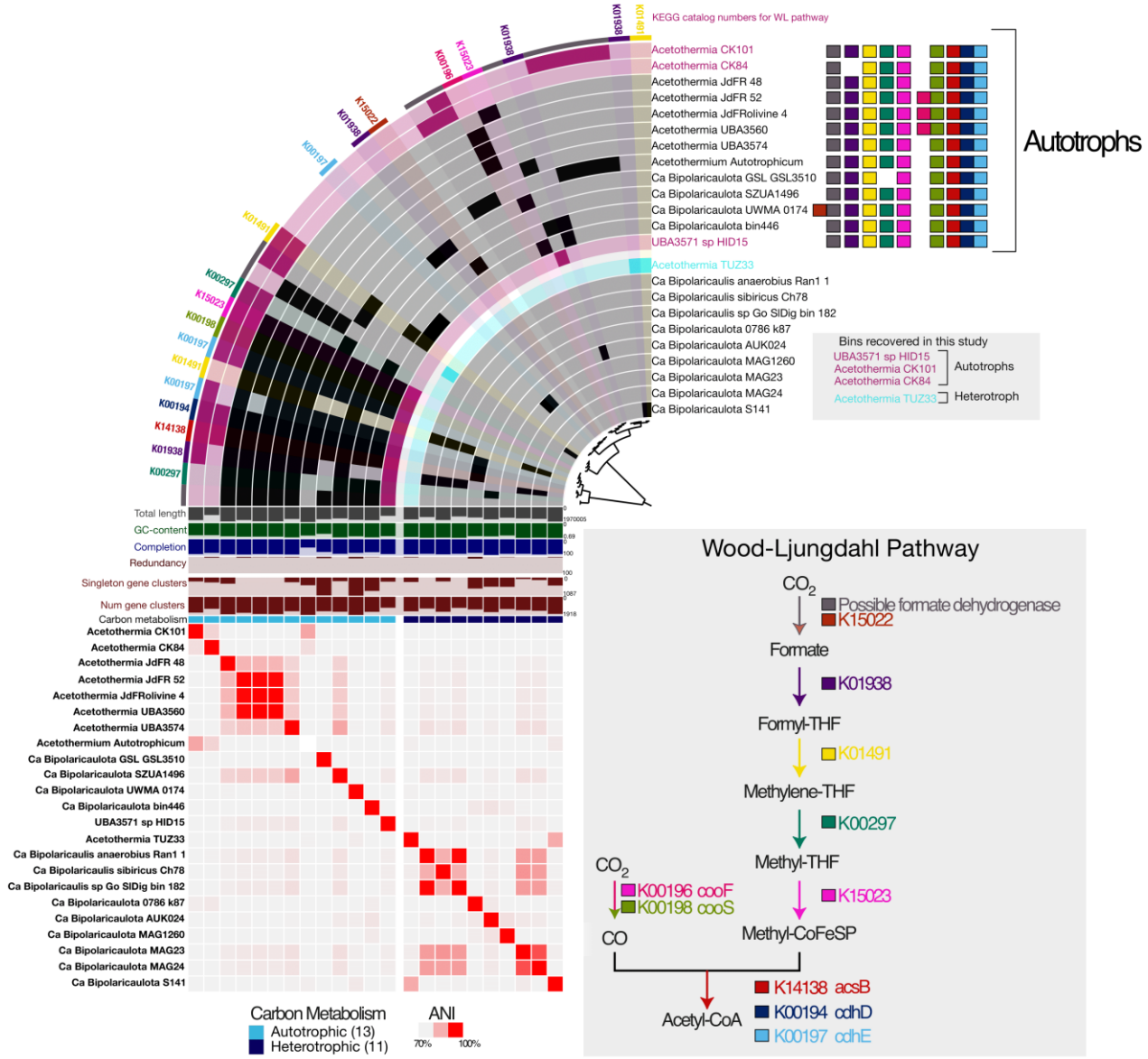

Figure 4: Phylogenetic tree shows the gene clusters only for the genes encoding WLP. Gene clusters were generated using 19 publicly available and 4 MAGs reconstructed in this study. The heatmap shows average nucleotide identity between MAGs. Values were calculated in the anvio v7 using pyANI (Pritchard et al. 2016). The colored squares represent the enzymes catalyzing WL pathway.

Table S1. Water chemistry and information of the sampling sites

	Field Measurements							
Sample	Depth of the well	Temperature (°C)	pH	Ec (uS/sn)	Oxygen (mg/lt) @T	Salinity (ppm or mg/lt)	Carbonate hardness (mmol/l)	Bicarbonate mg/l
Kestanbol	?	62	6,97	28600	2,2 @27	18,3	6,1 mmol/lt - 17 od	372,2
Güre collector	260 m	64	7,07	1083	0,79 @42	0,5	1,8 mmol/lt - 4,8 od	109,8
Büyük Ilica	?	43,6	6,97	1055	1,1 @43	0,5	11 mmol/lt - 30.6 od	671,2
Can	60 m	45,6	6,92	2200	0,49 @44	1,1 ppm	4,5 mmol/lt - 12.4 od	274,6
Entur Thermal Hotel	?	46,5	7,96	1095	0,48 @ 46	0,5	2,05 mmol/lt - 5,7 od	125,1
Güre deep well	1350 m	76,6**	8,2	1240	0,98 @44	0,5	2 mmol/lt - 6od	122,0
Hidirlar	Hot spring	78,5	8,13	889	1,38 @45	0,4	2,2 mmol/lt - 6 od	134,2
Kaz Mountain Hotel	750 m	61,7*	8,27	1514	1,64 @47	0,8 mg/lt	1,5 mmol/lt - 4od	91,5
Kaz Mountain Hotel	75 m	56,7	8,28	1340	0,99 @47	680 ppm	2 mmol/lt - 5.5 od	122,0
Nebiler	Hot spring	55	7,12	1390	0,83 @40	0,8	8,6 mmol/lt - 23,7 od	524,8
Tuzla	Hot spring	68,1	6,96	78100	1,46 @53	52,3	-	7083,2
Karallica	Hot spring	46,7	7,07	2380	0,61 @46	1,2	3,5 mmol/lt - 9,6 od	213,6

* Samples taken in 2019 and 2020 had 73 °C. For detailed explanation, please see materials and methods.

** The actual temperature of the well is 94 °C

	Field Measurements							
Incubation name	Depth of the well	Temperature (°C)	pH	Ec (uS/sn)	Oxygen (mg/lt) @T	Salinity (ppm or mg/lt)	Carbonate hardness (mmol/lt)	Bicarbonate mg/l (calculated from
10 mM $NaH^{13}CO_3$ incubation***	750	-	7,31	2190	1,35	1,1	-	-
5 mM $NaH^{13}CO_3$ incubation***	750	-	7,42	1870	1,23	0,9	-	-
1 mM $NaH^{13}CO_3$ incubation***	750	-	7,84	1598	0,75	0,8	-	-
10 mM $NaH^{12}CO_3$ incubation***	750	-	7,28	2160	1,05	1,1	-	-
5 mM $NaH^{12}CO_3$ incubation***	750	-	7,37	1909	1,09	1,1	-	-
1 mM $NaH^{12}CO_3$ incubation***	750	-	7,91	1610	1,04	0,8	-	-

	anions						cations					
Sample	Phosphate mg/l	Bromide mg/l	Chloride mg/l	Nitrate mg/L	Nitrite mg/L	Sulfate mg/L	dilution	Na (mg/l)	NH_4 (mg/l)	K (mg/l)	Mg (mg/l)	Ca (mg/l)
Kestanbol	n.a.	18,2	11222,9	3,8	n.a.	90,3	50,0	5430,1	n.a.	571,6	36,8	755,2
Güre collector	n.a.	n.a.	42,4	n.a.	n.a.	372,3	2,0	197,3	n.a.	5,4	n.a.	15,0
Büyük Ilica	n.a.	n.a.	16,4	n.a.	n.a.	58,1	1,0	67,0	n.a.	6,6	7,9	36,9
Can	n.a.	n.a.	171,0	n.a.	n.a.	1116,2	5,0	444,1	n.a.	21,5	8,6	218,2
Entur Thermal Hotel	n.a.	n.a.	51,6	n.a.	n.a.	346,8	2,0	182,3	n.a.	3,5	n.a.	37,2
Güre deep well	n.a.	n.a.	4,9	n.a.	n.a.	17,9	1,0	12,3	n.a.	1,0	3,0	35,1
Hidirlar	n.a.	n.a.	8,4	n.a.	n.a.	204,6	2,0	181,5	n.a.	5,8	n.a.	6,8
Kaz Mountain Hotel	n.a.	n.a.	18,0	n.a.	n.a.	556,0	2,0	244,1	n.a.	5,7	n.a.	74,2
Kaz Mountain Hotel	n.a.	n.a.	20,6	n.a.	n.a.	637,3	2,0	238,0	n.a.	6,0	n.a.	76,6
Nebiler	n.a.	n.a.	36,3	n.a.	n.a.	309,5	2,0	222,5	n.a.	8,0	12,7	51,2
Tuzla	n.a.	69,1	28954,9	n.a.	n.a.	92,7	200,0	14804,7	n.a.	1446,2	n.a.	2330,2
Karallica	n.a.	n.a.	77,0	n.a.	n.a.	957,1	5,0	376,8	n.a.	16,8	n.a.	132,5

	anions						cations					
Incubation name	Phosphate mg/l	Bromide mg/l	Chloride mg/l	Nitrate mg/L	Nitrite mg/L	Sulfate mg/L	dilution	Na (mg/l)	NH_4 (mg/l)	K (mg/l)	Mg (mg/l)	Ca (mg/l)
10 mM $NaH^{13}CO_3$ incubation***	n.a.	n.a.	21,2	n.a.	n.a.	318,2	5,0	488,4	n.a.	6,1	n.a.	15,6
5 mM $NaH^{13}CO_3$ incubation***	n.a.	n.a.	22,0	n.a.	n.a.	630,5	5,0	368,7	n.a.	5,5	n.a.	24,2
1 mM $NaH^{13}CO_3$ incubation***	-	-	-	-	-	-	-	-	-	-	-	-
10 mM $NaH^{12}CO_3$ incubation***	-	-	-	-	-	-	-	-	-	-	-	-
5 mM $NaH^{12}CO_3$ incubation***	-	-	-	-	-	-	-	-	-	-	-	-
1 mM $NaH^{12}CO_3$ incubation***	-	-	-	-	-	-	-	-	-	-	-	-

	water isotopes				DOC	methane		
Sample	d18O	d18O Stabw	d2H	d2H Stabw	NPOC (mg/l)	CH4 (mg/l)	d13C-CH4 d 13C	d13C-CH4 std dev
Kestanbol	-4,84	0,09	-36,55	0,58	1,2+-1,81%			
Güre collector	-7,20	0,12	-45,21	0,49	1,1+-0,5%	0,0813	-22,4	0,08
Büyük Ilica	-8,11	0,07	-48,01	0,41	2,7+-0,22%	0,0029		
Can	-7,29	0,11	-59,81	1,03	0,9+-0,06%	0,0091		
Entur Thermal Hotel	-7,31	0,10	-45,58	0,75	0,8+-0,52%	0,0300	-25,3	0,13
Güre deep well	-7,34	0,09	-40,19	0,47	2,9+-0,4%	0,0057	-29,8	
Hidirlar	-7,94	0,10	-49,28	0,66	0,7+-0,03%	0,0018		
Kaz Mountain Hotel	-9,51	0,09	-60,63	0,42	0,8+-1,99%	0,0079	-10,4	
Kaz Mountain Hotel	-9,54	0,09	-60,35	0,51				
Nebiler	-9,25	0,08	-60,76	0,57	,74+-1,61%	0,0679	-14,5	0,18
Tuzla	-6,42	0,07	-37,97	0,47	0,9+-0,21%	0,0041		
Karallica	-1,27	0,11	-19,00	0,70	1,15+-1,9%	0,0315	-15,5	0,19

	water isotopes				DOC	methane		
Incubation name	d18O	d18O Stabw	d2H	d2H Stabw	NPOC (mg/l)	CH4 (mg/l)	d13C-CH4 d 13C	d13C-CH4 std dev
10 mM $NaH^{13}CO_3$ incubation***	-9,20	0,00	-60,69	0,00	0,9+-1,38%	0,0032		
5 mM $NaH^{13}CO_3$ incubation***	-9,07	0,09	-59,86	0,41	0,5+-1,84%	0,0060		
1 mM $NaH^{13}CO_3$ incubation***	-	-	-	-	-	-	-	
10 mM $NaH^{12}CO_3$ incubation***	-	-	-	-	-	-	-	
5 mM $NaH^{12}CO_3$ incubation***	-	-	-	-	-	-	-	
1 mM $NaH^{12}CO_3$ incubation***	-	-	-	-	-	-	-	

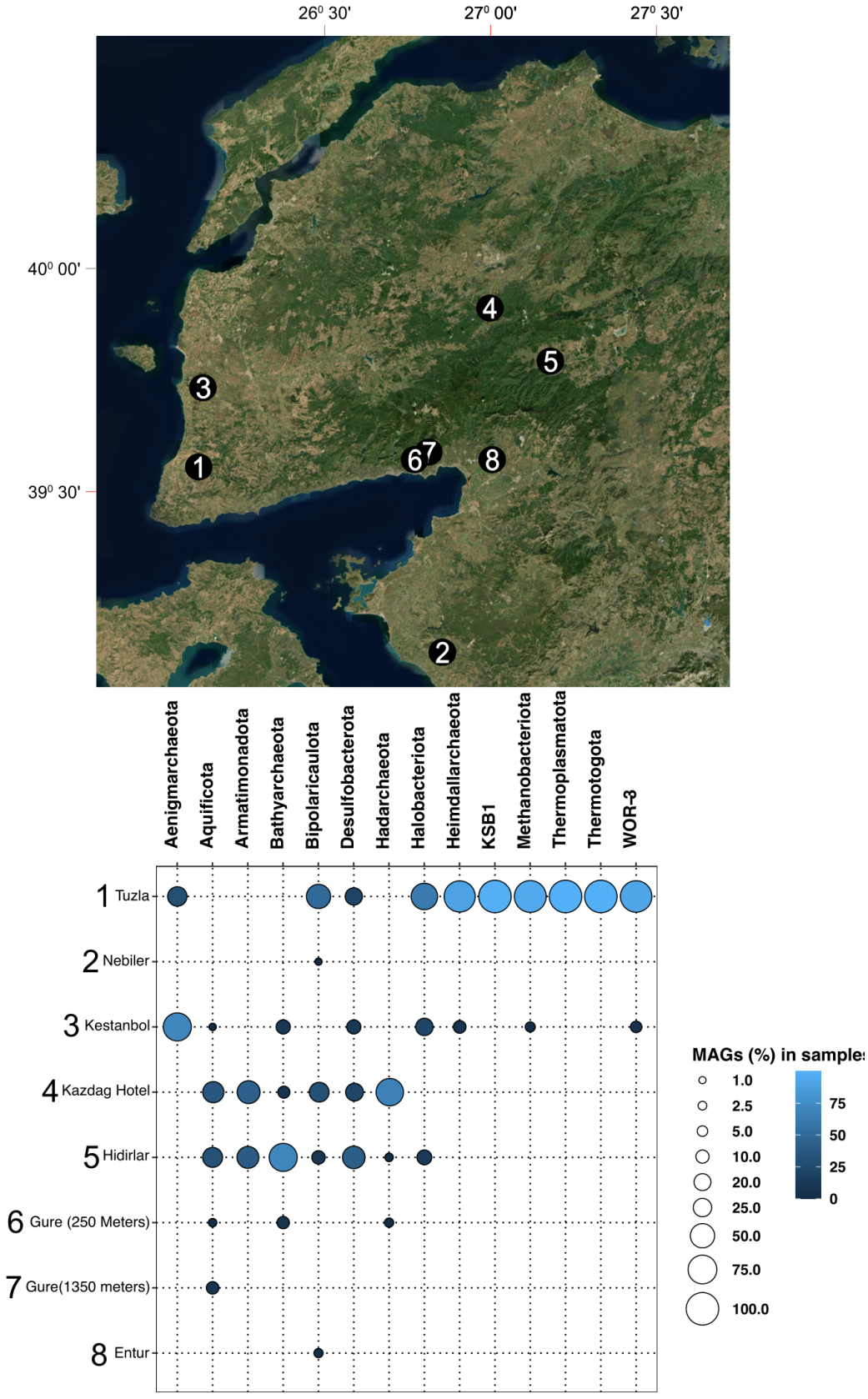

Figure S1: Relative coverages of the MAGs with assigned putative taxonomy across the sampling spots in Biga Peninsula, west of Turkey. The map is taken from Google Earth. Note that Tuzla sample (#1) represents geothermal brine. MAGs associated with *Ca.* Bipolaricaulota had the most coverages from Tuzla samples.

Concluding Discussion

Russell and Martin wrote in the abstract of their fundamental paper (Russell and Martin 2004): "Geologists have suggested that life might have emerged at hydrothermal vents, chemists have shown that metal sulfides such as FeS and NiS can catalyze biochemical reactions in the absence of proteins, and biologists have suggested that the acetyl-coenzyme-A (CoA) pathway of CO_2 fixation might be very ancient.". Field of the origin of life is the combination of these fundamental sciences and we need interdisciplinary fields to find out new clues on the origin of life. This thesis was built upon the hypotheses put forth by geologists, chemists, and biologists and tries to better understand the primordial carbon metabolism of the last universal common ancestor (LUCA) from a microbiological point of view. The imprints of ancient metabolism (chemistry) should be hidden in modern organisms (biology) thriving in proposed environments for the birthplace of life (geology). The thesis was first of all constructed on the sampling environments which were postulated as a possible hotspot for emergence of life in the Hadean Ocean. Thus, samples obtained from partially-serpentinized marine environment (Chapter 2), shallow-water hydrothermal setting (chapter 3), deep hydrothermal aquifer and hot springs (chapter 4, 5) were investigated to unravel microbial carbon cycling using a novel technique called quantitative DNA stable isotope probing (qSIP; (Hungate et al. 2015)). However, it should be noted that the sampled settings comprised complex microbial communities in the modern Earth conditions and therefore, my aim first was to understand the microbial ecology using stable isotope tracers. Afterwards, I tried to distill out the genes and species related to the origin of life hypothesis from the whole microbial community structure.

First signs of life in the geological record points towards biological carbon fixation under hydrothermal conditions, including biological methanogenesis in 3.6 billion years old rocks (Ueno et al. 2006), fossilized microbial structures in rocks from 3.7 billion years old rocks suggesting biological carbon fixation (Nutman et al. 2016), and stable isotope evidence for biological carbon fixation in 4.1 billion years old Zircons from the Jack Hills /Western Australia (Bell et al. 2015). These geological findings support the chemoautotrophic origin of life. Apart from geological record, alkaline hydrothermal settings gained importance after their discovery in the 2000s (Kelley et al. 2001) because gradients (pH, temperature, and energy) are needed for the emergence of the first life. Alkaline hydrothermal vents driven by serpentinization process have been proposed as a plausible setting for the origin of life (Russell et al. 1989; Russell and Martin 2004; Russell et al. 2010).

To find out the effect of hydrogen on carbon assimilation, the samples were collected from partially serpentinized peridotite mylonite from Saint Peter and Saint Paul Archipelago (Arquipélago de São Pedro e São Paulo, Brasil 'SPSPA') at the equatorial Mid-Atlantic Ridge (Chapter 2) (Coskun et al. 2021). Our motivation for this study comes from 3 scientific findings. First, before the cruise took place, shimmering water and hydrogen elevation were observed near SPSPA, which may indicate an ongoing serpentinization at the ocean bottom. The dives with remotely operated underwater vehicle (ROV) were organized to detect any serpentine-driven chimney structure similar to what have been

discovered in Lost City hydrothermal vent field (Kelley et al. 2005). Unfortunately, no vents were monitored, however samples from partially serpentinized mylonites were collected for qSIP experiments. This did not mask the importance of the study as H_2 is likely generated today at SPSPA through low-temperature aqueous alteration of peridotite, mechanoradical H_2 formation, or radiolysis, despite at slow rates (Coskun et al. 2021). Secondly, hydrogen oxidation is an important energy source, which yields low-potential electrons used in respiratory chains or fixing carbon (Greening et al. 2016). The active sites (iron-sulfur clusters) of metalloenzymes are mimicking in terms of structure and atomic coordination of naturally occurring minerals such as greigite, suggesting that mineral surfaces were catalyzing the first biochemical reaction in the absence of proteins (Russell and Martin 2004). Moreover, hydrogen is an entry in the Wood-Ljungdahl pathway which has been proposed as an ancient carbon fixation pathway (Ragsdale and Pierce 2008). Additionally, the genome of the last universal common ancestor (LUCA) has been predicted to be capable of fixing CO_2 with the Wood-Ljungdahl pathway in hydrothermal settings (Weiss et al. 2016). Lastly, methanogens and acetogens have been hypothesized to be deeply-branching and these organisms can be found in hydrothermal environments, including serpentinization-driven ecosystems (Schrenk et al. 2013).

To better understand the effects of H_2 on carbon anabolism in seafloor microbial communities associated with ultramafic rocks, we incubated the rocks on the cruise (SPSPA (AL170602) onboard the MV ALUCIA in 2017) with ^{13}C-labeled sodium-bicarbonate, formate and acetate with and without hydrogen gas (H_2). The results show that rock-associated microbes increased the assimilation of bicarbonate and acetate utilization while formate metabolism seems to be affected by increasing hydrogen concentration. Atribacteria, *Nitrospira* and Thaumarchaeota exhibited significant increase in ^{13}C-substrate assimilation in the presence of H_2. This data clearly supports the thermodynamic calculations predicting that oxidation of H_2 is energetically favorable for sea-floor microbes (Amend et al. 2011). For the future directions, here I think that hydrogen gas measurements from the headspace would be a great supporting data in addition to qSIP. Also, oxygen measurements should be continuously measured through the course of the experiment because we have shown in our previous study that oxygen gets consumed by the microbial communities (Coskun et al. 2019). The reason is that we used glass vials with gas-tight crimp seals to track the ^{13}C-labeled carbon. The necessity of gas-tight incubations comes from the fact that a fraction of bicarbonate turns into carbon dioxide (Kleypas et al. 1999). It is also the same issue when using acetate and formate because microbes can turn them into CO_2. Lastly, adding bicarbonate slightly changes the pH as we have shown in chapter 4. Hence, pH should be measured after the termination of the incubation.

Chapter 3 focuses on the activity of growing microbial populations in Estuarine sediments using quantitative DNA-stable isotope probing (qSIP) with $H_2{}^{18}O$ as a passive tracer (Schwartz 2007). Complex microbial communities found in estuarine sediments are primarily composed of uncultured lineages that facilitate aerobic, microaerophilic, and anaerobic metabolic pathways that influence the cycling of carbon, nitrogen, and sulfur (Baker et al. 2015). Although difficult, measuring the expansion of certain bacterial populations is essential for understanding ecosystem resilience and responsiveness to change (Luna et al. 2002). The Bowen et al. (2011) study found that while the structure of microbial communities in estuarine habitats can be resistant to environmental change, the levels of activity within populations can change significantly in response to shifting nutrient and

oxygen levels, with obvious effects on biogeochemical cycles (Kearns et al. 2016). This chapter was published before I become part of origin-of-life cluster and gave me great insights on how to further apply qSIP using different labeled substrates.

The paper 1 (Puzenat et al. 2021) deserves a special mention although only mentioned in the appendix because I learned how to apply qSIP technique to low biomass samples. This paper particularly describes a geological investigation to map the hyperthermalism in a shallow-water hydrothermal system in Milos using images taken from aerial drones and Autonomous Underwater Vehicle (AUV). I personally attended the fieldwork together with a great geologist/geomicrobiologist team. This research paper provides perspectives on the heat fluxes of the Milos system (Puzenat et al. 2021). It may shed light on shallow water hydrothermal systems in the Early Earth as 18th-century geologist James Hutton stated, “the present is key to the past”. Mantle and thermal convection generated a geochemical disequilibrium (Shock 1990; Russell et al. 2010) where inorganic CO2 was reduced to organic molecules leading to life's emergence in the Early Earth condition (Russell et al. 2010). The Paleochori Bay in Milos displays a nice example of geochemical disequilibrium with distinct outflow patches where temperature and chemistry changes sharply. Thus, shallow-water-hydrothermal systems are possible settings where life could have originated and emerged (Damer and Deamer 2019). The samples were collected from yellow-, white- and orange-colored sand patches in Milos where the temperature was around 50-80 ^{o}C. The 20 ml glass vials were filled with samples displaying different colors. ^{12}C- and ^{13}C-labeled sodium-bicarbonate was added into the sand samples to unravel the carbon cycling mediated by chemolithoautotrophs. During the incubation, a hybridization oven was used to heat the samples to their original temperature. The incubations were terminated after 3 days and sent back to Munich for laboratory analysis. After spending 3 months on the sample analysis using DNA-SIP methodology (Neufeld et al. 2007a), none of the samples showed a clear shift between ^{12}C- and ^{13}C-labeled DNA. A possible reason could be related to incubation setup. The biomass in the thermal sediments was low, thus, a successful labeling did not occur. Alternatively, the incubation conditions could be affected by small headspace in 20 ml glass vials, which may turn into anoxic conditions within a short time frame. On the other hand, this might indicate microbial activity in the incubations. It can be also speculated that chemolithoautotrophy was not the main metabolism in Milos shallow water hydrothermal setting, but studies on microbial composition found that *Sulfurovum* spp., a chemolithoautotrophic Epsilonbacterium, comprising 60% of the total reads (Giovannelli et al. 2013; Caramanna et al. 2021). Although the SIP experiment failed in Milos, it gave us a unique opportunity to review our incubation setup. The low biomass samples should be incubated in a larger volume so that a successful labeling would be guaranteed (if there are microbes which can utilize the given substrate) as we applied this in Turkey to thermal waters and ended up with clear shifts between unlabeled and labeled incubations (Chapter 4).

Chapter 4 and 5 are in preparation for a standalone publication which is a study targeting microbes dwelling in terrestrial hydrothermal settings. Hot springs (Damer and Deamer 2019) and deep subsurface hydrothermal aquifers (Gold 1992) may be a suitable setting for the emergence of life. To investigate the microbial carbon cycling dynamics, a 3-years of sampling campaign was conducted in Biga Peninsula, Turkey between 2019 and 2021. The qSIP incubations were done in 2020 and 2021, but only 2021 experiments were presented because the calculated bootstrap values for each OTU in

the experiments in 2020, i.e., the statistical indicators used in qSIP (Hungate et al. 2015), were quite big, indicating a huge variability in the replicate dataset. Therefore, we focused on the samples taken in the summertime of 2021. We have designed the experiments based on 2 latest papers: [1] DOC is stimulated more when more DIC is available to rTCA-encoding chemolithoautotrophs (Fullerton et al. 2021) and [2] TCA cycle can be reversed in the presence of high partial pressure of CO_2 (Steffens et al. 2021). We wanted to test these findings by supplementing differential bicarbonate concentrations to the thermal water from a 750-meter-deep hydrothermal aquifer. The incubations in 5 liters of glass bottles were amended with 1 mM, 5 mM and 10 mM unlabeled (^{12}C) and labeled (^{13}C) bicarbonate concentrations. Normally, we wanted to use 100 mM - 50 mM - 10 mM sodium bicarbonate, but the labeling compounds are not cheap. We assumed that 10 mM sodium bicarbonate incubations would yield more mean excess atom fraction (EAF) values; however, incubations receiving 1 mM sodium bicarbonate had the highest EAF. Furthermore, the 16S rRNA gene copies in the incubations did not change significantly, suggesting that DOC concentrations are not correlated with increased DIC. Therefore, chapter 4 provides substantial findings on the microbial carbon cycling in deep terrestrial hydrothermal aquifers and may contribute valuable knowledge on ecophysiology of microbial dark matter (Rinke et al. 2013). Chapter 5 focuses on the metabolic capacity of *Ca.* Bipolaricauolata MAGs reconstructed from the samples taken from Biga Peninsula and discusses the widespread distribution of halotolerant OTUs affiliated to this uncultured phylum. Chapter 4 and 5 will be finalized when the analysis showing the phylogenetic placement of the taxonomically unassigned metagenome-assembled-genomes (MAGs) were successfully implemented in the papers.

Consequently, this thesis has expanded our knowledge of carbon cycling driven by microorganisms in diverse geological settings, which have been proposed to plausible settings for the origin of life. It provides insight into the microbial ecology of microorganisms thriving in seafloor, hotsprings, shallow-water-hydrothermal marine environment and deep subsurface hydrothermal aquifers, with a focus on their metabolism associated with carbon assimilation pathways.

References

Akkuş, İbrahim, Hafize Akıllı, Selda Ceyhan, Ayşe Dilemre, and Zeki Tekin. 2005. *Türkiye jeotermal kaynakları envanteri* (Maden Tetkik ve Arama Genel Müdürlüğü).

Alneberg, Johannes, Brynjar Smári Bjarnason, Ino de Bruijn, Melanie Schirmer, Joshua Quick, Umer Z. Ijaz, Leo Lahti, Nicholas J. Loman, Anders F. Andersson, and Christopher Quince. 2014. 'Binning metagenomic contigs by coverage and composition', *Nat. Methods*, 11: 1144-46.

Altschul, S. F., W. Gish, W. Miller, E. W. Myers, and D. J. Lipman. 1990. 'Basic local alignment search tool', *J. Mol. Biol.*, 215: 403-10.

Amend, Jan P., Thomas M. McCollom, Michael Hentscher, and Wolfgang Bach. 2011. 'Catabolic and anabolic energy for chemolithoautotrophs in deep-sea hydrothermal systems hosted in different rock types', *Geochim. Cosmochim. Acta*, 75: 5736-48.

Anantharaman, Karthik, Bela Hausmann, Sean P. Jungbluth, Rose S. Kantor, Adi Lavy, Lesley A. Warren, Michael S. Rappé, Michael Pester, Alexander Loy, Brian C. Thomas, and Jillian F. Banfield. 2018. 'Expanded diversity of microbial groups that shape the dissimilatory sulfur cycle', *The ISME Journal*, 12: 1715-28.

Angel, Roey. 2019. 'Experimental Setup and Data Analysis Considerations for DNA- and RNA-SIP Experiments in the Omics Era.' in Marc G. Dumont and Marcela Hernández García (eds.), *Stable Isotope Probing: Methods and Protocols* (Springer New York: New York, NY).

Baba, Alper, Galip Yuce, Ozan Deniz, and Didem Yasin Ugurluoglu. 2009. 'Hydrochemical and Isotopic Composition of Tuzla Geothermal Field (Canakkale-Turkey) and its Environmental Impacts', *Environ. Forensics*, 10: 144-61.

Bach, Wolfgang, Holger Paulick, Carlos J. Garrido, Benoit Ildefonse, William P. Meurer, and Susan E. Humphris. 2006. 'Unraveling the sequence of serpentinization reactions: petrography, mineral chemistry, and petrophysics of serpentinites from MAR 15°N (ODP Leg 209, Site 1274)', *Geophys. Res. Lett.*, 33.

Bada, Jeffrey L., and Jun Korenaga. 2018. 'Exposed areas above sea level on Earth> 3.5 Gyr ago: implications for prebiotic and primitive biotic chemistry', *Life*, 8: 55.

Baker, Brett J, Cassandre Sara Lazar, Andreas P Teske, and Gregory J Dick. 2015. 'Genomic resolution of linkages in carbon, nitrogen, and sulfur cycling among widespread estuary sediment bacteria', *Microbiome*, 3: 1-12.

Baker, Brett J., Jimmy H. Saw, Anders E. Lind, Cassandre Sara Lazar, Kai-Uwe Hinrichs, Andreas P. Teske, and Thijs J. G. Ettema. 2016. 'Genomic inference of the metabolism of cosmopolitan subsurface Archaea, Hadesarchaea', *Nat Microbiol*, 1: 16002.

Balderer, Werner. 1997. 'Mechanisms and processes of groundwater circulation in tectonically active areas', *Active Tectonics of Northwestern Anatolia-The Marmara Poly-Project,(eds. Shindler, C. and Pfister, M.)(Hochschulverlag AG an der ETH Zurich-Swiss, 1997) p*: 375-416.

Barge, Laura M., Erika Flores, Marc M. Baum, David G. VanderVelde, and Michael J. Russell. 2019. 'Redox and pH gradients drive amino acid synthesis in iron oxyhydroxide mineral systems', *Proc. Natl. Acad. Sci. U. S. A.*, 116: 4828-33.

Barge, Laura M., John-Paul Jones, Jason J. Pagano, Eduardo Martinez, and John Bescup. 2020. 'Three-Dimensional Analysis of a Simulated Prebiotic Hydrothermal Chimney', *ACS Earth Space Chem.*, 4: 1663-69.

Baricz, Andreea, Cecilia Maria Chiriac, Adrian-Ștefan Andrei, Paul-Adrian Bulzu, Erika Andrea Levei, Oana Cadar, Karina Paula Battes, Mirela Cîmpean, Marin Șenilă, Adorján Cristea, Vasile Muntean, Mircea Alexe, Cristian Coman, Edina Kriszta Szekeres, Cosmin Ionel Sicora, Artur

Ionescu, David Blain, William Kenneth O'Neill, Jessica Edwards, John Edward Hallsworth, and Horia Leonard Banciu. 2021. 'Spatio-temporal insights into microbiology of the freshwater-to-hypersaline, oxic-hypoxic-euxinic waters of Ursu Lake', *Environ. Microbiol.*, 23: 3523-40.

Barnett, S. E., N. D. Youngblut, and D. H. Buckley. 2019. 'Data Analysis for DNA Stable Isotope Probing Experiments Using Multiple Window High-Resolution SIP', *Methods Mol Biol*, 2046: 109-28.

Baross, John A., and Sarah E. Hoffman. 1985. 'Submarine hydrothermal vents and associated gradient environments as sites for the origin and evolution of life', *Orig. Life Evol. Biosph.*, 15: 327-45.

Belduz, Ali Osman, Sabriye Dulger, and Zihni Demirbag. 2003. 'Anoxybacillus gonensis sp. nov., a moderately thermophilic, xylose-utilizing, endospore-forming bacterium', *Int. J. Syst. Evol. Microbiol.*, 53: 1315-20.

Bell, Elizabeth A., Patrick Boehnke, T. Mark Harrison, and Wendy L. Mao. 2015. 'Potentially biogenic carbon preserved in a 4.1 billion-year-old zircon', *Proc. Natl. Acad. Sci. U. S. A.*, 112: 14518-21.

Berney, Michael, Chris Greening, Ralf Conrad, William R. Jacobs, Jr., and Gregory M. Cook. 2014. 'An obligately aerobic soil bacterium activates fermentative hydrogen production to survive reductive stress during hypoxia', *Proc. Natl. Acad. Sci. U. S. A.*, 111: 11479-84.

Bjornsdottir, S. H., S. K. Petursdottir, G. O. Hreggvidsson, S. Skirnisdottir, S. Hjorleifsdottir, J. Arnfinnsson, and J. K. Kristjansson. 2009. 'Thermus islandicus sp. nov., a mixotrophic sulfur-oxidizing bacterium isolated from the Torfajokull geothermal area', *Int J Syst Evol Microbiol*, 59: 2962-6.

Blazewicz, Steven J, Egbert Schwartz, and Mary K Firestone. 2014. 'Growth and death of bacteria and fungi underlie rainfall-induced carbon dioxide pulses from seasonally dried soil', *Ecology*, 95: 1162-72.

Blomberg, Simon P., Theodore Garland, Jr., and Anthony R. Ives. 2003. 'Testing for phylogenetic signal in comparative data: behavioral traits are more labile', *Evolution*, 57: 717-45.

Bolger, Anthony M., Marc Lohse, and Bjoern Usadel. 2014. 'Trimmomatic: a flexible trimmer for Illumina sequence data', *Bioinformatics*, 30: 2114-20.

Bomberg, M., T. Lamminmäki, and M. Itävaara. 2016. 'Microbial communities and their predicted metabolic characteristics in deep fracture groundwaters of the crystalline bedrock at Olkiluoto, Finland', *Biogeosciences*, 13: 6031-47.

Bowen, Jennifer L, Bess B Ward, Hilary G Morrison, John E Hobbie, Ivan Valiela, Linda A Deegan, and Mitchell L Sogin. 2011. 'Microbial community composition in sediments resists perturbation by nutrient enrichment', *The ISME Journal*, 5: 1540-48.

Bowers, Robert M., Nikos C. Kyrpides, Ramunas Stepanauskas, Miranda Harmon-Smith, Devin Doud, T. B. K. Reddy, Frederik Schulz, Jessica Jarett, Adam R. Rivers, Emiley A. Eloe-Fadrosh, Susannah G. Tringe, Natalia N. Ivanova, Alex Copeland, Alicia Clum, Eric D. Becraft, Rex R. Malmstrom, Bruce Birren, Mircea Podar, Peer Bork, George M. Weinstock, George M. Garrity, Jeremy A. Dodsworth, Shibu Yooseph, Granger Sutton, Frank O. Glöckner, Jack A. Gilbert, William C. Nelson, Steven J. Hallam, Sean P. Jungbluth, Thijs J. G. Ettema, Scott Tighe, Konstantinos T. Konstantinidis, Wen-Tso Liu, Brett J. Baker, Thomas Rattei, Jonathan A. Eisen, Brian Hedlund, Katherine D. McMahon, Noah Fierer, Rob Knight, Rob Finn, Guy Cochrane, Ilene Karsch-Mizrachi, Gene W. Tyson, Christian Rinke, Consortium Genome Standards, Alla Lapidus, Folker Meyer, Pelin Yilmaz, Donovan H. Parks, A. M. Eren, Lynn Schriml, Jillian F. Banfield, Philip Hugenholtz, and Tanja Woyke. 2017. 'Minimum information about a single amplified genome (MISAG) and a metagenome-assembled genome (MIMAG) of bacteria and archaea', *Nat. Biotechnol.*, 35: 725-31.

Boynton, W., and W. M. Kemp. 1985. 'Nutrient Regeneration and Oxygen Consumption Along an Estuarine Salinity Gradient', *Marine Ecology-progress Series - MAR ECOL-PROGR SER*, 23: 45-55.

Braakman, Rogier, and Eric Smith. 2012. 'The emergence and early evolution of biological carbon-fixation', *PLoS Comput. Biol.*, 8: e1002455.

Braakman, Rogier, and Eric Smith. 2013. 'The compositional and evolutionary logic of metabolism', *Phys. Biol.*, 10: 011001.

Braun, A., M. Spona-Friedl, M. Avramov, M. Elsner, F. Baltar, T. Reinthaler, G. J. Herndl, and C. Griebler. 2021. 'Reviews and syntheses: Heterotrophic fixation of inorganic carbon – significant but invisible flux in environmental carbon cycling', *Biogeosciences*, 18: 3689-700.

Brisbarre, N., M. L. Fardeau, V. Cueff, J. L. Cayol, G. Barbier, V. Cilia, G. Ravot, P. Thomas, J. L. Garcia, and B. Ollivier. 2003. 'Clostridium caminithermale sp. nov., a slightly halophilic and moderately thermophilic bacterium isolated from an Atlantic deep-sea hydrothermal chimney', *Int J Syst Evol Microbiol*, 53: 1043-49.

Bristow, Laura A., Tage Dalsgaard, Laura Tiano, Daniel B. Mills, Anthony D. Bertagnolli, Jody J. Wright, Steven J. Hallam, Osvaldo Ulloa, Donald E. Canfield, Niels Peter Revsbech, and Bo Thamdrup. 2016. 'Ammonium and nitrite oxidation at nanomolar oxygen concentrations in oxygen minimum zone waters', *Proc. Natl. Acad. Sci. U. S. A.*, 113: 10601-06.

Bryant, F. O., and M. W. Adams. 1989. 'Characterization of hydrogenase from the hyperthermophilic archaebacterium, Pyrococcus furiosus', *J. Biol. Chem.*, 264: 5070-79.

Buchfink, Benjamin, Chao Xie, and Daniel H. Huson. 2015. 'Fast and sensitive protein alignment using DIAMOND', *Nat. Methods*, 12: 59-60.

Buckel, Wolfgang, and Rudolf K. Thauer. 2018. 'Flavin-Based Electron Bifurcation, Ferredoxin, Flavodoxin, and Anaerobic Respiration With Protons (Ech) or NAD+ (Rnf) as Electron Acceptors: A Historical Review', *Front. Microbiol.*, 9: 401.

Butler, I. B., M. A. Schoonen, and D. T. Rickard. 1994. 'Removal of dissolved oxygen from water: A comparison of four common techniques', *Talanta*, 41: 211-5.

Camanocha, Anuj, and Floyd E. Dewhirst. 2014. 'Host-associated bacterial taxa from Chlorobi, Chloroflexi, GN02, Synergistetes, SR1, TM7, and WPS-2 Phyla/candidate divisions', *Journal of Oral Microbiology*, 6: 25468.

Can, M., F. A. Armstrong, and S. W. Ragsdale. 2014. 'Structure, function, and mechanism of the nickel metalloenzymes, CO dehydrogenase, and acetyl-CoA synthase', *Chem Rev*, 114: 4149-74.

Caporaso, J. Gregory, Justin Kuczynski, Jesse Stombaugh, Kyle Bittinger, Frederic D. Bushman, Elizabeth K. Costello, Noah Fierer, Antonio Gonzalez Peña, Julia K. Goodrich, Jeffrey I. Gordon, Gavin A. Huttley, Scott T. Kelley, Dan Knights, Jeremy E. Koenig, Ruth E. Ley, Catherine A. Lozupone, Daniel McDonald, Brian D. Muegge, Meg Pirrung, Jens Reeder, Joel R. Sevinsky, Peter J. Turnbaugh, William A. Walters, Jeremy Widmann, Tanya Yatsunenko, Jesse Zaneveld, and Rob Knight. 2010. 'QIIME allows analysis of high-throughput community sequencing data', *Nat. Methods*, 7: 335-36.

Caramanna, Giorgio, Stefan M. Sievert, and Solveig I. Bühring. 2021. 'Submarine Shallow-Water Fluid Emissions and Their Geomicrobiological Imprint: A Global Overview', *Frontiers in Marine Science*, 8.

Carr, Stephanie A., Beth N. Orcutt, Kevin W. Mandernack, and John R. Spear. 2015. 'Abundant Atribacteria in deep marine sediment from the Adélie Basin, Antarctica', *Front. Microbiol.*, 6: 872.

Chen, Yin, and J. Colin Murrell. 2010. 'When metagenomics meets stable-isotope probing: progress and perspectives', *Trends Microbiol.*, 18: 157-63.

Chong, Zhi-Soon, Wei-Fen Woo, and Shu-Sin Chng. 2015. 'Osmoporin OmpC forms a complex with MlaA to maintain outer membrane lipid asymmetry in Escherichia coli', *Molecular Microbiology*, 98: 1133-46.
Colman, Daniel R., Saroj Poudel, Blake W. Stamps, Eric S. Boyd, and John R. Spear. 2017. 'The deep, hot biosphere: Twenty-five years of retrospection', *Proc. Natl. Acad. Sci. U. S. A.*, 114: 6895-903.
Cordero, P. R. F., K. Bayly, P. Man Leung, C. Huang, Z. F. Islam, R. B. Schittenhelm, G. M. King, and C. Greening. 2019. 'Atmospheric carbon monoxide oxidation is a widespread mechanism supporting microbial survival', *Isme j*, 13: 2868-81.
Corliss, John B., Jack Dymond, Louis I. Gordon, John M. Edmond, Richard P. von Herzen, Robert D. Ballard, Kenneth Green, David Williams, Arnold Bainbridge, Kathy Crane, and Tjeerd H. van Andel. 1979. 'Submarine Thermal Springs on the Galápagos Rift', *Science*.
Cornall, A., A. Rose, C. Streten, K. McGuinness, D. Parry, and K. Gibb. 2016. 'Molecular screening of microbial communities for candidate indicators of multiple metal impacts in marine sediments from northern Australia', *Environ Toxicol Chem*, 35: 468-84.
Coskun, Ömer K., Volkan Özen, Scott D. Wankel, and William D. Orsi. 2019. 'Quantifying population-specific growth in benthic bacterial communities under low oxygen using H218O', *ISME J.*, 13: 1546-59.
Coskun, Ömer K., Monica Pichler, Sergio Vargas, Stuart Gilder, and William D. Orsi. 2018. 'Linking Uncultivated Microbial Populations and Benthic Carbon Turnover by Using Quantitative Stable Isotope Probing', *Appl. Environ. Microbiol.*, 84.
Coskun, Ömer K., Aurèle Vuillemin, Florence Schubotz, Frieder Klein, Susanna E. Sichel, Wolfgang Eisenreich, and William D. Orsi. 2021. 'Quantifying the effects of hydrogen on carbon assimilation in a seafloor microbial community associated with ultramafic rocks', *ISME J.*
Craig, H. 1961. 'Isotopic Variations in Meteoric Waters', *Science*, 133: 1702-03.
Çelikoğlu, E., M. Y. Cankılıç, and Others. 2016. 'Prokaryotic diversity of hot springs in Balikesİr and Kütahya, Turkey', *Appl. Ecol. Environ. Res.*, 14: 429-40.
D'Avanzo, Charlene, and James N Kremer. 1994. 'Diel oxygen dynamics and anoxic events in an eutrophic estuary of Waquoit Bay, Massachusetts', *Estuaries*, 17: 131-39.
Daebeler, Anne, Craig W. Herbold, Julia Vierheilig, Christopher J. Sedlacek, Petra Pjevac, Mads Albertsen, Rasmus H. Kirkegaard, José R. de la Torre, Holger Daims, and Michael Wagner. 2018. 'Cultivation and Genomic Analysis of "Candidatus Nitrosocaldus islandicus," an Obligately Thermophilic, Ammonia-Oxidizing Thaumarchaeon from a Hot Spring Biofilm in Graendalur Valley, Iceland', *Front. Microbiol.*, 9: 193.
Damer, Bruce, and David Deamer. 2019. 'The Hot Spring Hypothesis for an Origin of Life', *Astrobiology*.
Darwin, Charles. 1871. 'Letter no. 7471', *Darwin Correspondence Project; University of Cambridge; Available online: https://www. darwinproject. ac. uk/letter/DCP-LETT-7471. xml (accessed on 30 November 2020)*.
De Simone, Giuseppina, Simona Maria Monti, Vincenzo Alterio, Martina Buonanno, Viviana De Luca, Mosè Rossi, Vincenzo Carginale, Claudiu T. Supuran, Clemente Capasso, and Anna Di Fiore. 2015. 'Crystal structure of the most catalytically effective carbonic anhydrase enzyme known, SazCA from the thermophilic bacterium Sulfurihydrogenibium azorense', *Bioorganic & Medicinal Chemistry Letters*, 25: 2002-06.
Dhillon, Ashita, Andreas Teske, Jesse Dillon, David A Stahl, and Mitchell L Sogin. 2003. 'Molecular characterization of sulfate-reducing bacteria in the Guaymas Basin', *Applied and environmental microbiology*, 69: 2765-72.
Diaz, Robert J, and Rutger Rosenberg. 2008. 'Spreading dead zones and consequences for marine ecosystems', *Science*, 321: 926-29.

Díaz, Robert J., and Rutger Rosenberg. 1995. 'Marine benthic hypoxia: a review of its ecological effects and the behavioural responses of benthic macrofauna', *Oceanography and Marine Biology*, 33: 245-303.
Dunford, Eric A., and Josh D. Neufeld. 2010. 'DNA stable-isotope probing (DNA-SIP)', *J. Vis. Exp.*
Dyksma, S., S. Lenk, J. E. Sawicka, and M. Mußmann. 2018a. 'Uncultured Gammaproteobacteria and Desulfobacteraceae Account for Major Acetate Assimilation in a Coastal Marine Sediment', *Frontiers in microbiology*, 9: 3124.
Dyksma, S., P. Pjevac, K. Ovanesov, and M. Mussmann. 2018b. 'Evidence for H(2) consumption by uncultured Desulfobacterales in coastal sediments', *Environ Microbiol*, 20: 450-61.
Dyksma, Stefan, Kerstin Bischof, Bernhard M. Fuchs, Katy Hoffmann, Dimitri Meier, Anke Meyerdierks, Petra Pjevac, David Probandt, Michael Richter, Ramunas Stepanauskas, and Marc Mußmann. 2016. 'Ubiquitous Gammaproteobacteria dominate dark carbon fixation in coastal sediments', *The ISME Journal*, 10: 1939-53.
Edgar, Robert C. 2004. 'MUSCLE: multiple sequence alignment with high accuracy and high throughput', *Nucleic Acids Res.*, 32: 1792-97.
Edgar, Robert C. 2010. 'Search and clustering orders of magnitude faster than BLAST', *Bioinformatics*, 26: 2460-61.
Edgar, Robert C. 2013. 'UPARSE: highly accurate OTU sequences from microbial amplicon reads', *Nat. Methods*, 10: 996-98.
Edwards, Katrina J., Keir Becker, and Frederick Colwell. 2012. 'The Deep, Dark Energy Biosphere: Intraterrestrial Life on Earth', *Annu. Rev. Earth Planet. Sci.*, 40: 551-68.
Einsiedl, F., A. Wunderlich, M. Sebilo, Ö K. Coskun, W. D. Orsi, and B. Mayer. 2020. 'Biogeochemical evidence of anaerobic methane oxidation and anaerobic ammonium oxidation in a stratified lake using stable isotopes', *Biogeosciences*, 17: 5149-61.
Emerson, J. B., B. C. Thomas, W. Alvarez, and J. F. Banfield. 2016. 'Metagenomic analysis of a high carbon dioxide subsurface microbial community populated by chemolithoautotrophs and bacteria and archaea from candidate phyla', *Environ Microbiol*, 18: 1686-703.
Eren, A. Murat, Özcan C. Esen, Christopher Quince, Joseph H. Vineis, Hilary G. Morrison, Mitchell L. Sogin, and Tom O. Delmont. 2015. 'Anvi'o: an advanced analysis and visualization platform for 'omics data', *PeerJ*, 3: e1319.
Etiope, Giuseppe. 2017. 'Abiotic Methane in Continental Serpentinization Sites: An Overview', *Procedia Earth and Planetary Science*, 17: 9-12.
Fernandez, Ana B., Maria C. Rasuk, Pieter T. Visscher, Manuel Contreras, Fernando Novoa, Daniel G. Poire, Molly M. Patterson, Antonio Ventosa, and Maria E. Farias. 2016. 'Microbial Diversity in Sediment Ecosystems (Evaporites Domes, Microbial Mats, and Crusts) of Hypersaline Laguna Tebenquiche, Salar de Atacama, Chile', *Frontiers in microbiology*, 7.
Fisher, Luke A., Alexandra Pontefract, Sanjoy M Som, Christopher E. Carr, Benjamin Klempay, Britney E Schmidt, Jeff S Bowman, and Douglas H. Bartlett. 2021. 'Current state of athalassohaline deep-sea hypersaline anoxic basin research-recommendations for future work and relevance to astrobiology', *Environ. Microbiol.*, 23: 3360-69.
Fones, E. M., D. R. Colman, E. A. Kraus, R. Stepanauskas, A. S. Templeton, J. R. Spear, and E. S. Boyd. 2021. 'Diversification of methanogens into hyperalkaline serpentinizing environments through adaptations to minimize oxidant limitation', *Isme j*, 15: 1121-35.
Fortunato, Caroline S., and Julie A. Huber. 2016. 'Coupled RNA-SIP and metatranscriptomics of active chemolithoautotrophic communities at a deep-sea hydrothermal vent', *ISME J.*, 10: 1925-38.
Früh-Green, Gretchen L., Deborah S. Kelley, Stefano M. Bernasconi, Jeffrey A. Karson, Kristin A. Ludwig, David A. Butterfield, Chiara Boschi, and Giora Proskurowski. 2003. '30,000 years of hydrothermal activity at the lost city vent field', *Science*, 301: 495-98.

Fuchs, Georg. 2011. 'Alternative pathways of carbon dioxide fixation: insights into the early evolution of life?', *Annu. Rev. Microbiol.*, 65: 631-58.

Fullerton, Katherine M., Matthew O. Schrenk, Mustafa Yücel, Elena Manini, Marco Basili, Timothy J. Rogers, Daniele Fattorini, Marta Di Carlo, Giuseppe d'Errico, Francesco Regoli, Mayuko Nakagawa, Costantino Vetriani, Francesco Smedile, Carlos Ramírez, Heather Miller, Shaunna M. Morrison, Joy Buongiorno, Gerdhard L. Jessen, Andrew D. Steen, María Martínez, J. Maarten de Moor, Peter H. Barry, Donato Giovannelli, and Karen G. Lloyd. 2021. 'Effect of tectonic processes on biosphere–geosphere feedbacks across a convergent margin', *Nat. Geosci.*, 14: 301-06.

Galperin, Michael Y., Yuri I. Wolf, Kira S. Makarova, Roberto Vera Alvarez, David Landsman, and Eugene V. Koonin. 2021. 'COG database update: focus on microbial diversity, model organisms, and widespread pathogens', *Nucleic Acids Res.*, 49: D274-D81.

Garcia, Ronald, and Rolf Müller. 2014. 'The Family Polyangiaceae.' in Eugene Rosenberg, Edward F. DeLong, Stephen Lory, Erko Stackebrandt and Fabiano Thompson (eds.), *The Prokaryotes: Deltaproteobacteria and Epsilonproteobacteria* (Springer Berlin Heidelberg: Berlin, Heidelberg).

Gat, J. R., and I. Carmi. 1970. 'Evolution of the isotopic composition of atmospheric waters in the Mediterranean Sea area', *J. Geophys. Res.*, 75: 3039-48.

Geets, Joke, Brigitte Borremans, Ludo Diels, Dirk Springael, Jaco Vangronsveld, Daniel van der Lelie, and Karolien Vanbroekhoven. 2006. 'DsrB gene-based DGGE for community and diversity surveys of sulfate-reducing bacteria', *Journal of Microbiological methods*, 66: 194-205.

Genderjahn, Steffi, Mashal Alawi, Kai Mangelsdorf, Fabian Horn, and Dirk Wagner. 2018. 'Desiccation- and Saline-Tolerant Bacteria and Archaea in Kalahari Pan Sediments', *Front. Microbiol.*, 9: 2082.

Ghai, Rohit, Carolina Megumi Mizuno, Antonio Picazo, Antonio Camacho, and Francisco Rodriguez-Valera. 2013. 'Metagenomics uncovers a new group of low GC and ultra-small marine Actinobacteria', *Scientific reports*, 3: 2471.

Giovannelli, Donato, Giuseppe d'Errico, Elena Manini, Michail Yakimov, and Costantino Vetriani. 2013. 'Diversity and phylogenetic analyses of bacteria from a shallow-water hydrothermal vent in Milos island (Greece)', *Front. Microbiol.*, 4: 184.

Giuffrè, Alessandro, Vitaliy B. Borisov, Marzia Arese, Paolo Sarti, and Elena Forte. 2014. 'Cytochrome bd oxidase and bacterial tolerance to oxidative and nitrosative stress', *Biochimica et Biophysica Acta (BBA) - Bioenergetics*, 1837: 1178-87.

Glein, Christopher R., John A. Baross, and J. Hunter Waite. 2015. 'The pH of Enceladus' ocean', *Geochim. Cosmochim. Acta*, 162: 202-19.

Glud, Ronnie N. 2008. 'Oxygen dynamics of marine sediments', *Marine Biology Research*, 4: 243-89.

Gold, T. 1992. 'The deep, hot biosphere', *Proc. Natl. Acad. Sci. U. S. A.*, 89: 6045-49.

Gouy, Manolo, Stéphane Guindon, and Olivier Gascuel. 2010. 'SeaView version 4: A multiplatform graphical user interface for sequence alignment and phylogenetic tree building', *Mol. Biol. Evol.*, 27: 221-24.

Graham, E. D., J. F. Heidelberg, and B. J. Tully. 2018. 'Potential for primary productivity in a globally-distributed bacterial phototroph', *Isme j*, 12: 1861-66.

Greening, Chris, Ambarish Biswas, Carlo R. Carere, Colin J. Jackson, Matthew C. Taylor, Matthew B. Stott, Gregory M. Cook, and Sergio E. Morales. 2016. 'Genomic and metagenomic surveys of hydrogenase distribution indicate H2 is a widely utilised energy source for microbial growth and survival', *ISME J.*, 10: 761-77.

Gudasz, Cristian, David Bastviken, Kristin Steger, Katrin Premke, Sebastian Sobek, and Lars J. Tranvik. 2010. 'Temperature-controlled organic carbon mineralization in lake sediments', *Nature*, 466: 478-81.

Guindon, Stéphane, Jean-François Dufayard, Vincent Lefort, Maria Anisimova, Wim Hordijk, and Olivier Gascuel. 2010. 'New algorithms and methods to estimate maximum-likelihood phylogenies: assessing the performance of PhyML 3.0', *Syst. Biol.*, 59: 307-21.

Gupta, Radhey S. 2014. 'The Phylum Aquificae.' in Eugene Rosenberg, Edward F. DeLong, Stephen Lory, Erko Stackebrandt and Fabiano Thompson (eds.), *The Prokaryotes: Other Major Lineages of Bacteria and The Archaea* (Springer Berlin Heidelberg: Berlin, Heidelberg).

Guven, Kemal, Fatma Matpan Bekler, and Reyhan Gul Guven. 2018. 'Thermophilic and Halophilic Microorganisms Isolated from Extreme Environments of Turkey, with Potential Biotechnological Applications.' in Dilfuza Egamberdieva, Nils-Kåre Birkeland, Hovik Panosyan and Wen-Jun Li (eds.), *Extremophiles in Eurasian Ecosystems: Ecology, Diversity, and Applications* (Springer Singapore: Singapore).

Haldane, J. B. S. 1929. 'The origin of life', *Rationalist Annual*, 148: 3-10.

Hao, Liping, Simon Jon McIlroy, Rasmus Hansen Kirkegaard, Søren Michael Karst, Warnakulasuriya Eustace Yrosh Fernando, Hüsnü Aslan, Rikke Louise Meyer, Mads Albertsen, Per Halkjær Nielsen, and Morten Simonsen Dueholm. 2018. 'Novel prosthecate bacteria from the candidate phylum Acetothermia', *ISME J.*, 12: 2225-37.

Hausmann, Bela, Claus Pelikan, Craig W. Herbold, Stephan Köstlbacher, Mads Albertsen, Stephanie A. Eichorst, Tijana Glavina del Rio, Martin Huemer, Per H. Nielsen, Thomas Rattei, Ulrich Stingl, Susannah G. Tringe, Daniela Trojan, Cecilia Wentrup, Dagmar Woebken, Michael Pester, and Alexander Loy. 2018. 'Peatland Acidobacteria with a dissimilatory sulfur metabolism', *The ISME Journal*, 12: 1729-42.

Hausmann, Bela, Claus Pelikan, Thomas Rattei, Alexander Loy, Michael Pester, and Mark J. Bailey. 2019. 'Long-Term Transcriptional Activity at Zero Growth of a Cosmopolitan Rare Biosphere Member', *mBio*, 10: e02189-18.

Hayer, Michaela, Egbert Schwartz, Jane C Marks, Benjamin J Koch, Ember M Morrissey, Alexa A Schuettenberg, and Bruce A Hungate. 2016. 'Identification of growing bacteria during litter decomposition in freshwater through quantitative stable isotope probing', *Environmental Microbiology Reports*, 8: 975-82.

Herschy, Barry, Alexandra Whicher, Eloi Camprubi, Cameron Watson, Lewis Dartnell, John Ward, Julian R. G. Evans, and Nick Lane. 2014. 'An origin-of-life reactor to simulate alkaline hydrothermal vents', *J. Mol. Evol.*, 79: 213-27.

Hoehler, Tori M., and Bo Barker Jørgensen. 2013. 'Microbial life under extreme energy limitation', *Nature Reviews Microbiology*, 11: 83-94.

Hu, Ping, Lauren Tom, Andrea Singh, Brian C. Thomas, Brett J. Baker, Yvette M. Piceno, Gary L. Andersen, and Jillian F. Banfield. 2016. 'Genome-Resolved Metagenomic Analysis Reveals Roles for Candidate Phyla and Other Microbial Community Members in Biogeochemical Transformations in Oil Reservoirs', *mBio*, 7: e01669-15.

Huerta-Cepas, Jaime, Damian Szklarczyk, Kristoffer Forslund, Helen Cook, Davide Heller, Mathias C. Walter, Thomas Rattei, Daniel R. Mende, Shinichi Sunagawa, Michael Kuhn, Lars Juhl Jensen, Christian von Mering, and Peer Bork. 2016. 'eggNOG 4.5: a hierarchical orthology framework with improved functional annotations for eukaryotic, prokaryotic and viral sequences', *Nucleic Acids Res.*, 44: D286-93.

Hugenholtz, P., C. Pitulle, K. L. Hershberger, and N. R. Pace. 1998. 'Novel division level bacterial diversity in a Yellowstone hot spring', *J. Bacteriol.*, 180: 366-76.

Hughes, Gareth W., Stephen C. L. Hall, Claire S. Laxton, Pooja Sridhar, Amirul H. Mahadi, Caitlin Hatton, Thomas J. Piggot, Peter J. Wotherspoon, Aneika C. Leney, Douglas G. Ward, Mohammed Jamshad, Vaclav Spana, Ian T. Cadby, Christopher Harding, Georgia L. Isom, Jack A. Bryant, Rebecca J. Parr, Yasin Yakub, Mark Jeeves, Damon Huber, Ian R. Henderson, Luke A. Clifton, Andrew L. Lovering, and Timothy J. Knowles. 2019. 'Evidence for phospholipid

export from the bacterial inner membrane by the Mla ABC transport system', *Nature Microbiology*, 4: 1692-705.
Hungate, Bruce A, Rebecca L Mau, Egbert Schwartz, J Gregory Caporaso, Paul Dijkstra, Natasja van Gestel, Benjamin J Koch, Cindy M Liu, Theresa A McHugh, and Jane C Marks. 2015. 'Quantitative microbial ecology through stable isotope probing', *Applied and environmental microbiology*, 81: 7570-81.
Hügler, Michael, and Stefan M. Sievert. 2011. 'Beyond the Calvin Cycle: Autotrophic Carbon Fixation in the Ocean', *Annual Review of Marine Science*, 3: 261-89.
Hyatt, Doug, Gwo-Liang Chen, Philip F. Locascio, Miriam L. Land, Frank W. Larimer, and Loren J. Hauser. 2010. 'Prodigal: prokaryotic gene recognition and translation initiation site identification', *BMC Bioinformatics*, 11: 119.
Inagaki, Fumio, Masae Suzuki, Ken Takai, Hanako Oida, Tatsuhiko Sakamoto, Kaori Aoki, Kenneth H. Nealson, and Koki Horikoshi. 2003. 'Microbial Communities Associated with Geological Horizons in Coastal Subseafloor Sediments from the Sea of Okhotsk', *Applied and environmental microbiology*, 69: 7224-35.
Islam, Zahra F., Caitlin Welsh, Katherine Bayly, Rhys Grinter, Gordon Southam, Emma J. Gagen, and Chris Greening. 2020. 'A widely distributed hydrogenase oxidises atmospheric H2 during bacterial growth', *The ISME Journal*.
Jansen, Kathrin, Rudolf K. Thauer, Fritz Widdel, and Georg Fuchs. 1984. 'Carbon assimilation pathways in sulfate reducing bacteria. Formate, carbon dioxide, carbon monoxide, and acetate assimilation by Desulfovibrio baarsii', *Archives of Microbiology*, 138: 257-62.
Jasechko, Scott. 2019. 'Global Isotope Hydrogeology—Review', *Reviews of Geophysics*, 57: 835-965.
Jenkins, Mark C., and W. Michael Kemp. 1984. 'The coupling of nitrification and denitrification in two estuarine sediments1,2', *Limnology and Oceanography*, 29: 609-19.
Ji, Mukan, Chris Greening, Inka Vanwonterghem, Carlo R. Carere, Sean K. Bay, Jason A. Steen, Kate Montgomery, Thomas Lines, John Beardall, Josie van Dorst, Ian Snape, Matthew B. Stott, Philip Hugenholtz, and Belinda C. Ferrari. 2017. 'Atmospheric trace gases support primary production in Antarctic desert surface soil', *Nature*, 552: 400-03.
Jia, Baolei, Hye Im Jeong, Kyung Hyun Kim, and Che Ok Jeon. 2016. 'Complete genome of Zhongshania aliphaticivorans SM-2T, an aliphatic hydrocarbon-degrading bacterium isolated from tidal flat sediment', *Journal of Biotechnology*, 226: 22-23.
Jiao, Jian-Yu, Lan Liu, Zheng-Shuang Hua, Bao-Zhu Fang, En-Min Zhou, Nimaichand Salam, Brian P. Hedlund, and Wen-Jun Li. 2021. 'Microbial dark matter coming to light: challenges and opportunities', *Natl Sci Rev*, 8: nwaa280.
Jochum, Lara M, Xihan Chen, Mark A Lever, Alexander Loy, Bo Barker Jørgensen, Andreas Schramm, and Kasper U Kjeldsen. 2017. 'Depth distribution and assembly of sulfate-reducing microbial communities in marine sediments of Aarhus Bay', *Applied and environmental microbiology*, 83: e01547-17.
Johnson Hope, A., Eric Hampton, and A. Lesley Scott. 2009. 'The Thermotoga maritima Trk Potassium Transporter—from Frameshift to Function', *J. Bacteriol.*, 191: 2276-84.
Jørgensen, B. B. 1977. 'Bacterial sulfate reduction within reduced microniches of oxidized marine sediments', *Marine Biology*, 41: 7-17.
Jungbluth, Sean P., Jan P. Amend, and Michael S. Rappé. 2017. 'Corrigendum: Metagenome sequencing and 98 microbial genomes from Juan de Fuca Ridge flank subsurface fluids', *Sci Data*, 4: 170080.
Kadnikov, V. V., A. V. Mardanov, A. V. Beletsky, Y. A. Frank, O. V. Karnachuk, and N. V. Ravin. 2019. 'Complete Genome Sequence of an Uncultured Bacterium of the Candidate Phylum Bipolaricaulota', *Microbiology*, 88: 461-68.

Kalyaanamoorthy, Subha, Bui Quang Minh, Thomas K. F. Wong, Arndt von Haeseler, and Lars S. Jermiin. 2017. 'ModelFinder: fast model selection for accurate phylogenetic estimates', *Nat. Methods*, 14: 587-89.

Kanehisa, M., and S. Goto. 2000. 'KEGG: kyoto encyclopedia of genes and genomes', *Nucleic Acids Res.*, 28: 27-30.

Kang, Dongwan, Feng Li, Edward S. Kirton, Ashleigh Thomas, Rob S. Egan, Hong An, and Zhong Wang. 2019. "MetaBAT 2: an adaptive binning algorithm for robust and efficient genome reconstruction from metagenome assemblies." In.: PeerJ Preprints.

Katayama, T., M. K. Nobu, H. Kusada, X. Y. Meng, N. Hosogi, K. Uematsu, H. Yoshioka, Y. Kamagata, and H. Tamaki. 2020. 'Isolation of a member of the candidate phylum 'Atribacteria' reveals a unique cell membrane structure', *Nat Commun*, 11: 6381.

Kearns, Patrick J, John H Angell, Evan M Howard, Linda A Deegan, Rachel HR Stanley, and Jennifer L Bowen. 2016. 'Nutrient enrichment induces dormancy and decreases diversity of active bacteria in salt marsh sediments', *Nature communications*, 7: 1-9.

Keck, François, Frédéric Rimet, Agnès Bouchez, and Alain Franc. 2016. 'phylosignal: an R package to measure, test, and explore the phylogenetic signal', *Ecol. Evol.*, 6: 2774-80.

Keeling, P. J., F. Burki, H. M. Wilcox, B. Allam, E. E. Allen, L. A. Amaral-Zettler, E. V. Armbrust, J. M. Archibald, A. K. Bharti, C. J. Bell, B. Beszteri, K. D. Bidle, C. T. Cameron, L. Campbell, D. A. Caron, R. A. Cattolico, J. L. Collier, K. Coyne, S. K. Davy, P. Deschamps, S. T. Dyhrman, B. Edvardsen, R. D. Gates, C. J. Gobler, S. J. Greenwood, S. M. Guida, J. L. Jacobi, K. S. Jakobsen, E. R. James, B. Jenkins, U. John, M. D. Johnson, A. R. Juhl, A. Kamp, L. A. Katz, R. Kiene, A. Kudryavtsev, B. S. Leander, S. Lin, C. Lovejoy, D. Lynn, A. Marchetti, G. McManus, A. M. Nedelcu, S. Menden-Deuer, C. Miceli, T. Mock, M. Montresor, M. A. Moran, S. Murray, G. Nadathur, S. Nagai, P. B. Ngam, B. Palenik, J. Pawlowski, G. Petroni, G. Piganeau, M. C. Posewitz, K. Rengefors, G. Romano, M. E. Rumpho, T. Rynearson, K. B. Schilling, D. C. Schroeder, A. G. Simpson, C. H. Slamovits, D. R. Smith, G. J. Smith, S. R. Smith, H. M. Sosik, P. Stief, E. Theriot, S. N. Twary, P. E. Umale, D. Vaulot, B. Wawrik, G. L. Wheeler, W. H. Wilson, Y. Xu, A. Zingone, and A. Z. Worden. 2014. 'The Marine Microbial Eukaryote Transcriptome Sequencing Project (MMETSP): illuminating the functional diversity of eukaryotic life in the oceans through transcriptome sequencing', *PLoS Biol*, 12: e1001889.

Kelley, D. S., J. A. Karson, D. K. Blackman, G. L. Früh-Green, D. A. Butterfield, M. D. Lilley, E. J. Olson, M. O. Schrenk, K. K. Roe, G. T. Lebon, P. Rivizzigno, and A. T. Shipboard Party. 2001. 'An off-axis hydrothermal vent field near the Mid-Atlantic Ridge at 30 degrees N', *Nature*, 412: 145-49.

Kelley, Deborah S., Jeffrey A. Karson, Gretchen L. Früh-Green, Dana R. Yoerger, Timothy M. Shank, David A. Butterfield, John M. Hayes, Matthew O. Schrenk, Eric J. Olson, Giora Proskurowski, Mike Jakuba, Al Bradley, Ben Larson, Kristin Ludwig, Deborah Glickson, Kate Buckman, Alexander S. Bradley, William J. Brazelton, Kevin Roe, Mitch J. Elend, Adélie Delacour, Stefano M. Bernasconi, Marvin D. Lilley, John A. Baross, Roger E. Summons, and Sean P. Sylva. 2005. 'A serpentinite-hosted ecosystem: the Lost City hydrothermal field', *Science*, 307: 1428-34.

Kemp, W Michael, Walter R Boynton, Jason E Adolf, Donald F Boesch, William C Boicourt, Grace Brush, Jeffrey C Cornwell, Thomas R Fisher, Patricia M Glibert, and Jim D Hagy. 2005. 'Eutrophication of Chesapeake Bay: historical trends and ecological interactions', *Marine ecology progress series*, 303: 1-29.

Kitadai, Norio, Masafumi Kameya, and Kosuke Fujishima. 2017. 'Origin of the Reductive Tricarboxylic Acid (rTCA) Cycle-Type CO2 Fixation: A Perspective', *Life*, 7.

Klein, Frieder, Wolfgang Bach, Susan E. Humphris, Wolf-Achim Kahl, Niels Jöns, Bruce Moskowitz, and Thelma S. Berquó. 2014. 'Magnetite in seafloor serpentinite—Some like it hot', *Geology*, 42: 135-38.

Klein, Frieder, Niya G. Grozeva, and Jeffrey S. Seewald. 2019. 'Abiotic methane synthesis and serpentinization in olivine-hosted fluid inclusions', *Proc. Natl. Acad. Sci. U. S. A.*, 116: 17666-72.
Klein, Frieder, Jesse D. Tarnas, and Wolfgang Bach. 2020. 'Abiotic Sources of Molecular Hydrogen on Earth', *Elements*, 16: 19-24.
Kleypas, J. A., R. W. Buddemeier, D. Archer, J. P. Gattuso, C. Langdon, and B. N. Opdyke. 1999. 'Geochemical consequences of increased atmospheric carbon dioxide on coral reefs', *Science*, 284: 118-20.
Koch, Benjamin J, Theresa A McHugh, Michaela Hayer, Egbert Schwartz, Steven J Blazewicz, Paul Dijkstra, Natasja van Gestel, Jane C Marks, Rebecca L Mau, and Ember M Morrissey. 2018. 'Estimating taxon-specific population dynamics in diverse microbial communities', *Ecosphere*, 9: e02090.
Koch, Hanna, Alexander Galushko, Mads Albertsen, Arno Schintlmeister, Christiane Gruber-Dorninger, Sebastian Lücker, Eric Pelletier, Denis Le Paslier, Eva Spieck, Andreas Richter, Per H. Nielsen, Michael Wagner, and Holger Daims. 2014. 'Growth of nitrite-oxidizing bacteria by aerobic hydrogen oxidation', *Science*, 345: 1052-54.
Kojima, Hisaya, Miho Watanabe, and Manabu Fukui. 2017. 'Sulfuritortus calidifontis gen. nov., sp. nov., a sulfur oxidizer isolated from a hot spring microbial mat', *International Journal of Systematic and Evolutionary Microbiology*, 67: 1355-58.
Konstantinidis, Konstantinos T., and James M. Tiedje. 2005. 'Genomic insights that advance the species definition for prokaryotes', *Proc. Natl. Acad. Sci. U. S. A.*, 102: 2567-72.
Köster, Johannes, and Sven Rahmann. 2012. 'Snakemake--a scalable bioinformatics workflow engine', *Bioinformatics*, 28: 2520-22.
Kwan, Patrick, Chelsea L. McIntosh, David P. Jennings, R. Chris Hopkins, Sanjeev K. Chandrayan, Chang-Hao Wu, Michael W. W. Adams, and Anne K. Jones. 2015. 'The [NiFe]-Hydrogenase of Pyrococcus furiosus Exhibits a New Type of Oxygen Tolerance', *J. Am. Chem. Soc.*, 137: 13556-65.
Lane, Nick, John F. Allen, and William Martin. 2010. 'How did LUCA make a living? Chemiosmosis in the origin of life', *Bioessays*, 32: 271-80.
Lang, Susan Q., David A. Butterfield, Mitch Schulte, Deborah S. Kelley, and Marvin D. Lilley. 2010. 'Elevated concentrations of formate, acetate and dissolved organic carbon found at the Lost City hydrothermal field', *Geochim. Cosmochim. Acta*, 74: 941-52.
Langmead, Ben, and Steven L. Salzberg. 2012. 'Fast gapped-read alignment with Bowtie 2', *Nat. Methods*, 9: 357-59.
Lau, Maggie C. Y., Thomas L. Kieft, Olukayode Kuloyo, Borja Linage-Alvarez, Esta van Heerden, Melody R. Lindsay, Cara Magnabosco, Wei Wang, Jessica B. Wiggins, Ling Guo, David H. Perlman, Saw Kyin, Henry H. Shwe, Rachel L. Harris, Youmi Oh, Min Joo Yi, Roland Purtschert, Greg F. Slater, Shuhei Ono, Siwen Wei, Long Li, Barbara Sherwood Lollar, and Tullis C. Onstott. 2016. 'An oligotrophic deep-subsurface community dependent on syntrophy is dominated by sulfur-driven autotrophic denitrifiers', *Proc. Natl. Acad. Sci. U. S. A.*, 113: E7927-E36.
Lavalleur, H. J., and F. S. Colwell. 2013. 'Microbial characterization of basalt formation waters targeted for geological carbon sequestration', *FEMS Microbiol Ecol*, 85: 62-73.
Lavik, Gaute, Torben Stührmann, Volker Brüchert, Anja Van der Plas, Volker Mohrholz, Phyllis Lam, Marc Mußmann, Bernhard M Fuchs, Rudolf Amann, and Ulrich Lass. 2009. 'Detoxification of sulphidic African shelf waters by blooming chemolithotrophs', *Nature*, 457: 581-84.
Lecoeuvre, A., B. Ménez, M. Cannat, V. Chavagnac, and E. Gérard. 2021. 'Microbial ecology of the newly discovered serpentinite-hosted Old City hydrothermal field (southwest Indian ridge)', *Isme j*, 15: 818-32.

Lee, Michael D. 2019. 'GToTree: a user-friendly workflow for phylogenomics', *Bioinformatics*, 35: 4162-64.
Letunic, Ivica, and Peer Bork. 2016. 'Interactive tree of life (iTOL) v3: an online tool for the display and annotation of phylogenetic and other trees', *Nucleic Acids Res.*, 44: W242-5.
Li, Dinghua, Chi-Man Liu, Ruibang Luo, Kunihiko Sadakane, and Tak-Wah Lam. 2015. 'MEGAHIT: an ultra-fast single-node solution for large and complex metagenomics assembly via succinct de Bruijn graph', *Bioinformatics*, 31: 1674-76.
Liu, Yi-Fan, Jing Chen, Zhong-Lin Liu, Li-Bin Shou, Dan-Dan Lin, Lei Zhou, Shi-Zhong Yang, Jin-Feng Liu, Wei Li, Ji-Dong Gu, and Bo-Zhong Mu. 2020. 'Anaerobic Degradation of Paraffins by Thermophilic Actinobacteria under Methanogenic Conditions', *Environ. Sci. Technol.*, 54: 10610-20.
Lopez-Fernandez, Margarita, Mats Åström, Stefan Bertilsson, and Mark Dopson. 2018. 'Depth and Dissolved Organic Carbon Shape Microbial Communities in Surface Influenced but Not Ancient Saline Terrestrial Aquifers', *Front. Microbiol.*, 9: 2880.
Lu, Zheng, and James A. Imlay. 2021. 'When anaerobes encounter oxygen: mechanisms of oxygen toxicity, tolerance and defence', *Nat. Rev. Microbiol.*, 19: 774-85.
Lueders, T., M. Manefield, and M. W. Friedrich. 2004. 'Enhanced sensitivity of DNA- and rRNA-based stable isotope probing by fractionation and quantitative analysis of isopycnic centrifugation gradients', *Environ Microbiol*, 6: 73-8.
Lueders, Tillmann. 2015. 'DNA-and RNA-based stable isotope probing of hydrocarbon degraders.' in, *Hydrocarbon and Lipid Microbiology Protocols* (Springer).
Luna, GM, E Manini, and R Danovaro. 2002. 'Large fraction of dead and inactive bacteria in coastal marine sediments: comparison of protocols for determination and ecological significance', *Applied and environmental microbiology*, 68: 3509-13.
Magnabosco, C., L. H. Lin, H. Dong, M. Bomberg, W. Ghiorse, H. Stan-Lotter, K. Pedersen, T. L. Kieft, E. van Heerden, and T. C. Onstott. 2018. 'The biomass and biodiversity of the continental subsurface', *Nat. Geosci.*, 11: 707-17.
Magnabosco, Cara, Kathleen Ryan, Maggie C. Y. Lau, Olukayode Kuloyo, Barbara Sherwood Lollar, Thomas L. Kieft, Esta van Heerden, and Tullis C. Onstott. 2016. 'A metagenomic window into carbon metabolism at 3 km depth in Precambrian continental crust', *ISME J.*, 10: 730-41.
Maia, Marcia, Susanna Sichel, Anne Briais, Daniele Brunelli, Marco Ligi, Nicolas Ferreira, Thomas Campos, Bérengère Mougel, Isa Brehme, Christophe Hémond, Akihisa Motoki, Denise Moura, Carla Scalabrin, Ivo Pessanha, Eliane Alves, Arthur Ayres, and Pedro Oliveira. 2016. 'Extreme mantle uplift and exhumation along a transpressive transform fault', *Nat. Geosci.*, 9: 619-23.
Mall, Achim, Jessica Sobotta, Claudia Huber, Carolin Tschirner, Stefanie Kowarschik, Katarina Bačnik, Mario Mergelsberg, Matthias Boll, Michael Hügler, Wolfgang Eisenreich, and Ivan A. Berg. 2018. 'Reversibility of citrate synthase allows autotrophic growth of a thermophilic bacterium', *Science*, 359: 563-67.
Marcy, Yann, Cleber Ouverney, Elisabeth M. Bik, Tina Lösekann, Natalia Ivanova, Hector Garcia Martin, Ernest Szeto, Darren Platt, Philip Hugenholtz, David A. Relman, and Stephen R. Quake. 2007. 'Dissecting biological "dark matter" with single-cell genetic analysis of rare and uncultivated TM7 microbes from the human mouth', *Proc. Natl. Acad. Sci. U. S. A.*, 104: 11889-94.
Martin, William, John Baross, Deborah Kelley, and Michael J. Russell. 2008. 'Hydrothermal vents and the origin of life', *Nat. Rev. Microbiol.*, 6: 805-14.
Martin, William F. 2020. 'Older Than Genes: The Acetyl CoA Pathway and Origins', *Front. Microbiol.*, 11: 817.

Martin, William, and Michael J. Russell. 2007. 'On the origin of biochemistry at an alkaline hydrothermal vent', *Philos. Trans. R. Soc. Lond. B Biol. Sci.*, 362: 1887-925.
Mason, O. U., C. A. Di Meo-Savoie, J. D. Van Nostrand, J. Zhou, M. R. Fisk, and S. J. Giovannoni. 2009. 'Prokaryotic diversity, distribution, and insights into their role in biogeochemical cycling in marine basalts', *Isme j*, 3: 231-42.
McCollom, Thomas M. 2016. 'Abiotic methane formation during experimental serpentinization of olivine', *Proc. Natl. Acad. Sci. U. S. A.*, 113: 13965-70.
McCollom, Thomas M., and Jeffrey S. Seewald. 2007. 'Abiotic synthesis of organic compounds in deep-sea hydrothermal environments', *Chem. Rev.*, 107: 382-401.
McCollom, Thomas M., and Jeffrey S. Seewald. 2013. 'Serpentinites, Hydrogen, and Life', *Elements*, 9: 129-34.
McDowall, Jennifer S., Bonnie J. Murphy, Michael Haumann, Tracy Palmer, Fraser A. Armstrong, and Frank Sargent. 2014. 'Bacterial formate hydrogenlyase complex', *Proc. Natl. Acad. Sci. U. S. A.*, 111: E3948-56.
McNichol, Jesse, Hryhoriy Stryhanyuk, Sean P. Sylva, François Thomas, Niculina Musat, Jeffrey S. Seewald, and Stefan M. Sievert. 2018. 'Primary productivity below the seafloor at deep-sea hot springs', *Proc. Natl. Acad. Sci. U. S. A.*, 115: 6756-61.
Meier, D. V., P. Pjevac, W. Bach, S. Markert, T. Schweder, J. Jamieson, S. Petersen, R. Amann, and A. Meyerdierks. 2019. 'Microbial metal-sulfide oxidation in inactive hydrothermal vent chimneys suggested by metagenomic and metaproteomic analyses', *Environ Microbiol*, 21: 682-701.
Merino, Nancy, Heidi S. Aronson, Diana P. Bojanova, Jayme Feyhl-Buska, Michael L. Wong, Shu Zhang, and Donato Giovannelli. 2019. 'Living at the Extremes: Extremophiles and the Limits of Life in a Planetary Context', *Front. Microbiol.*, 10: 780.
Mertoglu, Orhan, Sakir Simsek, and Nilgun Basarir. 2020. "Geothermal energy use: projections and country update for Turkey." In *Proceedings World Geothermal Congress*.
Middelburg, Jack J, Gerard Klaver, Joop Nieuwenhuize, Rinus M Markusse, Tom Vlug, and FJWA Van der Nat. 1995. 'Nitrous oxide emissions from estuarine intertidal sediments', *Hydrobiologia*, 311: 43-55.
Miller, S. L. 1953. 'A production of amino acids under possible primitive earth conditions', *Science*, 117: 528-29.
Momper, Lily, Sean P. Jungbluth, Michael D. Lee, and Jan P. Amend. 2017. 'Energy and carbon metabolisms in a deep terrestrial subsurface fluid microbial community', *ISME J.*, 11: 2319-33.
Morrill, P. L., W. J. Brazelton, L. Kohl, A. Rietze, S. M. Miles, H. Kavanagh, M. O. Schrenk, S. E. Ziegler, and S. Q. Lang. 2014. 'Investigations of potential microbial methanogenic and carbon monoxide utilization pathways in ultra-basic reducing springs associated with present-day continental serpentinization: the Tablelands, NL, CAN', *Frontiers in microbiology*, 5: 613.
Morrissey, Ember M., Rebecca L. Mau, Egbert Schwartz, J. Gregory Caporaso, Paul Dijkstra, Natasja van Gestel, Benjamin J. Koch, Cindy M. Liu, Michaela Hayer, Theresa A. McHugh, Jane C. Marks, Lance B. Price, and Bruce A. Hungate. 2016. 'Phylogenetic organization of bacterial activity', *ISME J.*, 10: 2336.
Morrissey, Ember M., Rebecca L. Mau, Egbert Schwartz, Benjamin J. Koch, Michaela Hayer, and Bruce A. Hungate. 2018. 'Taxonomic patterns in the nitrogen assimilation of soil prokaryotes', *Environ. Microbiol.*, 20: 1112-19.
Morrissey, Ember M., Rebecca L. Mau, Egbert Schwartz, Theresa A. McHugh, Paul Dijkstra, Benjamin J. Koch, Jane C. Marks, and Bruce A. Hungate. 2017. 'Bacterial carbon use plasticity, phylogenetic diversity and the priming of soil organic matter', *ISME J.*

Moser, D. P., T. M. Gihring, F. J. Brockman, J. K. Fredrickson, D. L. Balkwill, M. E. Dollhopf, B. S. Lollar, L. M. Pratt, E. Boice, G. Southam, G. Wanger, B. J. Baker, S. M. Pfiffner, L. H. Lin, and T. C. Onstott. 2005. 'Desulfotomaculum and Methanobacterium spp. dominate a 4- to 5-kilometer-deep fault', *Appl Environ Microbiol*, 71: 8773-83.

Muchowska, Kamila B., Elodie Chevallot-Beroux, and Joseph Moran. 2019a. 'Recreating ancient metabolic pathways before enzymes', *Bioorg. Med. Chem.*

Muchowska, Kamila B., Sreejith J. Varma, Elodie Chevallot-Beroux, Lucas Lethuillier-Karl, Guang Li, and Joseph Moran. 2017. 'Metals promote sequences of the reverse Krebs cycle', *Nat Ecol Evol*, 1: 1716-21.

Muchowska, Kamila B., Sreejith J. Varma, and Joseph Moran. 2019b. 'Synthesis and breakdown of universal metabolic precursors promoted by iron', *Nature*, 569: 104-07.

Müller, Albert Leopold, Kasper Urup Kjeldsen, Thomas Rattei, Michael Pester, and Alexander Loy. 2015. 'Phylogenetic and environmental diversity of DsrAB-type dissimilatory (bi) sulfite reductases', *The ISME Journal*, 9: 1152-65.

Müller, Bettina, Li Sun, and Anna Schnürer. 2013. 'First insights into the syntrophic acetate-oxidizing bacteria--a genetic study', *Microbiologyopen*, 2: 35-53.

Müller, Volker. 2003. 'Energy conservation in acetogenic bacteria', *Appl. Environ. Microbiol.*, 69: 6345-53.

Mützenberg, Stefan. 1997. 'Nature and origin of the thermal springs in the Tuzla area, Western Anatolia, Turkey', *Active Tectonic of Northwestern Anatolia—The Marmara Poly-Project*: 301-17.

Neufeld, Josh D., Jyotsna Vohra, Marc G. Dumont, Tillmann Lueders, Mike Manefield, Michael W. Friedrich, and J. Colin Murrell. 2007a. 'DNA stable-isotope probing', *Nat. Protoc.*, 2: 860-66.

Neufeld, Josh D., Michael Wagner, and J. Colin Murrell. 2007b. 'Who eats what, where and when? Isotope-labelling experiments are coming of age', *ISME J.*, 1: 103-10.

Nigro, Lisa M., Andrew S. Hyde, Barbara J. MacGregor, and Andreas Teske. 2016. 'Phylogeography, Salinity Adaptations and Metabolic Potential of the Candidate Division KB1 Bacteria Based on a Partial Single Cell Genome', *Front. Microbiol.*, 7: 1266.

Nixon, Scott W. 1981. 'Remineralization and nutrient cycling in coastal marine ecosystems.' in, *Estuaries and nutrients* (Springer).

Nobu, Masaru K., Jeremy A. Dodsworth, Senthil K. Murugapiran, Christian Rinke, Esther A. Gies, Gordon Webster, Patrick Schwientek, Peter Kille, R. John Parkes, Henrik Sass, Bo B. Jørgensen, Andrew J. Weightman, Wen-Tso Liu, Steven J. Hallam, George Tsiamis, Tanja Woyke, and Brian P. Hedlund. 2016. 'Phylogeny and physiology of candidate phylum 'Atribacteria' (OP9/JS1) inferred from cultivation-independent genomics', *ISME J.*, 10: 273-86.

Nogales, Balbina, Edward R. B. Moore, Enrique Llobet-Brossa, Ramon Rossello-Mora, Rudolf Amann, and Kenneth N. Timmis. 2001. 'Combined Use of 16S Ribosomal DNA and 16S rRNA To Study the Bacterial Community of Polychlorinated Biphenyl-Polluted Soil', *Applied and environmental microbiology*, 67: 1874-84.

Nutman, Allen P., Vickie C. Bennett, Clark R. L. Friend, Martin J. Van Kranendonk, and Allan R. Chivas. 2016. 'Rapid emergence of life shown by discovery of 3,700-million-year-old microbial structures', *Nature*, 537: 535-38.

Okay, Aral, Muzaffer Siyako, and Kerem Bürkan. 1991. 'Geology and tectonic evolution of the Biga Peninsula', *Bulletin of the Technical University Istanbul*, 44: 191-255.

Okubo, Takashi, and Hideto Takami. 2021. 'Metabolic potential of the imperfect denitrifier Candidatus Desulfobacillus denitrificans in an anammox bioreactor', *Microbiologyopen*, 10: e1227.

Oremland, Ronald S., Laurence G. Miller, and Michael J. Whiticar. 1987. 'Sources and flux of natural gases from Mono Lake, California', *Geochim. Cosmochim. Acta*, 51: 2915-29.
Oren, Aharon. 2008. 'Microbial life at high salt concentrations: phylogenetic and metabolic diversity', *Saline Systems*, 4: 2.
Orsi, W. D., R. Morard, A. Vuillemin, M. Eitel, G. Wörheide, J. Milucka, and M. Kucera. 2020a. 'Anaerobic metabolism of Foraminifera thriving below the seafloor', *Isme j*, 14: 2580-94.
Orsi, William D. 2018. 'Ecology and evolution of seafloor and subseafloor microbial communities', *Nature Reviews Microbiology*, 16: 671-83.
Orsi, William D., Jason M. Smith, Shuting Liu, Zhanfei Liu, Carole M. Sakamoto, Susanne Wilken, Camille Poirier, Thomas A. Richards, Patrick J. Keeling, Alexandra Z. Worden, and Alyson E. Santoro. 2016. 'Diverse, uncultivated bacteria and archaea underlying the cycling of dissolved protein in the ocean', *ISME J.*, 10: 2158-73.
Orsi, William D., Jason M. Smith, Heather M. Wilcox, Jarred E. Swalwell, Paul Carini, Alexandra Z. Worden, and Alyson E. Santoro. 2015. 'Ecophysiology of uncultivated marine euryarchaea is linked to particulate organic matter', *ISME J.*, 9: 1747-63.
Orsi, William D., Aurèle Vuillemin, Paula Rodriguez, Ömer K. Coskun, Gonzalo V. Gomez-Saez, Gaute Lavik, Volker Mohrholz, and Timothy G. Ferdelman. 2020b. 'Metabolic activity analyses demonstrate that Lokiarchaeon exhibits homoacetogenesis in sulfidic marine sediments', *Nature Microbiology*, 5: 248-55.
Orsi, William D., Susanne Wilken, Javier del Campo, Thierry Heger, Erick James, Thomas A. Richards, Patrick J. Keeling, Alexandra Z. Worden, and Alyson E. Santoro. 2018. 'Identifying protist consumers of photosynthetic picoeukaryotes in the surface ocean using stable isotope probing', *Environmental Microbiology*, 20: 815-27.
Ortega-Arbulú, Ana-Sofia, Monica Pichler, Aurèle Vuillemin, and William D. Orsi. 2019. 'Effects of organic matter and low oxygen on the mycobenthos in a coastal lagoon', *Environmental Microbiology*, 21: 374-88.
Osburn, M. R., D. E. LaRowe, L. M. Momper, and J. P. Amend. 2014. 'Chemolithotrophy in the continental deep subsurface: Sanford Underground Research Facility (SURF), USA', *Frontiers in microbiology*, 5: 610.
Pagel, M. 1999. 'Inferring the historical patterns of biological evolution', *Nature*, 401: 877-84.
Papp, Katerina, Bruce A Hungate, and Egbert Schwartz. 2018. 'Microbial rRNA synthesis and growth compared through quantitative stable isotope probing with H218O', *Applied and environmental microbiology*, 84: e02441-17.
Parada, Alma E., David M. Needham, and Jed A. Fuhrman. 2016. 'Every base matters: assessing small subunit rRNA primers for marine microbiomes with mock communities, time series and global field samples', *Environ. Microbiol.*, 18: 1403-14.
Parks, Donovan H., Christian Rinke, Maria Chuvochina, Pierre-Alain Chaumeil, Ben J. Woodcroft, Paul N. Evans, Philip Hugenholtz, and Gene W. Tyson. 2017. 'Recovery of nearly 8,000 metagenome-assembled genomes substantially expands the tree of life', *Nat Microbiol*.
Pedersen, K. 2000. 'Exploration of deep intraterrestrial microbial life: current perspectives', *FEMS Microbiol. Lett.*, 185: 9-16.
Pedersen, Karsten. 1997. 'Microbial life in deep granitic rock', *FEMS Microbiol. Rev.*, 20: 399-414.
Pepe-Ranney, C., A. N. Campbell, C. N. Koechli, S. Berthrong, and D. H. Buckley. 2016a. 'Unearthing the Ecology of Soil Microorganisms Using a High Resolution DNA-SIP Approach to Explore Cellulose and Xylose Metabolism in Soil', *Frontiers in microbiology*, 7: 703.
Pepe-Ranney, C., C. Koechli, R. Potrafka, C. Andam, E. Eggleston, F. Garcia-Pichel, and D. H. Buckley. 2016b. 'Non-cyanobacterial diazotrophs mediate dinitrogen fixation in biological soil crusts during early crust formation', *Isme j*, 10: 287-98.

Perner, M., M. Hansen, R. Seifert, H. Strauss, A. Koschinsky, and S. Petersen. 2013. 'Linking geology, fluid chemistry, and microbial activity of basalt- and ultramafic-hosted deep-sea hydrothermal vent environments', *Geobiology*, 11: 340-55.

Pester, Michael, Norbert Bittner, Pinsurang Deevong, Michael Wagner, and Alexander Loy. 2010. 'A 'rare biosphere' microorganism contributes to sulfate reduction in a peatland', *The ISME Journal*, 4: 1591-602.

Phelps, Craig D., Lee J. Kerkhof, and Lily Y. Young. 1998. 'Molecular characterization of a sulfate-reducing consortium which mineralizes benzene', *FEMS Microbiology Ecology*, 27: 269-79.

Pichler, Monica, Ömer K. Coskun, Ana-Sofia Ortega-Arbulú, Nicola Conci, Gert Wörheide, Sergio Vargas, and William D. Orsi. 2018. 'A 16S rRNA gene sequencing and analysis protocol for the Illumina MiniSeq platform', *Microbiologyopen*: e00611.

Pierson, Beverly K, and Richard W Castenholz. 1974. 'A phototrophic gliding filamentous bacterium of hot springs, Chloroflexus aurantiacus, gen. and sp. nov', *Archives of Microbiology*, 100: 5-24.

Preiner, Martina, Kensuke Igarashi, Kamila B. Muchowska, Mingquan Yu, Sreejith J. Varma, Karl Kleinermanns, Masaru K. Nobu, Yoichi Kamagata, Harun Tüysüz, Joseph Moran, and William F. Martin. 2020. 'A hydrogen-dependent geochemical analogue of primordial carbon and energy metabolism', *Nature Ecology & Evolution*, 4: 534-42.

Pritchard, Leighton, Rachel H. Glover, Sonia Humphris, John G. Elphinstone, and Ian K. Toth. 2016. 'Genomics and taxonomy in diagnostics for food security: soft-rotting enterobacterial plant pathogens', *Analytical Methods*, 8: 12-24.

Probst, Alexander J., Cindy J. Castelle, Andrea Singh, Christopher T. Brown, Karthik Anantharaman, Itai Sharon, Laura A. Hug, David Burstein, Joanne B. Emerson, Brian C. Thomas, and Jillian F. Banfield. 2017. 'Genomic resolution of a cold subsurface aquifer community provides metabolic insights for novel microbes adapted to high CO2 concentrations', *Environ. Microbiol.*, 19: 459-74.

Probst, Alexander J., Felix J. Elling, Cindy J. Castelle, Qingzeng Zhu, Marcus Elvert, Giovanni Birarda, Hoi-Ying N. Holman, Katherine R. Lane, Bethany Ladd, M. Cathryn Ryan, Tanja Woyke, Kai-Uwe Hinrichs, and Jillian F. Banfield. 2020. 'Lipid analysis of CO2-rich subsurface aquifers suggests an autotrophy-based deep biosphere with lysolipids enriched in CPR bacteria', *The ISME Journal*, 14: 1547-60.

Probst, Alexander J., Bethany Ladd, Jessica K. Jarett, David E. Geller-McGrath, Christian M. K. Sieber, Joanne B. Emerson, Karthik Anantharaman, Brian C. Thomas, Rex R. Malmstrom, Michaela Stieglmeier, Andreas Klingl, Tanja Woyke, M. Cathryn Ryan, and Jillian F. Banfield. 2018. 'Differential depth distribution of microbial function and putative symbionts through sediment-hosted aquifers in the deep terrestrial subsurface', *Nature Microbiology*, 3: 328-36.

Puzenat, Valentine, Javier Escartín, Jean-Emmanuel Martelat, Thibaut Barreyre, Sven Le Moine Bauer, Paraskevi Nomikou, Nuno Gracias, Pascal Allemand, Varvara Antoniou, Omer Coskun, Rafael Garcia, Philippe Grandjean, Steffen Leth Jørgensen, Lluís Magí, Manolis Mandalakis, William Orsi, Paraskevi Polymenakou, Anders Schouw, Guillem Vallicrosa, and Othonas Vlasopoulos. 2021. 'Shallow-water hydrothermalism at Milos (Greece): Nature, distribution, heat fluxes and impact on ecosystems', *Mar. Geol.*, 438: 106521.

Qin, Wei, Shady A. Amin, Willm Martens-Habbena, Christopher B. Walker, Hidetoshi Urakawa, Allan H. Devol, Anitra E. Ingalls, James W. Moffett, E. Virginia Armbrust, and David A. Stahl. 2014. 'Marine ammonia-oxidizing archaeal isolates display obligate mixotrophy and wide ecotypic variation', *Proc. Natl. Acad. Sci. U. S. A.*, 111: 12504-09.

Quast, Christian, Elmar Pruesse, Pelin Yilmaz, Jan Gerken, Timmy Schweer, Pablo Yarza, Jörg Peplies, and Frank Oliver Glöckner. 2013. 'The SILVA ribosomal RNA gene database project: improved data processing and web-based tools', *Nucleic Acids Res.*, 41: D590-6.

Quince, Christopher, Alan W. Walker, Jared T. Simpson, Nicholas J. Loman, and Nicola Segata. 2017. 'Shotgun metagenomics, from sampling to analysis', *Nat. Biotechnol.*, 35: 833-44.

Rabus, Ralf, Sofia S. Venceslau, Lars Wöhlbrand, Gerrit Voordouw, Judy D. Wall, and Inês A. C. Pereira. 2015. 'Chapter Two- A Post-Genomic View of the Ecophysiology, Catabolism and Biotechnological Relevance of Sulphate-Reducing Prokaryotes.' in Robert K. Poole (ed.), *Advances in Microbial Physiology* (Academic Press).

Radajewski, S., I. R. McDonald, and J. C. Murrell. 2003. 'Stable-isotope probing of nucleic acids: a window to the function of uncultured microorganisms', *Curr Opin Biotechnol*, 14: 296-302.

Ragsdale, Stephen W. 2003. 'Pyruvate ferredoxin oxidoreductase and its radical intermediate', *Chem. Rev.*, 103: 2333-46.

Ragsdale, Stephen W. 2004. 'Life with carbon monoxide', *Crit. Rev. Biochem. Mol. Biol.*, 39: 165-95.

Ragsdale, Stephen W., and Elizabeth Pierce. 2008. 'Acetogenesis and the Wood-Ljungdahl pathway of CO(2) fixation', *Biochim. Biophys. Acta*, 1784: 1873-98.

Rappé, Michael S., and Stephen J. Giovannoni. 2003. 'The uncultured microbial majority', *Annu. Rev. Microbiol.*, 57: 369-94.

Ravenschlag, K., K. Sahm, J. Pernthaler, and R. Amann. 1999. 'High bacterial diversity in permanently cold marine sediments', *Appl Environ Microbiol*, 65: 3982-9.

Rempfert, Kaitlin R., Hannah M. Miller, Nicolas Bompard, Daniel Nothaft, Juerg M. Matter, Peter Kelemen, Noah Fierer, and Alexis S. Templeton. 2017. 'Geological and Geochemical Controls on Subsurface Microbial Life in the Samail Ophiolite, Oman', *Frontiers in microbiology*, 8: 56-56.

Reveillaud, J., E. Reddington, J. McDermott, C. Algar, J. L. Meyer, S. Sylva, J. Seewald, C. R. German, and J. A. Huber. 2016. 'Subseafloor microbial communities in hydrogen-rich vent fluids from hydrothermal systems along the Mid-Cayman Rise', *Environ Microbiol*, 18: 1970-87.

Reysenbach, Anna-Louise, Emily St John, Jennifer Meneghin, Gilberto E. Flores, Mircea Podar, Nina Dombrowski, Anja Spang, Stephane L'Haridon, Susan E. Humphris, Cornel E. J. de Ronde, Fabio Caratori Tontini, Maurice Tivey, Valerie K. Stucker, Lucy C. Stewart, Alexander Diehl, and Wolfgang Bach. 2020. 'Complex subsurface hydrothermal fluid mixing at a submarine arc volcano supports distinct and highly diverse microbial communities', *Proc. Natl. Acad. Sci. U. S. A.*, 117: 32627-38.

Rho, Mina, Haixu Tang, and Yuzhen Ye. 2010. 'FragGeneScan: predicting genes in short and error-prone reads', *Nucleic Acids Res.*, 38: e191.

Rice, Peter, Ian Longden, and Alan Bleasby. 2000. 'EMBOSS: the European molecular biology open software suite', *Trends in genetics*, 16: 276-77.

Rickard, David, and George W Luther. 2007. 'Chemistry of iron sulfides', *Chemical reviews*, 107: 514-62.

Rinke, Christian, Patrick Schwientek, Alexander Sczyrba, Natalia N. Ivanova, Iain J. Anderson, Jan-Fang Cheng, Aaron Darling, Stephanie Malfatti, Brandon K. Swan, Esther A. Gies, Jeremy A. Dodsworth, Brian P. Hedlund, George Tsiamis, Stefan M. Sievert, Wen-Tso Liu, Jonathan A. Eisen, Steven J. Hallam, Nikos C. Kyrpides, Ramunas Stepanauskas, Edward M. Rubin, Philip Hugenholtz, and Tanja Woyke. 2013. 'Insights into the phylogeny and coding potential of microbial dark matter', *Nature*, 499: 431-37.

Rosenberg, Eugene. 2006. 'Hydrocarbon-Oxidizing Bacteria.' in Martin Dworkin, Stanley Falkow, Eugene Rosenberg, Karl-Heinz Schleifer and Erko Stackebrandt (eds.), *The Prokaryotes: Volume 2: Ecophysiology and Biochemistry* (Springer New York: New York, NY).

Roslev, Peter, Mariann Brøndum Larsen, Dennis Jørgensen, and Martin Hesselsoe. 2004. 'Use of heterotrophic CO2 assimilation as a measure of metabolic activity in planktonic and sessile bacteria', *J. Microbiol. Methods*, 59: 381-93.

Rotthauwe, Jan-Henrich, Karl-Paul Witzel, and Werner Liesack. 1997. 'The ammonia monooxygenase structural gene amoA as a functional marker: molecular fine-scale analysis of natural ammonia-oxidizing populations', *Applied and environmental microbiology*, 63: 4704-12.

Russell, M. J., A. J. Hall, and W. Martin. 2010. 'Serpentinization as a source of energy at the origin of life', *Geobiology*, 8: 355-71.

Russell, Michael J., Laura M. Barge, Rohit Bhartia, Dylan Bocanegra, Paul J. Bracher, Elbert Branscomb, Richard Kidd, Shawn McGlynn, David H. Meier, Wolfgang Nitschke, Takazo Shibuya, Steve Vance, Lauren White, and Isik Kanik. 2014. 'The drive to life on wet and icy worlds', *Astrobiology*, 14: 308-43.

Russell, Michael J., Allan J. Hall, and Dugald Turner. 1989. 'In vitro growth of iron sulphide chimneys: possible culture chambers for origin-of-life experiments', *Terra Nova*, 1: 238-41.

Russell, Michael J., and William Martin. 2004. 'The rocky roots of the acetyl-CoA pathway', *Trends Biochem. Sci.*, 29: 358-63.

Salter, Susannah J., Michael J. Cox, Elena M. Turek, Szymon T. Calus, William O. Cookson, Miriam F. Moffatt, Paul Turner, Julian Parkhill, Nicholas J. Loman, and Alan W. Walker. 2014. 'Reagent and laboratory contamination can critically impact sequence-based microbiome analyses', *BMC Biol.*, 12: 87.

Sánchez-Andrea, Irene, Iame Alves Guedes, Bastian Hornung, Sjef Boeren, Christopher E. Lawson, Diana Z. Sousa, Arren Bar-Even, Nico J. Claassens, and Alfons J. M. Stams. 2020. 'The reductive glycine pathway allows autotrophic growth of Desulfovibrio desulfuricans', *Nat. Commun.*, 11: 5090.

Santelli, C. M., B. N. Orcutt, E. Banning, W. Bach, C. L. Moyer, M. L. Sogin, H. Staudigel, and K. J. Edwards. 2008. 'Abundance and diversity of microbial life in ocean crust', *Nature*, 453: 653-6.

Sarp, S, M Burçak, T Yıldırım, and N Yıldırım. 1998. 'Biga yarımadasının jeolojisi ve jeotermal enerji olanakları ile Balıkesir-Havran-Derman kaplıca sahasının detay jeotermal etüdü ve gradyan sondajları', *Gn. Directorate of Mineral Research and Exploration, Rep*, 10537.

Schink, B. 1997. 'Energetics of syntrophic cooperation in methanogenic degradation', *Microbiol. Mol. Biol. Rev.*, 61: 262-80.

Schmidtko, Sunke, Lothar Stramma, and Martin Visbeck. 2017. 'Decline in global oceanic oxygen content during the past five decades', *Nature*, 542: 335-39.

Schneider, Dominik, Daniela Zühlke, Anja Poehlein, Katharina Riedel, and Rolf Daniel. 2021. 'Metagenome-Assembled Genome Sequences from Different Wastewater Treatment Stages in Germany', *Microbiol Resour Announc*, 10: e0050421.

Schoell, Martin. 1988. 'Multiple origins of methane in the Earth', *Chem. Geol.*, 71: 1-10.

Schrenk, Matthew O., William J. Brazelton, and Susan Q. Lang. 2013. 'Serpentinization, Carbon, and Deep Life', *Rev. Mineral. Geochem.*, 75: 575-606.

Schubotz, Florence, Lindsay E. Hays, D'arcy R. Meyer-Dombard, Aimee Gillespie, Everett L. Shock, and Roger E. Summons. 2015. 'Stable isotope labeling confirms mixotrophic nature of streamer biofilm communities at alkaline hot springs', *Front. Microbiol.*, 6: 42.

Schuchmann, Kai, and Volker Müller. 2012. 'A bacterial electron-bifurcating hydrogenase', *J. Biol. Chem.*, 287: 31165-71.

Schuchmann, Kai, and Volker Müller. 2016. 'Energetics and Application of Heterotrophy in Acetogenic Bacteria', *Appl. Environ. Microbiol.*, 82: 4056-69.

Schwartz, Egbert. 2007. 'Characterization of growing microorganisms in soil by stable isotope probing with H218O', *Applied and environmental microbiology*, 73: 2541-46.

Schwartz, Egbert, Michaela Hayer, Bruce A Hungate, Benjamin J Koch, Theresa A McHugh, William Mercurio, Ember M Morrissey, and Katerina Soldanova. 2016. 'Stable isotope probing with 18O-water to investigate microbial growth and death in environmental samples', *Current opinion in biotechnology*, 41: 14-18.

Schwartz, Egbert, David J Van Horn, Heather N Buelow, Jordan G Okie, Michael N Gooseff, John E Barrett, and Cristina D Takacs-Vesbach. 2014. 'Characterization of growing bacterial populations in McMurdo Dry Valley soils through stable isotope probing with 18O-water', *FEMS Microbiology Ecology*, 89: 415-25.

Seemann, Torsten. 2013. 'barrnap 0.9: rapid ribosomal RNA prediction', *Google Scholar*.

Seewald, Jeffrey S., Kenneth W. Doherty, Terence R. Hammar, and Stephen P. Liberatore. 2002. 'A new gas-tight isobaric sampler for hydrothermal fluids', *Deep Sea Res. Part I*, 49: 189-96.

Seewald, Jeffrey S., Mikhail Yu Zolotov, and Thomas McCollom. 2006. 'Experimental investigation of single carbon compounds under hydrothermal conditions', *Geochim. Cosmochim. Acta*, 70: 446-60.

Seyler, Lauren M., Lora R. McGuinness, Jack A. Gilbert, Jennifer F. Biddle, Donglai Gong, and Lee J. Kerkhof. 2018. 'Discerning autotrophy, mixotrophy and heterotrophy in marine TACK archaea from the North Atlantic', *FEMS Microbiol. Ecol.*, 94.

Shock, Everett L. 1990. 'Geochemical constraints on the origin of organic compounds in hydrothermal systems', *Orig. Life Evol. Biosph.*, 20: 331-67.

Sieber, Christian M. K., Alexander J. Probst, Allison Sharrar, Brian C. Thomas, Matthias Hess, Susannah G. Tringe, and Jillian F. Banfield. 2018. 'Recovery of genomes from metagenomes via a dereplication, aggregation and scoring strategy', *Nature Microbiology*, 3: 836-43.

Sieradzki, Ella T., Benjamin J. Koch, Alex Greenlon, Rohan Sachdeva, Rex R. Malmstrom, Rebecca L. Mau, Steven J. Blazewicz, Mary K. Firestone, Kirsten Hofmockel, Egbert Schwartz, Bruce A. Hungate, and Jennifer Pett-Ridge. 2020. 'Measurement error and resolution in quantitative stable isotope probing: implications for experimental design', *bioRxiv*.

Smith, Amy R., Brandon Kieft, Ryan Mueller, Martin R. Fisk, Olivia U. Mason, Radu Popa, and Frederick S. Colwell. 2019. 'Carbon fixation and energy metabolisms of a subseafloor olivine biofilm', *ISME J.*, 13: 1737-49.

Smith, Eric, and Harold J. Morowitz. 2004. 'Universality in intermediary metabolism', *Proc. Natl. Acad. Sci. U. S. A.*, 101: 13168-73.

Sojo, Victor, Barry Herschy, Alexandra Whicher, Eloi Camprubí, and Nick Lane. 2016. 'The Origin of Life in Alkaline Hydrothermal Vents', *Astrobiology*, 16: 181-97.

Spanevello, Mark D., and Bharat K. C. Patel. 2004. 'The phylogenetic diversity of Thermus and Meiothermus from microbial mats of an Australian subsurface aquifer runoff channel', *FEMS Microbiol. Ecol.*, 50: 63-73.

Spona-Friedl, Marina, Alexander Braun, Claudia Huber, Wolfgang Eisenreich, Christian Griebler, Andreas Kappler, and Martin Elsner. 2020. 'Substrate-dependent CO2 fixation in heterotrophic bacteria revealed by stable isotope labelling', *FEMS Microbiol. Ecol.*, 96.

Stamatakis, A. 2006. 'RAxML-VI-HPC: maximum likelihood-based phylogenetic analyses with thousands of taxa and mixed models', *Bioinformatics*, 22: 2688-90.

Steffens, Lydia, Eugenio Pettinato, Thomas M. Steiner, Achim Mall, Simone König, Wolfgang Eisenreich, and Ivan A. Berg. 2021. 'High CO2 levels drive the TCA cycle backwards towards autotrophy', *Nature*, 592: 784-88.

Stevens, T. 1997. 'Lithoautotrophy in the subsurface', *FEMS Microbiol. Rev.*, 20: 327-37.

Stevens, Todd O. 2018. 'Subsurface microbiology and the evolution of the biosphere.' in, *The Microbiology of the Terrestrial Deep Subsurface* (CRC Press).

Stevens, Todd O., and James P. McKinley. 1995. 'Lithoautotrophic Microbial Ecosystems in Deep Basalt Aquifers', *Science*, 270: 450-55.

Stott, M. B., J. A. Saito, M. A. Crowe, P. F. Dunfield, S. Hou, E. Nakasone, C. J. Daughney, A. V. Smirnova, B. W. Mountain, K. Takai, and M. Alam. 2008. 'Culture-independent characterization of a novel microbial community at a hydrothermal vent at Brothers volcano, Kermadec arc, New Zealand', *Journal of Geophysical Research: Solid Earth*, 113.

Suzuki, T., T. Murai, I. Fukuda, T. Tobe, M. Yoshikawa, and C. Sasakawa. 1994. 'Identification and characterization of a chromosomal virulence gene, vacJ, required for intercellular spreading of Shigella flexneri', *Mol Microbiol*, 11: 31-41.

Szewzyk, R., and N. Pfennig. 1987. 'Complete oxidation of catechol by the strictly anaerobic sulfate-reducing Desulfobacterium catecholicum sp. nov', *Archives of Microbiology*, 147: 163-68.

Takami, Hideto, Hideki Noguchi, Yoshihiro Takaki, Ikuo Uchiyama, Atsushi Toyoda, Shinro Nishi, Gab-Joo Chee, Wataru Arai, Takuro Nunoura, Takehiko Itoh, Masahira Hattori, and Ken Takai. 2012. 'A deeply branching thermophilic bacterium with an ancient acetyl-CoA pathway dominates a subsurface ecosystem', *PLoS One*, 7: e30559.

Tamames, Javier, and Fernando Puente-Sánchez. 2018. 'SqueezeMeta, A Highly Portable, Fully Automatic Metagenomic Analysis Pipeline', *Front. Microbiol.*, 9: 3349.

Taubert, M., W. A. Overholt, B. M. Heinze, G. A. Matanfack, R. Houhou, N. Jehmlich, M. von Bergen, P. Rösch, J. Popp, and K. Küsel. 2022. 'Bolstering fitness via CO(2) fixation and organic carbon uptake: mixotrophs in modern groundwater', *Isme j*, 16: 1153-62.

Team, Rstudio. 2015. 'RStudio: integrated development for R', *RStudio, Inc. , Boston, MA URL http://www. rstudio. com*.

Team, Rstudio, and Others. 2015. 'RStudio: integrated development for R', *RStudio, Inc. , Boston, MA URL http://www. rstudio. com*, 42: 14.

Teske, Andreas, Kai-Uwe Hinrichs, Virginia Edgcomb, Alvin de Vera Gomez, David Kysela, Sean P. Sylva, Mitchell L. Sogin, and Holger W. Jannasch. 2002. 'Microbial diversity of hydrothermal sediments in the Guaymas Basin: evidence for anaerobic methanotrophic communities', *Appl. Environ. Microbiol.*, 68: 1994-2007.

Thiel, Vera, Michael Hügler, David M. Ward, and Donald A. Bryant. 2017. 'The Dark Side of the Mushroom Spring Microbial Mat: Life in the Shadow of Chlorophototrophs. II. Metabolic Functions of Abundant Community Members Predicted from Metagenomic Analyses', *Front. Microbiol.*, 8: 943.

Tobler, Dominique J., and Liane G. Benning. 2011. 'Bacterial diversity in five Icelandic geothermal waters: temperature and sinter growth rate effects', *Extremophiles*, 15: 473-85.

Trifinopoulos, Jana, Lam-Tung Nguyen, Arndt von Haeseler, and Bui Quang Minh. 2016. 'W-IQ-TREE: a fast online phylogenetic tool for maximum likelihood analysis', *Nucleic Acids Res.*, 44: W232-5.

Tuorto, Steven J., Phillip Darias, Lora R. McGuinness, Nicolai Panikov, Tingjun Zhang, Max M. Häggblom, and Lee J. Kerkhof. 2014. 'Bacterial genome replication at subzero temperatures in permafrost', *ISME J.*, 8: 139-49.

Tyson, R. V., and T. H. Pearson. 1991. 'Modern and ancient continental shelf anoxia: an overview', *Geological Society, London, Special Publications*, 58: 1-24.

Ueno, Yuichiro, Keita Yamada, Naohiro Yoshida, Shigenori Maruyama, and Yukio Isozaki. 2006. 'Evidence from fluid inclusions for microbial methanogenesis in the early Archaean era', *Nature*, 440: 516-19.

Valiela, Ivan, Kenneth Foreman, Michael LaMontagne, Douglas Hersh, Joseph Costa, Paulette Peckol, Barbara DeMeo-Andreson, Charlene D'Avanzo, Michele Babione, and Chi-Ho Sham. 1992. 'Couplings of watersheds and coastal waters: sources and consequences of nutrient enrichment in Waquoit Bay, Massachusetts', *Estuaries*, 15: 443-57.

Van Kranendonk, Martin J. 2010. 'Two types of Archean continental crust: Plume and plate tectonics on early Earth', *Am. J. Sci.*, 310: 1187-209.

Varma, Sreejith J., Kamila B. Muchowska, Paul Chatelain, and Joseph Moran. 2018. 'Native iron reduces CO2 to intermediates and end-products of the acetyl-CoA pathway', *Nat Ecol Evol*, 2: 1019-24.

Vavourakis, Charlotte D., Adrian-Stefan Andrei, Maliheh Mehrshad, Rohit Ghai, Dimitry Y. Sorokin, and Gerard Muyzer. 2018. 'A metagenomics roadmap to the uncultured genome diversity in hypersaline soda lake sediments', *Microbiome*, 6.

Vengosh, Avner, Cahit Helvacı, and İsmail H. Karamanderesi. 2002. 'Geochemical constraints for the origin of thermal waters from western Turkey', *Appl. Geochem.*, 17: 163-83.

Vignais, Paulette M., and Bernard Billoud. 2007. 'Occurrence, classification, and biological function of hydrogenases: an overview', *Chem. Rev.*, 107: 4206-72.

Vuillemin, A., S. Vargas, K. Coskun Ö, R. Pockalny, R. W. Murray, D. C. Smith, S. D'Hondt, and W. D. Orsi. 2020. 'Atribacteria Reproducing over Millions of Years in the Atlantic Abyssal Subseafloor', *mBio*, 11.

Vuillemin, Aurèle, Scott D. Wankel, Ömer K. Coskun, Tobias Magritsch, Sergio Vargas, Emily R. Estes, Arthur J. Spivack, David C. Smith, Robert Pockalny, Richard W. Murray, Steven D'Hondt, and William D. Orsi. 2019. 'Archaea dominate oxic subseafloor communities over multimillion-year time scales', *Sci Adv*, 5: eaaw4108.

Wächtershäuser, G. 1990. 'Evolution of the first metabolic cycles', *Proc. Natl. Acad. Sci. U. S. A.*, 87: 200-04.

Waite, J. Hunter, J. Hunter Waite, Christopher R. Glein, Rebecca S. Perryman, Ben D. Teolis, Brian A. Magee, Greg Miller, Jacob Grimes, Mark E. Perry, Kelly E. Miller, Alexis Bouquet, Jonathan I. Lunine, Tim Brockwell, and Scott J. Bolton. 2017. 'Cassini finds molecular hydrogen in the Enceladus plume: Evidence for hydrothermal processes', *Science*, 356: 155-59.

Wang, Shang, Weiguo Hou, Hailiang Dong, Hongchen Jiang, Liuqin Huang, Geng Wu, Chuanlun Zhang, Zhaoqi Song, Yong Zhang, Huilei Ren, Jing Zhang, and Li Zhang. 2013. 'Control of temperature on microbial community structure in hot springs of the Tibetan Plateau', *PLoS One*, 8: e62901.

Wang, Wenxiu, Jianchang Tao, Ke Yu, Chen He, Jianjun Wang, Penghui Li, Hongmei Chen, Bu Xu, Quan Shi, and Chuanlun Zhang. 2021. 'Vertical Stratification of Dissolved Organic Matter Linked to Distinct Microbial Communities in Subtropic Estuarine Sediments', *Front. Microbiol.*, 12: 697860.

Wang, Zhaohui Aleck, Kevin D Kroeger, Neil K Ganju, Meagan Eagle Gonneea, and Sophie N Chu. 2016. 'Intertidal salt marshes as an important source of inorganic carbon to the coastal ocean', *Limnology and Oceanography*, 61: 1916-31.

Wankel, Scott D., Leonid N. Germanovich, Marvin D. Lilley, Gence Genc, Christopher J. DiPerna, Alexander S. Bradley, Eric J. Olson, and Peter R. Girguis. 2011. 'Influence of subsurface biosphere on geochemical fluxes from diffuse hydrothermal fluids', *Nature Geoscience*, 4: 461-68.

Wasmund, Kenneth, Marc Mußmann, and Alexander Loy. 2017. 'The life sulfuric: microbial ecology of sulfur cycling in marine sediments', *Environmental Microbiology Reports*, 9: 323-44.

Weiss, Madeline C., Filipa L. Sousa, Natalia Mrnjavac, Sinje Neukirchen, Mayo Roettger, Shijulal Nelson-Sathi, and William F. Martin. 2016. 'The physiology and habitat of the last universal common ancestor', *Nat Microbiol*, 1: 16116.

Westmeijer, George, Maliheh Mehrshad, Stephanie Turner, Linda Alakangas, Varvara Sachpazidou, Carina Bunse, Jarone Pinhassi, Marcelo Ketzer, Mats Åström, Stefan Bertilsson, and Mark Dopson. 2022. 'Connectivity of Fennoscandian Shield terrestrial deep biosphere microbiomes with surface communities', *Communications Biology*, 5: 37.

Wilcoxen, J., B. Zhang, and R. Hille. 2011. 'Reaction of the molybdenum- and copper-containing carbon monoxide dehydrogenase from Oligotropha carboxydovorans with quinones', *Biochemistry*, 50: 1910-6.

Wimmer, Jessica L. E., Andrey do Nascimento Vieira, Joana C. Xavier, Karl Kleinermanns, William F. Martin, and Martina Preiner. 2021. 'The Autotrophic Core: An Ancient Network of 404 Reactions Converts H2, CO2, and NH3 into Amino Acids, Bases, and Cofactors', *Microorganisms*, 9.

Wolf, Patricia G., Ambarish Biswas, Sergio E. Morales, Chris Greening, and H. Rex Gaskins. 2016. 'H2 metabolism is widespread and diverse among human colonic microbes', *Gut Microbes*, 7: 235-45.

Woods, Angela, Maribeth Watwood, and Egbert Schwartz. 2011. 'Identification of a toluene-degrading bacterium from a soil sample through H2 18O DNA stable isotope probing', *Applied and environmental microbiology*, 77: 5995-99.

Worman, Stacey L., Lincoln F. Pratson, Jeffrey A. Karson, and Emily M. Klein. 2016. 'Global rate and distribution of H 2 gas produced by serpentinization within oceanic lithosphere : H 2 FORMATION IN OCEAN LITHOSPHERE', *Geophys. Res. Lett.*, 43: 6435-43.

Wright, Jody J., Kishori M. Konwar, and Steven J. Hallam. 2012. 'Microbial ecology of expanding oxygen minimum zones', *Nat. Rev. Microbiol.*, 10: 381-94.

Wu, Yu-Wei, Blake A. Simmons, and Steven W. Singer. 2016. 'MaxBin 2.0: an automated binning algorithm to recover genomes from multiple metagenomic datasets', *Bioinformatics*, 32: 605-07.

Yalcin, Tolga. 2007. 'Geochemical characterization of the Biga Peninsula thermal waters (NW Turkey)', *Aquat. Geochem.*, 13: 75-93.

Yarza, Pablo, Pelin Yilmaz, Elmar Pruesse, Frank Oliver Glöckner, Wolfgang Ludwig, Karl-Heinz Schleifer, William B. Whitman, Jean Euzéby, Rudolf Amann, and Ramon Rosselló-Móra. 2014. 'Uniting the classification of cultured and uncultured bacteria and archaea using 16S rRNA gene sequences', *Nat. Rev. Microbiol.*, 12: 635-45.

Ye, Qi, Ying Wu, Zhuoyi Zhu, Xiaona Wang, Zhongqiao Li, and Jing Zhang. 2016. 'Bacterial diversity in the surface sediments of the hypoxic zone near the Changjiang Estuary and in the East China Sea', *Microbiologyopen*, 5: 323-39.

Youngblut, N. D., and D. H. Buckley. 2014. 'Intra-genomic variation in G + C content and its implications for DNA stable isotope probing', *Environ Microbiol Rep*, 6: 767-75.

Youngblut, Nicholas D., Samuel E. Barnett, and Daniel H. Buckley. 2018a. 'HTSSIP: An R package for analysis of high throughput sequencing data from nucleic acid stable isotope probing (SIP) experiments', *PLoS One*, 13: e0189616.

Youngblut, Nicholas D., Samuel E. Barnett, and Daniel H. Buckley. 2018b. 'SIPSim: A Modeling Toolkit to Predict Accuracy and Aid Design of DNA-SIP Experiments', *Front. Microbiol.*, 9: 570.

Youssef, Noha H., Ibrahim F. Farag, Christian Rinke, Steven J. Hallam, Tanja Woyke, and Mostafa S. Elshahed. 2015. 'In Silico Analysis of the Metabolic Potential and Niche Specialization of Candidate Phylum "Latescibacteria" (WS3)', *PLoS One*, 10: e0127499.

Youssef, Noha H., Ibrahim F. Farag, Sydney Rudy, Ace Mulliner, Kara Walker, Ford Caldwell, Malik Miller, Wouter Hoff, and Mostafa Elshahed. 2019. 'The Wood-Ljungdahl pathway as a key component of metabolic versatility in candidate phylum Bipolaricaulota (Acetothermia, OP1)', *Environ. Microbiol. Rep.*, 11: 538-47.

Zhou, Zhichao, Yang Liu, Jie Pan, Brandi R. Cron, Brandy M. Toner, Karthik Anantharaman, John A. Breier, Gregory J. Dick, and Meng Li. 2020. 'Gammaproteobacteria mediating utilization of methyl-, sulfur- and petroleum organic compounds in deep ocean hydrothermal plumes', *ISME J.*, 14: 3136-48.

Declaration

I hereby confirm that my thesis entitled **Quantifying carbon fixation in microbial dark matter from low-temperature hydrothermal settings: experimental validation using quantitative stable isotope probing**, is the result of my own original work. Furthermore, I certify that this work contains no material which has been accepted for the award of any other degree or diploma in my name, in any university and, to the best of my knowledge and belief, contains no material previously published or written by another person, except where due reference has been made in the text. In addition, I certify that no part of this work will, in the future, be used in a submission in my name, for any other degree or diploma in any university or other tertiary institution without the prior approval of the Ludwig-Maximilians-Universität München.

Place and Date	Signature
München, 02.03.2022	Ömer Kürşat Coşkun

Acknowledgements

I would like to thank my supervisor Prof.Dr. William D. Orsi for his continuous support and guidance. His overall insights, patience and encouragement through this project have been invaluable for me. I am so grateful to have had a supervisor who was continuously showing me great empathy by recognizing my low-concentration times and giving me enough time to gain energy. I would like to express my thanks to my good friend and colleague Dr. Aurèle Vuillemin, whom I shared the office and the lab with for 4 years, for all his support and lively discussions.

My thanks are extended to Volkan Özen whom I have shared almost an entire year together with in Munich. I would like to acknowledge here that I missed those days when we discussed different aspects of life.

I would like to thank Baran Karapunar whom I studied together at Middle East Technical University, and MGAP master program at LMU for being a good company in the department. I would like to thank to Marina Waldmann for our walks and inviting me over her and Baran's house. I would also like to thank my close friends in the Alfred und Karl Marchionini dormitory, especially Suna Günay, Ibrahim Mutlu, Ibrahim Orhan, Tuğba Sel, Sedef Akkuş, Viktor Elkin, Michael Birth, and Firas Nassar.

I would like to thank to my friends in Turkey for their support during my Ph.D., especially to Yunus Emre Polat, Nurgül Polat, Cenk Parlatan, Meltem Parlatan, Emre Gözübüyük, Çağdaş Çelebi, Tuğrul Eynur, Sena Eynur, Erhan Yılmaz, Büşra Yılmaz, İsmail Metehan Gültekin, Muhittin Serhat Mutlu, and Senem Mutlu.

I am extremely grateful to my girlfriend who supported me every single day with her smiling face.

I am greatly indebted to my family members, especially to my parents Ayla Coşkun and Mustafa Coşkun, my sister Zeynep Nihan Coşkun, and my uncle Şerafettin Coşkun for their continuous and endless support throughout whole my life.

Finally, this project could have never happened without the financial support of the Deutsche Forschung Gemeinschaft (DFG) --- project ID 364653263 --- TRR-235.